Conference Proceedings of the Society for Experimental Mechanics Series

Vijay Chalivendra
Allison M Beese
Ryan B. Berke *Editors*

Mechanics of Composite, Hybrid and Multifunctional Materials, Fracture, Fatigue, Failure and Damage Evolution, Volume 3

Proceedings of the 2021 Annual Conference on Experimental and Applied Mechanics

SEM

Springer

Conference Proceedings of the Society for Experimental Mechanics Series

Series Editor

Kristin B. Zimmerman
Society for Experimental Mechanics, Inc.,
Bethel, CT, USA

The Conference Proceedings of the Society for Experimental Mechanics Series presents early findings and case studies from a wide range of fundamental and applied work across the broad range of fields that comprise Experimental Mechanics. Series volumes follow the principle tracks or focus topics featured in each of the Society's two annual conferences: IMAC, A Conference and Exposition on Structural Dynamics, and the Society's Annual Conference & Exposition and will address critical areas of interest to researchers and design engineers working in all areas of Structural Dynamics, Solid Mechanics and Materials Research.

More information about this series at http://www.springer.com/series/8922

Vijay Chalivendra • Allison M Beese • Ryan B. Berke
Editors

Mechanics of Composite, Hybrid and Multifunctional Materials, Fracture, Fatigue, Failure and Damage Evolution, Volume 3

Proceedings of the 2021 Annual Conference on Experimental and Applied Mechanics

Springer

Editors
Vijay Chalivendra
University of Massachussetts
North Dartmouth, MA, USA

Ryan B. Berke
Mechanical and Aerospace Engineering
Utah State University
Logan, UT, USA

Allison M Beese
Materials Science and Engineering and
Mechanical Engineering
Pennsylvania State University
University Park, PA, USA

ISSN 2191-5644 ISSN 2191-5652 (electronic)
Conference Proceedings of the Society for Experimental Mechanics Series
ISBN 978-3-030-86740-9 ISBN 978-3-030-86741-6 (eBook)
https://doi.org/10.1007/978-3-030-86741-6

This Springer imprint is published by the registered company Springer Nature Switzerland AG
The registered company address is: Gewerbestrasse 11, 6330 Cham, Switzerland

Preface

Mechanics of Composite, Hybrid and Multifunctional Materials, Fracture, Fatigue, Failure and Damage Evolution represents one of four volumes of technical papers presented at the 2021 SEM Annual Conference & Exposition on Experimental and Applied Mechanics organized by the Society for Experimental Mechanics held on June 14–17, 2021. The complete Proceedings also includes volumes on *Dynamic Behavior of Materials; Challenges in Mechanics of Time-Dependent Materials, Mechanics of Biological Systems and Materials, Micro- and Nanomechanics; Thermomechanics & Infrared Imaging, Inverse Problem Methodologies, Mechanics of Additive & Advanced Manufactured Materials;* and *Advancement of Optical Methods & Digital Image Correlation.*

The commercial market for composite continues to expand with a wide range of applications from sporting equipment to aerospace vehicles. This growth has been fueled by new material developments, greater understanding of material behaviors, novel design solutions, and improved manufacturing techniques. The broad range of applications and the associated technical challenges require an increasingly multidisciplinary and collaborative approach between the mechanical, chemical, and physical sciences to sustain and enhance the positive impact of composites on the commercial and military sectors.

New materials are being developed from recycled source materials, leading to composites with unique properties and more sustainable sources. Existing materials are also being used in new and critical applications, which requires a deeper understanding of material behaviors and failure mechanisms on multiple length and time scales. In addition, the unique properties of composites present many challenges in manufacturing and in joining with other materials. New testing methods must be developed to characterize the novel composite properties, to evaluate application and product life cycle performance, as well as to evaluate impacts and merits of new manufacturing methods.

The first section of this volume presents early research findings from experimental and computational investigations related to the processing, characterization, and testing of composite, hybrid, and multifunctional materials.

The fracture, fatigue, failure, and damage evolution section of this volume covers some of the most critical considerations in engineering design. Understanding and characterizing fatigue and fracture has remained as one of the primary focus areas of experimental mechanics for several decades. Advances in experimental techniques, such as digital image correlation, acoustic emissions, and electron microscopy, have allowed for deeper study of phenomena related to fatigue and fracture. This volume contains the results of investigations of several aspects of fatigue and fracture such as microstructural effects, the behavior of interfaces, the behavior of different and/or complex materials such as composites, and environmental and loading effects. The collection of experimental mechanics research included here represents another step toward solving the long-term challenges associated with fatigue and fracture.

North Dartmouth, MA, USA — Vijaya Chalivendra
University Park, PA, USA — Allison M. Beese
Logan, UT, USA — Ryan B. Berke

Contents

Chapter 1
Effects of Water Saturation and Low Temperature Coupling on the Mechanical Behavior of Carbon and E-Glass Epoxy Laminates

James LeBlanc, Paul Cavallaro, Jahn Torres, Eric Warner, David Ponte, Irine Chenwi, and Arun Shukla

Abstract Advanced composite materials exhibit many desirable characteristics which make them viable candidates for utilization in harsh marine environments. An experimental investigation has been conducted to quantify the effects of coupled water saturation and low temperatures on the mechanical and dynamic behavior of E-glass and carbon epoxy laminates. The relative performance of the materials as a function of water saturation and decreasing temperature was characterized through detailed experiments, specifically in-plane (tensile/compressive) and shear material properties, static and dynamic Mode-I fracture, and impact/flexure after impact strength. The temperature range considered in the study corresponds to a range from room temperature (20 °C) down to Arctic seawater and extreme ocean depth conditions (−2 °C). The materials utilized in the study, carbon/epoxy and E-glass/epoxy, are chosen due to their primary interest to the marine and undersea vehicle communities. The results of the mechanical and dynamic material experiments show that all properties are affected by both water saturation and decreasing temperature, although the trends are specific to the property of consideration.

Keywords Composite materials · Low temperatures · Mechanical characterization · Water ingression · Dynamic mechanical analysis

1.1 Introduction

Fiber-reinforced polymer (FRP) composites provide exclusive performance advantages over traditional structural materials when designed for operational use in the subsea domain. These materials produce components that have high strength to weight ratios, lighter overall weight, superior resistance to corrosion, and overall reductions in required maintenance. However, there are also many unique considerations that must be taken when using these materials in the design of a structure. These include reduced resistance to impact damage and cyclic loading conditions, post-damage residual strengths, complex failure and damage mechanisms, repair difficulty, and stringent certification processes. The understanding of the performance of these materials when operating in extreme marine environments is key in ensuring a structurally adequate design that will ensure robustness throughout the intended life cycle. The focus of the current work is on the conditions found in Arctic environments, deep ocean depths, and applications with long seawater exposure times such as drilling operations. The conditions associated with these environments include near freezing seawater temperatures and water ingression into the structural laminates. The specific quantities of interest are those that potentially affect operating capabilities of submerged components/structures arising from low temperature/water ingression exposures, namely material strength (tensile, shear, compression), damage resistance (fracture toughness, crack propagation/stability), and impact loading resistance.

The understanding of the complex mechanical and fracture characteristics of advanced composite materials is generally much more limited than the knowledge associated with historical metallic materials. This limited understanding can be compounded by the introduction of use in long-term submergence and low temperature conditions. The use of polymer-based materials in cold and Arctic temperature environments results in higher stiffnesses but oftentimes lower toughness properties

J. LeBlanc (✉) · P. Cavallaro · J. Torres · E. Warner · D. Ponte
Naval Undersea Warfare Center (Division Newport), Newport, RI, USA
e-mail: James.M.LeBlanc@Navy.MIl; paul.cavallaro@navy.mil; jahn.torres-jove@navy.mil; eric.warner@navy.mil; david.ponte@navy.mil

I. Chenwi · A. Shukla
Dynamic Photo Mechanics Laboratory, Department of Mechanical, Industrial and Systems Engineering, University of Rhode Island, Kingston, RI, USA
e-mail: mforneba@uri.edu; shuklaa@uri.edu

V. Chalivendra et al. (eds.), *Mechanics of Composite, Hybrid and Multifunctional Materials, Fracture, Fatigue, Failure and Damage Evolution, Volume 3*, Conference Proceedings of the Society for Experimental Mechanics Series,
https://doi.org/10.1007/978-3-030-86741-6_1

which may lead to the onset of unique failure mechanisms such as matrix cracking, ply delaminations, etc. When considering the design of structures and vehicles comprised of composite materials to be operated in a cold water environment, there is a certain need to understand the unique relationships between lamina stress distributions, the mechanics of the interlaminar ply interfaces, water absorption behavior, and fracture properties. In low temperature cases where impact type loading, such as wave slap or collisions, is a concern, there is a greater desire to improve the fracture toughness of the materials and associated laminates. These material choices and characterizations are typically made and driven by the results of detailed laboratory testing in controlled environments. Future advancements in the knowledgebase of the effects of Arctic ocean temperatures and long-term water saturation on the failure characteristics of advanced composite materials will further the expanded use of these material in marine applications.

1.2 Materials

The materials studied in the current investigation consisted of carbon/epoxy and E-glass/epoxy laminates. The carbon and E-glass fabrics were "plain weave" styles in which the yarns were woven in a one-over/one-under pattern, resulting in balanced yarn counts along the warp and weft directions. The E-glass fabric had an areal weight density of 5.61 oz./yd^2 with equal yarn counts of 18 per inch in both the warp and weft directions. The carbon fabric had an areal weight density of 5.88 oz./yd^2 with equal yarn counts of 12.5 per inch in both the warp and weft directions.

1.3 Results

A comprehensive experimental investigation of the effects of water saturation coupled with low temperatures on the mechanical, fracture, and impact dependent material properties of E-glass/epoxy and carbon/epoxy laminates has been conducted to quantify the mechanical and damage behavior of these advanced material systems when water saturation is coupled with decreasing temperatures down to the lowest expected water temperatures of the Arctic/deep ocean environments. Under tensile loading there are measurable drops in both Young's moduli and tensile strengths with water saturation, although the magnitudes of the drops are dependent upon material property and temperature. Similarly, the compressive behavior of the laminates exhibit reductions in both compressive Young's modulus and strength when saturated with water as compared to the dry condition. The short beam shear strength characteristics of the E-glass and carbon/epoxy laminates display common trends with water saturation and decreasing temperature, namely a near-uniform decrease in short beam shear strength across the 20 °C to −2 °C temperature range. A direct dependence of G_{IC} on water saturation and temperature is observed, with the carbon laminate showing a clear overall reduction in G_{IC} when the laminates become saturated whereas the E-glass laminate shows that G_{IC} increases with the presence of entrapped water. Observations of dynamic fracture experiments highlight no quantifiable dependence of G_{ICd} on water saturation condition at a given temperature for the carbon laminates while the E-glass laminates exhibited higher G_{ICd} values in the saturated state than the dry state. When subjected to drop tower impact loading, the E-glass and carbon laminates show lower peak impact forces in a saturated state than the corresponding dry state—an indicator of reduced dynamic flexural stiffness. Finally, the four-point flexure after impact behavior of the carbon laminates result in a trend where the saturated material has higher post-impact flexural strength than the dry carbon laminates. However, the E-glass laminate in a saturated state exhibits a significant reduction in flexure after impact strength as compared to the dry laminate.

Acknowledgements The research presented in this study has been generously supported through the Internal Investment Program and In-House Laboratory Independent Research (ILIR) programs at the Naval Undersea Warfare Center (Division Newport). The help of undergraduate students Ms. Juliana Martinez and Mr. Timothy Pickard in conducting the dynamic fracture experiments is gratefully acknowledged.

Chapter 2
Initiation and Propagation Fracture Toughness of AA7475-T7651 Under Different Loading Conditions

Purnashis Chakraborty, Anoop Kumar Pandouria, Sanjay Kumar, M. K. Singha, and Vikrant Tiwari

Abstract Fracture toughness of an engineering material is an essential parameter for the damage and the safety assessment of a structure exposed to different loading conditions in applications like defense, automotive, and aircraft structure. In this article, an effort is made to evaluate the fracture toughness of AA7475-T7351 alloy under different loading rates. Single edge three-point bend experiments are conducted at four different loading rates 1 mm/min, 10 mm/min, 100 mm/min, and 1000 mm/min. Quasi-static experiments are conducted using two different electromechanical universal testing machines (Zwick-Roll/Z-50 and MTS). Quasi-static initiation and propagation fracture toughness are evaluated from the load vs. crack mouth opening displacement (CMOD) diagram. It is observed that the fracture toughness of the material increases with the increase of loading rates. The fracture propagation toughness of the material also shows a positive sensitivity towards the loading rates.

Keywords Fracture toughness · Propagation toughness · TBP specimen · AA7475-T7651

2.1 Introduction

The key factor behind the rapid use of the 7XXX series aluminum alloy in aerospace, defense, and automotive industries over the previous few decades is the high strength to density ratio, high resistance against fatigue crack growth, high fracture toughness, and corrosion resistance [1–3]. These structures are more prone to face different uncertain loads such as blast, crash, and impact. Metallic material's mechanical behavior is sensitive to loading rate and temperature [4, 5]. 7XXX alloy series has a face-centered cubic (FCC) crystal structure. Different metallic solutes are used to form precipitates in the metal matrix to make more superior alloys in terms of strength and ductility [6, 7]. The concept of dynamic fracture toughness plays a vital role in structural analysis and design. As many components of the different structures may fail under the action of impulsive loads (e.g., airplane crashes, the impact of flying objects, projectile impacts, and earthquakes). Different researcher [8–12] used different setup (one bar or tow bar setup) and technique (one-point, two-point strain gauge method and high-speed optical measurement) to study the fracture toughness of a material. Bacon et al. [8] studied the fracture behavior of glass and PMMA on glass and PMMA under different loading rates using a modified Hopkinson pressure bar. The author evaluated the stress intensity factor and established a relationship between the stress intensity factor and applied dynamic load. The effect of inertia was emphasized to evaluate the correct value of the stress intensity factor. It is reported that the stress intensity factor of PMMA is proportional to load point displacement for the first vibration mode. The author also performed a comparison of fracture toughness evaluated from two different techniques (load point displacement and two-point strain measurement). Rubio et al. [9] performed three-point bend experiments to evaluate the dynamic fracture initiation toughness of AA7075-T651 under dynamic load using input load, displacement, and CMOD as input parameters. A high-speed imaging system was used to determine crack mouth displacement of three-point bend specimen. Numerical analysis using ABAQUS was performed to validate the experimental results. Xing et al. [10] used a drop tower mechanism to determine the fracture toughness of two different aluminum alloys, AA2014 and AA7075, under different loading conditions. The author observed a

P. Chakraborty (✉) · A. K. Pandouria · M. K. Singha · V. Tiwari
Department of Applied Mechanics, Indian Institute of Technology Delhi, New Delhi, India
e-mail: purnashis.chakraborty@am.iitd.ac.in; maloy@am.iitd.ac.in; tiwariv@am.iitd.ac.in

S. Kumar
Mechanical Engineering Department, Delhi Technological University, Delhi, India
e-mail: sanjaykumar@dtu.ac.in

V. Chalivendra et al. (eds.), *Mechanics of Composite, Hybrid and Multifunctional Materials, Fracture, Fatigue, Failure and Damage Evolution, Volume 3*, Conference Proceedings of the Society for Experimental Mechanics Series,
https://doi.org/10.1007/978-3-030-86741-6_2

constant increase of initiation fracture toughness and propagation toughness for both aluminum alloys with the increase of loading rates. Moreover, it is observed that AA2014 offers higher initiation toughness but AA7075 offers better propagation toughness. The author observed transgranular and intergranular of AA2014 and AA7075 under scanning electron microscope. Singh et al. [11] studied the dynamic fracture behavior of sandwich aluminum and brittle Homolite-100 under dynamic loading conditions on a single notch three-point bend specimen using modified Hopkinson pressure bar. The applied load and the load point displacement were measured by using a two-point strain measurement technique. Two high-speed cameras were used to find crack initiation, delamination, and crack re-initiation velocity of sandwich three-point bend specimen. It was observed that crack initiation, delamination, and crack re-initiation time decrease with the increase of loading rate. The presence of a thin aluminum layer increases the overall fracture toughness of the specimen. Galvez et al. [12] investigate the dynamic fracture toughness of high-strength armor steel using split Hopkinson pressure bar. The author directly placed the cracked specimen between the incident and transmitted bar. The specimen displacement was measured by strain gauges mounted on the bars where fracture initiation time was obtained using fracture gauge pasted on the specimen. The author observed that the fracture toughness of armor steel is insensitive towards loading rate. This article investigates the fracture toughness of AA7474-T7351 aluminum alloy under different loading rates and temperatures.

2.2 Material Description

The 7475-T7351aluminum alloy used in the present study was procured from Falcon Aerospace (USA) in the form of a rolled plate of 12.75 mm thick and T7351 temper. AA7475-T7351 is the purified version of the AA7075 aluminum alloy with higher yield strength, ductility, and fracture toughness. The percentage of the chemical composition obtained from EDX was compared with the manufacturer's data and allowable limits of those compositions in Table 2.1.

2.2.1 Sample Preparation and Specimen Geometry

All samples are obtained by cutting the strip from the large AA7475-T7351 aluminum alloy panels and making the notch using EDM wire cut. Single edge three-point bend specimens are adopted for quasi-static with width $W = 20$ mm, thickness $B = W/2 = 10$ mm, and span length $S = 4W = 80$ mm as shown in Fig. 2.1.

At the middle, a crack of uniform width 1.5 mm and length 7 mm is made; subsequently, a V-notch of length 1.5 mm at 30° angles is created using EDM wire cut. A prefixing flaw (fatigue crack) of length 1.5 is developed using a 100 kN capacity

Table 2.1 Chemical composition of aluminum alloy 7475-T7351

Elements	Al	Zn	Mg	Cu	Fe	Si	Ni	Mn	Cr	Ti	V	Sn	Pb
As per present study EDX W (%)	90.85	5.2203	2.12	1.4216	0.074	0.0506	0.0023	0.005	0.1944	0.0379	0.0097	<0.001	0.0011
As per manufacturer W (%)	89.88	5.9	2.3	1.7	0.07	0.04	0.0029	0.01	0.2	0.03	0.01	0.0012	0.0015
Allowable limit W (%)	88.5–91.5	5.2–6.2	1.9–2.6	1.2–1.9	0.00–0.12	0.00–0.10	–	0.00–0.08	0.18–0.025	0.00–0.06	0.00–0.05	–	–

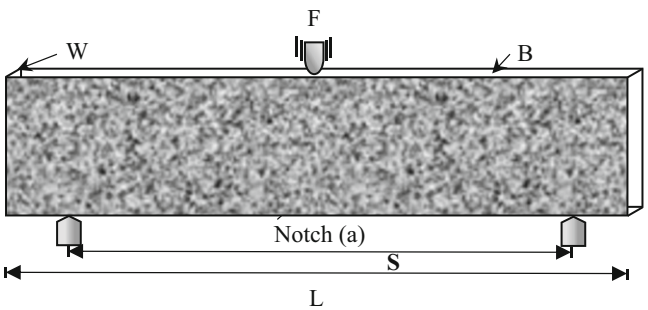

Fig. 2.1 Geometry of TBP specimen

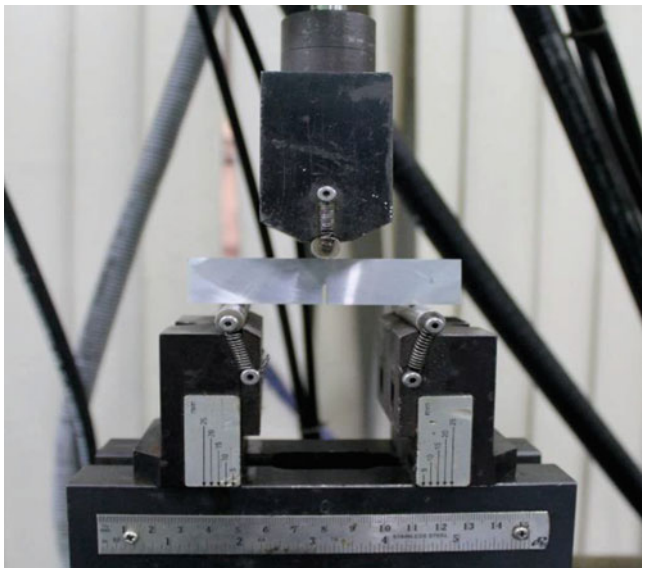

Fig. 2.2 Fatigue crack preparation

MTS machine, as shown in Fig. 2.2. The minimum and maximum loads applied during fatigue crack in the TBP specimen are 200 N and 2000 N, respectively. The mean load and load amplitude are measured 1100 N and 825 N. The loading frequency set at 25 Hz, and the number of cycles needed to obtain the required fatigue crack length was between 41,450 and 44,250.

2.3 Experimental Procedure

The characterization of the material's fracture behavior under a wide range of loading rates using one mechanical testing machine is very impractical because of their limited crosshead velocity range. Thus, based on the magnitude of the loading rate, various devices are used to evaluate fracture toughness. A Zwick-Roll/Z50 electromechanical universal testing machine is used to determine the fracture toughness for loading rate 1–100 mm/min, whereas for loading rate 1000–5000 mm/min a 250 kN capacity MTS machine with hydraulic grip is used.

2.3.1 The Theoretical Aspect of Static Fracture Toughness

All quasi-static three-point bend experiments usually conducted using a clip gauge to measure crack mouth opening displacement (CMOD). The static fracture toughness (K_{Ic}) for the single edge 3-point bend specimen is calculated using

$$K_{Ic} = \frac{3S\sqrt{a}}{2BW^2} Y\left(\frac{a}{W}\right) F \tag{2.1}$$

where a is the total crack length (notch + fatigue crack), B is the thickness, S is span length, L is the specimen length, F is the force applied on the specimen and

$$Y\left(\frac{a}{W}\right) = \frac{1.99 - \left(\frac{a}{W}\right)\left(1 - \frac{a}{W}\right)\left(2.15 - 3.93\frac{a}{W} + 2.7\left(\frac{a}{W}\right)^2\right)}{\left(1 + 2\frac{a}{W}\right)\left(1 - \frac{a}{W}\right)^{3/2}} \tag{2.2}$$

Here F can be calculated from the Load vs. CMOD diagram.

2.4 Experiments and Results

A three-point bend specimen with a single edge has been mounted on Zwick/Roll-Z50 and MTS machine as shown in Fig.2.3a to achieve three-point bend loading conditions. In order to quantify the crack mouth opening displacement (CMOD), a clip gauge is attached to the specimen at the mouth of the notch. Two knife-edges are pasted at the mouth of the notch to hold the clip gauge. The applied load on the specimen and corresponding CMOD of the specimen are recorded in the computer attached with the machine. Zwick-Roll/Z-50 is used for loading range between 1 and 100 mm/min, whereas for above 500 mm/min loading rate MTS machine has been used. The specimen before and after the experiment is shown in Fig. 2.3b.

2.5 Results and Discussion

The Load vs. CMOD of AA7475-T7351 aluminum experiments performed at a different loading rate (1–1000 mm/min) are reported in Fig. 2.4. It can be observed that with the increase of loading rate, the specimen required a higher load to deform. The fracture toughness of metal is evaluated corresponding to the maximum load of load vs. CMOD diagram. To evaluate

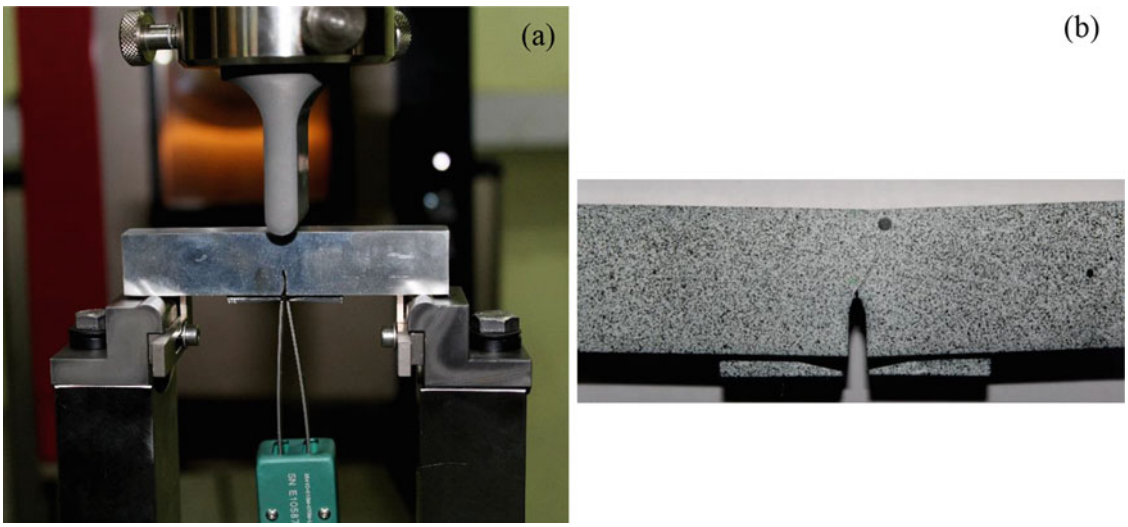

Fig. 2.3 (**a**) TBP specimen fixing in UTM (**b**) TBP specimen after experiment

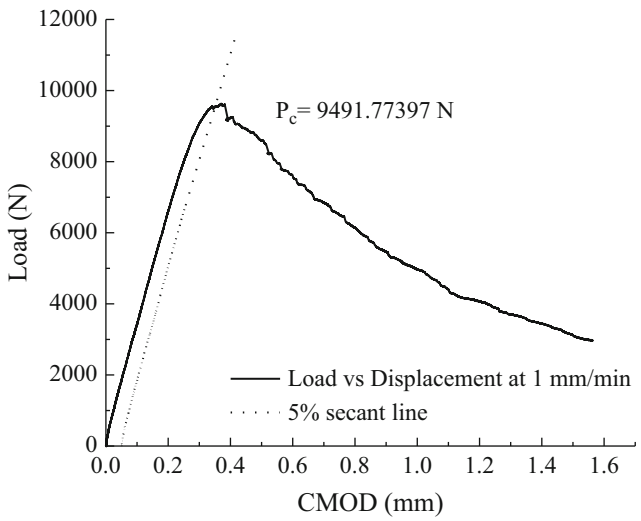

Fig. 2.4 Load vs. CMOD diagram

Table 2.2 Fracture toughness under different loading rates

Loading rate (mm/min)	1	10	100	1000
Fracture toughness (MPa $m^{1/2}$)	55.51946	56.01403	57.60076	58.92683

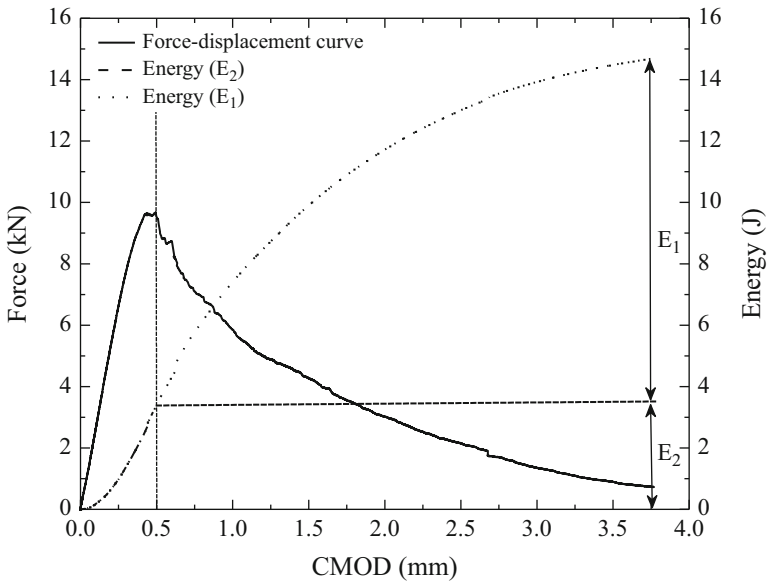

Fig. 2.5 Force and energy absorbed by the TBP specimen vs. CMOD effect of loading rate

fracture toughness, a 5% secant line is drawn parallel to the elastic region of the load-CMOD diagram. The critical load (P_c) is identified as the overlapping point between the load-CMOD diagram and the 5% secant line.

The fracture toughness calculated corresponding to critical load (PC) and Eq. (2.1) under different loading rates reported in Table 2.2.

2.5.1 Calculation of Propagation Fracture Toughness

Fracture initiation toughness is usually referred to as fracture toughness, physically explained as the resistance against crack initiation in a material. However, the propagation toughness is expressed as the resistance against a propagating crack under a specific loading condition. The propagation toughness of a material is directly linked with energy absorbed during the failure process. So, a purely energy-based method is used to determine the propagation fracture toughness.

The energy absorption by a material during failure may be divided into two parts; energy absorbed corresponding to maximum force, $\boldsymbol{E_1}$, and $\boldsymbol{E_2}$, after passing the maximum load. The total energy absorbed during the failure process is expressed as $\boldsymbol{E = E_1 + E_2}$. All these energies $\boldsymbol{E_1}$, $\boldsymbol{E_2}$, and $\boldsymbol{E}$ can be evaluated by successive integration of the load-CMOD curve during the failure process, as described in Fig. 2.5. Here it is assumed that the $\boldsymbol{E_1}$ is the amount of energy required to initiate the crack and $\boldsymbol{E_2}$ is energy used to propagate the crack [13]. Under plane strain condition, the average propagation fracture toughness is expressed as [14]:

$$K_{\mathrm{Ic}}^{P} = \sqrt{G_{\mathrm{C}} Y/(1-\nu^2)} \tag{2.3}$$

where $G_{\mathrm{C}} = \frac{E_2}{A_c}$, Y is the Young's modulus, ν is the Poisson's ratio and A is the fracture area.

2.5.2 *Effect of Loading Rate*

The loading rate have significant influence on the initiation and propagation toughness of a material. In this study, the experiments are performed at 1 mm/min, 10 mm/min, 100 mm/min, and 1000 mm/min, respectively. The effect of loading rate on the load-CMOD is shown in Fig. 2.6.

The initiation fracture toughness of AA7475-T7351 aluminum alloy at different loading rates is plotted on the log scale as shown in Fig. 2.7a. The propagation toughness of AA7475-T7351 aluminum at particular displacements is plotted on the log scale in Fig. 2.7b. It can be observed that the fracture initiation and propagation toughness of AA7475-T7351 significantly depend upon the loading rates.

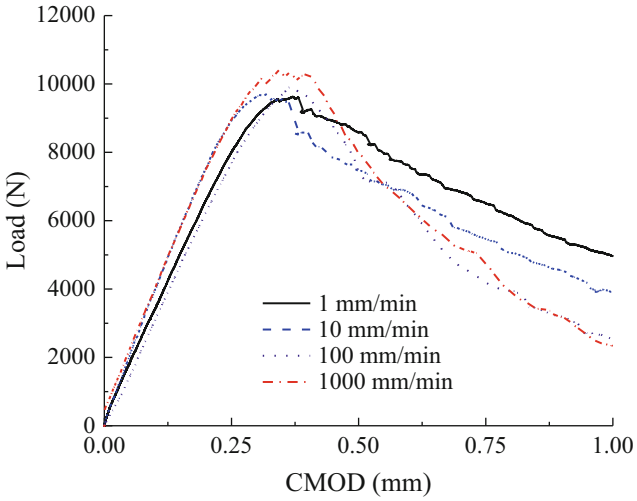

Fig. 2.6 Load vs. CMOD under different rate of loading

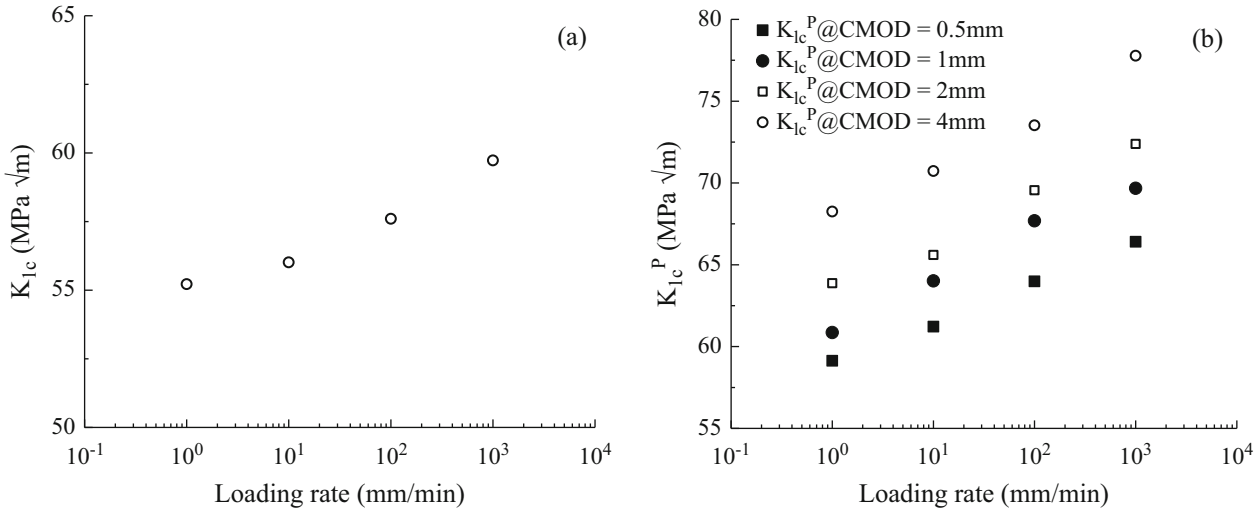

Fig. 2.7 (**a**) Initiation fracture toughness at different loading rates (**b**) Propagation fracture toughness at particular displacement under different loading rates

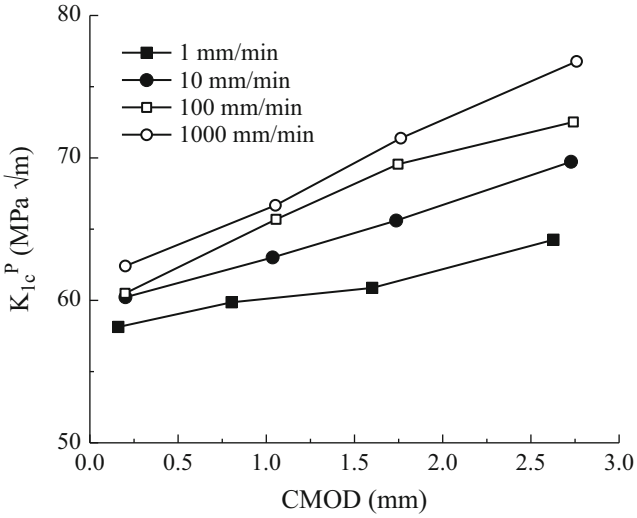

Fig. 2.8 Effect of displacement on the propagation toughness

2.5.3 Effect of Displacement on the Propagation Toughness

The effect of accumulated strain or successive displacement has an important influence on the propagation toughness. The propagation fracture toughness at a particular displacement is plotted under different loading rates in Fig. 2.8. So, it's clear that the propagation toughness of material is largely dependent upon the accumulated displacement.

2.6 Conclusion

A single edge notched three-point bend specimen is used to investigate the fracture behavior of AA7475-T7351 aluminum alloy under quasi-static loading conditions. The initiation fracture toughness is evaluated at different loading rates. The average propagation fracture toughness of AA7475-T7351 aluminum alloy is also evaluated. The initiation and propagation fracture toughness are evaluated as a function of loading rates. It is observed that loading rate has a significant effect on initiation and propagation toughness and AA7475-T7351 aluminum alloy shows positive loading rate sensitivity towards loading rate.

References

1. Tabei, A., Shih, D.S., Garmestani, H., Liang, S.Y.: Dynamic recrystallization of Al alloy 7075 in turning. J. Manuf. Sci. Eng. **138**(7) (2016)
2. Driemeier, L., Brünig, M., Micheli, G., Alves, M.: Experiments on stress-triaxiality dependence of material behavior of aluminum alloys. Mech. Mater. **42**(2), 207–217 (2010)
3. Teimouri, R., Amini, S., Mohagheghian, N.: Experimental study and empirical analysis on effect of ultrasonic vibration during rotary turning of aluminum 7075 aerospace alloy. J. Manuf. Process. **26**, 1–12 (2017)
4. Rusinek, A., Klepaczko, J.R.: Shear testing of a sheet steel at wide range of strain rates and a constitutive relation with strain-rate and temperature dependence of the flow stress. Int. J. Plast. **17**(1), 87–115 (2001)
5. Nemat-Nasser, S., Guo, W.G.: Thermomechanical response of DH-36 structural steel over a wide range of strain rates and temperatures. Mech. Mater. **35**(11), 1023–1047 (2003)
6. Cavaliere, P., Squillace, A.: High temperature deformation of friction stir processed 7075 aluminium alloy. Mater. Charact. **55**(2), 136–142 (2005)
7. Taleghani, M.J., Navas, E.R., Salehi, M., Torralba, J.M.: Hot deformation behaviour and flow stress prediction of 7075 aluminium alloy powder compacts during compression at elevated temperatures. Mater. Sci. Eng. A. **534**, 624–631 (2012)
8. Bacon, C., Färm, J., Lataillade, J.L.: Dynamic fracture toughness determined from load- point displacement. Exp. Mech. **34**(3), 217–223 (1994)
9. Rubio, L., Fernández-Sáez, J., Navarro, C.: Determination of dynamic fracture-initiation toughness using three-point bending tests in a modified Hopkinson pressure bar. Exp. Mech. **43**(4), 379–386 (2003)

10. Xing, M.Z., Wang, Y.G., Jiang, Z.X.: Dynamic fracture behaviors of selected aluminum alloys under three-point bending. Defence Technol. **9** (4), 193–200 (2013)
11. Singh, R.P., Parameswaran, V.: An experimental investigation of dynamic crack propagation in a brittle material reinforced with a ductile layer. Opt. Lasers Eng. **40**(4), 289–306 (2003)
12. Gálvez, F., Cendon, D., García, N., Enfedaque, A., Sánchez-Gálvez, V.: Dynamic fracture toughness of a high strength armor steel. Eng. Fail. Anal. **16**(8), 2567–2575 (2009)
13. Chen, Y., Pedersen, K.O., Clausen, A.H., Hopperstad, O.S.: An experimental study on the dynamic fracture of extruded AA6xxx and AA7xxx aluminium alloys. Mater. Sci. Eng. A. **523**(1–2), 253–262 (2009)
14. Huang, S., Luo, S., Xia, K.: Dynamic fracture initiation toughness and propagation toughness of PMMA. In: Proceedings of the SEM annual conference, Albuquerque, pp. 1–4 (2009)

Chapter 3
Flow Stress and Fracture Toughness Behavior of AA5083 Under Quasi-Static Loading

Anoop Kumar Pandouria, Sanjay Kumar, Purnashis Chakraborty, Kuldeep Yadav, Amit Kumar, and Vikrant Tiwari

Abstract In this study, an effort has been made to investigate the mechanical behavior including the fracture toughness of AA5083 aluminum alloy under different loading rates. EDX-spectroscopy is performed to evaluate the chemical composition of the aluminum alloy AA5083. The quasi-static tensile and compressive experiments are performed on a universal testing machine. The quasi-static three-point bend experiments are performed using the MTS-810 machine to obtain the static fracture toughness of AA5083 aluminum alloy. The quasi-static tensile tests and compression tests are performed at different strain rates (10^{-4} to 10^{-1}/s) and flow stresses have been obtained for the corresponding strain rates. It is found that the aluminum alloy shows strain rate sensitivity in both tension and compression; however, this sensitivity was relatively more dominant in tension than in compression.

Keywords AA5083 · Spectroscopy · Static fracture toughness · Flow stress and strain rate sensitivity

3.1 Introduction

The important factors in selecting aluminum (Al) alloys for manufacturing of structural components are their high strength to weight ratio, resistance to corrosion with different chemicals, and high thermal as well as electrical conductivity. AA5083 is used as sheet metal work, hydraulic tubes and in marine [1]. Due to its good corrosion properties of AA5xxx series, it is used for marine applications [2]. Due to lightweight, generally aluminum alloys are preferred for automotive body in automobile industries, so that it improves fuel economy [3]. As we know that before existence of concepts of fracture mechanics, the design engineers used mechanical properties such as yield strength and tensile strength as failure stress, but due to presence of pre-existing cracks the mechanical components fail at lower stress. After development of fracture mechanics concepts, the important mechanical property known as fracture toughness has been used as an important design parameter [4]. The fracture toughness is an important mechanical property defined as the resistance of material for crack extension. Different authors obtained fracture toughness of aluminum alloys of different series. Kumar et al. [5] experimentally obtained the static fracture toughness of AA2014-T6 using MTS machine.

In addition to evaluation of fracture toughness, several researchers also performed tensile and compression tests on aluminum alloys for determination of flow stress and strain rate sensitivity behavior of aluminum alloys at different strain rates. Prakash et al. [6] found the deformation behaviors of Al2014-T6 at different strain rates and temperatures. Sharma et al. [7] obtained the flow stresses at different strain rates and constitutive behavior of 2014-T652.

A. K. Pandouria (✉) · P. Chakraborty · K. Yadav · A. Kumar · V. Tiwari
Department of Applied Mechanics, Indian Institute of Technology, Delhi, New Delhi, India
e-mail: purnashis.chakraborty@am.iitd.ac.in; tiwariv@am.iitd.ac.in

S. Kumar
Department of Applied Mechanics, Indian Institute of Technology, Delhi, New Delhi, India

Department of Mechanical Engineering, Delhi Technological University, Delhi, India
e-mail: sanjaykumar@dtu.ac.in

V. Chalivendra et al. (eds.), *Mechanics of Composite, Hybrid and Multifunctional Materials, Fracture, Fatigue, Failure and Damage Evolution, Volume 3*, Conference Proceedings of the Society for Experimental Mechanics Series,
https://doi.org/10.1007/978-3-030-86741-6_3

3.2 Theory and Specimen

3.2.1 Quasi-Static Fracture Toughness Test

Three-point bend notched specimen shown in Fig. 3.1a was used during experiments for evaluation of static fracture toughness (K_{Ic}). The chemical composition of AA5083 specimen is shown in Table 3.1. The major alloying element in AA5083 is magnesium used as corrosion resistant. The length, width, and thickness of specimen were considered 100, 20, and 10 mm, respectively. The notch with its dimensions shown in specimen was made using wire electric discharge machining. The dimensions of notched specimens are as follows: The length of uniform crack having 1.5 mm width is 7 mm. The uniform crack followed with V-notch with depth 1.5 mm and angle 30°. The natural crack of length 1.5 mm was also created at tip of V-notch using MTS machine of capacity 25 kN. The minimum and maximum load were maintained 40 and 400 kN at frequency 10 Hz for creation of the fatigue crack. Total cycles required to create fatigue crack was 2108 cycles.

The three-point bend experiments have been performed on UTM machine, as shown in Fig. 3.1b, with cross-head speed maintained at 1mm/min. The loads and crack mouth opening displacements for two different experiments were recorded using clip gauges. The load verses displacement curves for two experiments have been drawn in Fig. 3.3a. Both experiments were performed at same travel speed, so both curves shown in Fig. 3.3a are approximately matched.

$$K_{Ic} = \frac{3S\sqrt{a}}{2BW^2} Y\left(\frac{a}{W}\right) F \tag{3.1}$$

$$Y\left(\frac{a}{W}\right) = \frac{1.99 - \left(\frac{a}{W}\right)\left(1 - \frac{a}{W}\right)\left(2.15 - 3.93\frac{a}{W} + 2.7\left(\frac{a}{W}\right)^2\right)}{\left(1 + 2\frac{a}{W}\right)\left(1 - \frac{a}{W}\right)^{3/2}} \tag{3.2}$$

3.2.2 Quasi-Static Tensile and Compression Test

The quasi-static tensile tests on AA5083 specimens were performed using universal testing machine (UTM) of capacity 100kN. The photographs of tensile specimen and UTM machine are shown in Fig. 3.2a, b, respectively. The gauge length and gauge diameter of specimen are taken 45 and 9 mm according to ASTM E8M standard. The tensile tests were performed at two strain rates 10^{-4}/s and 10^{-1}/s.

The cylindrical specimens were used for compression experiments with diameter to length ratio 1:1, as described in Fig. 3.2c. The quasi-static compression tests on AA5083 were performed at four strain rates 10^{-4}/s, 10^{-3}/s, 10^{-2}/s, and 10^{-1}/s on universal testing machine shown in Fig. 3.2d. The compression specimens after experiments at different strain rates 10^{-4}/s, 10^{-3}/s, 10^{-2}/s, and 10^{-1}/s are shown with (ii), (iii), (iv), and (v), respectively. Total change in length was maintained 6 mm

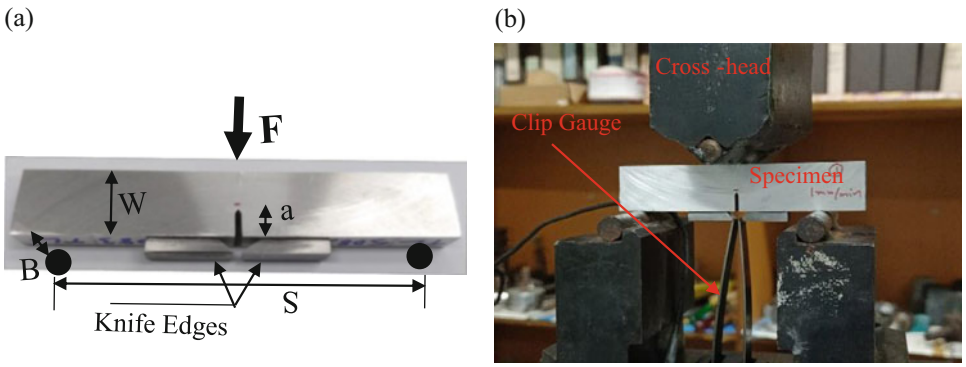

Fig. 3.1 (**a**) Single edge notched specimen (**b**) Quasi-static three-point bend experiment setup

Table 3.1 The chemical composition of AA5083

Elements	Al	Cr	Cu	Fe	Mg	Mn	Si	Ti	Zn	Ni
Present weight percentage (wt%)	94.58	0.007	0.023	0.241	4.251	0.653	0.106	0.026	0.216	0.004

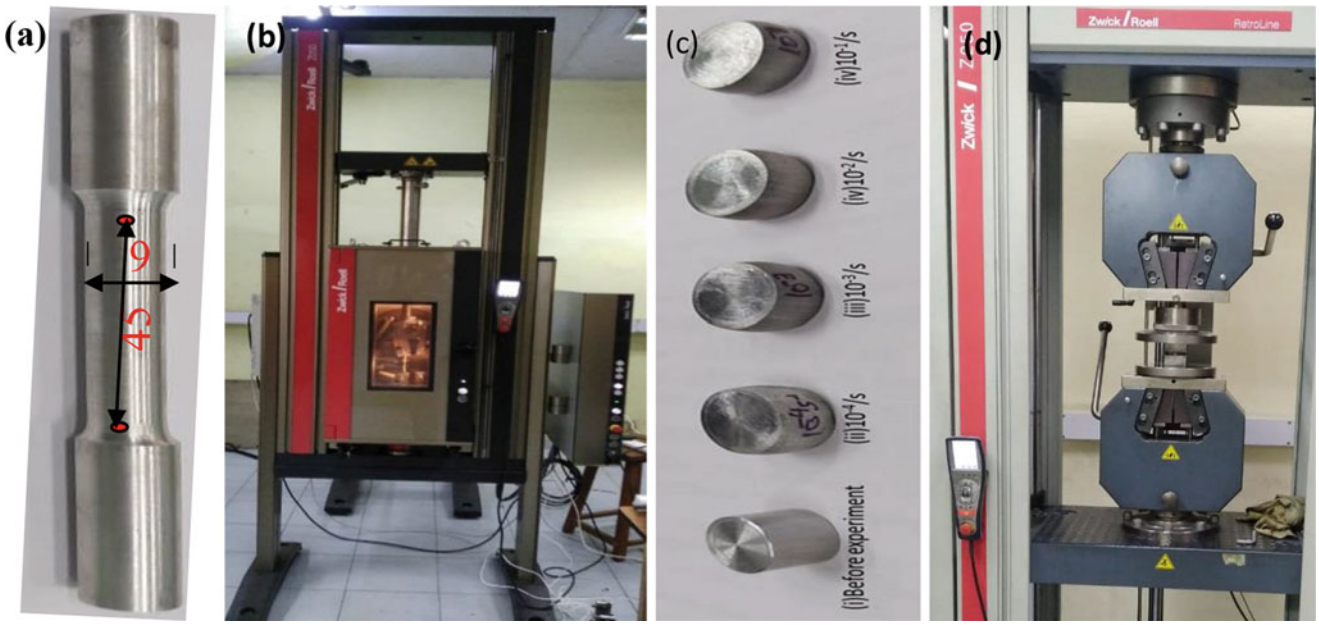

Fig. 3.2 (**a**) Tensile test specimen (**b**) Universal testing machine of 100 kN (**c**) Compression test specimen (i) Before experiment (ii) strain rate 10^{-4}/s (iii) strain rate 10^{-3}/s (iv) strain rate 10^{-2}/s and (v) strain rate 10^{-1}/s (**d**) Universal testing machine of 250 kN

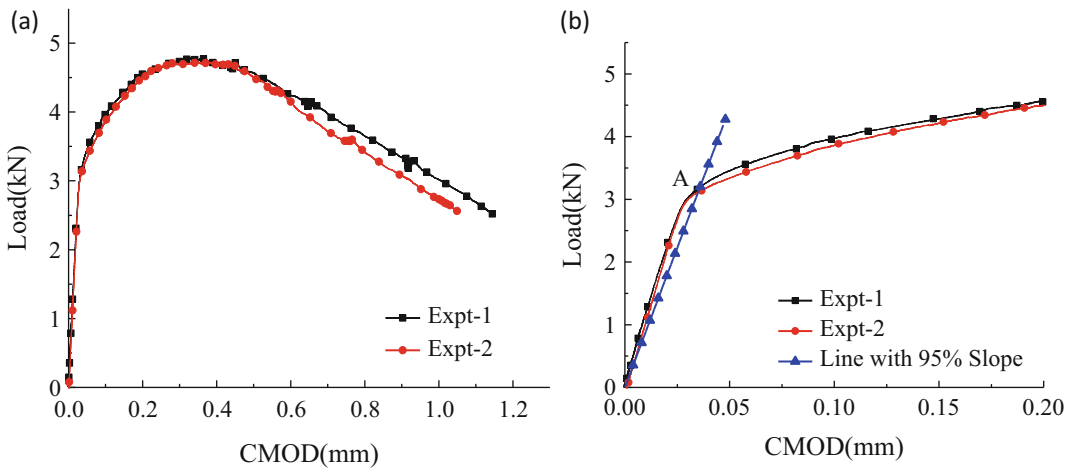

Fig. 3.3 (**a**) Load versus CMOD curve (**b**) Load vs CMOD and line with 95% slope of elastic region line

after experiment of all specimen. Different strain rates 10^{-4}/s, 10^{-3}/s, 10^{-2}/s, and 10^{-1}/s were obtained by providing travel speeds of cross head of 0.078, 0.78, 7.8, and 78 mm/min, respectively. Total reduction in length for all experiments was fixed 8 mm and its final length after compression was found 5 mm, whereas percentage increase in strain was around 60%.

3.3 Results and Discussions

In Fig. 3.3b, a line of slope 95% of that line which coincides with elastic curve region is drawn which intersects the load-deflection curve at a point A and load corresponding to this point is used for evaluation of fracture toughness. The load determined corresponding to point A is 3050 N used for the determination of fracture toughness. Having substituted values of different parameters such as span length ($S = 80$ mm), width ($B = 20$ mm), thickness ($W = 10$ mm), and force ($F = 3050$ N),

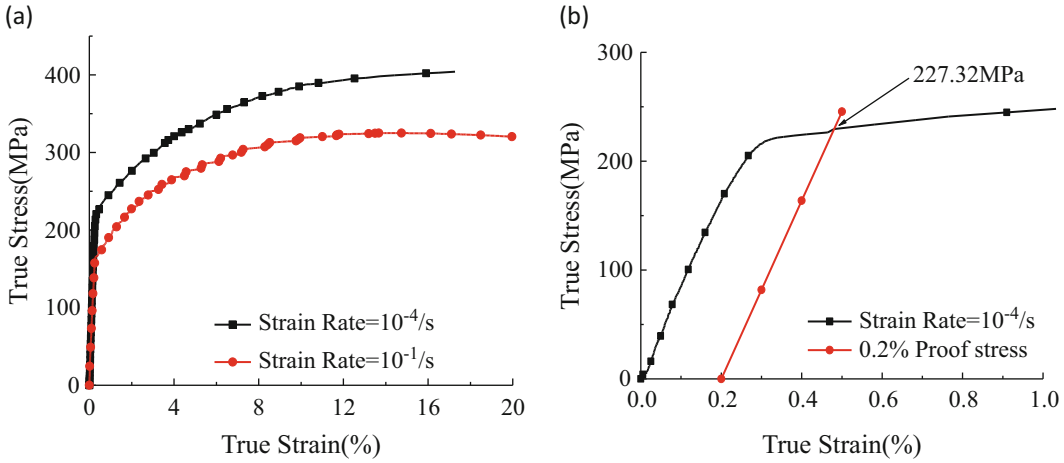

Fig. 3.4 (**a**) True stress vs True strain for tensile test (**b**) Proof stress at 0.2% offset

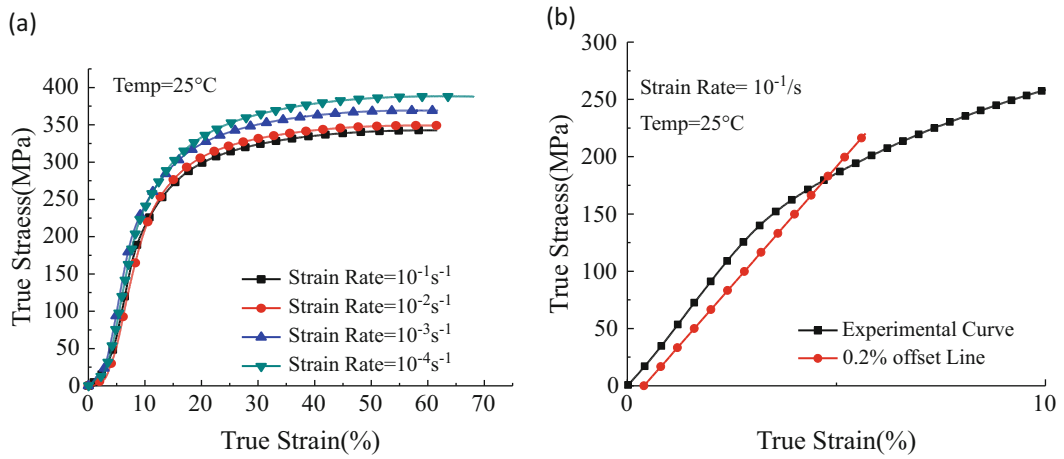

Fig. 3.5 (**a**) True stress vs. true strain for compression test (**b**) Proof stress at 0.2% offset

the value of static fracture toughness obtained is 23.34 MPa$\sqrt{m}$. The expression used for the evaluation of static fracture toughness is Eq. (3.1). A factor $Y(a/W)$ used for assessment of fracture toughness is obtained from Eq. (3.2).

The true stress-strain curve for the tensile test at two different strain rates, 10^{-4}/s and 10^{-1}/s conducted on UTM, is shown in Fig. 3.4a. The proof stress obtained at 0.2% offset at strain rate 10^{-4}/s is shown in Fig. 3.4b, and the corresponding yield stress obtained was 227.32 MPa, as shown in the diagram. Similarly, proof stress obtained at strain rate 10^{-1}/s was 170.10 MPa. So it is found that at a higher strain rate, the yield stress decreases, and it indicates that AA5083 has negative strain sensitivity. The percentage change in flow stress for two strain rates 10^{-4}/s and 10^{-1}/s is 25.17%. Clausen et al. [2] also found the strain rate negative sensitive behavior of aluminum alloy AA5083-H116.

The compression tests for the quasi-static condition for different strain rates were also performed, and true stress-strain curve were drawn for different strain rates as shown in Fig. 3.5a. The curve reveals that the flow stress is higher at lower strain rates and decreases with an increase in strain rates. The flow stress at different strain rates was obtained with the 0.2% offset shown in Fig. 3.5b for strain rate 10^{-3}/s. The flow stress obtained at different strain rates 10^{-4}/s, 10^{-3}/s, 10^{-2}/s, and 10^{-1}/s are 198.05, 184.02, 174.2, and 164.08 MPa. It is observed that the flow stress decreases with an increase in strain rates. So AA5083 also shows the negative strain rate sensitivity in compression. The percentage change in flow stress for two strain rates 10^{-4}/s and 10^{-1}/s is 17.19% which is lower than the flow stress obtained with tensile experiments.

3.4 Conclusions

Different mechanical properties of aluminum alloys AA5083 were studied in quasi-static conditions. The static fracture toughness obtained for AA5083 was 23.34 MPa$\sqrt{m}$. The tensile tests at two different strain rates (10^{-4}/s and 10^{-1}/s) were conducted, and their flow stresses were found 227.32 and 170.10 MPa, respectively. The compression tests at four different strain rates, 10^{-4}/s, 10^{-3}/s, 10^{-2}/s, and 10^{-1}/s, were also conducted, and their flow stresses were found 198.05, 184.02, 174.2, and 164.08 MPa, respectively. It was observed that aluminum alloys AA5083 showed negative strain sensitivity in tension as well as compression, but the decrease in flow stress is higher in the case of tension as compared to compression for the same range of strain rates. So it can be safely stated that the alloy is more strain sensitive in tension than in compression.

References

1. Jian, S.K., Schmid, S.R.: Manufacturing engineering and technology, 7th edn. Pearson Education (2014)
2. Clausen, A.H., Børvik, T., Hopperstad, O.S., Benallal, A.: Flow and fracture characteristics of aluminium alloy AA5083-H116 as function of strain rate, temperature and triaxiality. Mater. Sci. Eng. A. **364**(1–2), 260–272 (2004)
3. Smerd, R., Winkler, S., Salisbury, C., Worswick, M., Lloyd, D., Finn, M.: High strain rate tensile testing of automotive aluminum alloy sheet. Int. J. Impact Eng. **32**, 541–560 (2005)
4. Kumar, P.: Elements of fracture mechanics. Tata McGraw Hill, New Delhi (2004)
5. Kumar, S., Tiwari, V.: Evaluation of static fracture toughness (KIc) of Al2014-T6. In: International conference on recent advances in mechanical engineering, pp. 341–345 (2016)
6. Prakash, G., Singh, N.K., Gupta, N.K.: Deformation behaviours of Al2014-T6 at different strain rates and temperatures. Structures. **26**, 193–203 (2020)
7. Sharma, P., Chandel, P., Bhardwaj, V., Singh, M., Mahajan, P.: Ballistic impact response of high strength aluminium alloy 2014-T652 subjected to rigid and deformable projectiles. Thin-Walled Struct. **126**, 205–219 (2018)

Chapter 4
Development of Carbon-Glass Fiber Reinforced Hybrid Composites: Applications in Offshore Wind Turbine Blades

Eren Celik, Gamze Sacmaozu, and Alaeddin Burak Irez

Abstract In this century, as fossil energy resources are becoming increasingly scarce and their negative effects on the environment are being felt more and more every day including global warming and air pollution, the trend towards renewable energy sources is growing worldwide. Among the various renewable energy systems, wind energy stands out for its cost-efficiency and sustainability. In favor of higher wind speeds, offshore wind turbines generate significant potential for electricity production for coastal countries. However, high wind speeds, as well as open sea rains, have certain disadvantages on turbine blades, such as wind erosion damage. In addition, the rotor blades are moving rapidly due to the high wind speeds and they are hardly noticed by the birds, resulting in bird collisions with the wind turbine blades. This generates an impact load on the blades, which damages the blades of the wind turbine. Therefore, the impact resistance of the wind turbine blades must be improved for reliable service life. This study aims to develop composite materials to be used in the manufacture of wind turbine blades. In this respect, effective reinforcements should be used to improve the impact resistance of the developed composites. Accordingly, epoxy-based carbon-glass fiber reinforced composites are manufactured by using fine silicon carbide (SiC) particles as secondary reinforcement. Experimental studies, tensile tests, and impact tests were carried out to characterize the mechanical properties of the manufactured composites. With this study, it is intended to examine the effects of reinforcements on mechanical properties, and to determine an optimal composition to achieve these properties.

Keywords Impact resistance · Tensile strength · Offshore wind turbine · Hybrid composites · Silicon carbide

4.1 Introduction

With growing concerns about the environmental impact of increasing conventional fuel use, there is a worldwide interest in renewable energy due to its sustainability and cleanness [1]. Amongst various types of renewable energy resources, wind energy has significant potential all around the world. Looking at the project from an environmental point of view, wind turbines do not generate waste, unlike fossil energy sources. Moreover, wind turbines reduce greenhouse gas emissions. In addition, since the wind is renewable, there is no raw material cost. This ensures the sustainability of this type of energy [2].

Wind turbines can be classified as onshore and offshore. Considering the wind potential, offshore-type turbines have higher energy generation potential in favor of high wind speeds. On the other hand, offshore turbines require a higher initial investment and their maintenance costs are much higher compared to onshore ones. From the structural point of view, wind turbine blades are subjected to various loading types throughout their lifetime. These loads are structural loadings such as weight, operational loadings such as wind and centrifugal forces, and impact loadings such as bird strikes. Therefore, the turbine blade material has to resist the loading conditions mentioned above. Moreover, migratory birds cannot notice the turbine blades due to high turbine rotation speeds, resulting in birds hitting the turbine blades, as the offshore turbines coincide with the changing migration paths of migratory birds because of global warming [3]. This situation creates dynamic loading on the turbine blades and causes either visible damage or micro-crack formation on the turbine blades. Since the blades are the most important and expensive part of a wind turbine, the maintenance and repair of the blades comes at a high cost.

Eren Celik and Gamze Sacmaozu contributed equally to this work.

E. Celik · G. Sacmaozu · A. B. Irez (✉)
Department of Mechanical Engineering, Faculty of Mechanical Engineering, Istanbul Technical University, Istanbul, Turkey
e-mail: celikere16@itu.edu.tr; sacmaozu16@itu.edu.tr; irez.burak@gmail.com

V. Chalivendra et al. (eds.), *Mechanics of Composite, Hybrid and Multifunctional Materials, Fracture, Fatigue, Failure and Damage Evolution, Volume 3*, Conference Proceedings of the Society for Experimental Mechanics Series,
https://doi.org/10.1007/978-3-030-86741-6_4

Considering the harsh environmental conditions and sudden loads on the offshore wind turbines, it is seen that the composite materials generally bring advantageous results in comparison to single constituent materials [4]. Composites consist of two main parts as fibers and matrices. Fibers are also known as primary reinforcements and the most commonly used fibers are glass and carbon fibers. E-glass fibers are used as the main reinforcement in borosilicate glass composites, which are called "electric glass" due to their high electrical resistance. As the volume ratio of the fibers increases (usually up to 80%), the hardness, tensile and compressive strength increases proportionally and shows good mechanical properties. Carbon fibers, as another type of fiber, can be used as an alternative to glass fibers. Carbon fibers are stiffer and have a lower density, thus allowing the manufacturing of thinner, stiff and lighter wings. However, the cost of carbon fibers is much higher than glass fibers [5, 6]. Hybrid composites are manufactured by using more than one fiber together. By using a hybrid composite, the cost of a turbine blade can be reduced up to 30–35% instead of the manufacturing composites only with carbon fibers [7]. Based on this, it is thought that it would be appropriate to use glass and carbon fibers in the manufacturing of hybrid composites. Another issue that affects the mechanical properties of composites is the orientation of the fibers used in the fabrication of composites. As glass fibers are more brittle than carbon fibers, they are damaged more rapidly. Apart from the fibers' characteristics, the matrix has also a crucial effect on the composite behavior. Matrices act as a binder for the fibers in the composites. Amongst the different matrix types, thermosets show high resistance to solvents and abrasives and have higher fatigue strength. Among the different thermoset types, epoxy is the most commonly used matrix type. Epoxy resins show high specific tensile and flexural strength and are more resistant than polyester matrices [6]. Another type of composites is particulate composites. In the particulate composites, the particles are homogeneously distributed in the matrix. These secondary reinforcements are used to improve the mechanical properties of the material. The reinforced composites can show increased properties such as erosion resistance, tensile strength, and hardness. Particle-reinforced polymer matrices have higher erosion resistance than non-reinforced ones [8]. Therefore, particle-reinforcements were used to improve the mechanical properties of the glass-carbon fiber hybrid composite. Consequently, fine silicon carbide powders were used as secondary reinforcement due to their beneficial properties including wear and impact resistance. Likewise, metal matrix composites can be reinforced with silicon carbide for different applications due to their excellent mechanical properties [9]. Moreover, mechanical effects have been investigated in epoxy-based composites as well as metal matrix composites. Tensile strength and elongation of the glass fiber epoxy (GFE) composite samples increase with an increase in wt. percent of SiC reinforcements. The stress transfer along the loading path is obstructed by particulates [10]. The weight ratio of reinforcement agents plays a critical role in the improvement of the mechanical properties. These concerns require particular attention to the design procedure.

This research presents the processing of carbon-glass fiber reinforced hybrid composites. The main objective of this research is to determine the mechanical properties of these composites. During this study, mechanical properties such as ultimate tensile strength (UTS), strain at break, and elasticity modulus were determined with tensile tests. Then, Charpy impact tests were carried out with notched specimens. Lastly, the microstructure was observed by optical microscopy.

4.2 Materials and Methods

Epoxy-based hybrid composites are manufactured with unidirectional carbon and glass fiber fabrics in this study. 330 GSM unidirectional E-glass fiber (Profabric®) and 300 GSM unidirectional carbon fiber (DowAksa®) fabrics were used for manufacturing hybrid composites. The hybrid composites consist of ten layers of fabrics as five glass fiber layers placed at 90° and five carbon fiber layers placed at 0° (See Fig. 4.1).

Fiber and matrix used with a weight ratio of 1:1. Hexion L285 epoxy resin and Hexion H285 hardener were used with a weight ratio of 5:2 (See Table 4.1).

Composites were manufactured by means of the vacuum-assisted resin transfer molding (VARTM) method. Carbon and glass fibers were laid by hand according to the predetermined angles as shown in Fig. 4.1, epoxy resin was impregnated to the carbon and glass fibers with the assistance of vacuum pressure. VARTM is a process in which dry reinforcement is transformed into high-quality composite structures [11]. In addition, particle-type reinforcements were added to the composite by means of epoxy resin. It should be noted that secondary particles must be homogeneously distributed within the epoxy resin. Due to the increased resin viscosity by microparticle incorporation, this process must be maintained carefully. Otherwise, reinforcement agglomerations can be seen along with the final composite which can cause a notch effect. After total impregnation, the resin was cured under vacuum pressure at room temperature (25 °C) for up to 18 h. Following the cure at room temperature, post-cure was performed inside a conditioning oven at 60 °C for up to 6 h. Micro SiC particles used as secondary reinforcement had an average diameter of 3 μm and three different percentages of the SiC particles were used in the

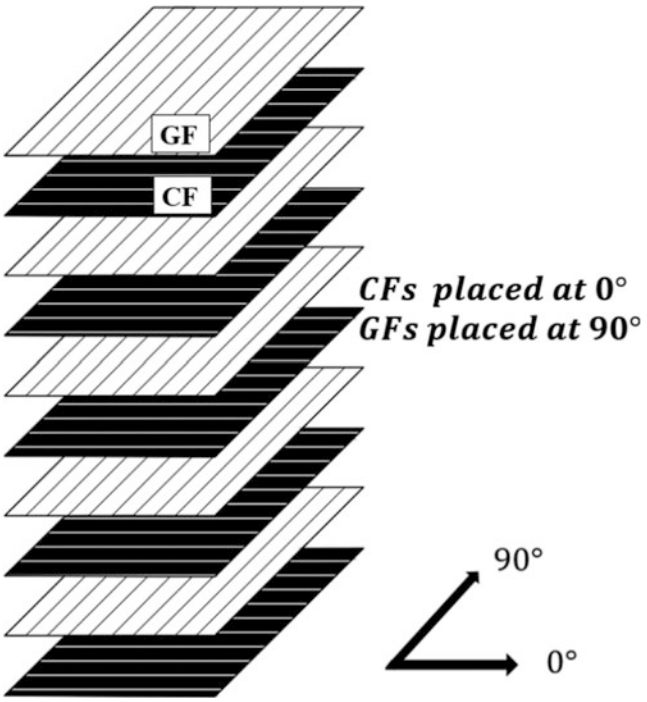

Fig. 4.1 Directions of unidirectional carbon and glass fiber fabrics

Table 4.1 Density and viscosity values for epoxy and hardener

	Density (g/cm^3)	Viscosity (mPas)
Hexion L285 epoxy	1.18–1.23	600–900
Hexion H285 hardener	0.94–0.97	50–100

Table 4.2 Compositions of hybrid composites

	wt. % of SiC
A	0
B	0.5
C	1.0
D	1.5

composite manufacturing. One reference group was manufactured by using only epoxy matrix without SiC. In the other groups, the resin was mixed with the SiC reinforcement depending on the composition chart in Table 4.2.

4.2.1 Material Characterization

After manufacturing of the composites, the specimens were prepared in order to examine the mechanical properties by tensile and Charpy impact tests. Test specimens were extracted from the composite plates by means of abrasive water jet.

Tensile tests were carried out according to the ASTM D3039 standard to examine the fundamental mechanical characteristics. Five rectangular specimens of 250 mm × 25 mm were prepared from all manufactured composites. Tensile tests were carried out using Dartec DY9 8SH Hydraulic Testing Machine with a loading rate of 2 mm/min. Ultimate tensile strength, strain at break, and elasticity modulus were determined via tensile tests [12].

Charpy impact tests were performed using a universal Charpy tester according to ASTM 6110 standard to study the impact resistance of the composites. Five rectangular samples of 125 mm × 12.7 mm with a standard notch were prepared from all manufactured composite [13]. E-glass fiber fabrics were parallel to the loading direction during the tests.

After sectioning composite plates, specimens were cold mounted. Then, polishing was performed. Optical microscopy was conducted to observe the microstructure of the manufactured composites. Carbon and glass fiber layers, as well as SiC distribution, were observed.

4.3 Results and Discussion

Experimental characterizations started with microscopical observation. Figure 4.2 shows the microstructure of the group C composites with wt. 1% SiC. Good adhesion of the matrix and the reinforcements was observed (See Fig. 4.2a, d). In addition, as seen from Fig. 4.2b no significant clustering was observed for SiC particles. The interface between carbon and glass fibers was well maintained under static conditions (See Fig. 4.2c).

After microscopic observation, densities of each group were measured and they are given in Table 4.3. Table 4.3 indicates that densities are sensible to the mass fractions of the reinforcing elements. In addition, it is quite probable that group B with the lowest density may have some voids in the microstructure due to manufacturing problems.

After density measurement, mechanical characterizations were performed and the results of tensile tests are presented in Table 4.4. The first deduction from Table 4.4 is that addition of SiC did not improve the mechanical properties significantly. A noticeable drop in the mechanical properties of group B was observed. This is attributed to the manufacturing problems which is also detected in density measurements. During the tests, main damage mechanism was observed as delamination and incorporation of SiC may have generated discontinuities in the matrix resulting in the degraded mechanical properties.

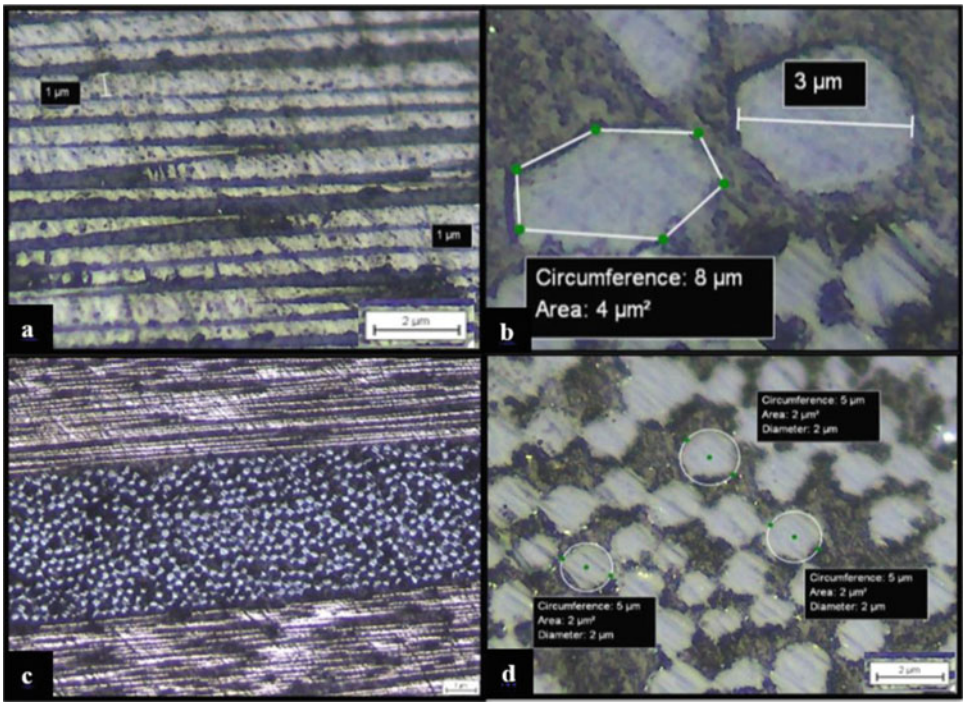

Fig. 4.2 Microstructural observation of group C: (**a**) carbon fibers (**b**) SiC/epoxy resin (**c**) glass/carbon laminates (**d**) glass fibers

Table 4.3 Densities of the manufactured composites

	Density (g/cm^3)
A	1.578 ± 0.02
B	1.203 ± 0.01
C	1.561 ± 0.025
D	1.592 ± 0.015

Table 4.4 Tensile test results of carbon-glass hybrid composite

Specimen group	wt. % SiC	Elasticity modulus (GPa)	UTS (MPa)	Strain at break
A	0	11.125 ± 0.52	880.1 ± 28.78	0.111 ± 0.002
B	0.5	6.379 ± 0.175	501.867 ± 7.01	0.153 ± 0.005
C	1	10.318 ± 0.14	690.133 ± 66.34	0.121 ± 0.004
D	1.5	11.204 ± 0.06	835.15 ± 15.31	0.108 ± 0.002

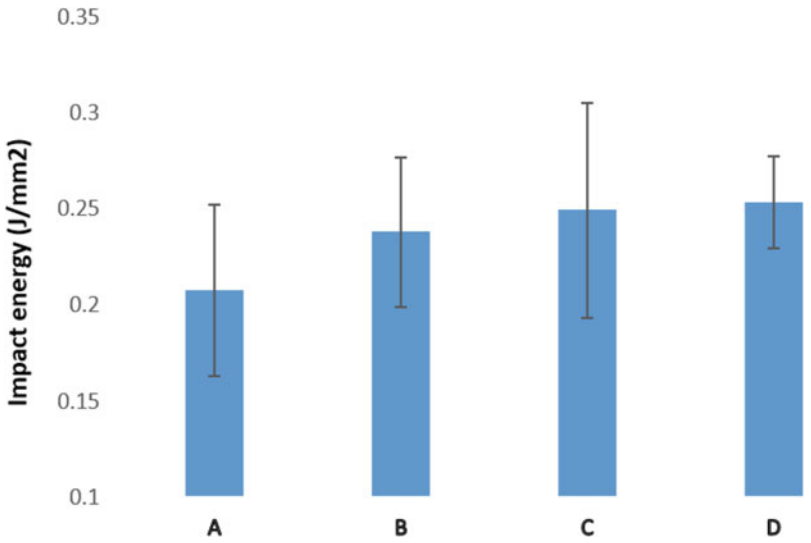

Fig. 4.3 Charpy impact test results of carbon-glass hybrid composite

Following tensile tests, Charpy impact tests showed that addition of SiC particles improved the impact resistance of the composites. High deviations in the absorbed energy values are thought to be a consequence of the local heterogeneities in the microstructure [14]. It is thought that any improvement in the interface quality between epoxy and SiC can promote higher absorbed energy in these composites (Fig. 4.3).

4.4 Conclusion

In the frame of this research, novel composites were developed to be used in offshore wind turbines. After manufacturing composites by means of VARTM method, a detailed experimental work was carried out. Microstructural observation showed a good interface between matrix and fibers. According to density measurement, unanticipated density drop was associated to the manufacturing related issues. These issues also affected the tensile test results as seen from the tensile test results of group B. Slight improvement in the UTS was observed with 1.5 wt. % SiC incorporation. On the other hand, incorporation of SiC increased the impact absorbance capacity of the manufactured composites. Fluctuations observed in the experimental characterizations can be originated from the local agglomerations of the reinforcements in the microstructure that should be eliminated to have much more homogeneous mixture by using high capacity ultrasound equipment. By considering all the obtained results, these novel composites can be used in the manufacturing of offshore wind turbine material after eliminating homogeneity-related insufficiencies. Fracture toughness examination and self-healing behavior of these composites constitute the main objectives of the future studies.

Acknowledgements The authors thank DowAksa™ Company R&D Department for their material support and valuable discussions in certain stages of this project.

References

1. Boyle, G.: Renewable Energy, vol. 456. Oxford University Press (2004)
2. Hayli, S.: The importance of wind energy the situation in the world and Turkey. Fırat Univ. J. Soc. Sci. **11**(1), 1–26 (2001)
3. Hüppop, O., Dierschke, J., Exo, K.M., Fredrich, E., Hill, R.: Bird migration studies and potential collision risk with offshore wind turbines. Ibis. **148**, 90–109 (2006). https://doi.org/10.1111/j.1474-919X.2006.00536.x
4. Thomas, L., Ramachandra, M.: Advanced materials for wind turbine blade—a review. Mater. Today Proc. **5**(1–3), 2635–2640 (2018). https://doi.org/10.1016/j.matpr.2018.01.043
5. Mishnaevsky, L.: Composite materials in wind energy technology. Thermal to mechanical energy conversion: engines and requirements. EOLSS. **8**(3) (2012)

6. Mishnaevsky, L., Branner, K., Petersen, H.N., Beauson, J., McGugan, M., Sørensen, B.F.: Materials for wind turbine blades: an overview. Materials (Basel). **10**(11), 1285 (2017). https://doi.org/10.3390/ma10111285
7. Chikhradze, N.M., Marquis, F.D.S., Abashidze, G.S.: Hybrid fiber and nanopowder reinforced composites for wind turbine blades. J. Mater. Res. Technol. **4**(1), 60–67 (2015). https://doi.org/10.1016/j.jmrt.2015.01.002
8. Häger, A., Friedrich, K., Dzenis, Y.A., Paipetis, S.A.: Study of erosion wear of advanced polymer composites. In: Proceedings of ICCM-10, pp. 155–162 (1995)
9. Abdulsalam, H.M., Charles, O.T., Ahmed, B., Samuel, M.: The influence of silicon carbide particulate loading on tensile, compressive and impact strengths of Al-Sicp composite for sustainable development. Chem. Eng. Trans. **63**, 619–624 (2018). https://doi.org/10.3303/CET1863104
10. Bhattacharjee, A. & Nanda, B.K., Effect of Silicon Carbide as Filler Reinforcements on the Mechanical and Damping Properties of Glass Fiber/Epoxy Composites, 2017.
11. Williams, C., Summerscalests, J., Grove, S.: Resin infusion under flexible tooling (RIFT): a review. Compos. Part A: Appl. Sci. Manufact. **27**(7), 517–524 (1995). https://doi.org/10.1002/9781118097298.weoc216
12. American Society for Testing and Materials.: Standard Test Method for Tensile Properties of Polymer Matrix Composite Materials (ASTM Standard No. D3039/D3039M-17, 2017). https://www.astm.org/Standards/D3039
13. American Society for Testing and Materials.: Standard Test Method for Determining the Charpy Impact Resistance of Notched Specimens of Plastics (ASTM Standard No. D6110-18, 2018). https://www.astm.org/Standards/D6110
14. Irez, A.B., Bayraktar, E.: Design of epoxy modified recycled rubber-based composites: effects of different contents of nano-silica, alumina and graphene nanoplatelets modification on the toughening behavior. Gazi Univ. J. Sci. **33**(1), 188–199 (2020)

Chapter 5
Effect of the Graphene Nanoplatelets (GnPs) on the Mechanical Properties in Recycled PP-Based Hybrid Composites

Cem Okan, Ramazan Kaya, Alaeddin Burak Irez, and Emrullah Cebe

Abstract In the day we fight against Covid-19, the use of disposable masks and isolation clothing is multiplied by 12 compared to the time before the Covid-19 pandemic. Considering that these disposable masks are made of polypropylene (PP), an average of 480 kilotons of PP waste is produced each year, exclusively from masks. After the use of these masks, it is important to collect and re-evaluate them in a controlled manner so as not to pose a risk of contamination and not to threaten the environment. Because of its advantageous properties, PP is used in the production of many parts in the automotive industry. With this study, it is aimed to develop composite materials to be used in car bumper manufacturing by using recycled PP obtained from melt blown PP fabrics (surgical mask fabric). Due to accidents or road conditions, impact damage can occur on the bumpers. Therefore, the impact resistance of the bumpers must be improved. In addition, in case of microscale damage resulting from the impacts received, microcracks may develop and cause material failure below the maximum tensile stress. In summary, effective reinforcements should be used to improve impact strength in composites for use in car bumpers. Accordingly, novel recycled PP (rPP) based composites are manufactured by using elastomer-styrene-ethylene-butylene-styrene (SEBS) and graphene nanoplatelets (GnPs) as compatible reinforcements with rPP. As experimental characterization, three-point bending tests and Charpy impact tests were carried out. Incorporation of GnPs increased the flexural strength and blending with SEBS improved the impact resistance of the developed composites. Certain clusters of the graphene nanoplatelets were observed by means of microscopy.

Keywords Eco-composites · Graphene nanoplatelets · Recycled polypropylene · Impact resistance

5.1 Introduction

In the COVID-19 epidemic, which emerged in 2019 and continues to affect our lives, the World Health Organization (WHO) stated that the use of masks is an important measure to prevent disease [1]. For this reason, the mask demands have become higher than ever before. Besides, the use of protective equipment has increased rapidly in hospitals and daily life. The protective equipment market has expanded by approximately 20% from 2019 to 2020 in the world [2]. Production volumes increased by making investments in US-based companies upon increasing demand [3]. On the other hand, single-use protective equipment has a crucial waste potential. The uncontrolled disposal of the waste of protective equipment, which includes nonwoven fabric as its content, causes environmental pollution and an increase in the risk of disease transmission. Protective equipment must be collected and recycled in a controlled manner to prevent this risk. To reduce the risk of contamination, the virus that stuck to the mask must be inactivated. According to the studies about inactivating SARS-CoV-2, the virus can be inactivated by applying temperatures of 56 °C, 65 °C, and 95 °C for 30 min, 15 min, and 3 min, respectively [4]. In this way, both environmental pollutions and the risk of contamination can be decreased.

Plastics are the most widely used raw material for protective equipment. With the increased number of protective equipment, the value of plastics used in the personal protective equipment market becomes US $3.6 billion in 2020 [5]. Polypropylene (PP), which is the most important raw material of the nonwoven fabric used in protective equipment, is

Cem Okan, Ramazan Kaya, and Alaeddin Burak Irez contributed equally to this work.

C. Okan · R. Kaya · A. B. Irez (✉) · E. Cebe
Department of Mechanical Engineering, Faculty of Mechanical Engineering, Istanbul Technical University (ITU), Istanbul, Turkey
e-mail: okan16@itu.edu.tr; kayara16@itu.edu.tr; irez@itu.edu.tr; cebe16@itu.edu.tr

V. Chalivendra et al. (eds.), *Mechanics of Composite, Hybrid and Multifunctional Materials, Fracture, Fatigue, Failure and Damage Evolution, Volume 3*, Conference Proceedings of the Society for Experimental Mechanics Series,
https://doi.org/10.1007/978-3-030-86741-6_5

used as matrix material after its recycling in this study. PP obtained after recycling will bring a significant added economic value to this study.

Because of its advantageous properties, PP is the second most used polymer material with a market share of 19% and it is used in the production of many parts in the industry. In particular, it can be used as a raw material in automobile bumpers. However, mechanical properties of PP are not sufficient for an automobile bumper. Therefore, it is aimed to improve the impact resistance of recycled PP by using certain reinforcements in this study. Nano-graphene is a very significant nanoscale addition for polymer nanocomposites. The main reason for this property is that it has a 2-dimensional honeycomb structure. This unique property makes nano-graphenes different from other nanoscale inclusions. Mechanical strength and specific elasticity modulus are respectively 130 GPa and 1 TPa. These mechanical strength values are magnificent. Also, it has a higher surface area than other microscale filling materials. Thanks to this feature, succeeding results can be obtained in composite properties even if it is used in small amounts [6, 7]. There are studies that have been conducted on PP-based GnP. It is observed that if the GnP content is less than 0.4 wt% and it gives the best results in terms of impact strength in this study [8]. SEBS is a good compatibilizer which is used for polymers [9]. There are studies that are related to rPP-based GnP. It is observed an improvement in impact strength when SEBS was used in the study on rPP-based SEBS composites [10].

This research presents processing of recycled PPs blended with GnPs and SEBS to create novel composites in an economic way. Main objective of this research is to determine the mechanical properties of these composites. During this study, mechanical properties such as flexural strength (UTS), strain at break and modulus were determined with three-point bending tests. Then, Charpy impact tests were carried out with notched specimens. Lastly, microstructure was observed by optical microscopy.

5.2 Materials and Methods

In this project, materials used in the composite manufacturing were procured from the industry. First, in order to observe the effect of recycling on PP, rPP was characterized without any reinforcement. Recycled PP was provided by Ersem Plastic and it was totally recycled from melt blown PP fabrics. As the principal reinforcing agent, graphene nanoplatelets were procured from Alfa Aesar® with the specific name of "Graphene nanoplatelets aggregates, sub-micron particles, S.A. 500 m^2/g". This product consists of sub-micron platelets which have a diameter of less than 2 μm and a thickness of around 5 nm. The tensile modulus and the density of the GnPs were listed as 1 TPa and 2.25 g/cm^3. As the second blending element, SEBS provided by Elastron TR was used. The density of SEBS is 0.89 g/cm^3.

5.2.1 Preparation of Materials

In order to obtain the desired efficiency in improving the final properties of the manufactured composites, it is necessary to ensure a homogeneous distribution of GnPs in the matrix without any agglomeration. In addition, the adhesion of the GnPs with the matrix must be maintained. For this reason, surface activation of GnPs is usually performed. Surface activation of GnPs were made by the use of oxidation or chemicals. Chemicals used for surface activation of GnPs are polyvinyl pyrrolidone (PVP), vinyl triethoxysilane, and nitric acid (HNO_3).

During the surface activation process, GNPs were added to 65% nitric acid (HNO_3) solution in a volume of 10 ml for each 0.1 g of GnP at 60 °C and the solution was mixed for 2 h. Then, this solution was filtered through a paper filter with a pore size of 40 μm, the resulting mixture was subjected to a cold-water bath with distilled water until a constant 7 pH value was obtained. The GNPs obtained after the bathing process were dried at 80 °C for 24 h, then powderized with a rotary mill and used in composite production. By creating new functional groups on the surfaces of GnPs with surface activation, GnPs bond with the matrix more effectively [11].

In the second stage, after surface activation of GnPs, rPP and SEBS were mixed in pre-defined ratios then the blend was milled for 1 h with a water cooled fast-rotating toothed-wheel mill to obtain a fine and homogeneous compound. After that, GnPs were added to this mixture and homogenization was performed by using ball milling. In the end, this final blend was used in composite manufacturing. In order to manufacture the composites, the final blend was hot pressed in a rectangular steel mold by using a hydraulic hot press machine of MKA Hidrolik&Hidromekanik Makina. The temperature was maintained at 190 °C at a pressure of approximately 15 bar for 20 min. After this procedure, the steel mold was removed from the hot press and it was allowed to cool down to room temperature. After completion of the manufacturing process, the specimens were extracted from the composite plates. Composite manufacturing procedure is graphically summarized in Fig. 5.1 below.

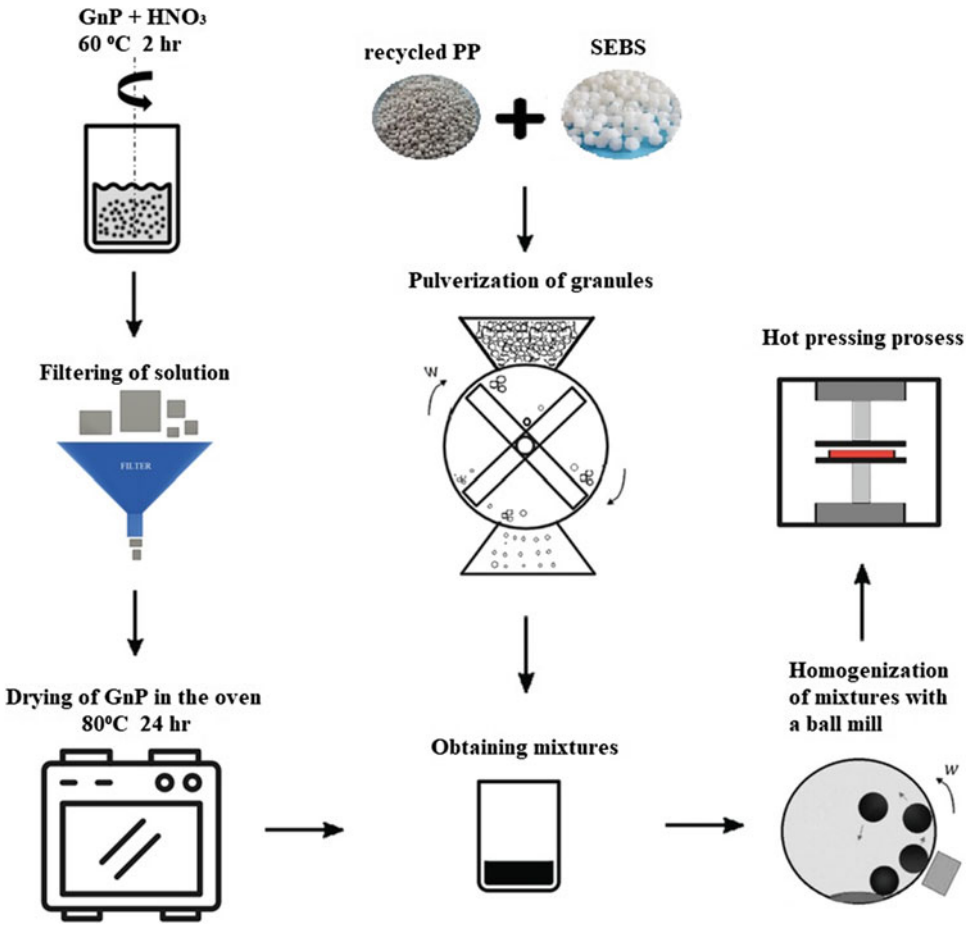

Fig. 5.1 Graphical illustration of the manufacturing procedure of the composites

Table 5.1 Preparation parameters for PP/GnP/SEBS

Composite code	rPP (wt. %)	GnP (wt. %)	SEBS (wt. %)
rPP	100	–	–
rPS	95	–	5
rPSG3	94.7	0.3	5
rPSG5	94.6	0.5	5

5.2.2 Material Characterization

A Shimadzu AG-IS testing system was used for tensile tests. Displacement of the specimen was measured by using crosshead displacement and crosshead speed was selected as 1 mm/min. Ultimate tensile strength (UTS), yield strength (σ_y), and elongation at break (ε_failure) were obtained from the test results.

Impact tests were performed out according to ASTM 6110 standard to study the impact energy [12]. A universal Charpy impact test machine was used in the tests. The specimen size is 127 × 12.7 mm and notch depth is 2.5 mm.

At least five specimens for each composition were used, and average values of the results were given together with standard deviations and all tests have been done at room temperature.

In Table 5.1, the compositions of recycled PP-based SEBS–GnP blended composites are given in detail.

5.3 Results and Discussions

After hot press, a specimen from rPSG4 group was sectioned after mounting they were polished. According to Fig. 5.2a, shiny spherical SEBS particles were observed along the matrix with various dimensions. In Fig. 5.2b, a SEBS particle was observed in a magnified scale. In Fig. 5.2c, small clusters of GnPs were observed in the matrix.

Three-Point Bending (3PB) tests have been carried out for each different type of composites and flexural stress, modulus, and strain at break are presented in Table 5.2.

Table 5.2 shows that, in general, blending rPP with SEBS resulted in a decrease in the flexural strength of the composites. Strain at break follows a similar trend for this blend. Graphene nanoplatelets incorporation has improved all mechanical properties for 0.3% wt. GnP content. However, by the increase in the GnP weight fraction, flexural strength and modulus were dropped. This can be associated to the possible clustering of GnPs which is consistent with the observations in Fig. 5.2c.

Subsequent to three-point bending tests, to assess the impact resistance of the manufactured composites Charpy impact tests were conducted. The results are normalized dividing by the impacted section and they are given in Fig. 5.3.

According to Charpy impact tests, energy absorbing capacity of the rPP was improved by incorporating SEBS. Adding GnPs to the rPP and SEBS blend leads to a degradation in the impact strength of the composites. Deviations in the absorbed

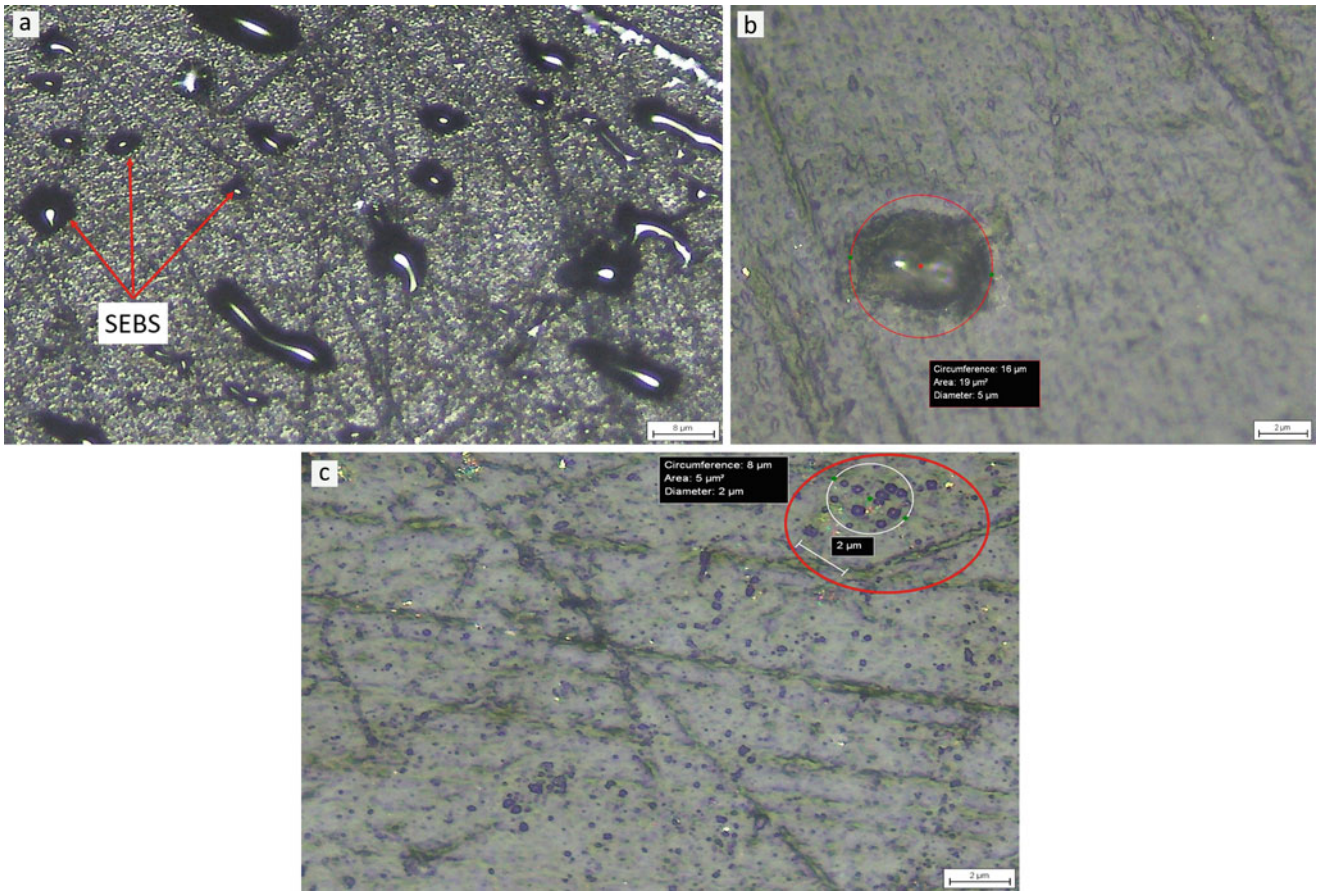

Fig. 5.2 Microstructural observation for a rPSG5 specimen

Table 5.2 Three-point bending test results for manufactured composites

Specimen numbers	Flexural strength (MPa)	Flexural modulus (MPa)	Strain at break (%)
rPP	38.92 ± 0.24	422.437 ± 2.17	9.21 ± 0.42
rPS	32.77 ± 0.32	467.754 ± 3.28	7.01 ± 0.15
rPSG3	41.60 ± 0.51	468.3143 ± 5.13	8.88 ± 0.37
rPSG5	34.65 ± 0.73	304.0333 ± 1.16	11.40 ± 0.49

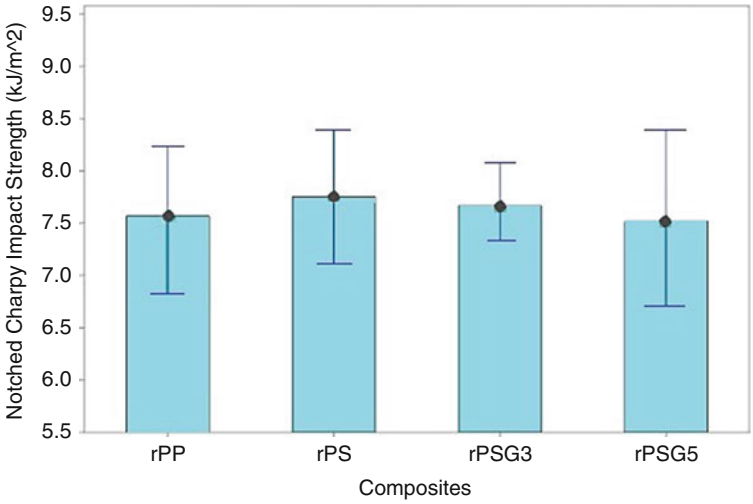

Fig. 5.3 Charpy impact test results for the developed composites

energy values are considered to be a consequence of the local heterogeneities in the microstructure [13]. Besides, high shear stresses generation in the interface of rPP and SEBS can occur. For this reason, fracture occurs only along the main crack propagation line in the absence of interfacial cracks between rPP and the SEBS. Therefore, it is claimed that interface quality improvement between rPP and SEBS can improve energy absorbing capacity of the composites.

5.4 Conclusion

A cost-efficient solution proposal to the PP recycling problem constituted the main motivation of this study. With this project, by recycling PP from disposable masks, the risk of infection by used masks is eliminated, pollution arisen from the masks can be avoided. During the manufacture step of the composites, recycled PPs were blended with SEBS and various contents of graphene nanoplatelets were incorporated to this blend to reinforce the resulting composites. Compared to our former studies, it is thought that the surface activation has brought positive outcomes. After the manufacturing step, mechanical properties were investigated by implementing a series of experimental methods. Three-point bending tests showed beneficial effects of reinforcements on flexural strength of the composites. According to the Charpy impact test, increasing content of GnPs combined with SEBS degrades the energy absorbing capability of the composites toughness which is attributed to formation of agglomerates in the microstructure at higher loadings of the reinforcements under laboratory conditions. These agglomerations should be eliminated to have a much more homogeneous mixture by using high capacity ultrasound equipment. By considering all results, these composites are promising candidates for the various applications in automotive industry such as bumper material.

Acknowledgements This research was supported by the Istanbul Technical University Office of Scientific Research Projects (ITU BAPSIS), under grant MAB-2021-42811. The authors thank Elastron TR and Ersem Plastik for their material support and valuable discussions during this project.

References

1. World Health Organization (WHO).: Rational use of personal protective equipment for coronavirus disease (COVID-19) and considerations during severe shortages [Internet] (2020). https://www.who.int/publications-detail/rational-useof-personal-protective-equipment-for-coronavirusdisease-(covid-19)-and-considerations-during-severeshortages. Accessed 24 Jan 2021
2. Markets, R.A.: Global healthcare personal protective equipment (PPE) market 2020–2030: COVID-19 impact, growth and change for the $7.83 billion market. PR Newswire (2020). https://www.prnewswire.com/news-releases/global-healthcare-personal-protective-equipment-ppe-market-2020-2030-covid-19-impact-growth-and-change-for-the-7-83-billion-market-301172679.html. Accessed 20 Sept 2020
3. Technologies, M.: Maskco Technologies, Inc. announces a strategic manufacturing partnership and investment with Gredale, LLC. PR Newswire (2020). https://www.prnewswire.com/news-releases/maskco-technologies-inc-announces-a-strategic-manufacturing-partnership-and-investment-with-gredale-llc-301171072.html. Accessed 11 Nov 2020

4. Batéjat, C., Grassin, Q., Manuguerra, J.C.: Heat inactivation of the severe acute respiratory syndrome coronavirus 2. bioRxiv. (2020)
5. Arnold, S.: Plastics in personal protective equipment market analysis, COVID-19 impact, outlook, opportunities, size, share forecast and supply demand 2021–2027| Trusted Business Insights, TECHNOWEEKLY. https://technoweekly.com/news/1122781/plastics-in-personal-protective-equipment-market-analysis-covid-19-impactoutlook-opportunities-size-share-forecast-and-supply-demand-2021-2027trusted-business-insights/. Accessed 12 Nov 2020
6. Geim, A.K., Novoselov, K.S.: The rise of graphene. Nat. Mater. **6**, 183–191 (2007)
7. Irez, A.B., Bayraktar, E., Miskioglu, I.: Fracture toughness analysis of epoxy-recycled rubber-based composite reinforced with graphene nanoplatelets for structural applications in automotive and aeronautics. Polymers. **12**(2), 448 (2020)
8. Liang, J.Z.: Impact fracture behavior and morphology of polypropylene/graphene nanoplatelets composites. Polym. Composit. **40**(S1), E511–E516 (2019)
9. Bassani, A., Pessan, L.A., Hage, E.: Toughening of polypropylene with styrene/ethylene-butylene/styrene tri-block copolymer: effects of mixing condition and elastomer content. J. Appl. Polym. Sci. **82**(9), 2185–2193 (2001)
10. Lin, J.H., Lin, Z.Y., Chen, J.M., Lou, C.W.: Recycled polypropylene/SEBS polyblends: manufacture and mechanical property evaluation. In: Applied Mechanics and Materials, vol. 457, pp. 53–56. Trans Tech Publications Ltd (2014)
11. Yang, W., Jiang, Z., Hu, X., Li, X., Wang, H., Xiao, R.: Enhanced activation of persulfate by nitric acid/annealing modified multi-walled carbon nanotubes via non-radical process. Chemosphere. **220**, 514–522 (2019)
12. American Society for Testing and Materials. Standard Test Method for Determining the Charpy Impact Resistance of Notched Specimens of Plastics (ASTM Standard No. D6110-18, 2018). https://www.astm.org/Standards/D6110
13. Irez, A.B., Bayraktar, E., Miskioglu, I.: Toughening mechanism in epoxy resin modified recycled rubber based composites reinforced with gamma-alumina, graphene and CNT. In: Mechanics of Composite, Hybrid and Multifunctional Materials, vol. 5, pp. 31–39. Springer, Cham (2019)

Chapter 6
Static and Dynamic Behaviour of Recycled AA7075 Based Composites Reinforced with ZrO_2-γ-Al_20_3 Fibre and SiC

H. M. Enginsoy, I. Miskioglu, E. Bayraktar, and D. Katundi

Abstract In this study, the microstructural formation and static/dynamic compression behaviour of recycled AA7075 based hybrid composites reinforced with $ZrO_2$and Al_2O_3 fibres were investigated. The effects of the hybrid metal matrix composites on the mechanical behaviour (quasi-static compression, dynamic compression, three-point bending and microhardness) have been investigated in detail by using ZrO_2 as a reinforcement element in two different proportions. It is aimed to be an alternative to traditional alloys used in the aeronautic industry. These composites were produced using by combined sinter + forging processes. The static and dynamic properties have been evaluated in detail, taking into account the relevant Scanning Electron Microscopy (SEM) microstructures (including the distribution of reinforcement elements).

Keywords Recycled composites · SEM · Static and dynamic tests

6.1 Introduction

Hybrid metal matrix composites are widely used in manufacturing engineering due to light and improved mechanical properties. Recycled aluminium-based hybrid metal composites are the most useful for the engineering applications [1–6]. The recycling of a material such as AA7075 is of great importance in this context. In the frame of this research project, here, a fresh scrap aluminium alloy "AA7075", ZrO_2 as a variable reinforcement and also, γ-Al_2O_3 fibre and SiC powders Al_2O_3 and SiC powders were used for the design of these composites that were produced with a combined "Sinter + Forging" production method. This production method has a useful and practical manufacturing process for the novel composites and provides a more rigid internal structure as well as the possibility of rapid and mass production [7–9]. Actually this project is going on and here only, the partial results have been presented under the permission of the French Aeronautical industrial partners.

6.2 Materials and Methods: Experimental Conditions

AA7075 (in fresh scrap chips) provided by the French Aeronautical company was identified as the main matrix component. After the atomization followed by ball milling processes on this component was doped with ZrO_2. After the addition of the other reinforcing elements, γ-Al_2O_3 fibre and SiC powders all of the composition were homogenized for approximately 4 h ball milling with a ball/powder ratio of 10/1. To obtain a homogenous mixture with a good wettability of the reinforcements with the matrix, a small amount of pure nano aluminium (3 wt %) powder was added in each mixture. Again, 2 wt % Zn-Stearate was also added in each mixture for the lubrication and hindering the oxidation of the mixture during the milling. Final compositions were given in Table 6.1.

H. M. Enginsoy · E. Bayraktar (✉) · D. Katundi
School of Mechanical and Manufacturing Engineering, Supmeca-Paris, Saint-Ouen, France
e-mail: bayraktar@supmeca.fr; dhurat.katundi@supmeca.fr

I. Miskioglu
ME-EM Department, Michigan Technological University, Houghton, MI, USA
e-mail: imiski@edu.mtu

V. Chalivendra et al. (eds.), *Mechanics of Composite, Hybrid and Multifunctional Materials, Fracture, Fatigue, Failure and Damage Evolution, Volume 3*, Conference Proceedings of the Society for Experimental Mechanics Series,
https://doi.org/10.1007/978-3-030-86741-6_6

Table 6.1 Compositions of the specimens (wt. %)

Specimen name	AA7075 (Matrix)	ZrO_2	γ-Al_2O_3 fibre	SiC	Zn Stearate
Specimen-1	B	5	5	20	2
Specimen-2	B	10	5	20	2

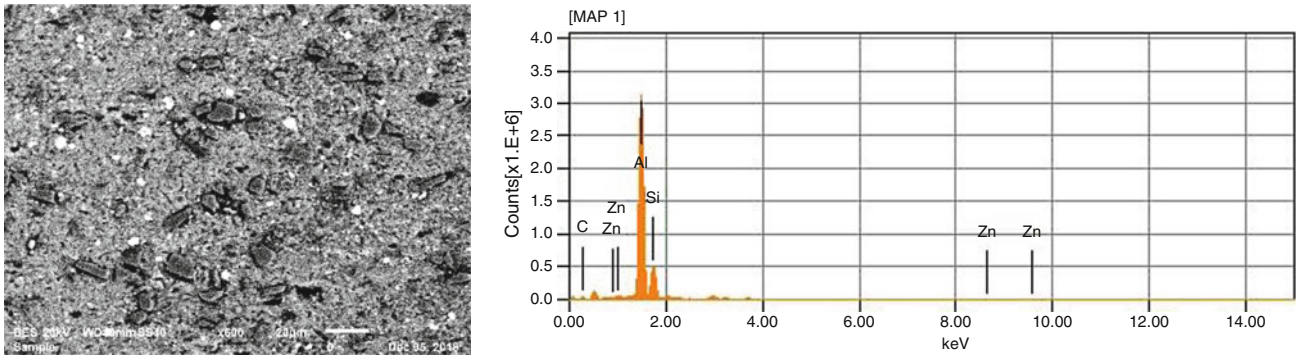

Fig. 6.1 EDS analysis and microstructure taken from SEM for Composite-1

Microstructural analyses are performed by using scanning electron microscope (SEM). The dispersion of reinforcement particles in the matrix and interface at matrix/reinforcements was also evaluated by Electro Discharge Spectrum "EDS" and mapping analyses.

Microhardness tests ($HV_{0.1}$) tests were conducted on the polished and etched specimens. The microhardness values were measured and the values are variables between 150 and 450 HVN with ±15% accuracy for the composites designed here under the laboratory conditions.

All the density measurements of the specimens were carried out by using Archimedes method. These values changed between 3.10 and 3.35 g/cm^3 with ±05% accuracy, respectively.

All of the mechanical tests such as static compression (DIN 50106), 3-point bending (ASTM D790) and dynamic compression (Drop Weight) tests were carried out with a Zwick mechanical test system at the strain rate of 1 mm/min. For each manufacturing process, 3–4 cylindrical specimens (H/D $\geq$ 1.5) were used.

6.3 Results and Discussion

6.3.1 Microstructural Analyses

All of the microstructural analyses were given here for two composites produced by "sinter + Forging".

In both specimens, one may observe that the reinforcement elements used in the internal structure were as homogeneously distributed so finely.

Electro Discharged Spectrum "EDS" analysis and general microstructure taken from SEM were presented in Fig. 6.1 for the Composite-1. It seems that the internal structure of the specimen was homogeneous and tough. A good cohesion/interface was observed in the structure as a result of a mutual chemical bonding diffusion between the reinforcements and matrix components in the composite.

The distributions of all the components used in the first composite (N°I) have been analyzed by using mapping analysis as shown in Fig. 6.2. One may observe that the distributions of the reinforcements in the structure are more and less homogeneous.

EDS analysis and general microstructure obtained on the SEM for the composite n° 2 are given in Fig. 6.3. As a result of these examination, it was observed that the internal structure of the specimen was homogeneous. It has been observed that a good chemical bonding diffusion occurs mutually between the matrix and the reinforcements. This is a basic reason of the toughening of the composite. Fibres added in the microstructures play an important role as a bridge and eliminate the early failure and also reduce debonding of the reinforcements from the matrix under the service conditions.

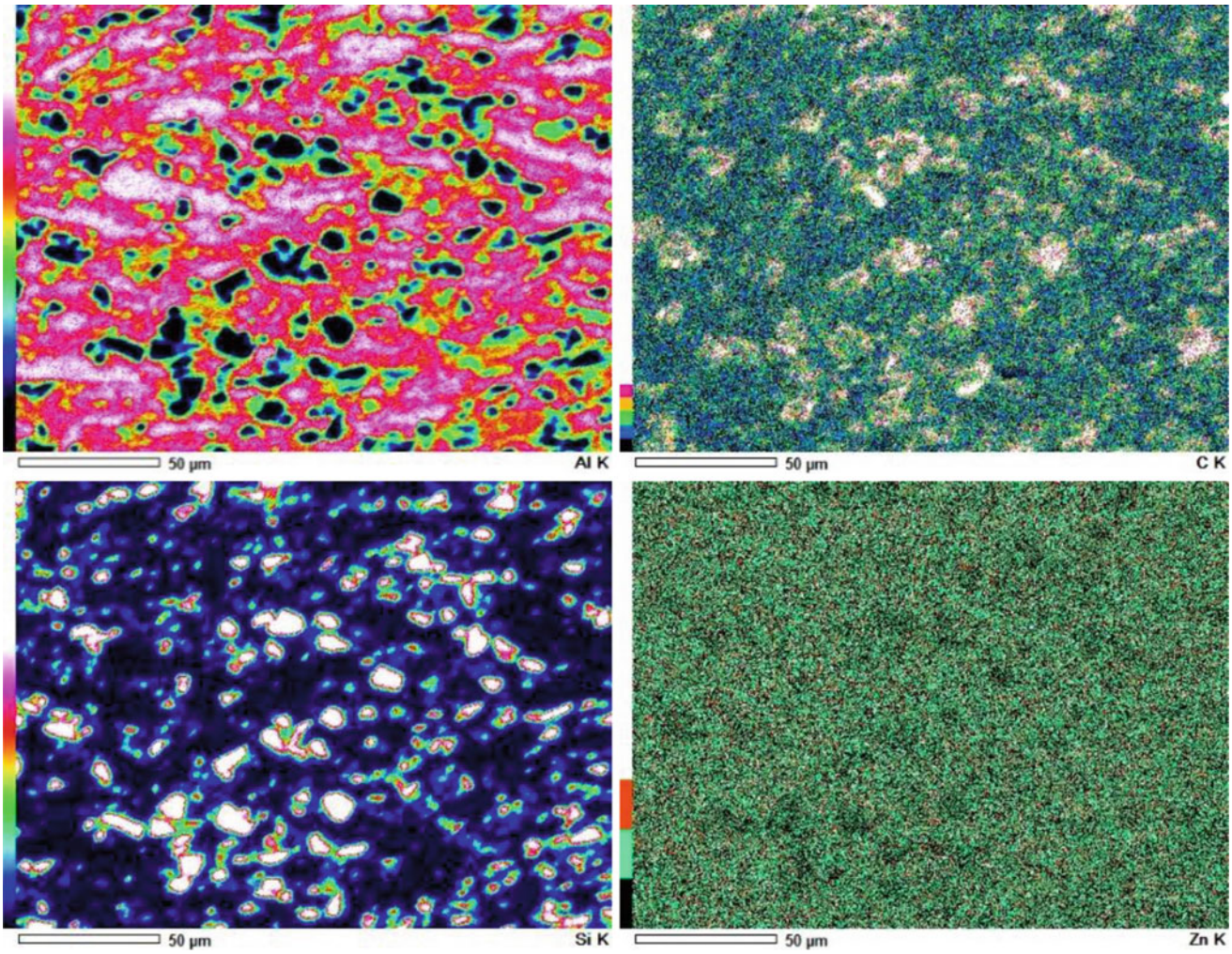

Fig. 6.2 Mapping analyses of the Composite-I

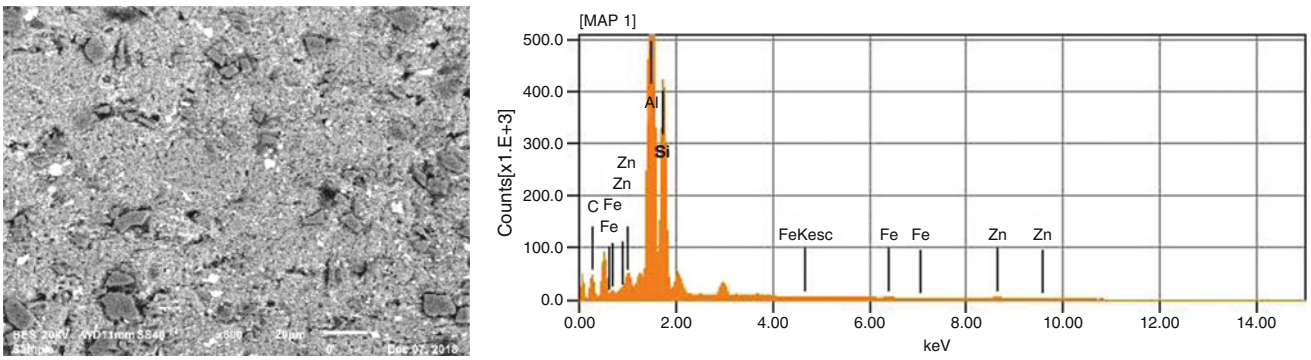

Fig. 6.3 EDS analysis and microstructure taken from SEM for the Composite-2

The distributions of all the components used in the first composite (N° 2) have been analyzed by using mapping analysis as shown in Fig. 6.4. One may observe that the distributions of the reinforcements in the structure are more and less homogeneous.

The mean values of the quasi-static compression tests for the two composites are presented in Fig. 6.5. The first preliminary results show that there are not so much difference between two composites. These tests should be multiplied to optimize the microstructure of the composites.

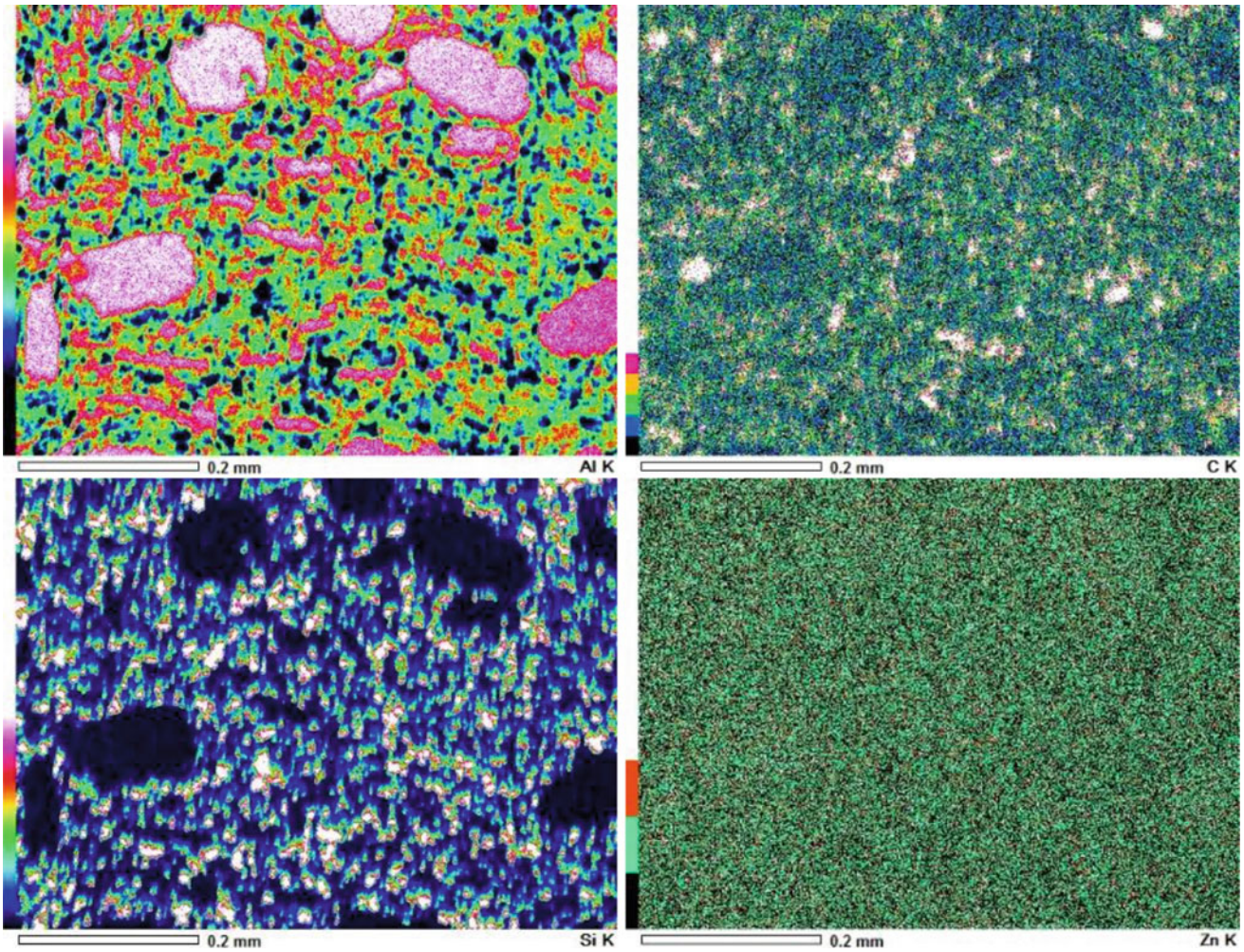

Fig. 6.4 Mapping analyses of the Composite-II

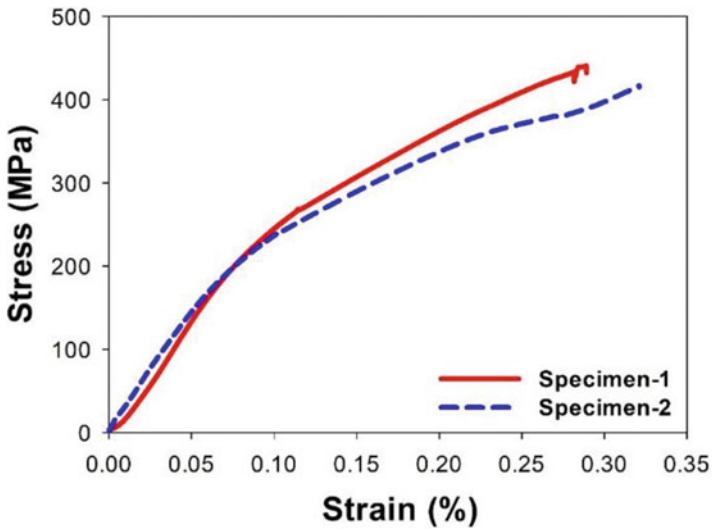

Fig. 6.5 Quasi-static compression test results

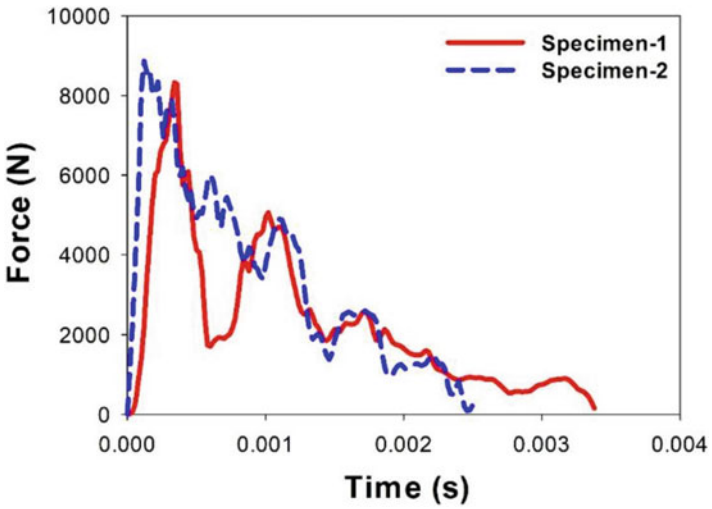

Fig. 6.6 Dynamic compression test results

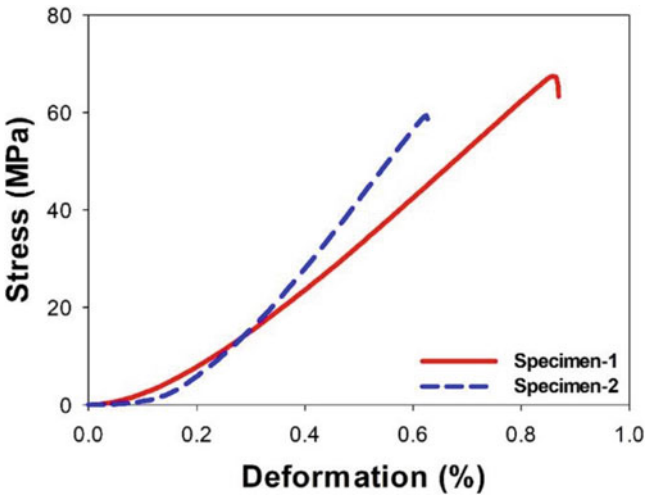

Fig. 6.7 Three-point bending test results

Dynamic compression test (low velocity impact/drop weight) results are presented in Fig. 6.6. As observed in this figure, both of the evaluations for two composites are quasi the same. It means that these values are only the preliminary results and it is difficult to observe the evolution of the test results by using only two compositions. It should be multiply the tests on the different compositions to observe the influence of the reinforcements.

The same evaluations are the same for the 3-point bending test results given in Fig. 6.7. These preliminary results cannot give an objective evaluation of the test results by using only two compositions. It should be multiply the tests on the different compositions to observe the influence of the reinforcements. One point for this test is clear that the first composition containing lower reinforcement values shows a ductile behaviour with regard to the second compositions. This appearance could be clarified with different compositions.

6.4 Conclusions

This preliminary work carried out here in the frame of the research project that is going on evaluates the microstructural evolution depending on the different reinforcements as the hybrid composite. Mechanical behaviour for the toughening mechanism of these composites (here are given only two compositions) were observed by carrying out through the static compression and dynamic test and also 3-point bending test, respectively. As the matrix, fresh scrap recycled aluminium

alloy, AA7075 was used doped later with different reinforcements such as ZrO_2SiC and γ-Al_2O_3 fibres, etc. These novel composites are aimed to be used for the aeronautical applications. As an advantage of these composites, a combined production process called "sinter + forging" has been carried out for the tougher microstructure. Scanning Electron Microscopy (SEM) results give an optimistic future for these recycled constituent composites due to homogenous distribution of the reinforcements in the microstructure with a good cohesion without debonding.

Acknowledgments The authors thank Dr. Georges Zambelis from Airbus-Helicopter Paris/FR for his support and also for his valuable discussion for this research project. The authors thank Mr. Christophe Ben Brahim and Mr. A. Larbi from electronics and mechanical laboratory in Supmeca/Paris for their technical help.

References

1. Thakur, S.K., Kong, T.S., Gupta, M.: Microwave synthesis and characterization of metastable (Al/Ti) and hybrid (Al/Ti + SiC) composites. Mater. Sci. Eng. A. **452**, 61–69 (2007). https://doi.org/10.1016/j.msea.2006.10.156
2. Ferreira, L.M.P., Robert, M.H., Bayraktar, E.: Production of aluminum/SiC/NiAl2O4 MMCs by thixoforming of recycled chips. Solid State Phenom. **217**, 286–293 (2014). https://doi.org/10.4028/www.scientific.net/SSP.217-218.286
3. Tokaji, K.: Effect of stress ratio on fatigue behaviour in SiC particulate-reinforced aluminium alloy composite. Fatigue Fract. Eng. Mater. Struct. **28**, 539–545 (2005). https://doi.org/10.1111/j.1460-2695.2005.00894.x
4. Ferreira, L.F.P., Bayraktar, E., Miskioglu, I., Katundi, D.: Design of hybrid composites from scrap aluminum bronze chips. In: Mechanics of Composite and Multi-functional Materials, vol. 7, pp. 131–138. Springer, Cham (2016). https://doi.org/10.1007/978-3-319-41766-0_15
5. Zhanga, P., Zhanga, L., Weib, D., Wub, P., Caob, J., Shijiab, C., Qua, X.: A high-performance copper-based brake pad for high-speed railway trains and its surface substance evolution and wear mechanism at high temperature. Wear. **444-445**, 203182 (2020)
6. Enginsoy, H.M., Bayraktar, E., Katundi, D., Gatamorta, F., Miskioglu, I.: Comprehensive analysis and manufacture of recycled aluminum-based hybrid metal matrix composites through the combined method; sintering and sintering + forging. Compos. Part B. **194**, 108040 (2020)
7. Choi, D.H., Kim, Y.H., Ahn, B.W., Kim II, Y., Jung, S.B.: Microstructure and mechanical property of A356 based composite by friction stir processing. Trans. Nonferrous Met. Soc. China. (2013). https://doi.org/10.1016/S1003-6326(13)62466-8
8. Ferreira, L.F.P., Bayraktar, E., Robert, M.H., Miskioglu, I.: Particles reinforced scrap aluminium-based composites by combined processing sintering + thixoforming. SEM Mech. Composit. Multi-funct. Mater. **17**, 145–152 (2016)
9. Sadoun, A.M., Fathy, A.: Experimental study on tribological properties of Cu–Al_2O_3 nanocomposite hybridized by graphene nanoplatelets. Ceram. Int. **45**, 24784–24792 (2019)

Chapter 7
Recycled "Al431 + A1050" Based Composites Reinforced with "TiC" Ceramic Powders for Aeronautical Applications

F. Gatamorta, H. M. Enginsoy, E. Bayraktar, and I. Miskioglu

Abstract In this study, a novel recycled Al 431 + 1050 based composites reinforced with "TiC" were designed for aeronautical applications with high resistant structure against to choc and static loading under service conditions. Static/dynamic compression behaviours of these composites were evaluated. Basically, laboratory-scale test samples were produced using combined "sinter + forging" production methods. Al 431 + 1050, a mixture of recycled and modified aluminium alloys, was used as the main matrix material. Different proportions of TiC (10, 15 and 20 wt %) were used as a major reinforcement element. As minor reinforcements, Mo and Cu metal powders and a small amount of Graphene Nano Platelets, (GNPs), and Alumina, (γ-Al_2O_3) fibre were used to compare their influence on the mechanical properties of these hybrid composite structures.

Keywords Recycled and mixed aluminium · Hybrid metal composites, TiC · Static compression test · Dynamic compression test

7.1 Introduction

Novel design of high toughness hybrid metal matrix composites for aeronautical applications where exceptional specific static and dynamic compressive properties should allow us for weight reduction of the pieces. These new composite groups [1–7] afford multifunctional properties that are impossible to find in conventional materials. In fact, heterogeneous and anisotropic materials are useful structures for decreasing damage zone by creating dynamic instabilities such as local plastic deformation, buckling, etc. It means that the behaviour of these materials can be changed by the heterogeneous structures. For this reason a novel hybrid composites are very attractive candidates with micro- and/or nano-size reinforcing particles [6–10]. Our common research project that is going on has shown that the reinforcements of the fine TiC (1–5 μm) ceramic particles, and nano molybdenum and copper particles improve mechanical properties of these composites very efficiently [10]. For this reason, as a parallel reserach was carried out a new alternative composite was produced through combined method called "Sinter + Forging" that is very efficient and economic manufacturing process for these composites. By means of this method, a tough and sound microstructure can be obtained with high toughening capacity.

In the present work, static and dynamic behaviour of these composites were evaluated to compare them with the former studies carried out by the same research group.

F. Gatamorta
University of Campinas, UNICAMP-FEM, Campinas, SP, Brazil
e-mail: fabiog@fem.unicamp.br

H. M. Enginsoy
School of Mechanical and Manufacturing Engineering, Supmeca-Paris, Saint-Ouen, France

E. Bayraktar (✉)
University of Campinas, UNICAMP-FEM, Campinas, SP, Brazil

School of Mechanical and Manufacturing Engineering, Supmeca-Paris, Saint-Ouen, France
e-mail: bayraktar@supmeca.fr

I. Miskioglu
ME-EM Department, Michigan Technological University, Houghton, MI, USA
e-mail: imiski@edu.mtu

V. Chalivendra et al. (eds.), *Mechanics of Composite, Hybrid and Multifunctional Materials, Fracture, Fatigue, Failure and Damage Evolution, Volume 3*, Conference Proceedings of the Society for Experimental Mechanics Series,
https://doi.org/10.1007/978-3-030-86741-6_7

7.2 Experimental Conditions

A novel aluminium mixed (Al 431+ A1050) matrix composites (AMCs) were designed from the recycled chips supplied by Brazilian aeronautic company, through combined method of powder metallurgy followed by "Sintering + Forging". Recycled aluminium (AA 431) chips were gas atomized after mixing with pure A1050 (50 wt %) that prepared by high energy milling in a planetary ball mill with an inert argon atmosphere to prevent oxidation of the powders (20/1 ball/powder ratio). Chemical compositions of the matrix were given as Al-5.5Zn-2.5Mg-0.5Cu; additionally 4 wt % of zinc stearate was used as a lubricant with 1 wt % PVA during the preparation of the composite. After milling operation, thermal behaviour of AA431 powder was evaluated with DSC-TGA diagram. All of the details were given in the former paper [10] for experimental conditions.

This matrix was reinforced basically with TiC (10, 15 and 20 wt %) and as a secondary reinforcements, molybdenum and copper (Mo 4 wt%, Cu 4% wt) were used, respectively. During the milling, pure nano AA1050 (5 wt %) was added to facilitate and homogenize the mixture of two types of recycled aluminium. Sintering was under argon gas in the oven. At the first stage of the sintering, compacted samples were heated at 375 °C for 30 min for eliminating lubricant and other artefact. At the second stage of sintering, heating was conducted up to the maximum sintering temperature (550 °C). After that, the hot forging was carried out to complete the manufacturing processes at the lower temperature than the sintering temperature. Mechanical and physical properties were evaluated through microhardness, static compression tests in three different deformation rates (0.5, 1 and 1.5 mm/min) and low velocity impact/drop weight tests were carried out only at one energy level.

7.3 Results and Discussion

Figure 7.1 shows only as an example of the homogeneous distribution of TiC (10 wt %) for a first composition (F-I) and Differential Scanning Calorimetry (DSC) diagram measured for AA431 and also simulation of fraction of solid depending on the temperature calculated with Thermo-Calc in the matrix to determine the critical transformation points during the heating

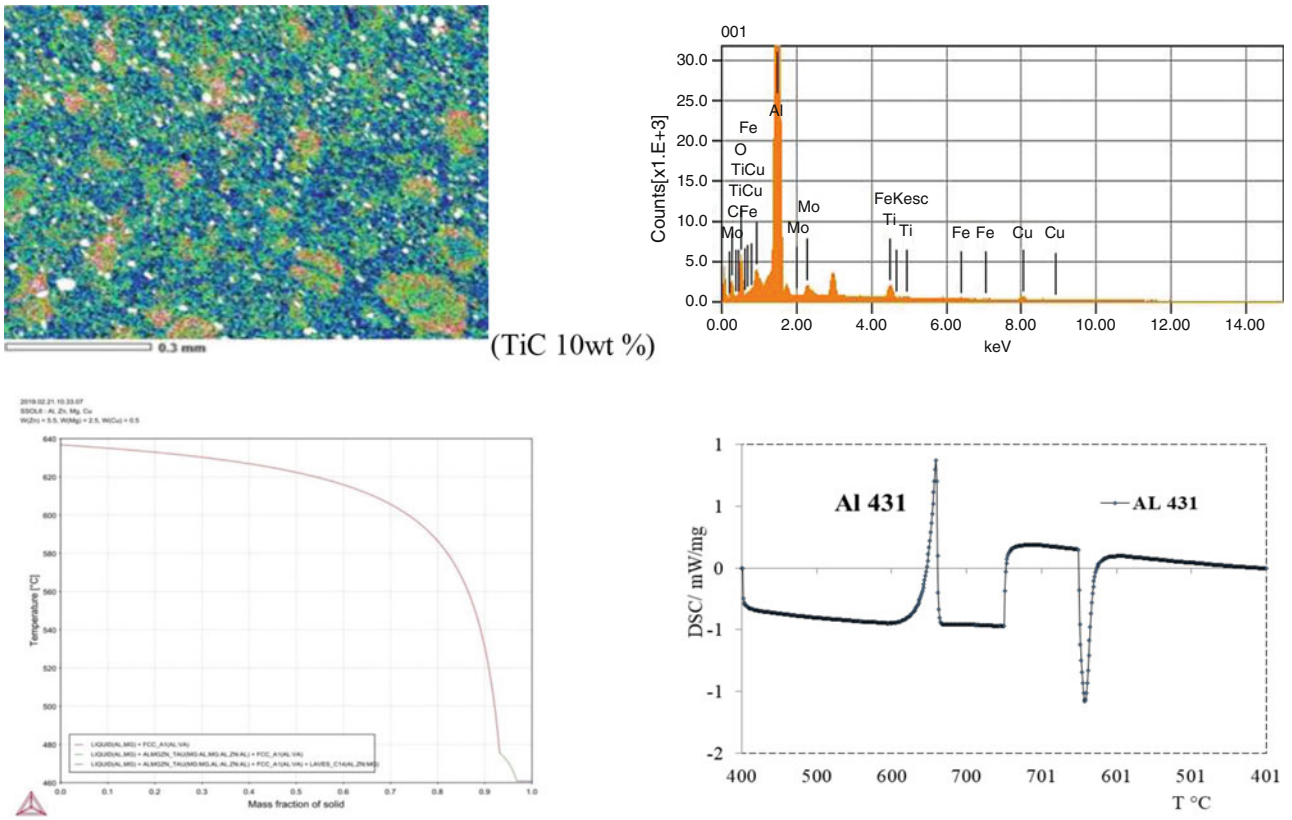

Fig. 7.1 Homogeneous distribution of TiC (10 wt %, F-I) and Differential Scanning Calorimetry (DSC) diagram measured for AA431 and also simulation of the fraction of solid depending on the temperature [10]

Table 7.1 Compositions of the specimens (wt. %)

Specimen name	Al 431 (50%) 1050 (50%) (Matrix)	TiC	Mo	Cu	Zn-Stearate	GNPs	γ-Al_2O_3 fibre
F-II	B	10	4	4	4	0.25	0.5
F-III	B	15	4	4	4	0.25	0.5
F-IV	B	20	4	4	4	0.25	0.5

Table 7.2 Electrical and thermal properties measured for three compositions with microhardness values

Composition	Electrical conductivity at 20 °C (S/m)	Thermal conductivity (W/mK)	Microhardness ($HV_{0,1}$)
F-II	$6.15 * 10^9$	4.398	117 ± 10
F-III	$5.28 * 10^9$	3.776	186 ± 20
F-IV	$3.40 * 10^9$	2835	225 ± 12

and cooling stages. Additional information was given for "EDS" chemical analysis. Fine distribution of the reinforcements and fine grain size are attributed to the presence of molybdenum in the structure (4 wt %). Molybdenum improves also the mechanical resistance for toughening mainly due to a strong cohesion at the interface between the matrix and reinforcements.

Table 7.1 presents all the three compositions formulated for the hybrid composite design. Beside the major reinforcement (TiC) and Mo-Cu, a small amount of GNPs and γ-Al_2O_3 play a strong binding and bridge on the grain boundaries. These results are only indicative and the composition will be improved during the actual project.

Electrical properties (conductivity) were measured with an Agilent 4338B milliohm metre. Five specimens were used for each manufacturing condition (sinter+forging) and then, the mean values of conductivity and resistivity values were given in Table 7.2. For measurements, DC regulated power supply voltage and current were set as 20 V and 20 A, respectively. Data acquisition Card "NI9234" was connected in parallel with the output of the power to acquire the voltage data (voltage input accuracy was 24 bits). A high precision multi-metre "Agilent U1253N" was connected in series to measuring the current intensity (*A*). Also, thermal property (conductivity) and microhardness values were given in Table 7.1.

All of the data (electrical and thermal) from the measurements above were displayed and stored with LabVIEW program. That is the reason that all the samples were produced under the same conditions and polished carefully on both of their surfaces to keep a parallelism. These results evidently should be considered as preliminary results and give an indicative data. It seems that form and surface conditions should be improved again.

Static compression tests have been performed to evaluate the mechanical behaviour of these novel composites produced with the combined method; "sintered-forging". Figure 7.2 gives these static compression test results obtained in three different deformation rate (0.5, 1 and 1.5 mm/min).

These graphs present the mean values obtained from three/four test specimens for each composition. One may see that the lower deformation rates ($v = 0.5$ mm/min in the present work) give, in general trend, higher resistance regarding to the higher deformation rates.

Even if it is difficult to conclude from here with three compositions and/or with three deformation rates, it seems that the composition with lower reinforcement show more ductile behaviour that is related to the tough and sound microstructure. There is a strong trend on the influence of the deformation rates; lower deformation rates give higher resitance related to probably the recovering of the microstructure at the intreface of the reinforcemlent/matrix.

Low velocity (drop weight) or dynamic compression tests results were presented in Fig. 7.3 for three compositions. These values were obtained only for one energy level. Maximum force was evaluated there by the values from both support data points. Here, a series of impact tests were performed at room temperature at the centre of cylindrical specimens using the instrumented drop weight test device as explained in detail in the experimental conditions. Three test specimens were tested for each composition and the mean values were compared for each composition.

All of these test results obtained from Fig. 7.3 show very clearly high damping and/or high absorbed capacity of the "sintered-forging" specimens. It means that impact resistance is directly related to absorbed energy. In fact, all of the specimens have shown that the most part of the impact force was used to maintain the balance with the inertia force, and only a small portion of the impact force was actually used to damage the specimen via deformation and/or fracture.

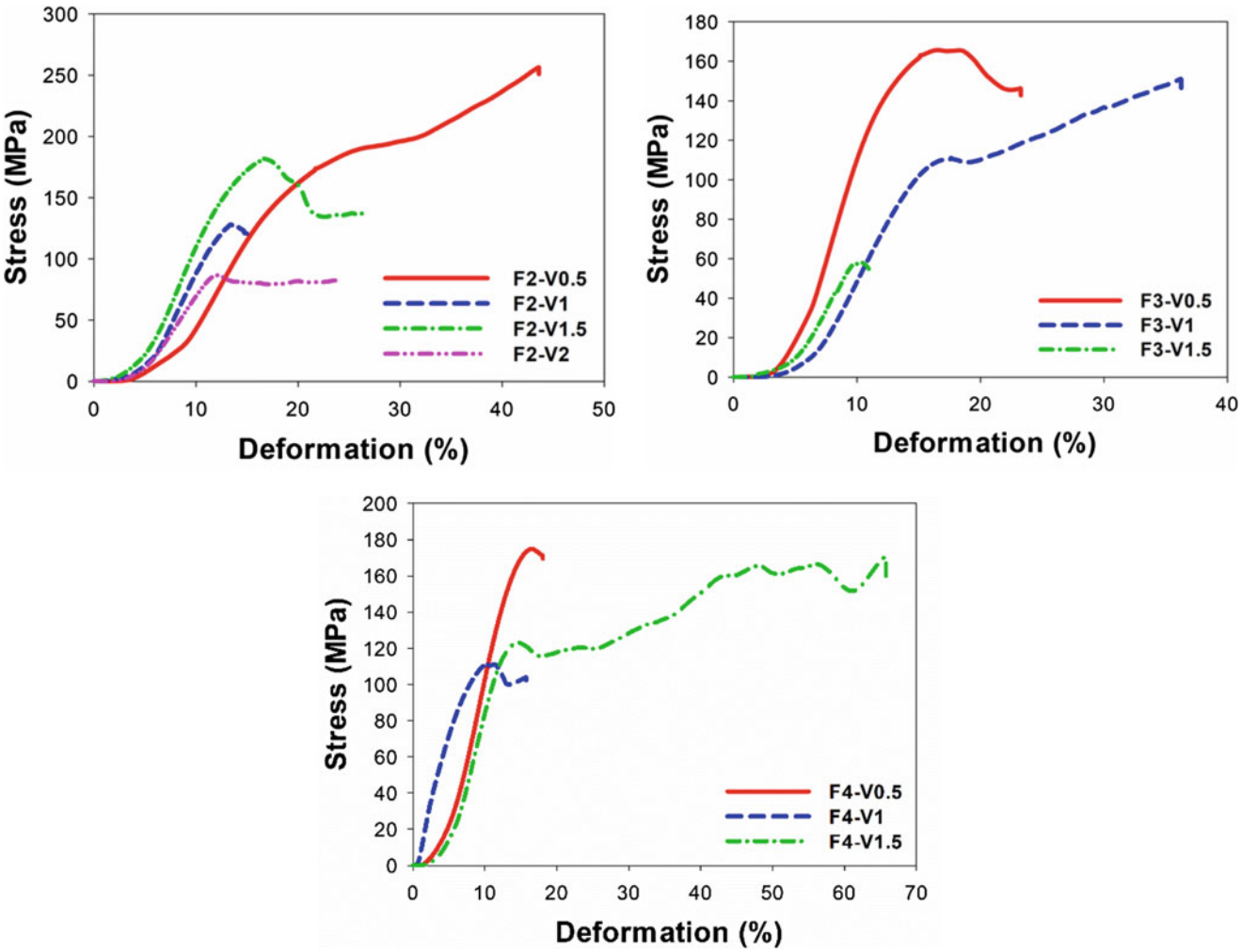

Fig. 7.2 Static compression test results for three compositions at the different deformation rates

Absorbed energy should be related with the process used here that this energy increases considerably in the structure obtained with higher reinforcements. Three compositions investigated here under the laboratory conditions, have given us a clear idea on the considerable effect of the reinforcements of the TiC fine ceramic particles together with molybdenum and the alumina fibre. These results should be improved evidently with detail analyses for industrial applications.

7.4 Conclusions

A novel aluminium mixed (Al 431 + A1050) matrix composites (AMCs) were designed from the recycled chips supplied by Brazilian aeronautic company, through combined method of powder metallurgy followed by "Sintering + Forging". Three different compositions reinforced with TiC/Cu/Mo/GNPs/γ-Al_2O_3 fibre were designed as a low cost manufacturing to propose for industrial partners.

In general way, this research results give encouraging results that could be very useful for industrial applications. For the next stage of this work, more materials and operational parameters should be taken into account to optimize the combined effect of the deformation rate and the composition variable with the reinforcements.

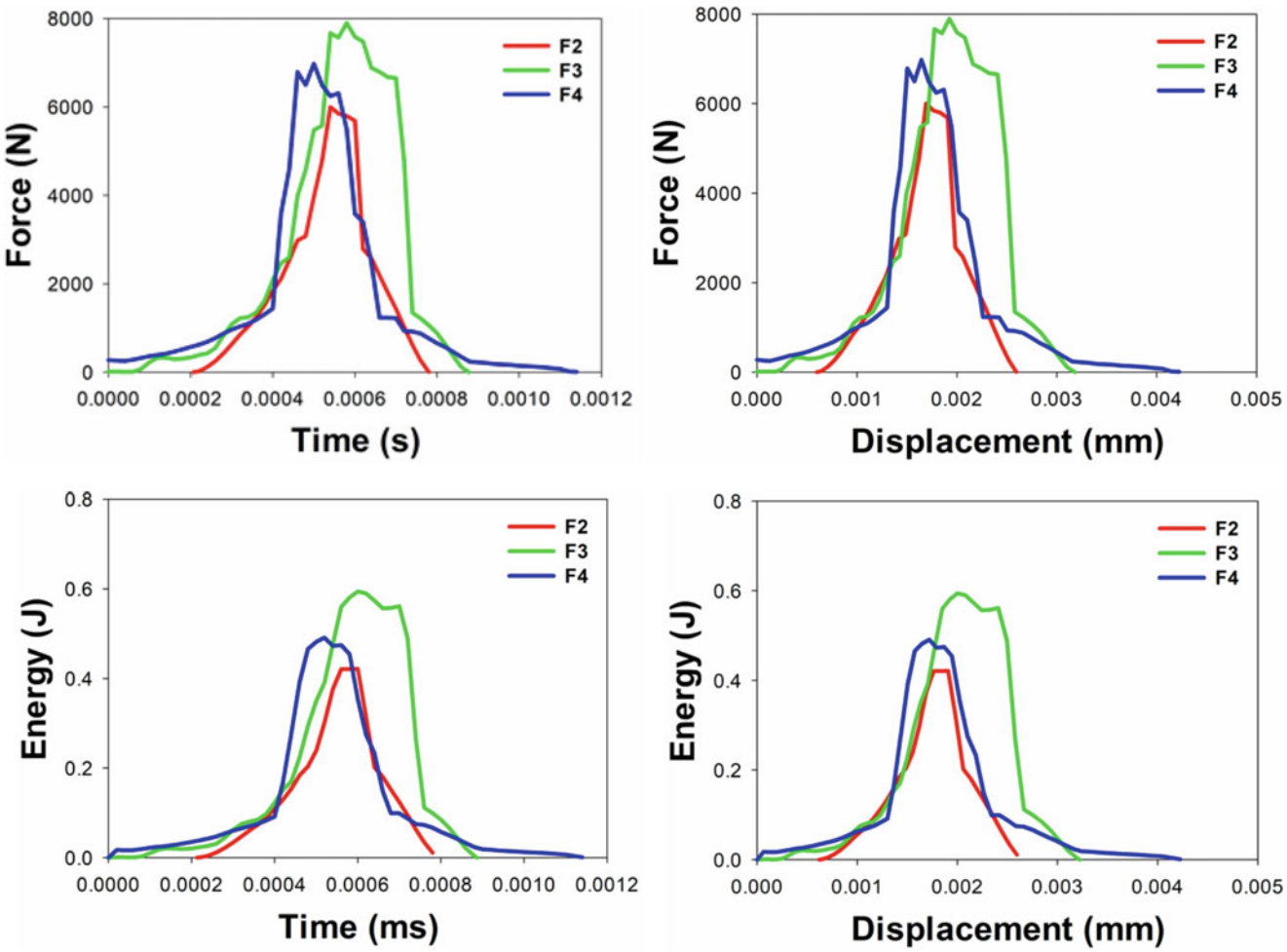

Fig. 7.3 Low velocity impact test result: Force (N)—Time (s) left and Force (N)—Displacement (mm) right diagrams again, Energy (J)—Time (s) left, and Energy (J)—Displacement (mm) right, diagrams obtained for the specimens produced with sintered + forging process

Acknowledgements Authors acknowledge financial support from CNPq—National Council for Scientific and Technological Development, (Brazil) and Program French Cathedra UNICAMP/French Consulate in São Paulo, Brazil. Third author, E. Bayraktar thanks personally to the French Consulate in Sao Paulo for partial financial support for this research project.

References

1. Bagheri, G.A.: The effect of reinforcement percentages on properties of copper matrix composites reinforced with TiC particles. J. Alloy Comp. **676**, 120–126 (2016)
2. Enginsoy, H.M., Gatamorta, F., Larbi, A., Bayraktar, E., Miskioglu, I.: Design of copper and silicon carbide (SiC) reinforced recycled aluminium matrix composites through sintering + forging (Chapter 7). In: Composite, Hybrid and Multifunctional Materials, vol. 6. Springer (2020, ISBN 978-3-030-59867-9). https://doi.org/10.1007/978-3-030-59868-6-7
3. Ferreira, L.-M.-P., Bayraktar, E., Miskioglu, I., Robert, M.H.: Design and physical properties of multifunctional structural composites reinforced with nanoparticles for aeronautical applications. JAMPT Adv. Mater. Process. Technol. **3**(1), 33–44 (2017)
4. Ferreira, L.F.P., Bayraktar, E., Miskioglu, I., Katundi, D.: Design of hybrid composites from scrap aluminium bronze chips (Chapter 15). In: SEM, pp. 131–138. Springer. (2016, ISBN 978-3-319-41766-0)
5. Wang, F., Li, Y., Wang, X., Koizumi, Y., Kenta, Y., Chiba, A.: In-situ fabrication and characterization of ultrafine structured Cu-TiC composites with high strength and high conductivity by mechanical milling. J. Alloy Comp. **657**, 122–132 (2016)
6. Bayraktar, E., Gatamorta, F., Enginsoy, H.M., Polis, J.E., Miskioglu, I.: New design of composites from fresh scraps of niobium for tribological applications (Chapter 6). In: Composite, Hybrid and Multifunctional Materials, vol. 6. Springer (2020, ISBN 978-3-030-59867-9). https://doi.org/10.1007/978-3-030-59868-6_6

7. Popov, V.A., Shelekhov, E.V., Prosviryakov, A.S., Kotov, A.D., Khomutov, M.G.: Particulate metal matrix composites development on the basis of in situ synthesis of TiC reinforcing nanoparticles during mechanical alloying. J. Alloy Comp. **707**, 365–370 (2017)
8. Tian, W.-S., Zhou, D.-S., Qiu, F., Jiang, Q.-C.: Superior tensile properties of in situ nano sized TiCp/Al-Cu composites fabricated by reaction in melt method. Mater. Sci. Eng. A. **658**, 409–414 (2016)
9. Ferreira, L.F.P., Gatamorta, F., Bayraktar, E., Robert, M.H.: Manufacturing of low cost composites with porous structures from scrap aluminium (AA2014) chips. In: Mechanics of Composite and Multi-functional Materials, vol. 7, pp. 233–240. Springer, Cham (2017). https://doi.org/10.1007/978-3-319-41766-0_28
10. Gatamorta, F., Miskioglu, I., Bayraktar, E., Melo, M.L.N.M.: Recycling of aluminium-431 by high energy milling reinforced with TiC-Mo-Cu for new composites in connection applications. In: Mechanics of Composite and Multi-functional Materials, vol. 5, pp. 41–46. Springer (2019). https://doi.org/10.1007/978-3-030-30028-9_6

Chapter 8
Experimental and Finite Element Study of Recycled Aluminium (AA7075) Matrix Composites Reinforced of TiC/MoS_2/γ-Al_2O_3Fibre/Nb_2Al

L. Mihlyuzova, H. M. Enginsoy, Stanislav Slavov, D. Dontchev, and E. Bayraktar

Abstract In the present work, the hybrid aluminium based composites coming from recycled AA7075 chips are produced by using the different levels of reinforcements. As a major one is TiC ceramic carbide ($d \leq$ 1–3 micron) at three levels (2.5%, 5%, 10%), whereas the minor addition of MoS_2, Nb2Al and γ-Al_2O_3 fibre were fixed as 2, 3 and 3 wt %, respectively. These compositions are targets for the application of the connection link in a mechanism to transfer motion in aeronautical industry. For this reason, the machinability of these composites should be significant engineering case for the tailored behaviour of the composites produced through combined method of powder metallurgy route: sintering + Forging. Certain characteristics of the composites were carried out according to the optimization conditions of the reinforcements. Static and dynamic-crash tests will be performed. The microstructure analyses (matrix/interface) were carried out by Scanning Electron Microscope (SEM).

A three-dimensional non-linear finite element model was used to simulate the static compression tests behaviour of these composites. A subroutine, VUMAT, will be written to use with ABAQUS/Explicit to analyze the effect of sintered-forging on the micro- and macrostructure of the manufactured materials. Different ratios of reinforcing particulates using in the experimental specimens were used in Representative Volume Element (RVE) (and other distribution techniques, etc.) for the microstructure modelling. Then, numerical models for the macrostructure were created using these micro-structures under the multiscale modelling process conditions.

Keywords Recycled hybrid composites · AA7075 · Sinter-forging · Nano hardness · Nano wearing · SEM analyses · Finite element analyses

8.1 Introduction

Our common research project that is going on has shown that the reinforcements of the fine TiC (1–5 μm) ceramic particles, and the minor addition of different fine particles improve the mechanical properties of these composites very efficiently under the extreme service conditions [1–6]. In the same work, we have used this time MoS_2, Nb_2Al and γ-Al_2O_3 fibre to optimize the mechanical behaviour with new formulation in order to obtain low cost and efficient composites for certain types of auxiliary applications in aeronautical industry. For this reason, a new alternative composite was produced through combined method called "Sinter + Forging" that is very efficient and economic manufacturing process for these composites. By means of this method, our former experiences have shown that a tough and sound microstructure with high toughening capacity can be carried out by this production route [1, 2, 4–6].

In other idea directly related to the application of the powder metallurgy to the aeronautical engineering. Altered powder metallurgy methods are reflected for the lightweight high performance composites; these are hot isostatic pressing, hot isostatic pressing (HIP) + hot isothermal forging, hot isostatic pressing and/or hot unidirectional pressing+ hot extrusion + hot

L. Mihlyuzova
UTCM, University of Chemical Technology and Metallurgy, Sofia, Bulgaria

School of Mechanical and Manufacturing Engineering, Supmeca-Paris, Saint-Ouen, France

H. M. Enginsoy · E. Bayraktar (✉)
School of Mechanical and Manufacturing Engineering, Supmeca-Paris, Saint-Ouen, France
e-mail: bayraktar@supmeca.fr

S. Slavov · D. Dontchev
UTCM, University of Chemical Technology and Metallurgy, Sofia, Bulgaria
e-mail: stanislav.slavov@uctm.edu; dontchev@uctm.edu

V. Chalivendra et al. (eds.), *Mechanics of Composite, Hybrid and Multifunctional Materials, Fracture, Fatigue, Failure and Damage Evolution, Volume 3*, Conference Proceedings of the Society for Experimental Mechanics Series,
https://doi.org/10.1007/978-3-030-86741-6_8

isothermal forging, etc. [1, 5–8]. Essentially, near net shape forming process through the powder metallurgy method is used for aeronautical and aerospace applications for high quality structure. However, many of these processes such as HIP are very expensive and have low efficiency [1, 5–7].

Therefore, for the low cost and efficient manufacturing of these pieces, we propose a new design powder metallurgy route that give low cost and high toughened production produced by the combined method: "sinter Forging" from the fresh scrap metallic parts. In the frame of this present work, AA7075 fresh scrap aluminium coming from the aeronautic company was used as matrix of the composites developed here. It is very easy to adapt the combined method to green compacts for light metal matrix (Al, Mg, Ti, etc.) because the porosity and other micro-defects are efficiently removed due to compression strain which leads more and less to the theoretical density [9–17].

In the present work, static and dynamic behaviour of these composites were evaluated to compare them with the former studies carried out by the same research group.

8.2 Experimental Conditions

The hybrid aluminium based composites coming from recycled AA7075 chips were processed by using the different levels of reinforcements. As a major one is TiC ceramic carbide ($d \leq$ 1–3 μm) at three levels (2.5%, 5%, 10%), whereas the minor addition of MoS_2, Nb2Al and γ-Al_2O_3 fibre were fixed as 2, 3 and 3 wt %, respectively. These composites were produced through the combined method called "Sintering + Forging" of powder metallurgy. Recycled aluminium chips were gas atomized after mixed with the reinforcements by high energy milling in a planetary ball mill with an inert argon atmosphere to prevent oxidation of the powders (20/1 ball/powder ratio). Thermal behaviour of the powder of AA7075 was evaluated with DSC-TGA diagram. All of the details were given in the former paper [1, 4–6] for experimental conditions.

During the milling, pure nano AA1050 (5 wt %) was added to facilitate and homogenize the mixture. Sintering was under argon gas in the oven. At the first stage of the sintering, compacted samples were heated at 300 °C for 30 min for eliminating lubricant and other artefact. At the second stage of sintering, heating was conducted up to the maximum sintering temperature (650 °C). After that, the hot forging was carried out to complete the manufacturing processes at the lower temperature than the sintering temperature. Mechanical and physical properties were evaluated through micro-hardness, static compression tests in three different deformation rates (0.5, 1 and 1.5 mm/min) and low velocity impact/drop weight tests were carried out only at one energy level.

The microstructure analyses (matrix/interface) have been carried out by Scanning Electron Microscope (SEM).

8.3 Results and Discussion

Chemical composition of scrap AA7075 powder was given in Table 8.1 and Fig. 8.1 presents the results of DSC analysis and the solid fraction in the structure depending on the temperature were simulated by means of Thermo-Calc software.

Table 8.1 Chemical composition of scrap AA7075 powder (wt. %)

Element	Al	Cu	Fe	Mg	Mn	Si	Ni	Zn	Cr	Zr
wt. %	Balance	1.48	0.23	2.11	0.07	0.10	0.01	5.29	0.22	0.02

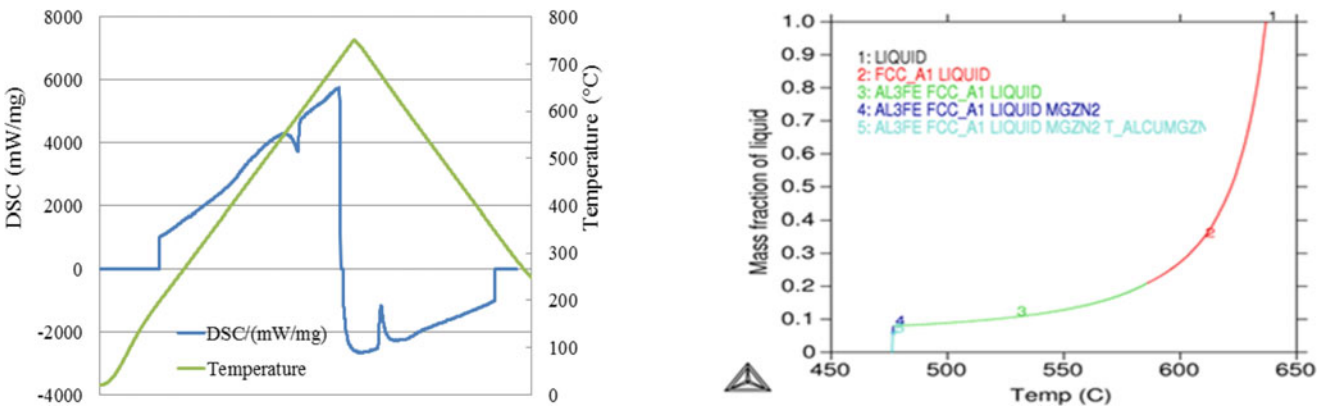

Fig. 8.1 DSC analysis and the solid fraction in the structure as a function of the temperature simulated by means of Thermo-Calc software

It is very easy to observe the heat treatment evolution after the identification of the parameters of the matrix such as the transformation points during the heating and cooling stages.

In Table 8.2, the general compositions of the three composites are presented with the major and minor reinforcements. These compositions are actually under the developments to optimize the interface matrix/reinforcements for the research project that is going on.

Figure 8.2 shows the original of the AA7075 chip morphology as received from the company and atomized size, green compact just before sinter-forging operation followed by mechanical testing.

Figure 8.3 presents a general information about the microstructural analyses that have been carried out by EDS, chemical analyses and following pictures give a detail mapping information on the distribution of the reinforcements in the matrix

Table 8.2 Compositions of the specimens (wt. %)

Specimen name	AA7075 matrix	TiC	MoS_2	γ-Al_2O_3 fibre	Nb_2Al	Pure nano AA1050	Zn stearate
N-I	B	2.5	2	3	3	5	2
N-II	B	5	2	3	3	5	2
N-III	B	10	2	3	3	5	2

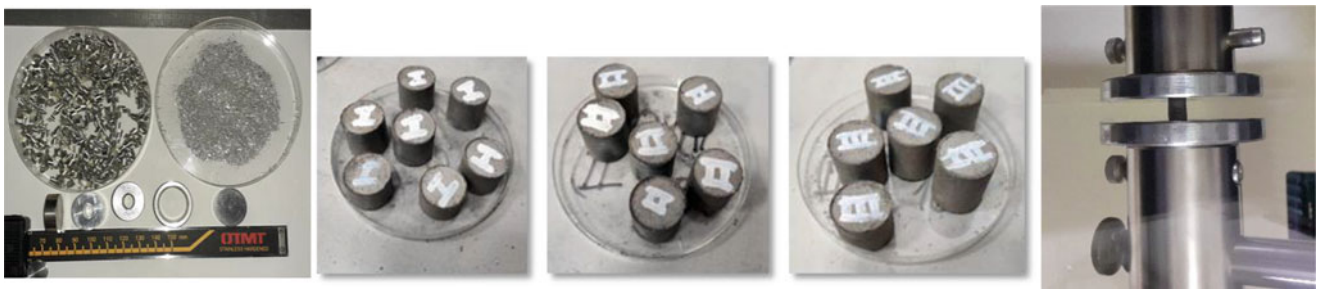

Fig. 8.2 Original of the AA7075 chip morphology as received from the company and atomized size, green compact just before sinter-forging operation followed by mechanical testing

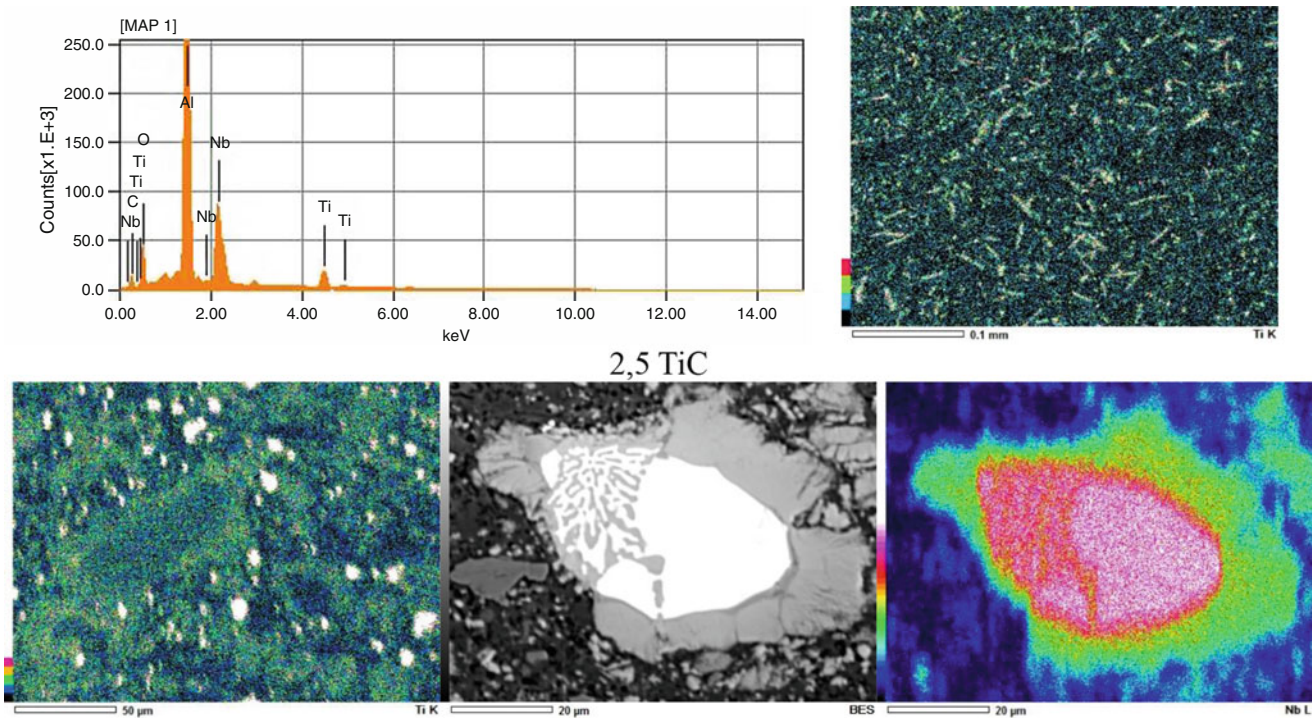

Fig. 8.3 "EDS" chemical analyses and mapping history showing the chemical bonding diffusion occurred at the interface matrix/reinforcement for the composites developed in the present work

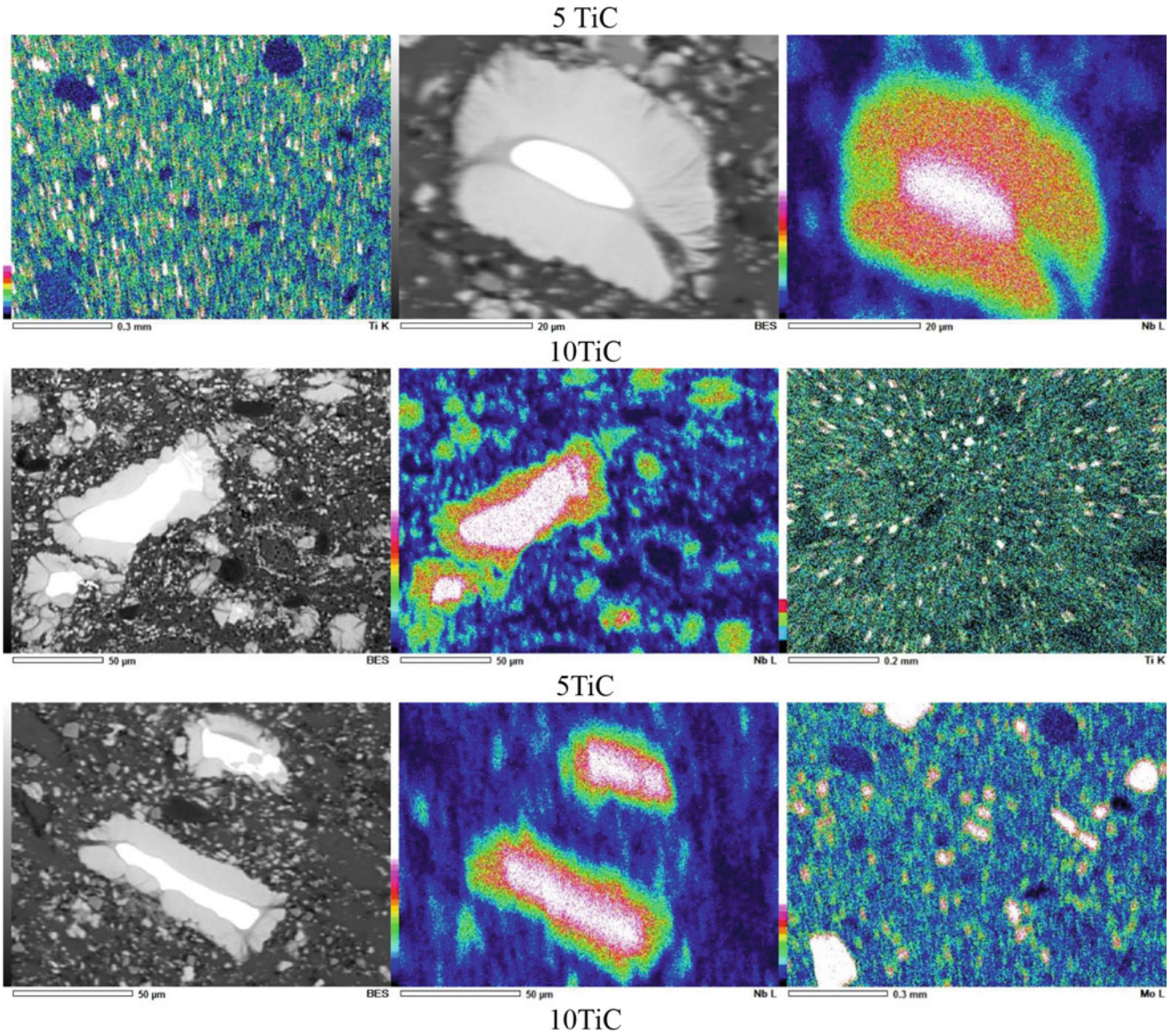

Fig. 8.3 (continued)

homogenously and also to observe the intermetallic phases occurred during the heat treatment sinter-forging. Essentially, TiC and Nb_2Al are the very suitable elements for the chemical bonding diffusion during the heat treatment operations. This diffusion mechanism is accelerated by the eutectic reaction in the structure mainly around the high activated elements. In this case, a considerable chemical diffusion bonding occurs around the Nb2Al and also TiC. If their quantity passes a threshold value, this diffusion mechanism absolutely occurs between aluminium matrix and the reinforcements.

Fracture surface analyses were given in Fig. 8.4 for only one composition (N-I), because damage analyses have shown that a brittle fracture surface and crack propagation are very similar. A strong cohesion of the reinforcements with matrix has shown that there is any debonding history of the reinforcement particles on the matrix generally observed in the microstructure.

The mechanical behaviour and damage analyses of the structure have been carried out for the sinter-forging. Static compression tests have been carried out at the different deformation rates as presented in Fig. 8.5. All of the test results of the three compositions have shown more and less the same behaviour but the first composition containing relatively lower TiC has more ductile behaviour regarding two other compositions. These results are compared for three different deformation rates and also the results were justified with a detail numerical study.

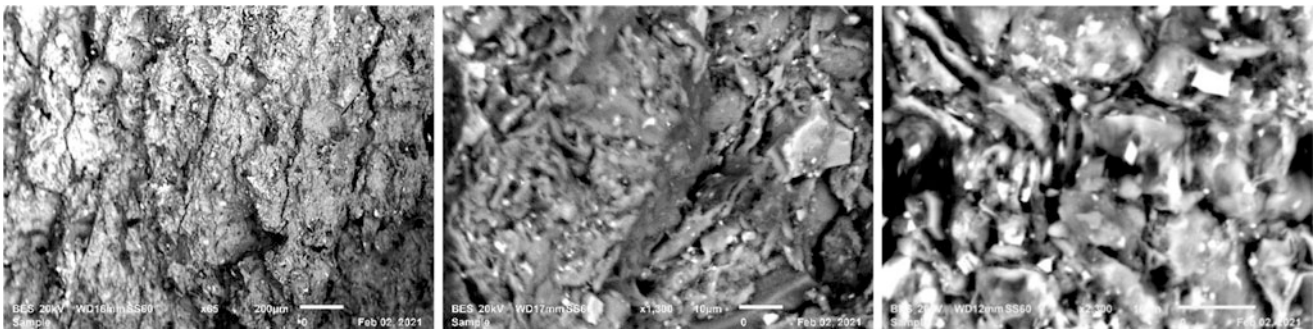

Fig. 8.4 Fracture surfaces observed on the specimen of the first composition (N-I) shows the position of the fine reinforcement particles added in the matrix

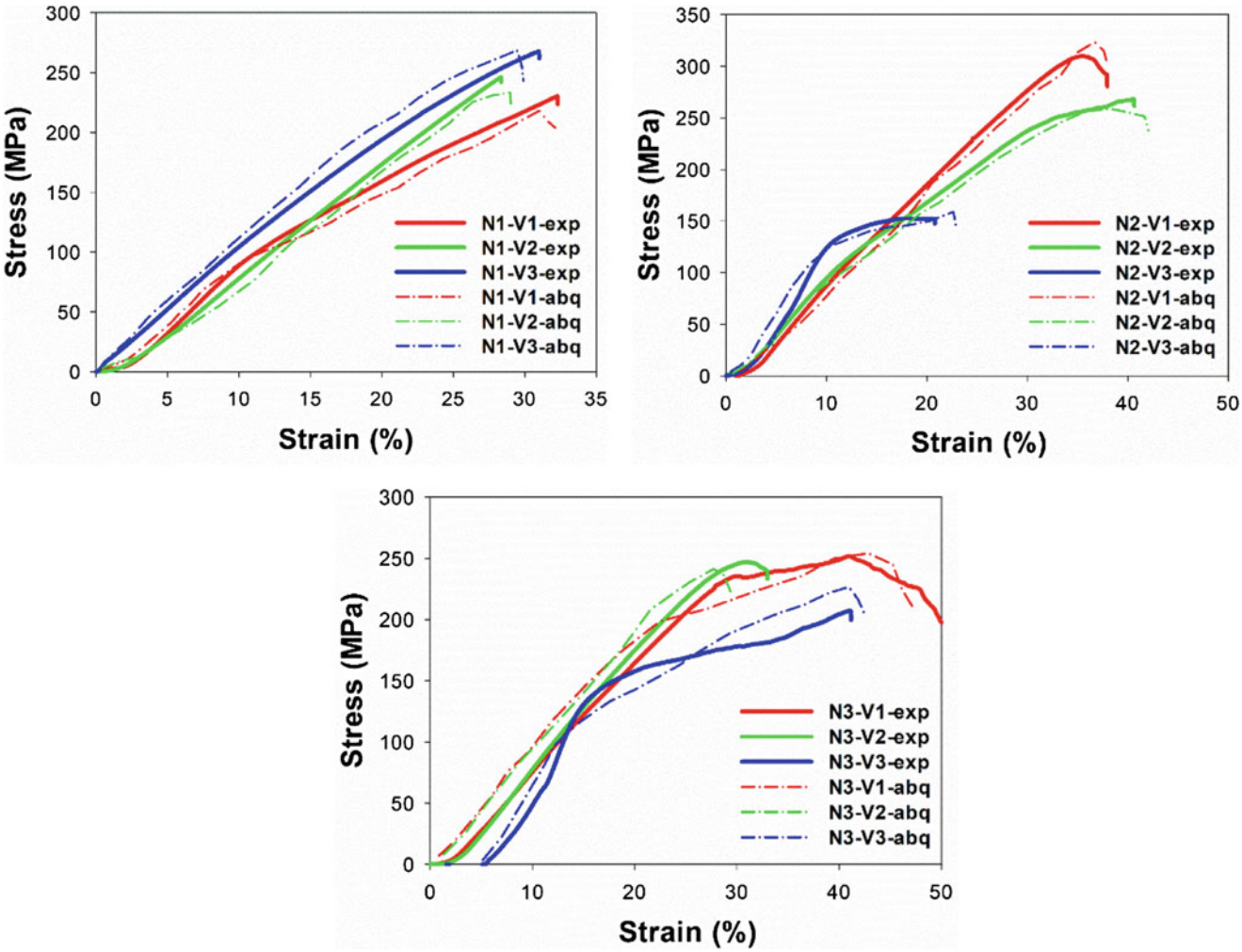

Fig. 8.5 Comparison of the static compression test results for the specimens N1, N2 and N3, respectively

As for the numerical study, it should be given a short history of the numerical application on the composites structure. In the literature, many different analytical and numerical studies have been carried out to analyze the characteristic structure of the MMCs. Analytical models developed based on experimental data are applied numerically through finite element method [1–5]. In the latter, the modelling of the interactions in the microstructure between the matrix and the reinforcement particles is of great importance. The basic parameters that influence these interaction of the particles (particle size, geometry, distribution,

quantity, etc.) with the matrix must be modelled. There are many mathematical techniques used in this modelling in the literature [7, 10–17]. One such model is Cohesive Zone Model (CZM) [6–17], although its implementation is time-consuming and detailed, it gives more realistic results.

In this work the microstructure of the composite were used and the specimens at the macro level were modelled. Modelling processes of both quasi-static compression tests were performed according to the test standards specified. In Fig. 8.5, static compression test specimens were modelled to be in cylindrical form. Quasi-static compression test apparatus (compression plate) of different linear test velocities are V1-V2-V3. This apparatus bottom surfaces in the macrostructure are completely ALLDOF fixed. Within both these test simulations, Al matrix and reinforcing particles were meshed using modified 10-node tetrahedral C3D10M mesh type with adaptive automatic meshing algorithm. The mesh element type was taken as four node-3D bilinear discrete rigid quadrilateral-R3D4 elements for mechanical loading.

Static compression test results, which are one of the mechanical behaviours of innovative composite specimens manufactured in our research, are shown in Fig. 8.5. These figures show quasi-static compression test results for both of experimental and multiscale modelling, obtained on the three types of composites under the different compression velocities. Within the scope of this test type, the maximum compression stress capacities of specimens manufactured from metal matrix composite material that we have designed innovative have been compared both experimentally and multiscale modelling simulations.

A parallel structural analyses have been carried out by low velocity impact tests (drop weight test) for three compositions at the same energy level. Absorption of the choc loading and evolution of the deformation under the choc application seem to be

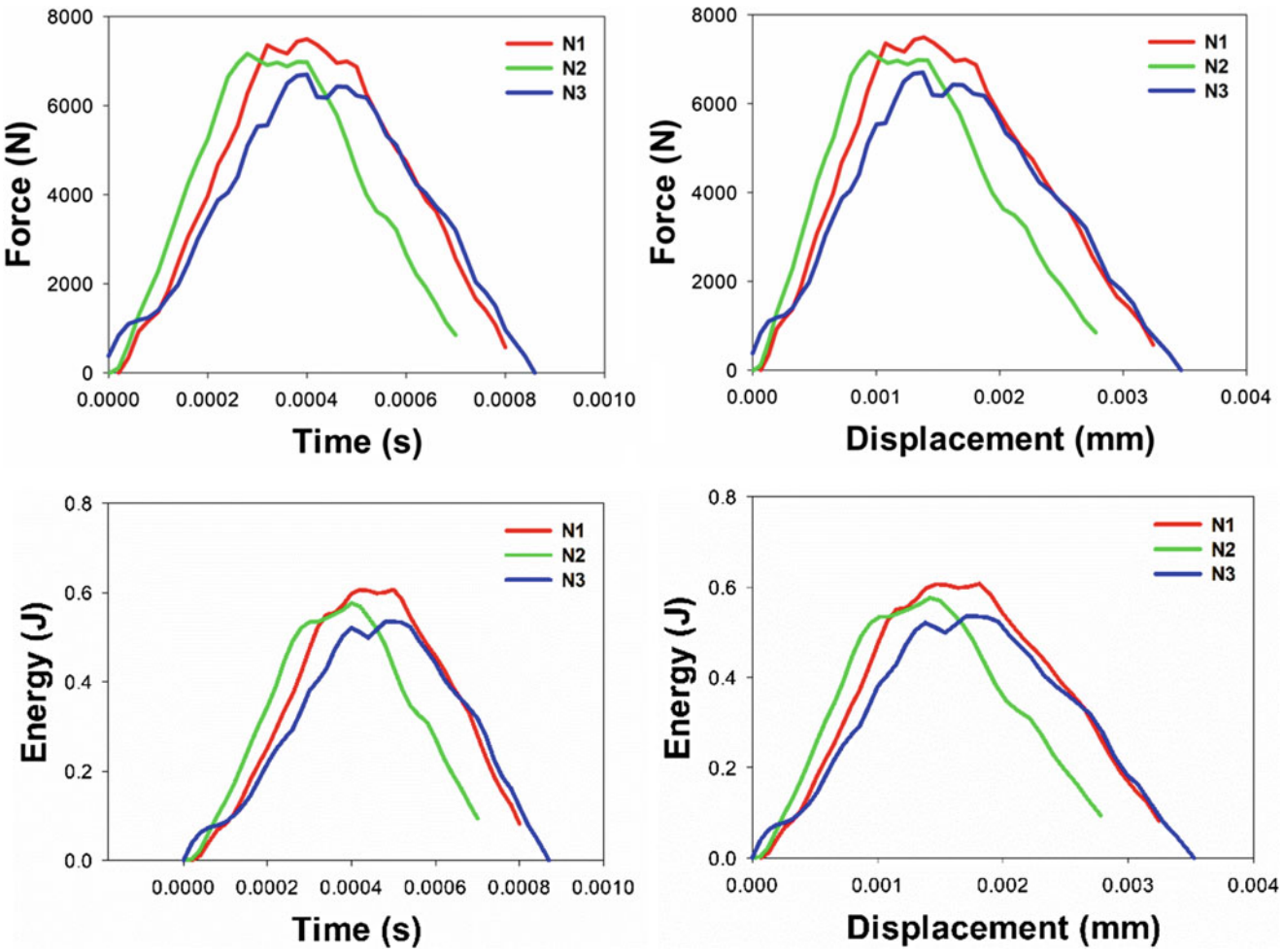

Fig. 8.6 Low velocity impact test results shown for three compositions

the same behaviour for the three compositions as given in Fig. 8.6. These results are only indicative test results and need to develop with more detail test conditions.

8.4 Conclusions

Recycled aluminium matrix composites reinforced with hard ceramic and intermetallic particles were designed through the combined method called Sinter + Forging for aeronautical applications.

In general meaning, this idea developed here in the frame of the common research project gives considerable results that could be very useful key for industrial applications. Absorbed/impact energy is directly related to the manufacturing process. Static compression tests have been compared with numerical applications. Static compression and low velocity impact tests results have justified very clearly that the composites produced with the combined method, sintered-forging give better results such as absorbed energy and/or high performance resistance capacity.

References

1. Ferreira, L.F.P., Bayraktar, E., Miskioglu, I., Katundi, D.: Design of hybrid composites from scrap aluminium bronze chips (Chapter 15). In: SEM, pp. 131–138. Springer (2016, ISBN 978-3-319-41766-0)
2. Ferreira, L.F.P., Bayraktar, E., Robert, M.H., Miskioglu, I.: Particles reinforced scrap aluminium based composites by combined processing sintering + thixoforming (Chapter 17). In: SEM, pp. 145–152. Springer (2016, ISBN 978-3-319-41766-0)
3. Saboori, A., Casati, R., Zanatta, A., Pavese, M., Badini, C., Vedani, M.: Effect of graphene nanoplatelets on microstructure and mechanical properties of AlSi10Mg nanocomposites produced by hot extrusion. Powder Metall. Met. Ceram. **56**, 647–655 (2018)
4. Enginsoy, H.M., Gatamorta, F., Larbi, A., Bayraktar, E., Miskioglu, I.: Design of copper and silicon carbide (SiC) reinforced recycled aluminium matrix composites through sintering + forging (Chapter 7). In: Composite, Hybrid and Multifunctional Materials, vol. 6. Springer (2020, ISBN 978-3-030-59867-9). https://doi.org/10.1007/978-3-030-59868-6-7
5. Ferreira, L.-M.-P., Bayraktar, E., Miskioglu, I., Robert, M.H.: Design and physical properties of multifunctional structural composites reinforced with nanoparticles for aeronautical applications. JAMPT Adv. Mater. Process. Technol. **3**(1), 33–44 (2017)
6. Gatamorta, F., Miskioglu, I., Bayraktar, E., Melo, M.L.N.M.: Recycling of aluminium-431 by high energy milling reinforced with TiC-Mo-Cu for new composites in connection applications. In: Mechanics of Composite and Multi-functional Materials, vol. 5, pp. 41–46. Springer (2019). https://doi.org/10.1007/978-3-030-30028-9_6
7. Saboori, A., Pavese, M., Badini, C., Fino, P.: Development of Al- and Cu-based nanocomposites reinforced by graphene nanoplatelets: fabrication and characterization. Front. Mater. Sci. **11**, 171–181 (2017)
8. Saboori, A., Novara, C., Pavese, M., Badini, C., Giorgis, F., Fino, P.: An investigation on the sinterability and the compaction behavior of aluminum/graphene nanoplatelets (GNPs) prepared by powder metallurgy. J. Mater. Eng. Perform. **26**, 993–999 (2017)
9. Williams, J.J., Segurado, J., LLorca, J., Chawla, N.: Three dimensional (3D) microstructure-based modeling of interfacial decohesion in particle reinforced metal matrix composites. Mater. Sci. Eng. A. **557**, 113–118 (2012)
10. Ekici, R., Kemal Apalak, M., Yildirim, M., Nair, F.: Simulated and actual micro-structure models on the indentation behaviors of particle reinforced metal matrix composites. Mater. Sci. Eng. A. **606**, 290–298 (2014)
11. Liu, F.R., Chan, K.C., Tang, C.Y.: Numerical modeling of the thermo-mechanical behavior of particle reinforced metal matrix composites in laser forming by using a multi-particle cell model. Compos. Sci. Technol. **68**(9), 1943–1953 (2008)
12. Çetin, A., Kalkanli, A.: Numerical simulation of solidification kinetics in A356/SiCp composites for assessment of as-cast particle distribution. J. Mater. Process. Technol. **209**, 4795–4801 (2009)
13. Galli, M., Botsis, J., Janczak-Rusch, J.: An elastoplastic three-dimensional homogenization model for particle reinforced composites. Comput. Mater. Sci. **41**, 312–321 (2008)
14. Chawla, N., Sidhu, R.S., Ganesh, V.V.: Three-dimensional visualization and microstructure-based modeling of deformation in particle-reinforced composites. Acta Mater. **54**, 1541–1548 (2006)
15. Su, Y., Ouyang, Q., Zhang, W., Li, Z., Guo, Q., Fan, G., Zhang, D.: Composite structure modeling and mechanical behavior of particle reinforced metal matrix composites. Mater. Sci. Eng. A. **597**, 359–369 (2014)
16. Yuan, Z., Li, F., Xue, F., He, M., Hussain, M.Z.: Analysis of the stress states and interface damage in a particle reinforced composite based on a micromodel using cohesive elements. Mater. Sci. Eng. A. **589**, 288–302 (2014)
17. Meng, Q., Wang, Z.: Prediction of interfacial strength and failure mechanisms in particle-reinforced metal-matrix composites based on a micromechanical model. Eng. Fract. Mech. **142**, 170–183 (2015)

Chapter 9
Tailored Behaviour of Scrap Copper Matrix Composites Reinforced with "Zn-Ni-Al" Low Cost Shape Memory Structures

L. Mihlyuzova, H.-M. Enginsoy, E. Bayraktar, S. Slavov, and D. Dontchev

Abstract The copper-aluminium (Cu-Al-Zn-Ni) based structures show shape memory behaviours that are low cost engineering applications, such as actuators, valves, etc., regarding to Ni-Ti-Al structures. These alloys have a useful transformation temperature that can be modified to lie between −100 and 100 °C (sometimes ±50 °C). For low cost production, a combined method through powder metallurgy processes (sinter-Forging) without using the grain size control additives.

In the frame of the common research project, production of the scrap thin sheet copper based composites reinforced with scrap commercially pure aluminium (AA1050) and zinc produced through the combined method, sinter-forging process will be discussed for a tough structure.

Keywords Scrap copper based composites · High strength · Memory shape effect · Compression Test · Bending test

9.1 Introduction

High performance metal based composites (HPMBC) are composed for the multifunctional materials for different application in aeronautical industry. One of the idea for the design of the novel composites is to develop a new type of shape memory materials from recycled constituent composites. The hint for the design and manufacturing of these composites is to create an optimal property with low cost materials partially coming from fresh scarp thin sheet in order to obtain more useful applications. Recently, these composites were improved by using alternative low cost manufacturing structures called the sandwich/layered structures. These structures contain several stacked thin sheets.

Several methods are generally used to create on the sheets such as diffusion bonding and deformation bonding, to prepare multilayer/sandwich composites. However, many of these processes are complex and expensive in process. This can limit the application of these structures in manufacturing engineering [1–6]. Among widely used processes for these structures is accumulative roll bonding (ARB) process that is an efficient method due to its simple operation and low cost manufacturing; however, this process also needs a long operation and is not so much practical for the mass production of these composites.

In the frame of the common research project, manufacturing of thin sheet "Cu-Zn-Al" based composites reinforced with certain reinforcement such as boron, titanium, zirconium niobium, etc., have been carried out through hot-forged bonding process of the composites. Interface and bonding characteristics have also been examined of hot-forged composites, heat treated at 550 °C depending on the operational parameters under laboratory conditions. Formability behaviour and delamination/decohesion phenomena have been analysed by 3P bending tests for toughening and hyperelasticity. A high strength bonding has been carried out by mechanical joining and mutual chemical bonding diffusion during this process as a function of process temperature and time for obtaining a tough composite structure.

L. Mihlyuzova
UTCM, University of Chemical Technology and Metallurgy, Sofia, Bulgaria

School of Mechanical and Manufacturing Engineering, Supmeca-Paris, Saint-Ouen, France

H.-M. Enginsoy · E. Bayraktar (✉)
School of Mechanical and Manufacturing Engineering, Supmeca-Paris, Saint-Ouen, France
e-mail: emin.bayraktar@isae-supmeca.fr

S. Slavov · D. Dontchev
UTCM, University of Chemical Technology and Metallurgy, Sofia, Bulgaria
e-mail: stanislavslavov@uctm.edu; dontchev@uctm.edu

V. Chalivendra et al. (eds.), *Mechanics of Composite, Hybrid and Multifunctional Materials, Fracture, Fatigue, Failure and Damage Evolution, Volume 3*, Conference Proceedings of the Society for Experimental Mechanics Series,
https://doi.org/10.1007/978-3-030-86741-6_9

As well known, the copper-zinc-aluminium (Cu-Zn-Al) binary alloy displays shape memory characteristics but has a transformation temperature that is generally considered too high for practical applications. The addition of zinc to the system produces a new ternary system, CuZnAl, which is of commercial importance. These alloys have a useful transformation temperature that can be modified to lie between −100 and 100 °C (sometimes ±50 °C). Another idea is to add small amount of certain elements as the reinforcements of the structure. Amongst them, boron, cerium, cobalt, iron, titanium, vanadium, zirconium, etc. are commonly used to control grain size of these composites [4–10]. These reinforcements decrease the grain size and prevent early failure. These reinforcements should be really small sizes to keep the stability of the structure like the shape memory characteristics.

In the frame of this research project, some preliminary results will be presented here, such as mechanical behaviour, hyperelasticity, transformation behaviour, recycled deformation behaviour, etc.

9.2 Experimental Conditions

Commercially pure Cu, Zn, Al and Ni thin sheets were used as basic structures in this research. The mean thickness of each thin sheet was variable between 0.1 and 0.2 mm, Cu, Zn, Al and Ni thin scrap sheets coming from French Aeronautical Company were cut into circles shape with 50 mm in diameter (Table 9.1). After cleaning to degrease them, a sandwich structure was stacked together and heated up to 250 °C under pressure in a matrix for 15 min. For certain special composites, these thin sheets were reinforced with fine Nb, B, Zr and/or Ti, powders in very low percentages to improve the certain properties, Actually this common research project is going on for certain auxiliary aeronautical applications for turbo-compressors. At the second stage, these structure was hot forged as a heat treatment process at 550 °C depending on the operational parameters under laboratory conditions. Formability behaviour and delamination/decohesion phenomenon have been analysed by 3P bending tests (ASTM D790). Finally a high strength bonding has been carried out by mechanical joining and mutual chemical bonding diffusion during this process as a function of process temperature and time. Dynamic Scanning Calorimetric Analyses (DSC) have also been done to observe the transformation point during the hot forging process.

9.3 Results and Discussion

Figure 9.1 shows a general schematic presentation of experimental set-up for hot forging of the stacked structure and set-up of the 3P bending test (ASTM790) equipment and rules with final shape of the bended specimen. 3P Bending tests (ASTM D790) have been carried out on the Zwick testing machine to evaluate formability and mechanical behaviours of these structures.

Table 9.1 Compositions of the SMA specimen (wt. %)

Specimen name	Cu	Zn	Al	Ni	B	Nb	Zr	Ti
Novel-SMA-I	B	13	6	3	0.25	0.5	0.25	0.5

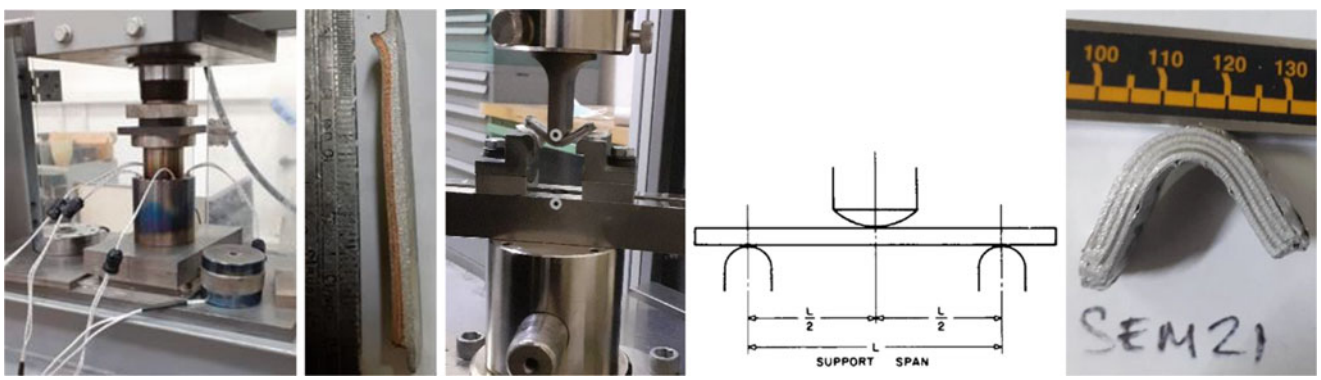

Fig. 9.1 Schematic presentation of experimental set-up for hot forging of the stacked structure and set-up of the 3P bending test (ASTM790) structure before and final shape of the bended specimen

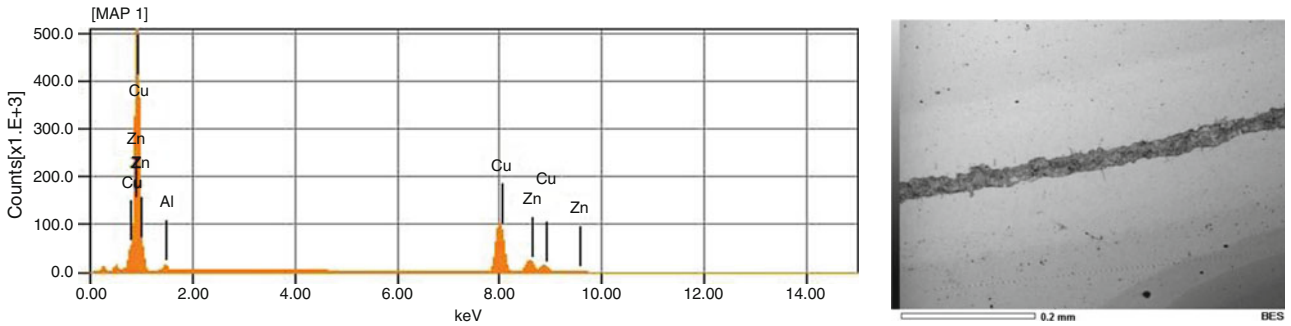

Fig. 9.2 EDS chemical analyses, mapping and microstructure of the Ni-Ti-Al composite after the 3P bending test for showing a strong cohesion due to the diffusion bonding

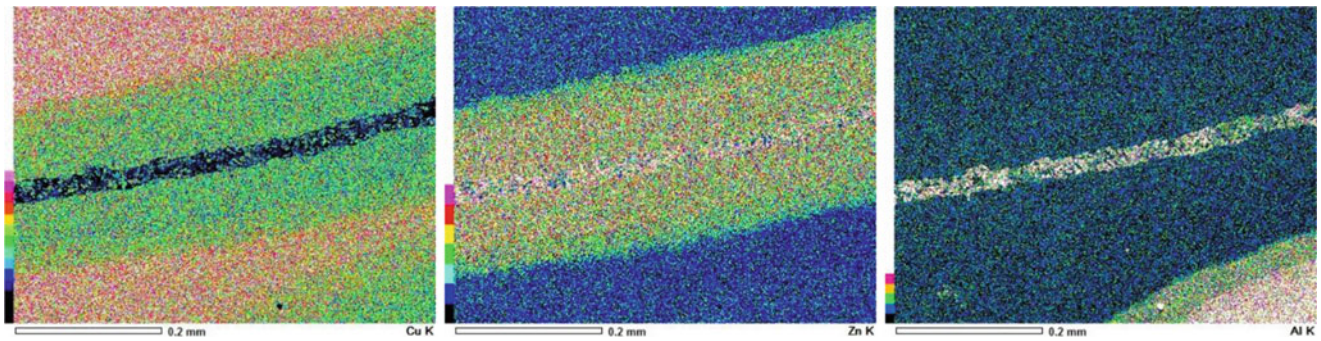

Fig. 9.3 Interface and diffusion bonding between each sheet part after the 3-point bending test

Microstructural and EDS chemical analyses were presented in Fig. 9.2 with the mapping analyses for the composite obtained by hot-forged compaction process.

Here there is a clear observation between thin sheets after the hot forging process. All of the mapping parts indicated that there is a very strong cohesion and fusion between thin sheets.

A detail interface analysis was also shown in Fig. 9.3. Here a strong cohesion between thin sheets is carried out during the hot forging and a strong diffusion between the sheets. Any decohesion was observed after the heavy deformation up to 25–30% with 3P bending tests.

Again, from Fig. 9.3, one may observe that a strong intermetallic phase layer has been carried out successfully between the copper and aluminium layers containing small amount of hard particle reinforcements during hot forging process. Finally a high strength bonding has also been carried out by mechanical joining and mutual chemical bonding diffusion during this process as a function of process temperature and time.

As well known, Differential Scanning Calorimetry (**DSC**) is a thermal **analysis** technique in which the heat flow into or out of a sample is measured as a function of temperature or time, while the sample is exposed to a controlled temperature program.

Figure 9.4 gives a detail information of DSC analyses on the "Cu-Al-Zn-Ni" composite that shows a transformation point at the level of 149–151 °C depending on the time and heating process.

As for 3P bending tests (ASTM D790) evaluation, the test results presented in Fig. 9.5 give a shape memory effect during the deformation (at the level of 10–113% of deformation. Stacked structure containing very thin sheets gives a hyperelasticity. During the test, thin stacked structure has undergone a heavily deformation and the test was stopped at this level.

Another interesting results were obtained thick Cu-Zn-Al-Ni stacked composite structure when they were undergone to cyclic deformation as presented in Fig. 9.6a, b. Two similar thick stacked specimens have been tested under the cyclic deformation as 10 and 20 cycles, respectively. Shape memory effect was observed on the both of the tests. A considerable recovering were observed at the first 5^{th} and 6^{st} cycles during the loading and unloading stages. These are preliminary results, and they give only a general idea on the recovering behaviour of these composites at the two stages in case of the cyclic deformations. It is worthy to evaluate these properties to well understand the hyperelasticity during the deformation of these stacked structure related to the shape memory effects.

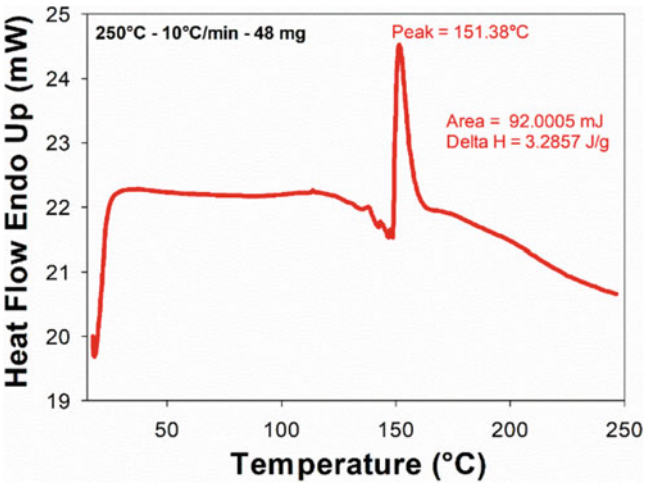

Fig. 9.4 Differential Scanning Calorimetric (DSC) analysis for the "Ni-Ti-Al" composite

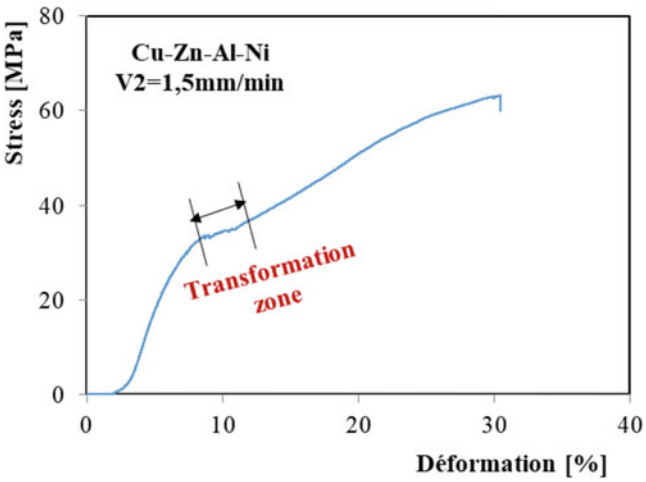

Fig. 9.5 Three-point bending test results for Cu-Zn-Al-Ni stacked composite structure

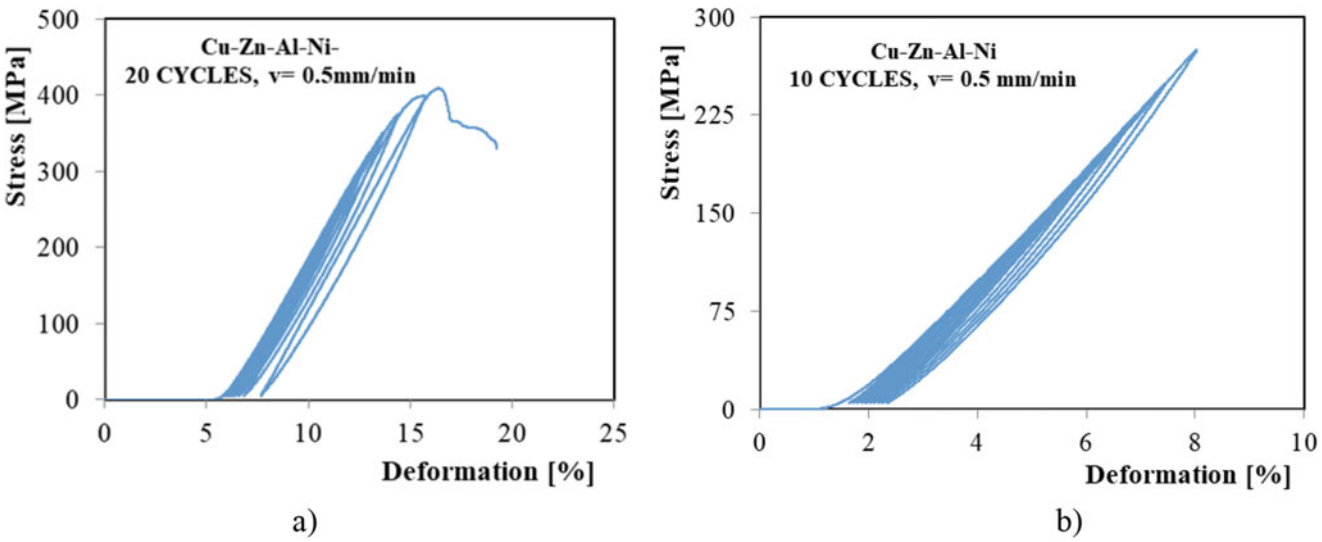

Fig. 9.6 Cyclic deformation behaviour of the "Cu-Zn-Al-Ni" stacked composite structure, in case of 10 cycles (**a**) and 20 cycles (**b**)

9.4 Conclusions

In the frame of the common research project, manufacturing of the scrap thin sheet "Cu-Zn-Al-Ni" based composites reinforced with small amount of hard particles have been carried out through hot-forged bonding process for obtaining an hyperelastic sandwich/stacked structure. Interface and bonding characteristics have also been examined of hot-forged composites, heat treated at 550 °C depending on the operational parameters under laboratory conditions.

A successful hyperelastic formability behaviour was observed and there was any delamination/decohesion phenomenon during the 3P bending tests. An intermetallic phase layer has been carried out between the copper and aluminium sheets during hot forging process. Finally a high strength bonding has been carried out by mechanical joining and mutual chemical bonding diffusion during this process as a function of process temperature and time. DSC results have given a detail information on the transformation behaviour of this composite.

"Cu-Zn-Al-Ni" stacked composite structure shows a considerable hyperelasticity during the cyclic deformation. Shape memory effect was observed on the both of the tests. A considerable recovering were observed at the first 5^{th} and 6^{st} cycles during the loading and unloading stages. It is worthy to evaluate these properties to well understand the hyperelasticity during the deformation of these stacked structure related to the shape memory effects.

References

1. Mihlyuzova, L., Enginsoy, H.M., Dontchev, D., Bayraktar, E.: Tailored behaviour of scrap copper matrix composites reinforced with zinc and aluminium: low cost shape memory structures (Chapter 5). In: Mechanics of Composite, Hybrid and Multifunctional Materials, vol. 6. Springer (2020, ISBN 978-3-030-59867-9). https://doi.org/10.1007/978-3-030-59868-6_5
2. Enginsoy, H.M., Bayraktar, E., Miskioglu, I., Katundi, D.: Manufacturing of "Ni-Ti" based composites from fresh scrap thin sheets reinforced with Nb and TiB_2 through hot-forged bonding: sandwich structures (Chapter 8). In: Composite, Hybrid and Multifunctional Materials, vol. 6. Springer (2020, ISBN 978-3-030-59867-9). https://doi.org/10.1007/978-3-030-59868-6_8
3. Wang, Z.G., Zu, X.T., Yu, H.J., He, X., Peng, C., Huo, Y.: Temperature memory effect in CuAlNi single crystalline and CuZnAl polycrystalline shape memory alloys. Thermochim. Acta. **448**, 69–72 (2006)
4. Firth, N., Afseth, A., Chapis, L., Athènes, C.: Making way for modern aluminium. Alum. Int. Today, 48–49 (2015)
5. Gatamorta, F., Miskioglu, I., Bayraktar, E., Melo, M.L.N.M.: Recycling of aluminium-431 by high energy milling reinforced with TiC-Mo-Cu for new composites in connection applications. In: Mechanics of Composite and Multi-functional Materials, vol. 5, pp. 41–46. Springer (2019). https://doi.org/10.1007/978-3-030-30028-9_6
6. Hekkert, M.P., Suurs, R.A., Negro, S.O., Kuhlmann, S., Smits, R.E.: Functions of innovation systems: a new approach for analysing technological change. Technol. Forecast. Soc. Chang. **74**(4), 413–432 (2007)
7. Singh, J., Chauhan, A.: Characterization of hybrid aluminum matrix composites for advanced applications—a review. J. Mater. Res. Technol. **5** (2), 159–169 (2016)
8. Gatamorta, F., Katundi, D., Bayraktar, E., Ferreira, L.M.P., Melo, M.L.N.M.: Magnetic shape memory composite (MSMC) design from intermetallic Cu-NiTi-MnAl-Fe_3O_4 alloy as an alternative replacement for actuators. In: Mechanics of Composite and Multi-functional Materials, vol. 5, pp. 47–54. Springer (2019). https://doi.org/10.1007/978-3-030-30028-9_7
9. Katundi, D., Ferreira, L.P., Bayraktar, E., Miskioglu, I., Robert, M.H.: Design of magnetic aluminium (A356) based composites through combined method of sinter + forging. SEM Mech. Composit. Multi-funct. Mater. **6**, 89–101 (2017)
10. Ramos, A.P., de Castro, W.B., Costa, J.D., de Santana, R.A.C.: Influence of zirconium percentage on microhardness and corrosion resistance of Ti50 Ni50-xZrx shape memory alloys. Mater Res. **22**(4), e20180604 (2019). https://doi.org/10.1590/1980-5373-MR-2018-0604

Chapter 10
Mechanical Properties of Recycled Rubber Modified Epoxy Resin Based Composites for Aircraft Auxiliary Structures

G. Zambelis, H.-M. Enginsoy, E. Bayraktar, A. Larbi, and D. Katundi

Abstract In this research, devulcanized recycled rubber modified phenolic epoxy based composites reinforced with different ceramic carbon, and/or glass fibres and also graphene nano plates (GnPs) based composites were designed for aircraft internal structure. After determination of the reinforcements and matrix, a hot bonding process was applied to complete successfully the manufacturing of these composites. After that, the relevant toughening mechanisms given by the reinforcements were analyzed in detail to evaluate the damage tolerance of aircraft internal structures. For this purpose, mechanical and physical properties, K_{IC}—Fracture toughness stress intensity factor and G_{Ic}—Critical energy release rate in mode I) have been determined by fracture toughness tests (static 3P bending test with single edge notch specimens, drop weight test, etc.).

Keywords Recycled composites · Epoxy, phenolic resin · Devulcanized Rubber · 3P bending

10.1 Introduction

Recycled rubber is largely used in manufacturing as a low cost engineering application by using different reinforcements to create high performance composites with multi-functional assets. As matrix, epoxies are generally used because they are very easy to combine with recycled rubber creating a good interface with other reinforcements. As the reinforcements, ceramic, carbon and/or glass fibres are largely used for aeronautical engineering applications for their high mechanical index (i.e. strength/weight). Many of them are ready for use and easily mixed to increase the resistance of the composite structure even if their homogenous distribution in the matrix can create sometimes some difficulties [1–4].

The procedure of the recycled rubber from fresh scrap rubber for manufacturing applications has been well industrialized as a very useful material for the composites. The elementary procedure contains very easy and safe chemical treatment called silanization followed by devulcanization treatments for cost effective composite designs [3–9].

The rubber modified epoxy based composites reinforced with different ceramic carbon, and/or glass fibres and also graphene nano plates (GnPs) are novel designs for aeronautic and aerospace applications. Another interesting mechanism called chemical bonding diffusion between rubber and reinforcement materials in the epoxy matrix can lead to improve the composite properties during the hot compaction processes [10–12].

In the frame of this common research work collaborated with French Aeronautical society, we try to develop a new alternative composite design with high performance capacity under the service conditions of aeronautic and/or aerospace, defence structures. Devulcanized recycled rubber modified phenolic epoxy based composites are extensively used for this research. Different reinforcements were used such as ceramic carbon, and/or glass fibres and also graphene nano plates (GnPs) for the application of aircraft internal structure.

G. Zambelis · D. Katundi
Airbus-Helicopters—Composites Research and Development Centre, Paris, France
e-mail: georges.zambelis@airbus.com; dhurata.katundi@isae-supmeca.fr

H.-M. Enginsoy · E. Bayraktar (✉) · A. Larbi
School of Mechanical and Manufacturing Engineering, Supmeca-Paris, Saint-Ouen, France
e-mail: emin.bayraktar@isae-supmeca.fr; abdelghani.larbi@isae-supmeca.fr

V. Chalivendra et al. (eds.), *Mechanics of Composite, Hybrid and Multifunctional Materials, Fracture, Fatigue, Failure and Damage Evolution, Volume 3*, Conference Proceedings of the Society for Experimental Mechanics Series,
https://doi.org/10.1007/978-3-030-86741-6_10

10.2 Experimental Conditions

After determination (in wt% percentages) of the reinforcements and respectively matrix, a special process was applied to complete successfully the manufacturing of these composites (silanization of the recycled rubber and devulcanization before blending it with epoxy resin and reinforcements). All of the details of these processes were given in former papers [2, 7, 10–13]. Chemical treatments followed devulcanized recycled rubber and were mixed with epoxy resin for obtaining a strong chemical bonding diffusion improved with different reinforcements (Table 10.1). After blending this mixture, they were milled during 4 h by adding "Zn-Stearate" as lubricant for homogenous distribution. To manufacture these composites, hot compaction was carried out at 230 °C during 20 min under the pressure of 6 tons to obtain the specimens with a diameter of 50 mm. Final rectangular shape specimens were cut for 3-point bending tests (ASTM STP 856) called Single Edge Notch Bending (SENB) test specimens (Fig. 10.1) to evaluate the fracture toughness (K_{IC}) and fracture energy (G_{Ic}) values of these composites.

3P bending tests (SENB) were carried out with a constant speed of 1 mm/min. Fracture surface analyses were carried out by using Scanning Electron Microscope (SEM) on the damaged specimens. Microstructural analyses have also been carried out on the polished surfaces of these specimens (Distribution of the particles by mapping and also chemical analyses by EDS—Electro Discharge Spectrum). All of the microhardness measurements have been carried out by using of "SHORE-D TESTS" following the ASTM 2240 and the results were presented in Table 10.2.

Table 10.1 Chemical compositions of the composites studied in this work (wt%)

Composites name	Rubber	Phenolic resin	TiB_2	(γ-Al_2O_3) fibre	Glass bubble	Al-fine chips	Glass fibre	GNP
LIAM-I-II	40	60						
YANNIS-EX	25	60			5	10		
PSYN-EX	30	50	10	5	5			
RTiB + LIAM	30	55	10	2.5	2.5			
LIAM-II	40	50		5		5		
LIAM-III	35	53					10	2

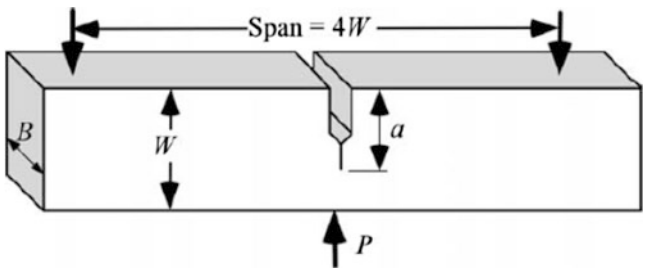

Fig. 10.1 3-Point single edge notched bending (SENB) test for fracture toughness, K_Ic and fracture energy, G_Ic characterization

Table 10.2 Shore-D hardness measurements of the composites

Composites name	Shore-D test ASTM 2240
LIAM-I-II	76 ± 2
YANNIS-EX	75 ± 4
PSYN-EX	82 ± 3
RTiB + LIAM	70 ± 2
LIAM-II	78 ± 2
LIAM-III	81 ± 3

10.3 Results and Discussion

10.3.1 Three-Point Bending Tests (SENB-ASTM D 790) and Fracture Surface Observations

3P bending tests have been carried out with a constant speed of 1 mm/min for the specimens produced from each different type of composites called single edge notched bending (SENB). Three to four specimens have been tested for each composition and evolution of stress levels depending on the deformation for each composition are presented in Fig. 10.2a, b. By using these graphs, fracture toughness and fracture energy values have been calculated.

Experimental set-up and geometry for the three-point bending (3 PB) tests (ASTM790/SENB-) were presented in Fig. 10.3.

Mechanical and physical properties are obtained by conducting the 3P bending test with single edge notch specimens suggested by ASTM D790 [5]. Flexural stress is calculated during three-point bending test as

$$\sigma_f = \frac{3PL}{2BW^2}$$

where L is the span length ($L = 4W$), P is the maximum bending load, B and W are respectively the sample width and thickness. Flexural strain is

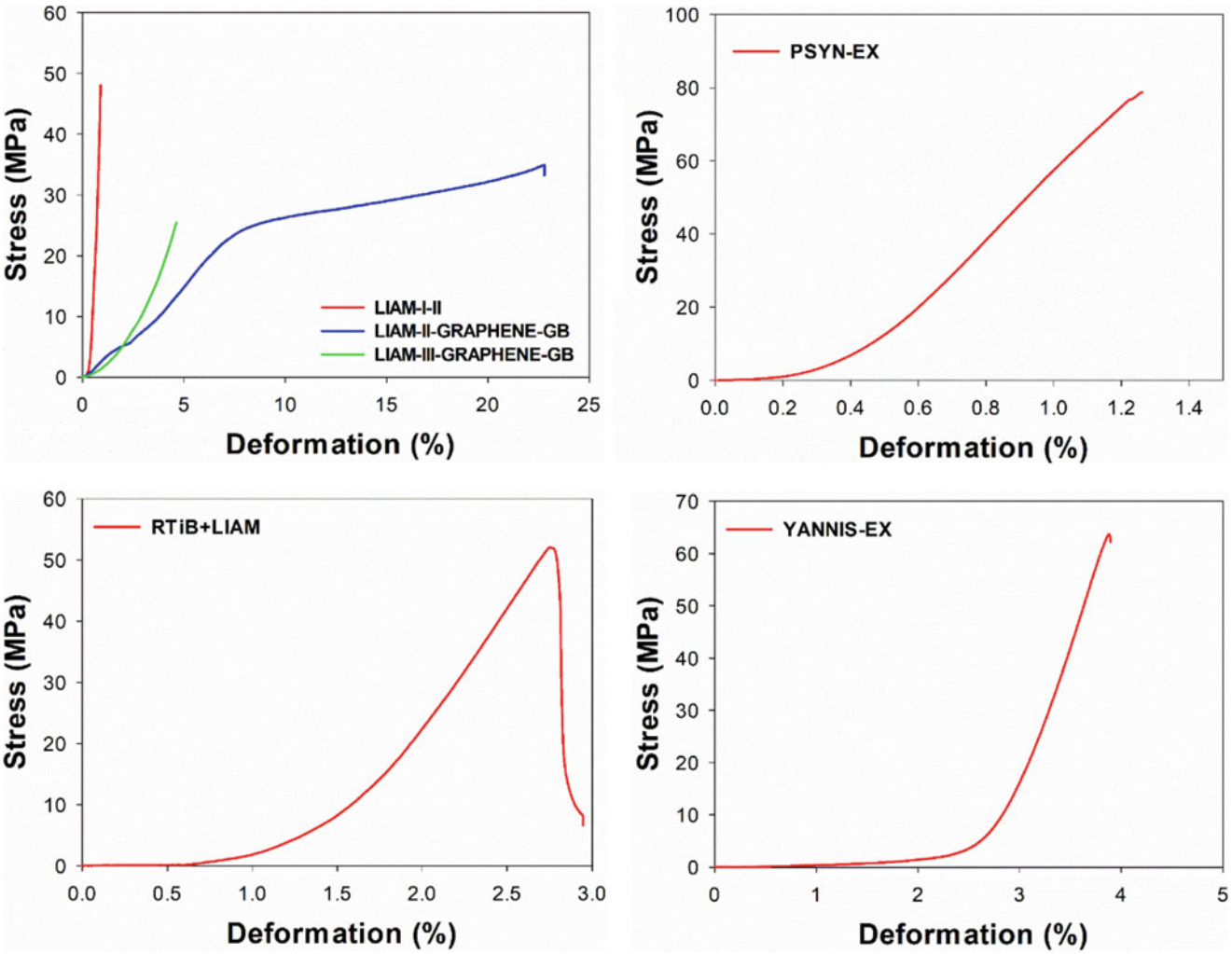

Fig. 10.2 (**a**) 3-Point single edge notched bending test results (3PB-SENB) for the specimen LIAM (left), and for the PSYN, right. (**b**) 3-Point single edge notched bending test results (3PB-SENB) for the specimen RTIB+LIAM (left), and for the YANNIS-EX, right

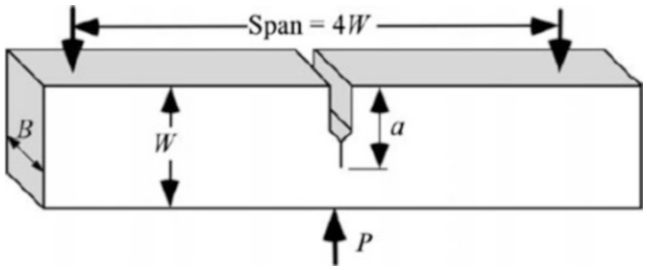

Fig. 10.3 SENB test set-up and model for numerical analysis

Table 10.3 Comparison of mechanical properties, fracture toughness and fracture energy

Composites name	Max flexural stress (MPa)	Flexural modulus (MPa)	Flexural strain (ε %)	K_{Ic} (MPa $m^{1/2}$)	G_{Ic} (kJ/m^2)
LIAM-I-II	48.1	7700	0.89	3.03	1.19
LIAM-II	34.9	1215	22.78	1.41	1.64
LIAM-III	25.5	622	4.63	1.60	4.13[a]
YANNIS-EX	63.7	5558	3.88	4.01	2.90
PSYN-EX	78.8	10,760	1.26	4.96	2.30
RTiB + LIAM	52.1	3548	2.75	3.28	3.04

[a]Not realistic value of G_{Ic} because the modulus is very low

$$\varepsilon_f = \frac{6DW}{L^2}$$

in which D is the maximum deflection at the centre of the specimen. The elasticity modulus in bending is calculated from

$$E_f = \frac{L^3 m}{4BW^3}$$

m is the tangent of the initial straight portion of the force-displacement curve.

The critical stress intensity factor in mode I loading is determined by testing the SENB specimens as

$$K_{Ic} = \frac{P}{BW^{\frac{1}{2}}} f(x), \quad x = a/W$$

This equation is valid for $0.2 < x < 0.8$, where P is the maximum force at fracture, B is the thickness of the specimen, W is the width, and "a" is the total notch length. $f(x)$ is the geometry correction factor which is obtained by

$$f(x) = 6x^{1/2}\left[\frac{1.99 - x(1-x)(2.15 - 3.93x + 2.7x^2)}{(1+2x)(1-x)^{3/2}}\right]$$

Critical strain energy release rate (fracture energy) is calculated as:

$$G_{Ic} = \frac{K_{Ic}^2}{E}$$

where E is the modulus of elasticity.

Table 10.3 presents the mechanical properties in bending mode. Fracture toughness values were also presented in the table. Here, the rubber modified epoxy based hybrid composites reinforced with different ceramic fibres, GB, GNP, etc. with a certain weight percentages have shown improvements in the mechanical properties. The flexural stress, the fracture toughness (K_{IC}) and fracture energy (G_{IC}) improved values explain a strong synergistic effect related to the basic physical properties of the individual reinforcements and chemical diffusion bonding between the matrix and/or between the reinforcements by means of mutual diffusion mechanism. As well known, the fracture toughness and fracture energy values of the hybrid composites are always higher than that of single composites, evidently, the synergistic effect plays a significant role.

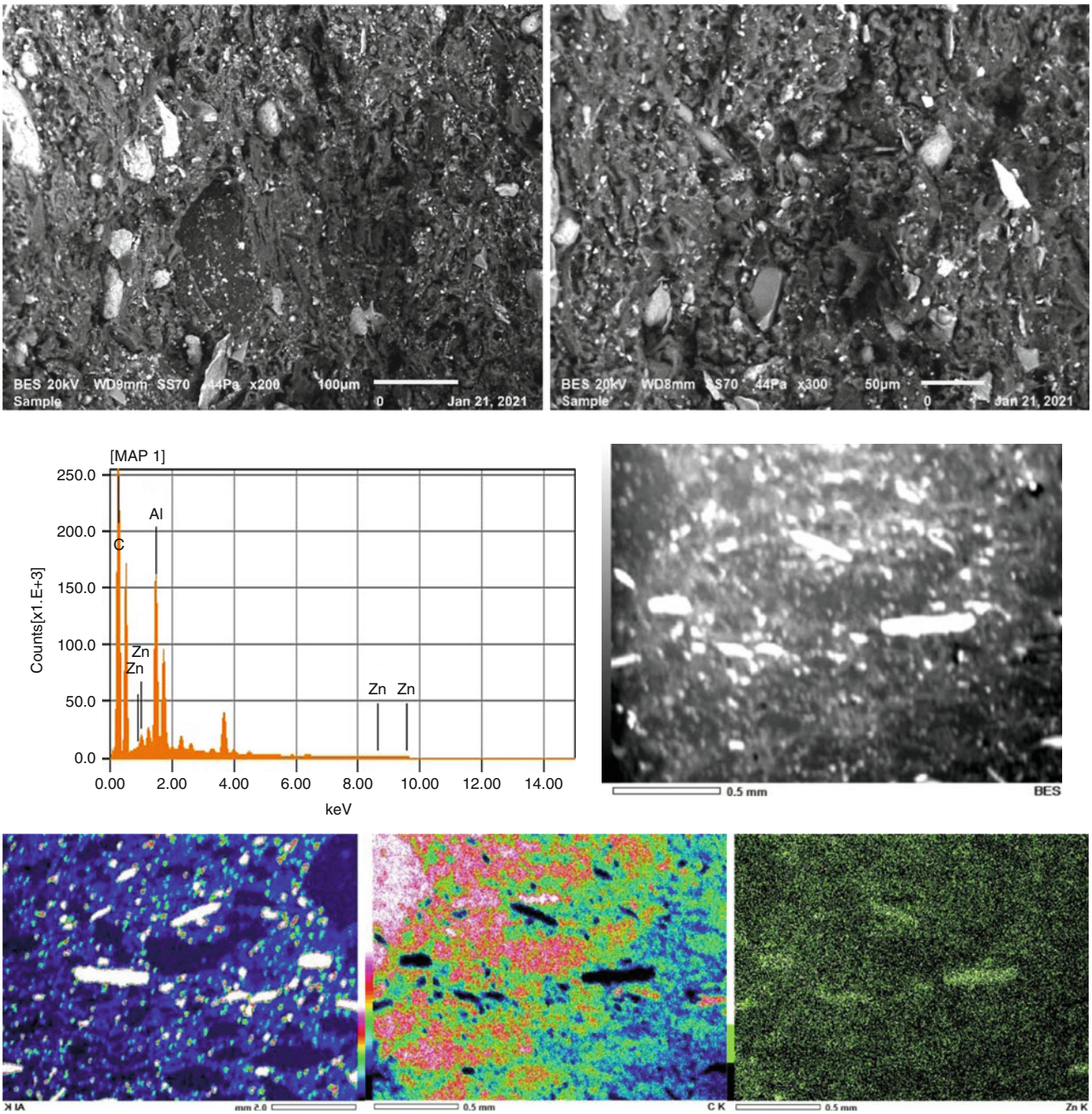

Fig. 10.4 (**a**) Fracture surface analyses for the composite of YANNIS-EX. (**b**) EDS chemical and microstructural and mapping analyses for the composite of YANNIS-EX-(Y-II)

For this reason, the fracture surface analyses of the composites have been carried out by using Scanning Electron Microscope (SEM) to justify this idea. At the same time, detailed mapping analyses have also been done on the microstructures of the polished specimens for each composite for observing the distribution of the reinforcement in the matrix. Figures 10.4, 10.5, 10.6, and 10.7 give all the details on the microstructure evolution with different reinforcements. In general way, we observe a homogenous distribution of the reinforcement in the matrix for each reinforcement on the mapping, even if

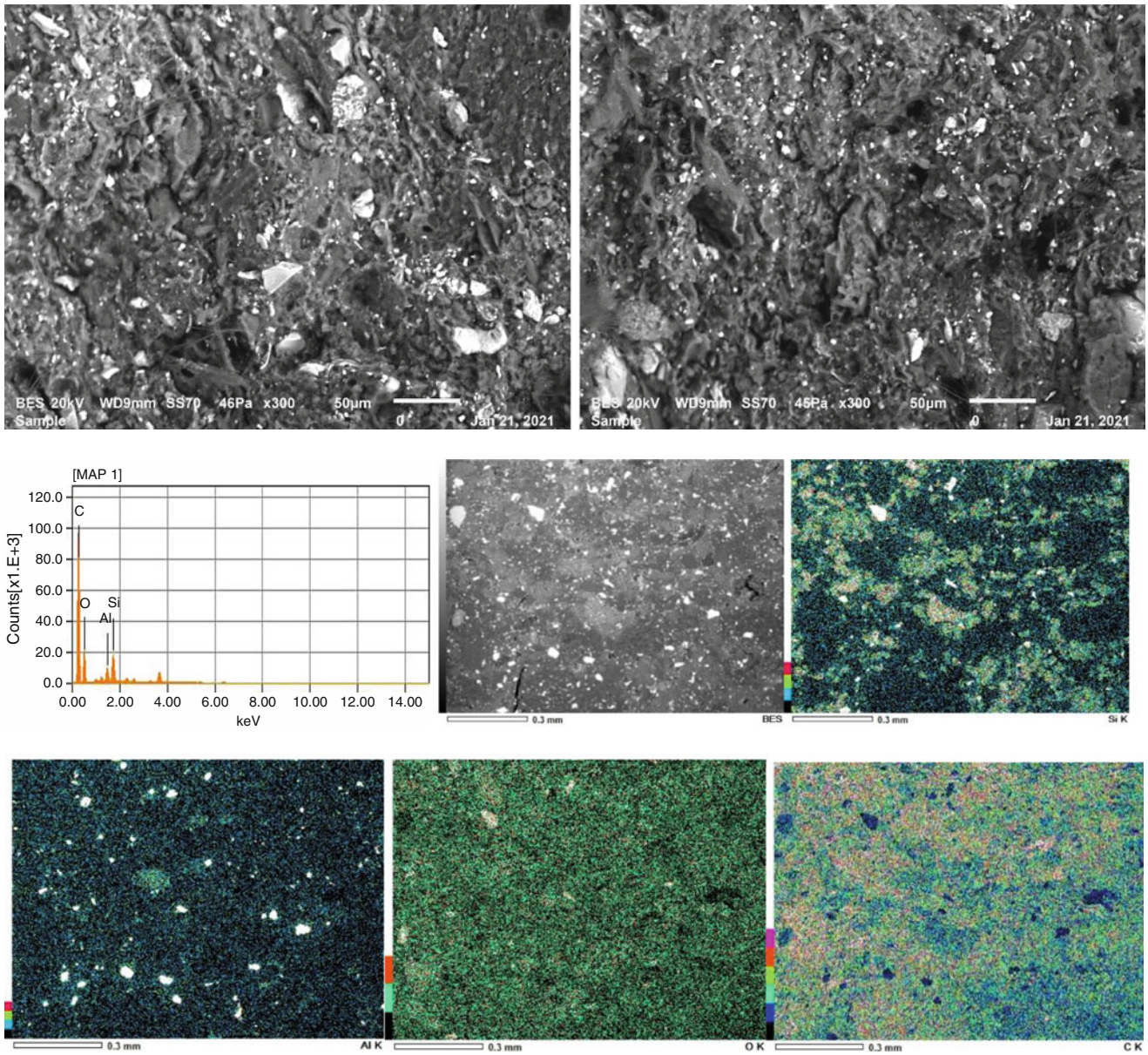

Fig. 10.5 (**a**) Fracture surface analyses for the composite of LIAMI_II. (**b**) EDS chemical and microstructural and mapping analyses for the composite of LII (LIAMI_II)

there are some local agglomerations of ceramic fibres and also glass bubbles in the matrix. As for the fracture surface analyses, all of the compositions have shown that there is a strong cohesion between the reinforcements and matrix. The ceramic fibres and glass bubbles seem to keep their position during the fracture and should play a mechanical bridge between the two parts of the microstructure. Additionally, some of the fracture surfaces present a layer structure due to the strong cohesion in the microstructure related to the chemical diffusion bonding. This property should be improved with the homogenous ball milling of the mixture.

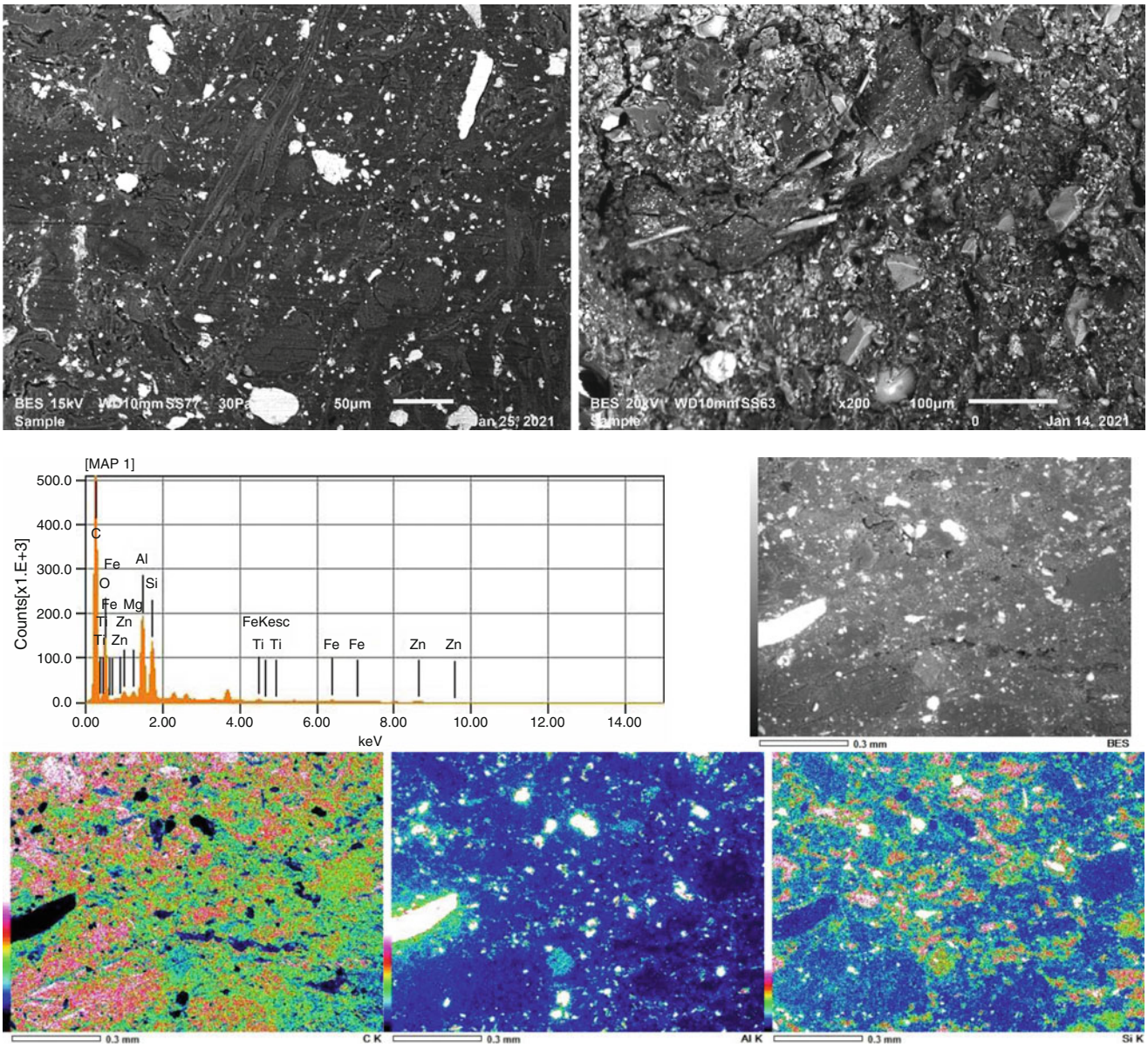

Fig. 10.6 (**a**) Microstructural (left) and fracture surface analyses (right) for the composite of RTiB-L. (**b**) EDS chemical and microstructural and mapping analyses for the composite of RTiB-L

10.4 Conclusions

The recycled rubber modified epoxy based composites reinforced with different ceramic fibres, GB and graphene nano platelets (GnPs) with a certain weight percentages have improved the mechanical properties of the composites such as flexural stress and fracture toughness (K_{IC}) and fracture energy ($G_{I}c$) values. These improvements are explained with a synergistic effect related to the basic physical properties of the individual reinforcements and chemical diffusion bonding between the matrix and/or between the reinforcements themselves by means of mutual diffusion mechanism. As well known, the fracture toughness and fracture energy values of the hybrid composites are always higher than that of single composites, evidently, the synergistic effect plays a significant role.

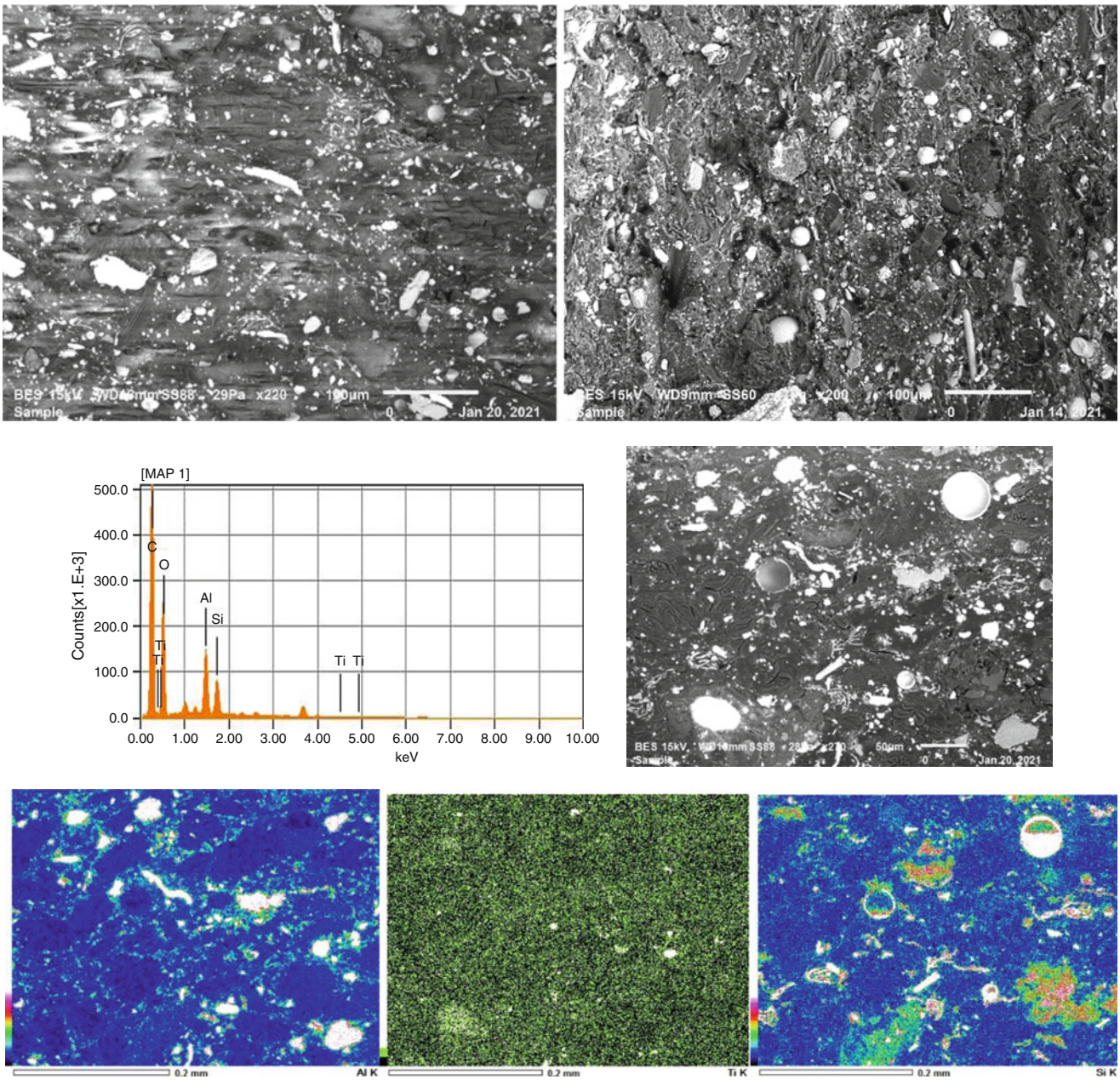

Fig. 10.7 (**a**) Microstructural, left and fracture surface analyses, right for the composite of PSYN-EX. (**b**) EDS chemical and microstructural and mapping analyses for the composite of PSYN-EX

The preliminary results obtained in the frame of the research project have given us an idea for the application of these novel composites designed with recycled rubber + epoxy. They can be used as the complementary components in the aircraft wings and/or in the helicopter. They can be also used as the internal structure in the aircraft after reducing problems with homogeneity. One interesting suggestion should be given here for aeronautical companies: the very high electrical conductivity of GnPs brings a new and original idea for the multi-functionality of these novel composites, and it may reduce the damage risk from lightning strikes.

Acknowledgments The authors thank Dr. Georges Zambelis from Airbus-Helicopters Paris/FR for his support and also for his valuable discussion for this research project. E. Bayraktar thanks Mr. Christophe BEN BRAHIM from electronic laboratory in Supmeca/Paris for materials and technical help.

References

1. Wan, C., Chen, B.: Reinforcement and interphase of polymer/graphene oxide nano composites. J. Mater. Chem. **22**, 3637–3646 (2012)
2. Burak Irez, A., Hay, J., Miskioglu, I., Bayraktar, E.: Scrap-rubber based composites reinforced with boron and alumina. In: Mechanics of Composite and Multi-functional Materials, vol. 6, pp. 1–10. Springer (2018)
3. Zhang, G., et al.: Effect of functionalization of graphene nanoplatelets on the mechanical and thermal properties of silicone rubber composites. Materials. **9**(2), 92 (2016)
4. Fu, S.-Y., Mai, Y.-W., Lauke, B., Yue, C.-Y.: Synergistic effect on the fracture toughness of hybrid short glass fiber and short carbon fiber reinforced polypropylene composites. Mater. Sci. Eng. **A323**, 326–335 (2002)
5. Dong, C., Davies, I.J.: Optimal design for the flexural behaviour of glass and carbon fibre reinforced polymer hybrid composites. Mater. Des. **37**, 450–457 (2012)
6. Zaimova, D., Bayraktar, E., Miskioglu, I.: Design and manufacturing of new elastomeric composites: mechanical properties, chemical and 179 physical analysis. Int. J. Composit. Part B. **1**(1), 1–12 (2016) (online 2017)
7. Irez, A.B., Bayraktar, E., Miskioglu, I.: Mechanical characterization of epoxy—scrap rubber based composites reinforced with alumina fibers. In: Mechanics of Composite and Multi-functional Materials, vol. 6, pp. 59–70. Springer (2017). ISBN 978-3-319-63408-1). https://doi.org/10.1007/978-3-319-63408-1
8. Ferreira, L.M.P., Miskioglu, I., Bayraktar, E., Katundi, D.: Mechanical and tribological properties of scrap rubber reinforced with Al_2O_3 fiber, aluminium and TiO_2. In: Mechanics of Composite and Multi-functional Materials, vol. 7, pp. 37–44. Springer (2016). ISBN 978-3-192 319-41766-0). https://doi.org/10.1007/978-3-319-41766-0
9. Masoud, F., Sapuan, S.M., Ariffin, M.K.A.M., Nukman, Y., Bayraktar, E.: Cutting processes of natural fiber-reinforced polymer composites. Polymers. **12**, 1332 (2020). https://doi.org/10.3390/polym12061332
10. Irez, A.B., Bayraktar, E.: Design of a low-cost aircraft structural material based on epoxy: recycled rubber composites modified with multifunctional nano. In: Mechanics of Composite and Multi-functional Materials, vol. 5, pp. 73–80. Springer (2019). https://doi.org/10.1007/978-3-030-30028-9_11
11. Burak Irez, A., Bayraktar, E., Miskioglu, I.: Flexural fatigue damage analyses of recycled rubber—modified epoxy-based composites reinforced with alumina fibres. FFEMS Fatigue Fract. Eng. Mater. Struct. (2019)
12. Burak, A., Zambelis, I.G., Bayraktar, E.: A new design of recycled ethylene propylene diene monomer rubber modified epoxy based composites reinforced with alumina fiber: fracture behavior and damage analyses. Materials. **12**(17), 2729 (2019). https://doi.org/10.3390/ma12172729
13. Burak Irez, A., Bayraktar, E., Miskioglu, I.: Fracture toughness analysis of epoxy-recycled rubber-based composite reinforced with graphene nanoplatelets for structural applications in automotive and aeronautics. Polymers. **12**, 448 (2020). https://doi.org/10.3390/polym12020448

Chapter 11
Manufacturing of Scrap Thin Sheet "Ni-Ti-Al" Based Composites Reinforced with Nb_2Al Through Hot-Forged Bonding: Sandwich Structures

H. M. Enginsoy, E. Bayraktar, D. Katundi, and A. Larbi

Abstract In the frame of the common research project, manufacturing of scrap thin sheet "Ni-Ti-Al" based composites reinforced with Nb_2Al/TiB_2 have been carried out through hot-forged bonding process of the composites for a high strength sandwich structure (>1500 MPa). Interface and bonding characteristics have also been examined of hot-forged composites, heat treated at 550 °C depending on the operational parameters under laboratory conditions. Formability behaviour and delamination phenomenon have been analysed by 3P bending tests. An intermetallic phase layer has been carried out between the titanium and aluminium sheets containing hard particles reinforcements during hot forging process. Finally, a high strength bonding has been carried out by mechanical joining and mutual chemical bonding diffusion during this process as a function of process temperature and time.

Numerical Approach: At this stage of the project, the primary objective would be to establish a continuum-based material model in order to capture the macroscopic behaviour of the targeted composite materials and numerically reproduce the results from the basic characterization tests (bending). The model was implemented for Finite Element Analysis Software ABAQUS/Explicit as a user subroutine VUMAT for explicit nonlinear finite element calculations. The second step would be modelling of the microstructure of the proposed hybrid Ni-Ti-Al based composites and simulate the behaviour of several RVEs and see the effect of the sintered-forging and different ratios of reinforcing particulates.

Keywords Ni-Ti-Al based composites · Sandwich structure · Bond strength · Chemical diffusion · Mechanical joining · 3P bending test

11.1 Introduction

High Strength Metal Based Composites (HSMBC) are composed of different types of different metals. The main idea for the design and manufacturing of these composites is to create the best properties of different materials to obtain more useful materials. The general properties of the metal based composites, such as strength, hardness, conductivity, etc. have been significantly improved by using an alternative low cost manufacturing structures called the sandwich structures. These structures contain several thin sheets from high strength materials. Several methods are generally used to create on the sheets such as such as diffusion bonding and deformation bonding, to prepare multilayer/sandwich composites. However, many of these processes are complex and expensive in process. This can limit the application of these structures in manufacturing engineering [1–6]. Among widely used processes for these structures is accumulative roll bonding (ARB) process that is an efficient method due to its simple operation and low cost manufacturing; however, this process also needs a long operation and is not so much practical for the mass production of these composites.

In the frame of the common research project, manufacturing of thin sheet "Ni-Ti-Al" based composites reinforced with Nb_2Al/TiB_2 have been carried out through hot-forged bonding process of the composites for a high strength sandwich structure (>1500 MPa). Interface and bonding characteristics have also been examined of hot-forged composites, heat treated at 550 °C depending on the operational parameters under laboratory conditions. Formability behaviour and delamination phenomenon have been analysed by 3P bending tests. An intermetallic phase layer has been carried out between the titanium

H. M. Enginsoy · E. Bayraktar (✉) · D. Katundi · A. Larbi
School of Mechanical and Manufacturing Engineering, Supmeca-Paris, Saint-Ouen, France
e-mail: emin.bayraktar@isae-supmeca.fr; dhurata.katundi@isae-supmeca.fr; abdelghani.larbi@isae-supmeca.fr

V. Chalivendra et al. (eds.), *Mechanics of Composite, Hybrid and Multifunctional Materials, Fracture, Fatigue, Failure and Damage Evolution, Volume 3*, Conference Proceedings of the Society for Experimental Mechanics Series,
https://doi.org/10.1007/978-3-030-86741-6_11

Table 11.1 Compositions of the specimens for sandwich composites (wt. %)

Specimen name	Ni	Ti	Al	Minors Nb, B, etc.
Ni-Ti-Al	30	30	40	X1, X2, X3

and aluminium layers containing hard particles reinforcements during hot forging process. Finally, a high strength bonding has been carried out by mechanical joining and mutual chemical bonding diffusion during this process as a function of process temperature and time. A practical numerical approach model was implemented for Finite Element Analysis Software ABAQUS/Explicit as a user subroutine VUMAT for explicit nonlinear finite element calculations.

11.2 Experimental Conditions

Commercially pure Ni, Ti, Al were used as initial materials in this research. The mean thickness of each thin sheet was variable between 0.1 and 0.2 mm, Ni, Ti and Al thin scrap sheets were cut into circles shape with 50 mm in diameter (Table 11.1). After cleaning to degrease them, a sandwich structure was stacked together and heated up to 250 °C under pressure in a matrix for 15 min. For certain special composites, these thin sheets were reinforced with fine Nb_2Al and/or TiB_2 powder to improve certain properties. Actually this common research project is going on for certain aeronautical applications for turbo-compressors. At the second stage, this structure was hot forged as a heat treatment process at 550 °C depending on the operational parameters under laboratory conditions. Formability behaviour and delamination phenomenon have been analysed by 3P bending tests (ASTM D790). An intermetallic phase layer has been carried out between the titanium and aluminium layers containing hard particles reinforcements during hot forging process. Finally, a high strength bonding has been carried out by mechanical joining and mutual chemical bonding diffusion during this process as a function of process temperature and time. Dynamic Scanning Calorimetric Analyses (DSC) have also been done to observe the transformation point during the hot forging process. A practical numerical approach model was implemented for Finite Element Analysis Software ABAQUS/Explicit as a user subroutine VUMAT for explicit nonlinear finite element calculations.

11.3 Results and Discussion

Figure 11.1 shows a detail manufacturing process of these sandwich structures by using a hot forging heat treatment process.

3P Bending tests (ASTM D790) have been carried out on the Zwick testing machine to evaluate formability and mechanical behaviours of these structures.

Microstructural and EDS chemical analyses were presented in Fig. 11.2 with the mapping for the composite obtained by hot-forged compaction process.

Here there is a clear observation between thin sheets after the hot forging process. All of the mapping parts indicated that there is a very strong cohesion and fusion between thin sheets.

Detail interface analyses were also shown in Fig. 11.3. Here a strong cohesion between thin sheets is carried out during the hot forging and a strong diffusion between the sheets. Any decohesion was observed after the heavily deformation up to 25–30% with 3P bending tests.

Again, from Fig. 11.3, one may observe that an intermetallic phase layer has been carried out successfully between the titanium and aluminium layers containing hard particles reinforcements during hot forging process. Finally, a high strength bonding has also been carried out by mechanical joining and mutual chemical bonding diffusion during this process as a function of process temperature and time.

As well known, Differential Scanning Calorimetry (**DSC**) is a thermal **analysis** technique in which the heat flow into or out of a sample is measured as a function of temperature or time, while the sample is exposed to a controlled temperature program. Figure 11.4 gives a detail information of DSC analyses on the "Ni-Ti-Al" composite that show a transformation point at the level of 230 °C depending on the time and heating process.

As for 3P bending tests (ASTM D790), all of the test results have been presented in Fig. 11.5 deformed at the three different deformation speed. To observe the stress distribution in case of the deformation under the 3P bending test conditions, ABAQUS/Explicit® was used for modelling under different test conditions.

Fig. 11.1 Manufacturing process by using a hot forging process; forging tool (matrix) is heated under pressure and the control is carried hot by using a hot compaction software

A subroutine was created in FORTRAN for microstructural simulation of the constituents and modelling of the Representative Volume Element (RVE) for composites with different ratios of the reinforcement particles [7–11]. Three-point bending impact test specimens were modelled with average thickness of 4 mm and width value of 12.5 mm in Figs. 11.5 and 11.6.

Also, the total length between the bottom supports was taken as 20 mm and all support contacts used during the test were modelled as 5 mm radius. Three-point bending test apparatus of linear test velocities are V1-V2-V3. This apparatus bottom surfaces in the macrostructure are completely ALLDOF fixed. Within both these test simulations, Al matrix and reinforcing particles were meshed using modified 10-node tetrahedral C3D10M mesh type with adaptive automatic meshing algorithm.

Figure 11.5 shows these 3PB test results for both of experimental and multiscale modelling, obtained on the three different velocities of composites. The same idea was given in Fig. 11.6 to observe the maximum stress distribution under the punch during the 3P bending test for three different bending velocities, respectively.

11.4 Conclusions

In the frame of the common research project, manufacturing of the scrap thin sheet “Ni-Ti-Al” based composites reinforced with Nb_2Al/TiB_2 have been carried out through hot-forged bonding process of the composites for a high strength sandwich structure. Interface and bonding characteristics have also been examined of hot-forged composites, heat treated at 550 °C depending on the operational parameters under laboratory conditions.

A successful formability behaviour was observed and there was any delamination/decohesion phenomenon during the 3P bending tests. An intermetallic phase layer has been carried out between the titanium and aluminium sheets containing hard particles reinforcements during hot forging process. Finally, a high strength bonding has been carried out by mechanical joining and mutual chemical bonding diffusion during this process as a function of process temperature and time. DSC results have given a detail information on the transformation behaviour of this composite. ABAQUS/Explicit® was used for modelling under different test conditions. A subroutine was created in FORTRAN for microstructural simulation of the constituents and modelling of the Representative Volume Element (RVE) for composites.

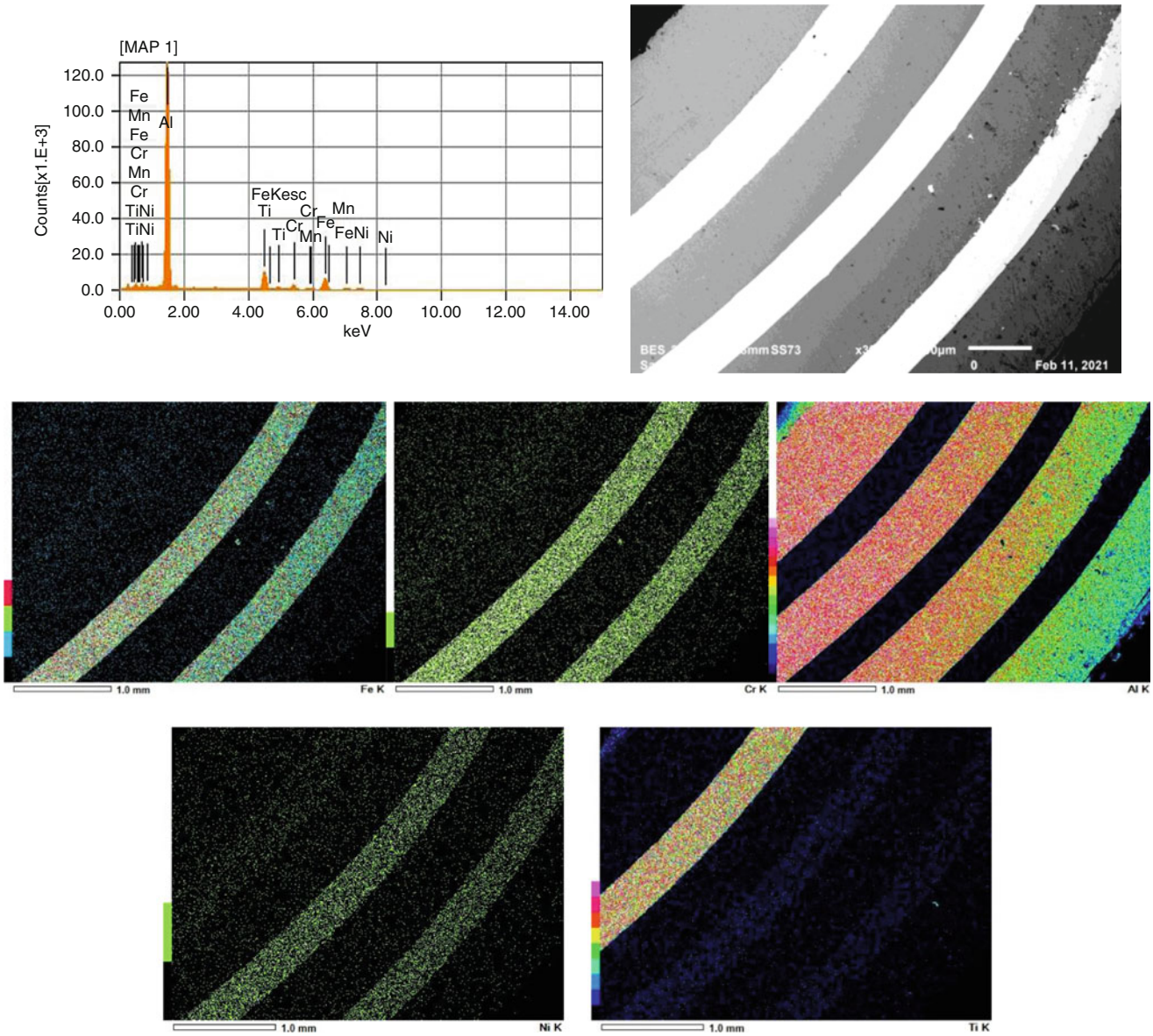

Fig. 11.2 EDS chemical analyses, mapping and microstructure of the Ni-Ti-Al composite after the 3P bending test for showing a strong cohesion due to the diffusion bonding

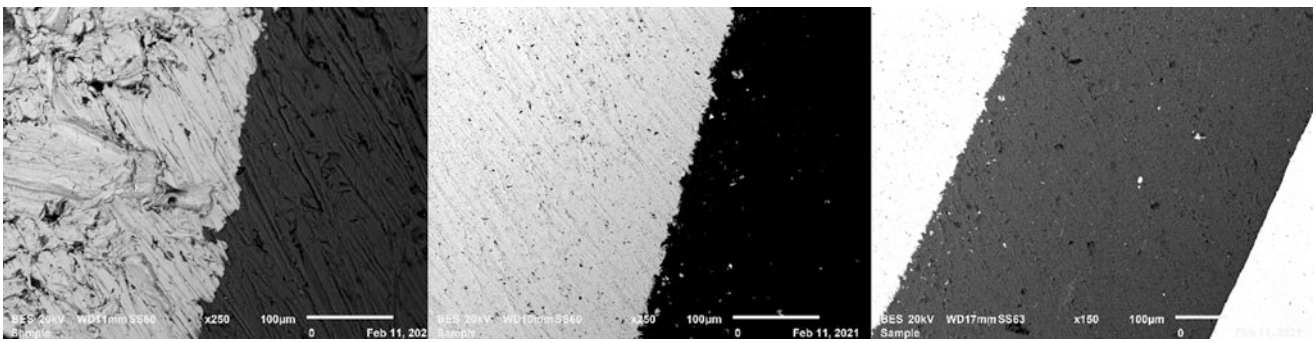

Fig. 11.3 Interface and diffusion bonding between each sheet part after the 3-point bending test

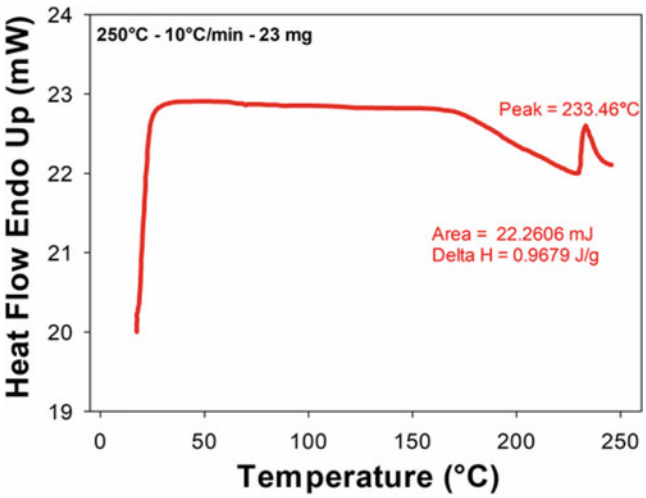

Fig. 11.4 Differential Scanning Calorimetric (DSC) analysis for the "Ni-Ti-Al" composite

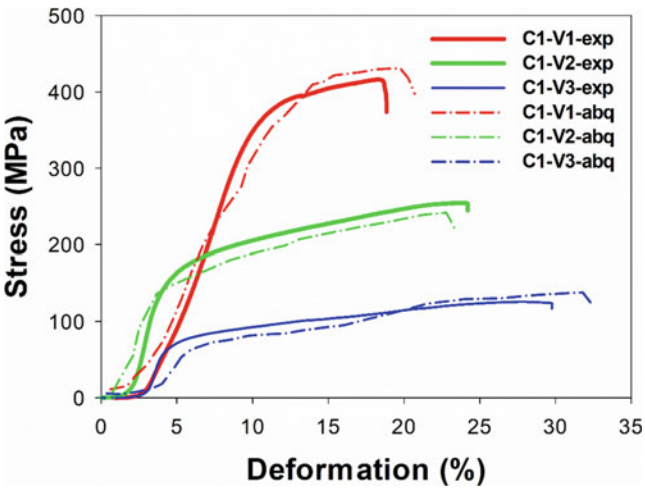

Fig. 11.5 Three-point bending test results

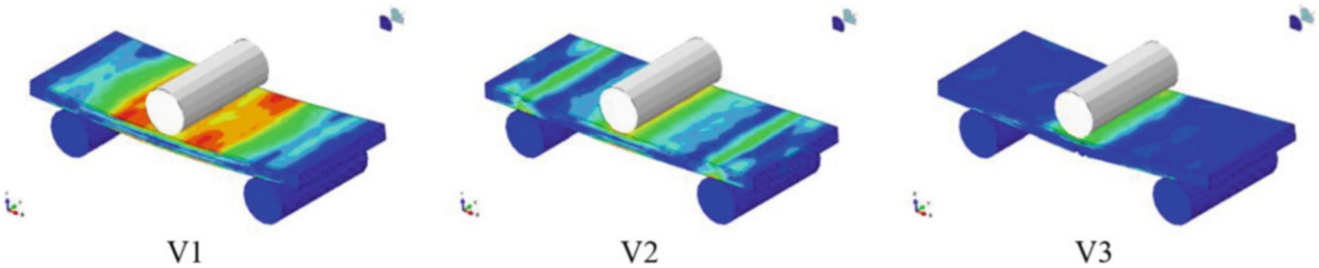

Fig. 11.6 3P Bending test final maximum stress results for three different bending velocities respectively

References

1. Mozaffari, A., Manesh, H.D., Janghorban, K.: Evaluation of mechanical properties and structure of multilayered Al/Ni composites produced by accumulative roll bonding (ARB) process. J. Alloys Compd. **489**, 103–109 (2010)
2. Mahdavian, M.M., Khatami-Hamedani, H., Abedi, H.R.: Macrostructure evolution and mechanical properties of accumulative roll bonded Al/Cu/Sn multilayer composite. J. Alloys Compd. **703**, 605–613 (2017)

3. Min, G., Lee, J.M., Kang, S.B., Kim, H.W.: Evolution of microstructure for multilayered Al/Ni composites by accumulative roll bonding process. Mater. Lett. **60**(27), 3255–3259 (2006)
4. Williams, J.J., Segurado, J., LLorca, J., Chawla, N.: Three dimensional (3D) microstructure-based modeling of interfacial decohesion in particle reinforced metal matrix composites. Mater. Sci. Eng. A. **557**, 113–118 (2012)
5. Ye, N., Rena, X., Liang, J.: Microstructure and mechanical properties of Ni/Ti/Al/Cu composite produced by accumulative roll bonding (ARB) at room temperature. J. Mater. Res. Technol. **9**(3), 5524–5532 (2020)
6. Bayraktar, E., Katundi, D., Gatamorta, F., Miskioglu, I., Murat Enginsoy, H.: Design of recycled thin sheet "Ti-Al" based composites 3Reinforced with AA1050, boron, TiB_2, TiC, and B_4C through hot-forged bonding (Chapter 10). In: Composite, Hybrid and Multifunctional Materials, vol. 6. Springer (2020, ISBN 978-3-030-59867-9). https://doi.org/10.1007/978-3-030-59868-6-10
7. Ekici, R., Kemal Apalak, M., Yildirim, M., Nair, F.: Simulated and actual micro-structure models on the indentation behaviors of particle reinforced metal matrix composites. Mater. Sci. Eng. A. **606**, 290–298 (2014)
8. Liu, F.R., Chan, K.C., Tang, C.Y.: Numerical modeling of the thermo-mechanical behavior of particle reinforced metal matrix composites in laser forming by using a multi-particle cell model. Compos. Sci. Technol. **68**(9), 1943–1953 (2008)
9. Çetin, A., Kalkanli, A.: Numerical simulation of solidification kinetics in A356/SiCp composites for assessment of as-cast particle distribution. J. Mater. Process. Technol. **209**, 4795–4801 (2009)
10. Galli, M., Botsis, J., Janczak-Rusch, J.: An elastoplastic three-dimensional homogenization model for particle reinforced composites. Comput. Mater. Sci. **41**, 312–321 (2008)
11. Chawla, N., Sidhu, R.S., Ganesh, V.V.: Three-dimensional visualization and microstructure-based modeling of deformation in particle-reinforced composites. Acta Mater. **54**, 1541–1548 (2006)

Chapter 12
Recycled Niobium-Aluminium (Nb_2Al) Intermetallics Based Composite Design: An Experimental and Numerical Approach for Toughening Mechanism

H. M. Enginsoy, E. Bayraktar, F. Gatamorta, D. Katundi, and I. Miskioglu

Abstract In this project, design of niobium-aluminium (Nb_2Al) intermetallics based composites is proposed by using the fresh scrap recycled niobium and aluminium alloy AA7075. These compositions will be the target for aeronautical engineering applications for high temperature service conditions. Manufacturing of these composites is an important engineering case for tailored behaviour of the composites produced through combined method of powder metallurgy route; sintering followed by forging. Different materials and operational (process) parameters will be used for optimization of the compositions. All of the analyses will be devoted to the static (compression, 3-point bending) test conditions. Microstructure analyses (matrix/interface) will be carried out by Scanning Electron Microscope (SEM). At this stage of the project, the primary objective would be to establish a continuum-based material model in order to capture the macroscopic behaviour of the targeted composite materials and numerically reproduce the results from the basic characterization tests (3P bending). The model will be implemented for Finite Element Analysis Software ABAQUS/Explicit as a user subroutine VUMAT for explicit nonlinear finite element calculations. The second step would be modelling of the microstructure of the proposed hybrid Nb_2Al based composites and simulate the behaviour of several RVEs and see the effect of the sintered-forging and different ratios of reinforcing particulates.

Keywords Intermetallic composites · Nb-Al · Sinter-forging · Fracture toughness · SEM analyses · Finite element analyses

12.1 Introduction

Niobium is a noble metal for engineering applications. Actually, Brazil has a major niobium mining and produces 90% of the niobium in the world as a raw material. However, the processing of this metal beginning from mining up to the advance processing for the real manufacturing engineering applications is very expensive and requires a sophisticated equipment and investment. However, very huge amount of scraps of the niobium coming from manufacturing of the pieces is not reprocessed efficiently as valuable and economic way because quasi all of the scarps goes to the waste. The niobium scraps as an important secondary source of the raw materials should be evaluated for the manufacturing of the new composite design. As not possible to extract in an economical way, the recycling of niobium could be a sustainable occasion for the aeronautical and nuclear power plants applications [1–6].

H. M. Enginsoy · D. Katundi
School of Mechanical and Manufacturing Engineering, Isae-Supmeca-Paris, Saint-Ouen, France
e-mail: dhurata.katundi@isae-supmeca.fr

E. Bayraktar (✉)
School of Mechanical and Manufacturing Engineering, Isae-Supmeca-Paris, Saint-Ouen, France

University of Campinas-UNICAMP-FEM, Campinas, SP, Brazil
e-mail: emin.bayraktar@isae-supmeca.fr

F. Gatamorta
University of Campinas-UNICAMP-FEM, Campinas, SP, Brazil
e-mail: fabiog@fem.unicamp.br

I. Miskioglu
ME-EM Department, Michigan Technological University, Houghton, MI, USA
e-mail: imiski@edu.mtu

V. Chalivendra et al. (eds.), *Mechanics of Composite, Hybrid and Multifunctional Materials, Fracture, Fatigue, Failure and Damage Evolution, Volume 3*, Conference Proceedings of the Society for Experimental Mechanics Series,
https://doi.org/10.1007/978-3-030-86741-6_12

The present work review of the efficient and sustainable recycling of the fresh scraps of niobium metal and also aluminium (AA 7075) alloy in the frame of the common research project is carried out between UNICAMP-Brazil and SUPMECA-France. In this work, Nb2Al intermetallic matrix composites were designed by using the combined method, sinter+forging through the powder metallurgy route. Niobium powder obtained fresh scrap by using high energy milling was used as main reinforcement element for the present work. As secondary reinforcements, fine Ni–Al intermetallics, TiC, Zr_2O_3, Cu powders were added in the matrix in order to prepare three different compositions. This process consists of the mixing, blending by high energy milling and compacting of the final composition through the combined method, sinter+forging. In the final stage, material parameters were optimized for improving physical and mechanical properties of these composites. Microstructures were analyzed by the Scanning Electron Microscope (SEM). The continuum-based material model will be implemented for Finite Element Analysis Software ABAQUS/Explicit as a user subroutine VUMAT for explicit nonlinear finite element calculations. The second step would be modelling of the microstructure of the proposed hybrid Nb_2Al based composites and simulate the behaviour of several RVEs and see the effect of the sintered-forging and different ratios of reinforcing particulates.

12.2 Materials, Experimental Methods and Finite Element Analysis

In this study, a new design alternative Nb-Al and Nb_2Al intermetallics based composites were designed by aeronautic company in Brazil. Fresh scrap niobium chips coming from the machining and other scraps in different sizes were gas atomized. After atomization, aluminium and niobium scraps were homogenized by high energy milling with planetary ball mill for 1 h and doped to prepare the matrix. At the second stage, other reinforcements were added to prepare three different compositions. Each composition was homogenized by ball milling for 4 h again with a ratio of ball/powder 20:1. To obtain a homogenous mixture with good wettability of the reinforcements with the matrix, pure nano aluminium (3 wt %) powder was added in each mixture. Again, 2 wt % Zn-Stearate was also added in each mixture for the lubrication and hindering the oxidation of the mixture during the milling. Final compositions used were given in Tables 12.1 and 12.2. After solid state sintering (700 °C) of all of the composites, all of the three composites (Nb-I, Nb-II and Nb-III, called after here as C1, C2 and C3) were processed by the combined method called sinter + forging [2–6].

Microstructural analyses are performed by scanning electron microscope (SEM). The dispersion of reinforcement particles in the matrix and interface at matrix/reinforcements was also evaluated.

Microhardness tests ($HV_{0.1}$) were conducted on the polished and etched specimens. The microhardness values were measured and the values are variables between 450 and 600 HVN with ±15% accuracy for the composites designed here under the laboratory conditions.

All the density measurements of the specimens were carried out by using Archimedes method. These values changed between 3 and 3.25 g/cm^3 with ±10% accuracy, respectively.

Quasi-static compression tests (DIN 50106) were carried out with a Zwick mechanical test system at the three different strain rates of 1 mm/min. For each manufacturing process, 3–4 cylindrical specimens ($H/D \geq 1.5$) were used. In the same way, 3-Point Bending (3 PB) tests (ASTM D 790) were carried out for only at the strain rate of 1 mm/min.

Figure 12.1 shows XRD diagram and fine scrap chips from the Nb and Nb_2Al composites. At the first stage, these fresh scraps were used after atomization followed by ball milling and the same process was applied for fine chip for AA7075 alloy before preparing the compositions.

Table 12.1 Compositions of the composites prepared in two groups (wt. %)

Composition name	Nb2Al + Recycled Nb	Recycled AA7075	TiC	NiAl	Zr_2O_3	Cu	Zn	TiH_2
C-I	B	30		8	5	2	0. 5	
C-II	B	40	5	2		2	0.5	0.1
C-III	B	30	2	2	2	2	2	

Table 12.2 Chemical composition of scrap AA 7075 alloy (wt. %)

Element	Al	Cu	Fe	Mg	Mn	Si	Ni	Zn	Cr	Zr
wt. %	Balance	1.48	0.23	2.11	0.07	0.10	0.01	5.29	0.22	0.02

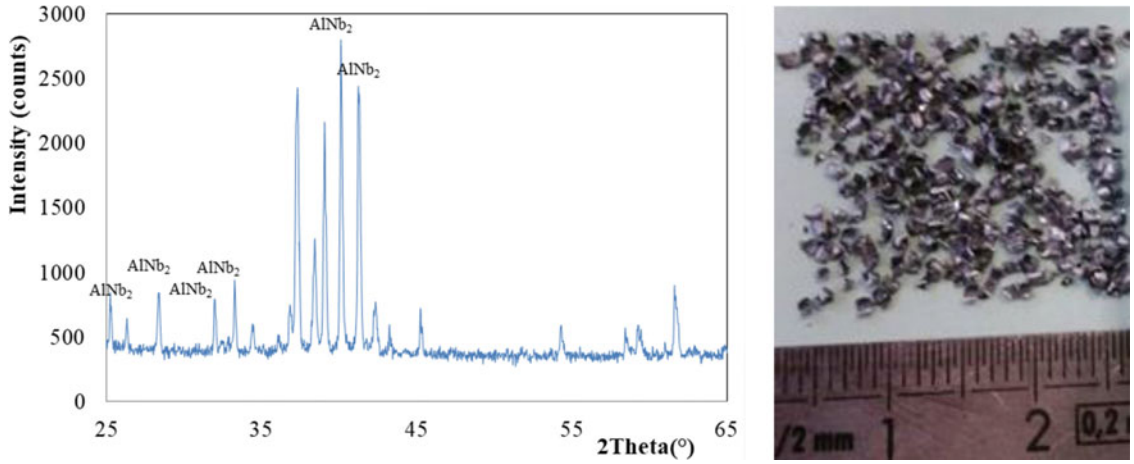

Fig. 12.1 XRD diagram and fine scrap chips from the Nb-Al composites

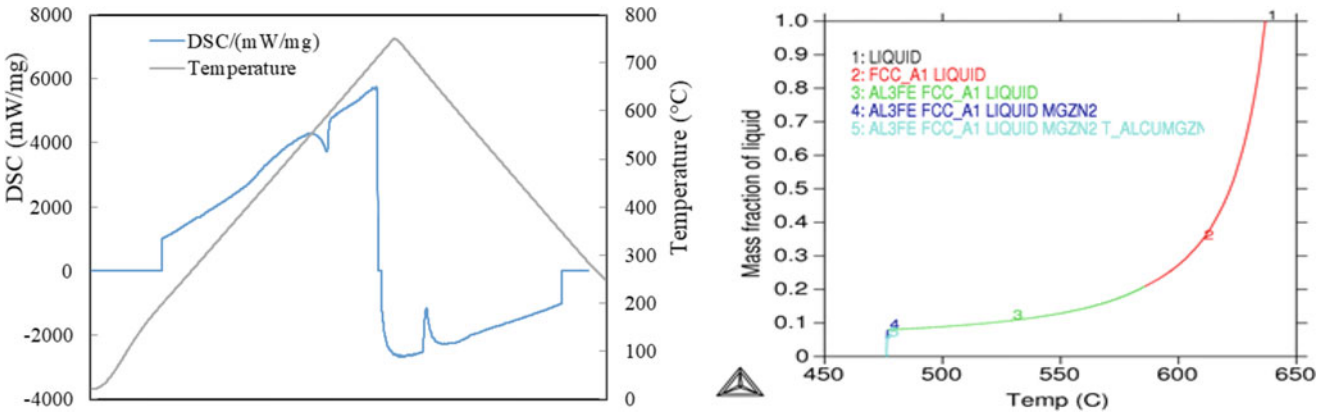

Fig. 12.2 Differential Scanning Calorimetry (DSC) diagram and heating conditions of AA7075 fine chips

Figure 12.2 shows Differential Scanning Calorimetry (DSC) result for AA7075 used as the matrix in this work, to determine the critical transformation points during the heating and cooling stages. Different conditions of AA7075 fine chips and general microstructure were also presented in Fig. 12.1 before milling prepared for the sintered specimen.

In Fig. 12.3, binary phase diagram of Niobium-Aluminium (Nb-Al) couple was shown. Regarding this diagram, the design of composites made in this work is found around certain intermetallic zones (Nb_2Al and Al_3Nb). The main reinforcement of Nb was at the same amount in the all of the five composites presented here [1].

Modelling of the mechanical behaviour of heterogeneous metal matrix composites under different physical conditions is very complex with finite element analysis. Particle shape/size and inhomogeneous spatial distribution of particles are important factors in the microstructural design for analytical and numerical modelling [7–12]. In this study, nonlinear simulations of micro- and macrostructures were studied by means of finite element method. A commercial software ABAQUS/Explicit® is used for macrostructural modelling under different test conditions. A subroutine was created in FORTRAN for microstructural simulation of the constituents and modelling of the Representative Volume Element (RVE) for composites with different ratios of the reinforcement particles.

The isotropic matrix hardening during plastic deformation is given in Eq. (12.1).

$$\sigma_m^{eq} = A\left[\varepsilon_m^p\right]^n \tag{12.1}$$

where σ_m^{eq}: Von Mises equivalent stress, $\left[\varepsilon_m^p\right]^n$: accumulated plastic strain, $A = 400$ MPa and $n = 0.15$, typical Al constants.

Representative Volume Element (RVE) is used for heterogenic distribution and close to realistic irregular particle microstructure modelling [13–17]. It describes that complex composite structure and boundary conditions of particle reinforced structural formation equation with metal matrix composites are defined in the RVE.

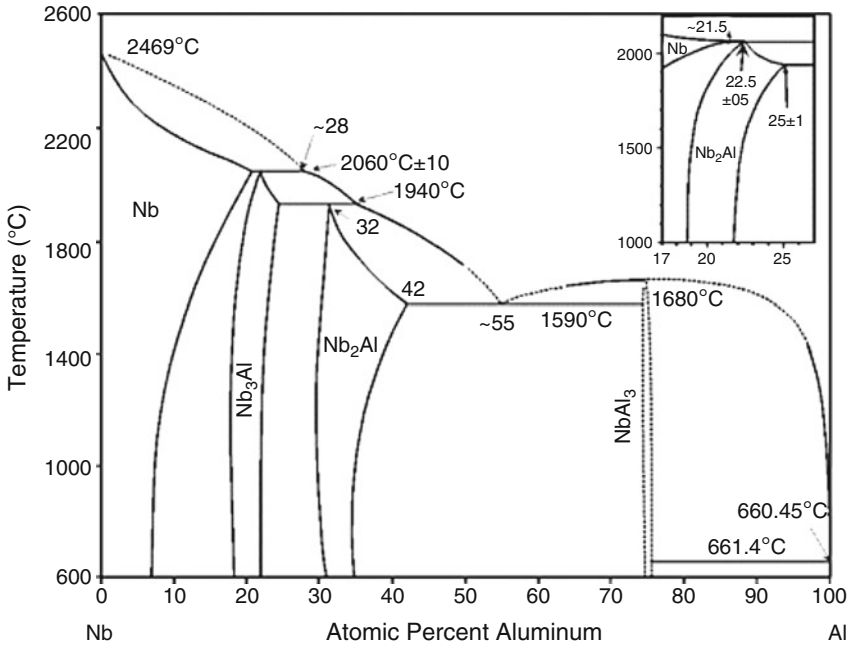

Fig. 12.3 Binary phase diagram of Nb Aluminium taken from ASM Metals Handbook [1]

Reinforcement particulates have been used for their phases respectively to determine each of the phases as volume in the RVE by Eqs. (12.2)–(12.5).

$$v_0 = \frac{V_0}{V} \tag{12.2}$$

$$v_1 = \frac{V_1}{V} = 1 - V_o \tag{12.3}$$

$$v_2 = \frac{V_2}{V} = 1 - (V_o + V_1) \tag{12.4}$$

$$v_n = \frac{V_n}{V} = 1 - (V_o + V_1 + \cdots + V_{n-1}) \tag{12.5}$$

where v_0, v_1, ...v_5 are volumes for reinforcement particulates in the RVE, respectively. Microstructure formed in the sintering result stress-strain behaviour is given in Eq. (12.6) [17].

$$\varepsilon_{ij} = \frac{\partial}{\partial \sigma_{ij}} [\Phi(d, D, T, \sigma_e, \sigma_m - \sigma_s)] \tag{12.6}$$

where d: grain size, D: relative density, T: sintering temperature, σ_e: Von Mises effective stress, σ_m: mean stress, σ_s: sintering potential.

High local stresses caused by particle surfaces are the principle responsabile of the initial damage that began in the microstructure. These results are also given by means of three-point bending tests. Then progressive damage occurred towards the macro-level of metal matrix composites.

Damage evolution law of exponential softening with evolution based on energy and stress components in traction-separation modelling of metal matrix composites is used with Eqs. (12.7) and (12.8).

$$\begin{aligned} t_n &= \begin{cases} (1 - \overline{D})\bar{t}_n, & \bar{t}_n \geq 0, \\ \bar{t}_n, & \text{if not,} \end{cases} \\ t_s &= (1 - \overline{D})\bar{t}_{s,} \\ t_t &= (1 - \overline{D})\bar{t}_t \end{aligned} \tag{12.7}$$

$$\overline{D} = \int_{\delta_m^0}^{\delta_m^f} \frac{T_{\text{eff}} d\delta}{G^C - G_0} \tag{12.8}$$

where $\overline{D}$: accumulated in the interface damage, G^C: fracture energy, G^0: elastic energy, T_{eff}: effective traction at damage initiation, $\overline{t}_n - \overline{t}_s - \overline{t}_t$: maximum nominal traction parameters, $\delta_m^0 - \delta_m^f$: initial thickness boundary conditions.

Cohesive Zone Model (CZM) is used to determinate relation as a surface based contact formula given in Eq. (12.9) between the reinforcement particles in the aluminium matrix phase in the microstructure.

$$\Gamma = \frac{1}{2} t \delta^f \tag{12.9}$$

where Γ: fracture energy, t: cohesive interfacial strength, δ^f: interfacial separation.

12.3 Results and Discussion of Experimental and Finite Element Analysis

12.3.1 Microstructural Analyses

In general way, mapping elementary analyses give a carefulness observation on the microstructure, the distribution of the reinforcements can be observed as very fine particles in micro size by means of "Mapping" analysis. All of the microstructures of the composites show the distribution of the reinforcements in the matrix very clearly. Even though the recycled chips used in this study were atomized before preparing the composite, the size of the chips varied between 10 and 30 μm. For this reason, the combined process that we call "sinter + forging" improves the distribution of reinforcements in the final structure homogenously. This difference should be more comprehensible with the mechanical test results.

That is the reason why we recommend this process especially for the recycled constituents as a low cost, alternative and more advantageous manufacturing process to design the composite efficiently [2–6].

More and less, all of the microstructures have shown the reinforcement effect on the microstructure. Many of these composites show a eutectic reaction due to chemical diffusion bonding between the reinforcements and the matrix basically, Nb, and Ni-Al due to easy diffusion of these elements in the matrix. For this reason, the combined process (Sinter + Forging) helps so much for a tough and sound microstructure of the hybrid composites.

Figure 12.4a–c present the microstructure of the composites taken from the "sintered + forged" specimen with "EDS" chemical analysis obtained on the "SEM" with BSE (Back Scattered) option.

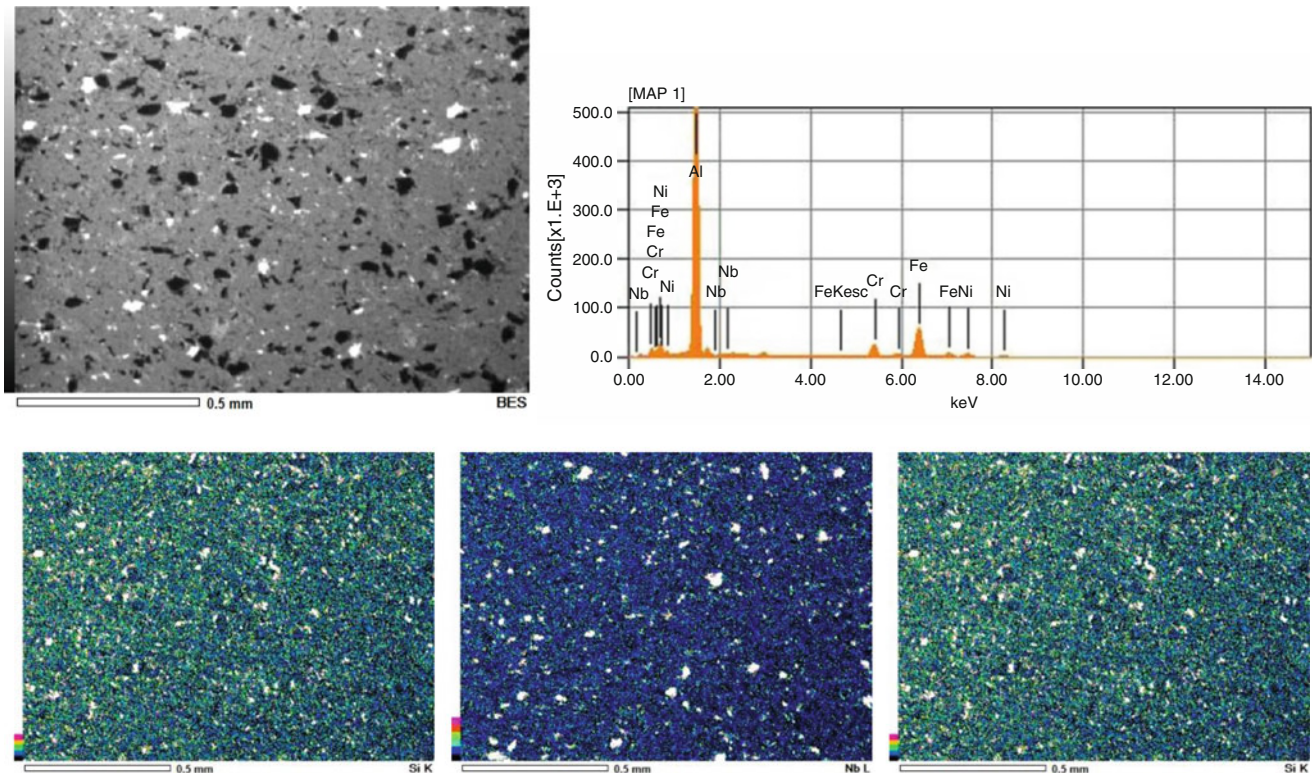

Fig. 12.4 Mapping elementary analyses of the three composites produced by the combined process; "Sinter + Forging" for showing the distribution of the reinforcements in the microstructure. (**a**) Mapping elementary analyses of the composite of C-I (Nb2Al-I). (**b**) Mapping elementary analyses of the composite of C-II (Nb2Al-II). (**c**) Mapping elementary analyses of the composite of C-III (Nb2Al-III)

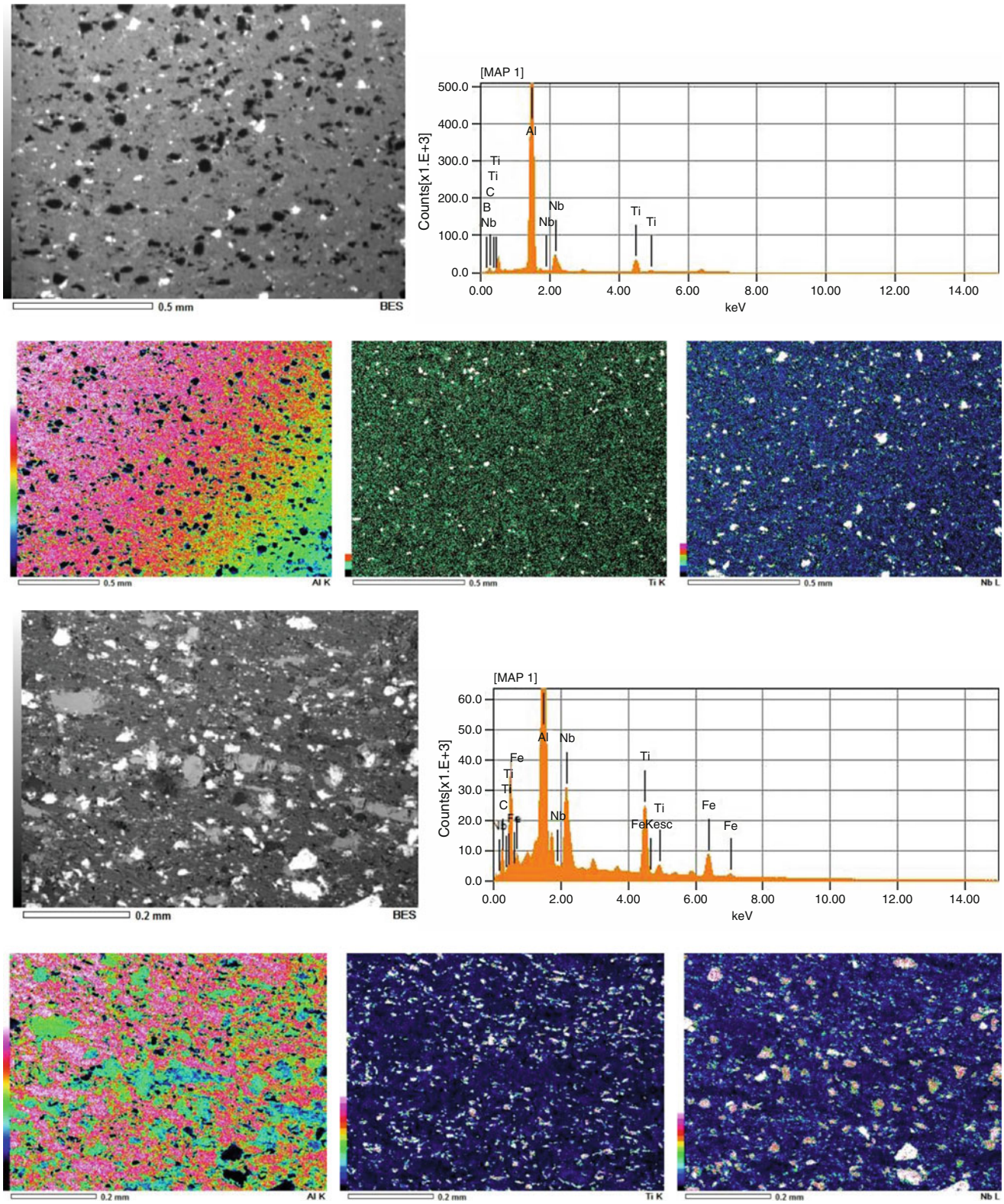

Fig. 12.4 (continued)

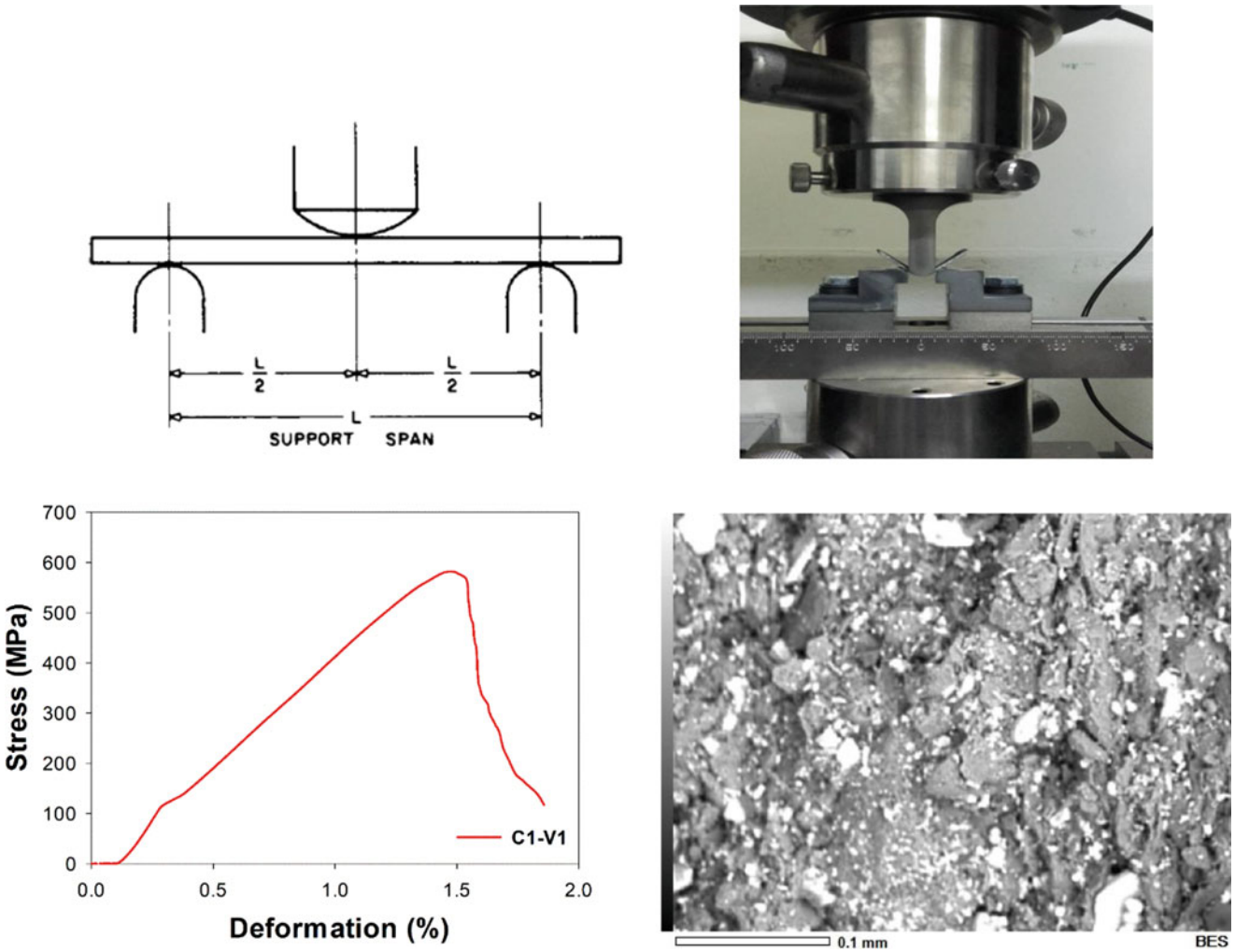

Fig. 12.5 Schematic presentation of the 3P bending test (ASTM790) and experimental set-up. Strain-deformation behaviour and fracture surface of the composite structure after the bending test

12.3.2 Three-Point Bending Test Results

Analyses of damage behaviour of the Nb2Al-Nb based composites have been evaluated by using 3P bending tests under quasi-static test conditions. The experimental test was carried out according to the ASTM 790. Standard test specimens were prepared from sintered forged composite. Figure 12.5 presents all of the set-up installed on the Zwick mechanical test system at the strain rate of 1 mm/min. Here, strain-deformation behaviour and fracture surface analyses of the composite structure were also presented after the bending test.

One may observe from these pictures an internal crack at the centre of the fracture surface after the test. Very tough structure is observed with very strong cohesion of the particles with the matrix.

12.3.3 Static Compression Test Results

In the frame of this present work, simple static compression tests were carried out under the laboratory scales to evaluate the mechanical behaviour of these novel composites produced with sinter + forging processes.

Figure 12.6a–c show all of the static compression test results at the three different strain rates obtained on the specimens produced by sinter + forging processes (Nb-Al-I, II, III called after here as CI, CII and C-III). These values are mean values obtained from 3 to 4 tests for each composition. Standard deviation is variable around ±30–40 MPa.

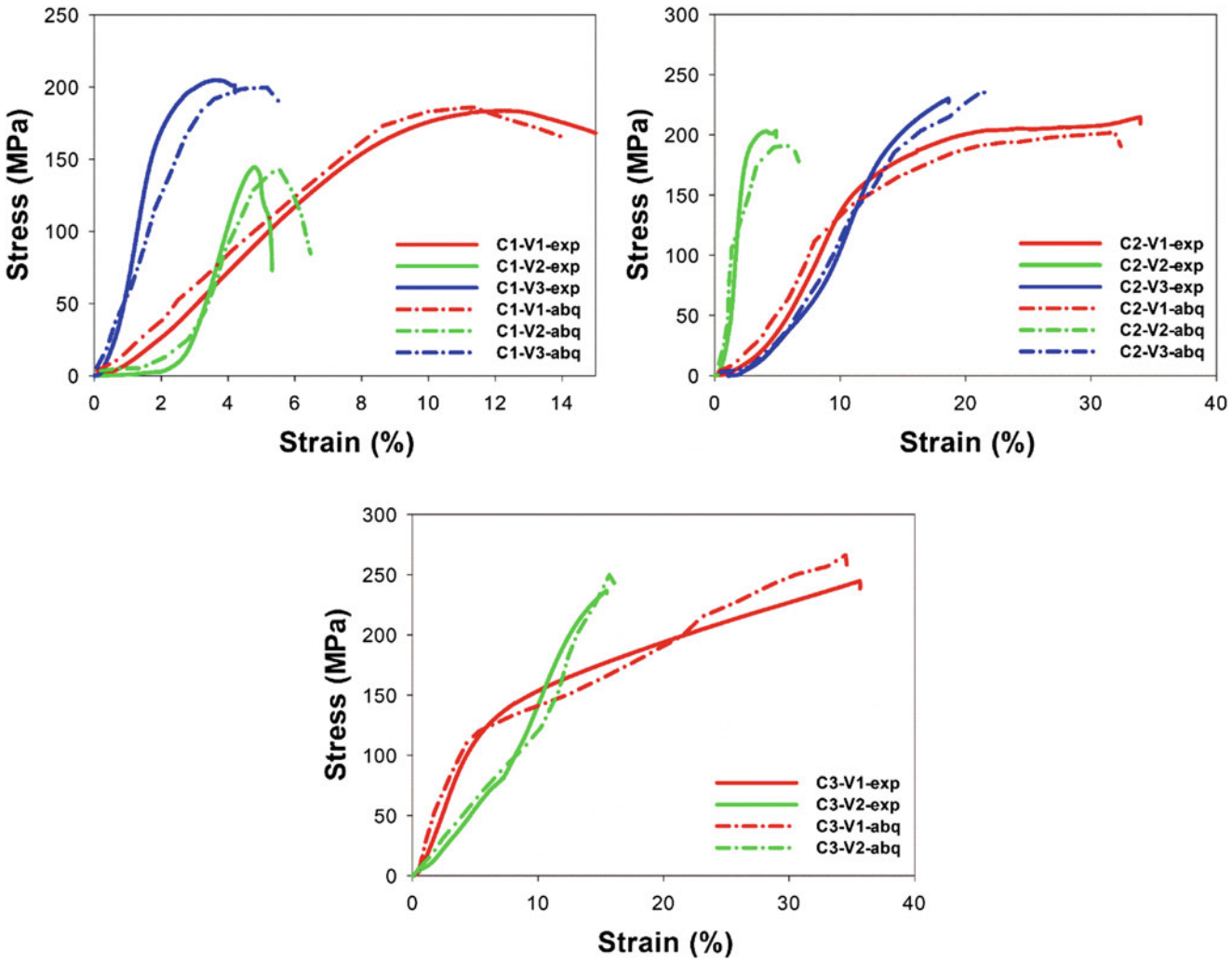

Fig. 12.6 (**a**) Quasi-static compression test (as a mean value) results for sintered + forged C1 specimens. (**b**) Quasi-static compression test (as a mean value) results for sintered + forged C2 specimens. (**c**) Quasi-static compression test (as a mean value) results for sintered + forged C3 specimens

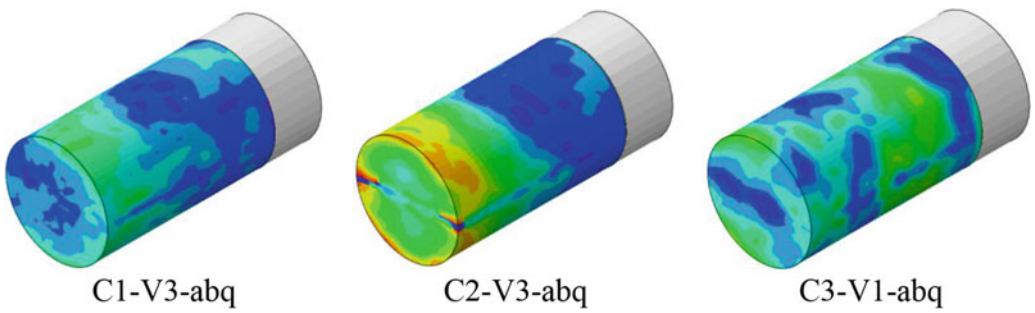

Fig. 12.7 Distribution of the maximum stresses in the compression test specimens from Fig. 12.6a–c

Distribution of the maximum stresses in the compression test specimens were shown here in Fig. 12.7. A nonlinear simulations of micro- and macrostructures have been carried out by means of finite element method. This macrostructural modelling was carried out under different experimental test conditions. Microstructural simulation of the constituents and modelling of the RVE for these composites have been carried out with different ratios of the reinforcement particles.

12.4 Conclusions

A new Nb-Al (Nb2Al) intermetallic based composites were designed from fresh scrap niobium with recycled chips of AA 7075 for the manufacturing of high resistant components for the high temperature applications as a low cost and high toughness alternative composite for turbo-compressors in aeronautical engineering. Low cost production of these composites have been successfully managed through the combined method of "sinter + forging". Microstructural analysis has shown a good chemical bonding diffusion at interface of matrix-reinforcement essentially in the specimens with a homogeneous distribution. These composites show a tough and sound microstructure generally without porosity thanks to the final stage of the manufacturing of these composite "sinter + forging".

In this study, a subroutine was developed with FORTRAN® software and embedded in the ABAQUS®/Explicit software to model the constituent material behaviour in the microstructural simulations. In this model, simulation of the interactions between the reinforcement particles and the matrix has been improved.

Good cohesion at the interface can only be achieved at high sintering temperatures, >700 °C and is recommended strongly followed forging operation for obtaining a healthy and sound microstructure.

By this way, a very stable vibrational chemical bonding between the matrix and intermetallic particles can be managed. Increasing the sintering temperature can provide easily vibrational chemical bonding under the effect of thermal diffusion. Therefore, reaction phases at the matrix/reinforcements interface can be caused by a stable interface. Actually this common research project is going on to optimize the operational parameters with experimental work supported by modelling to create real parts in the industrial scales.

Acknowledgements This work has been carried out on the frame of research collaboration between Supmeca/Paris-FRANCE and UNICAMP-FEM/ Campinas-SP/BRAZIL. Authors want to thank financial support from CNPq – Conselho Nacional de Desenvolvimento Científico e Tecnológico (Brazil); Program French Catedra UNICAMP/French Embassy in Brazil.

References

1. ASM International Handbook Committee: ASM Handbook, vol. 2–4, 10th edn, (1990)
2. Enginsoy, H., Gatamorta, F., Bayraktar, E., Robert, M., Miskioglu, I.: Experimental and numerical study of Al-Nb_2Al composites via associated procedure of powder metallurgy and thixoforming, JCOMB. Compos. Part B. **162**, 397–410 (2019). https://doi.org/10.1016/j.compositesb.2018.12.138
3. John, J.H.: Niobium alloys and high temperature applications. In: Niobium Science & Technology: Proceedings of the International Symposium Niobium 2001, Orlando, Florida, USA (2001)
4. Bewlay, B.P., Jackson, M.R., Zhao, J.-C., Subramanian, P.R.: A review of very-high-temperature Nb-silicide–based composites. Metall. Mater. Trans. A. **34A**, 2043–2555 (2003)
5. Kurşun, A., Bayraktar, E., Enginsoy, H.M.: Experimental and numerical study of alumina reinforced aluminium matrix composites: processing, microstructural aspects and properties. Compos. Part B. **90**, 302–314 (2016)
6. Kusaka, K., Fujine, M., Okabe, M., Endo, H.: Mechanical properties of Nb3Al-based intermetallics prepared by a ceramic mold-HIP process. Mater. Trans. JIM. **40**(7), 571–577 (1999)
7. Williams, J.J., Segurado, J., LLorca, J., Chawla, N.: Three dimensional (3D) microstructure-based modeling of interfacial decohesion in particle reinforced metal matrix composites. Mater. Sci. Eng. A. **557**, 113–118 (2012)
8. Ekici, R., Kemal Apalak, M., Yildirim, M., Nair, F.: Simulated and actual micro-structure models on the indentation behaviors of particle reinforced metal matrix composites. Mater. Sci. Eng. A. **606**, 290–298 (2014)
9. Liu, F.R., Chan, K.C., Tang, C.Y.: Numerical modeling of the thermo-mechanical behavior of particle reinforced metal matrix composites in laser forming by using a multi-particle cell model. Compos. Sci. Technol. **68**(9), 1943–1953 (2008)
10. Çetin, A., Kalkanli, A.: Numerical simulation of solidification kinetics in A356/SiCp composites for assessment of as-cast particle distribution. J. Mater. Process. Technol. **209**, 4795–4801 (2009)
11. Galli, M., Botsis, J., Janczak-Rusch, J.: An elastoplastic three-dimensional homogenization model for particle reinforced composites. Comput. Mater. Sci. **41**, 312–321 (2008)
12. Chawla, N., Sidhu, R.S., Ganesh, V.V.: Three-dimensional visualization and microstructure-based modeling of deformation in particle-reinforced composites. Acta Mater. **54**, 1541–1548 (2006)
13. Xu, Q., Qu, S.: Irreversible deformation of metal matrix composites: a study via the mechanism-based cohesive zone model. Mech. Mater. **89**, 72–84 (2015)
14. Breslin, M.C., Ringnalda, J., Xu, L., Fuller, M., Seeger, J., Daehn, G.S., Otani, T., Fraser, H.L.: Processing, microstructure, and properties of co-continuous alumina-aluminum composites. Mater. Sci. Eng. A. **195**, 113–119 (1995)
15. Zebarjad, S.M., Sajjadi, S.A.: Microstructure evaluation of Al-Al_2O_3 composite produced by mechanical alloying method. Mater. Des. **27**, 684–688 (2006)
16. Zebarjad, S.M., Sajjadi, S.A.: Dependency of physical and mechanical properties of mechanical alloyed Al-Al_2O_3 composite on milling time. Mater. Des. **28**, 2113–2120 (2007)
17. Fang, Z.Z.: Sintering of Advanced Materials. Woodhead Publishing, Cambridge (2010) ISBN 9781845695620

Chapter 13
Numerical Modeling of Recycled Rubber Based Composites Reinforced with Glass Fibers at High Strain Rates

G. K-Cakir, O. Aslan, and E. Bayraktar

Abstract Due to its high impact energy absorption properties, devulcanized recycled rubber based composites can be considered as a low cost candidate material for military applications which require lightweight protection against shock waves. This work aims at modeling of low cost devulcanized recycled rubber based composite behavior at high strain rates. In that framework, we established a continuum-based material model in order to capture the macroscopic behavior of the recycled rubber based composite material and numerically reproduce the results from the basic characterization tests. The model is implemented for Finite Element Analysis Software ABAQUS/Standard as a user subroutine UMAT for implicit nonlinear finite element calculations in order to simulate the behavior of several RVEs representing the microstructure of the composite and it is behavior at high strain rates.

Keywords Numerical modeling · Finite element analysis · Recycled composites · Devulcanized rubber · High strain rate

13.1 Introduction

In many industrial applications, rubber-based composites are subjected to different types of loading leading to various material failure [1]. Therefore, it is important to explore failure mechanisms and improve their mechanical properties efficiently to avoid failure and economic losses.

Continuum structures of polymer nanocomposites were modeled and their mechanical properties were predicted by finite element method and micromechanics in the literature [2–5]. Halpin–Tsai model, Nielsen's model, Mori–Tanaka model, Eshelby model, modified rule of mixtures and Shear Lag models, equivalent continuum model, and self-consistent model are some of the continuum methods used in polymer nanoparticle composites [6, 7]. These micromechanics models provide the prediction of the elastic properties of nanocomposite materials based on the geometry, orientation of the filler, and elastic properties of the filler and matrix. The Halpin–Tsai model is commonly used to predict the effective stiffness for fiber reinforced composites with perfect fiber alignment. Then, Mori–Tanaka is an effective field theory for inhomogeneity in an infinite medium to predict the modulus of nanocomposites.

When micromechanic models are applied to nanoparticle composites, some assumptions are considered such that nanoparticles and matrix behave as linearly elastic materials, perfect bonding exists between them, the nanoparticles are axisymmetric, identical in shape and size and can be described by their aspect ratio [8]. Finite element analysis was used for modeling of polymer nanoparticles with low nanoparticles content [9–12]. It was obtained that the nanoparticles should be distributed uniformly in the matrix. The reinforcements have different geometry and are distributed randomly in a polymeric composite. Hence, local agglomerations may occur and the microstructures become very complex. Therefore, the interrelationships between microstructures and the nanoparticles are analyzed with discretized numerical models which incorporate

G. K-Cakir
Department of Mechanical Engineering, Atilim University, Ankara, Turkey

School of Mechanical and Manufacturing Engineering, Isae-Supmeca-Paris, Saint-Ouen, France
e-mail: gamze.cakir@atilim.edu.tr

O. Aslan
Department of Mechanical Engineering, Atilim University, Ankara, Turkey

E. Bayraktar (✉)
School of Mechanical and Manufacturing Engineering, Isae-Supmeca-Paris, Saint-Ouen, France
e-mail: emin.bayraktar@isae-supmeca.fr

V. Chalivendra et al. (eds.), *Mechanics of Composite, Hybrid and Multifunctional Materials, Fracture, Fatigue, Failure and Damage Evolution, Volume 3*, Conference Proceedings of the Society for Experimental Mechanics Series,
https://doi.org/10.1007/978-3-030-86741-6_13

deformation and damage characteristics particularly on a local scale [6, 8]. The properties of nano reinforcements are obtained by the microstructure and the mechanical properties of the constituents. Homogenization-based multi-scale computational technique is used to observe relationships between microstructures and macro-behaviors. The most used homogenization method is Representative Volume Element (RVE) in FEM [13]. RVE was proposed by Nemat-Nasser and Hori [14] and is used in a repeating or periodic nature in the full-scale model. The dependency of the reported results should be verified to the RVE size for composite materials. The RVE includes the microscopic heterogeneities in an averaged sense. The studies in the literature showed that the theoretical results are in good agreement with available experimental data.

In this study, recycled rubber based composites reinforced with glass fibers were designed and the mechanical behavior of the composites were studied. Interface and bonding characteristics for recycled rubber and the reinforcements were analyzed under laboratory conditions. Formability behavior and damage analyses were also conducted by 3P bending tests. In addition, tests were carried out to study the fracture characteristics of the composites and toughening mechanisms were identified by using SEM on the fracture surfaces.

After investigating the fundamental mechanical characteristics of the composite experimentally obtained moduli were compared with a homogenization material model. A continuum-based material model was performed for the macroscopic behavior of the composite materials and the results were numerically reproduced from mechanical tests. The model was implemented for Finite Element Analysis Software ABAQUS/Standard as a user subroutine UMAT for implicit nonlinear finite element calculations. Then, microstructure of the composite material was modeled and the behavior of several representative volume elements (RVEs) were simulated.

13.2 Material Characterization Methods

Flexural tests, fatigue tests, and impact tests were conducted to determine mechanical properties. The most common flexural test is the three-point bending test for composite materials. After manufacturing of the composites, three-point bending tests are conducted and deflection of the specimen was measured by the crosshead position. Then, flexural strength, elasticity modulus in bending and strain were also obtained from the test results. In addition, fracture toughness indicators such as critical stress intensity factor and critical strain energy release rate were investigated with notched specimens. It is important to determine the microstructure of the composites because all of the compositions should show a homogenous distribution of the reinforcements in the structure. Moreover, creating ideal interface for each composition is needed to observe good adhesion of the reinforcements in the rubber-based matrix. For this reason, after the realization of bending tests, fracture surfaces were analyzed by means of Scanning Electron Microscopy (SEM) to observe the microstructure and to identify damage and toughening mechanisms. Furthermore, Shore D hardness test measurements on the polished flat surfaces of the specimens were carried out using Shore D hardness tester. Then, dynamic compression tests (drop weight tests) were carried out to observe impact behavior of the manufactured composites with the force-time curves. Time dependent behavior was identified by nano indentation testing.

13.3 Numerical Analysis

For numerical approach, the continuum-based model was performed by a user material subroutine UMAT in ABAQUS. Numerical analysis was studied to calibrate the experimental results. To provide verification, composite material parameters obtained by the mechanical characterization experiments were applied to the model until the optimum parameters were achieved. First, mechanical properties derived from mechanical tests were implemented to the continuum-based model. Then, a numerical study was carried out to observe the evolution of the strain energy release rate along the crack front. The model was implemented for Finite Element Analysis Software ABAQUS/Standard as a user subroutine UMAT for implicit nonlinear finite element calculations.

The primary objective was to establish a continuum-based material model in order to capture the macroscopic behavior of the targeted composite materials and numerically reproduce the results from the basic characterization tests (3P bending tests, fatigue tests, impact tests, etc.). After investigating the macroscopic behavior such as mechanical strength, flexural modulus and strain at break, experimentally obtained moduli were compared with a homogenization material model. There are several analytical models to determine the theoretical modulus of these composites. Among these analytical models, Halpin–Tsai model was chosen due to its convenience to estimate the experimental results in case of homogeneous distribution of the fillers. Halpin–Tsai homogenization adapted to composites can be preferred to estimate the moduli of the composites and to

compare with the 3PB test results. In addition, 3PB tests was simulated by finite element method incorporating the homogenization model and the resulting stress-strain curves were compared with the experimental results. Halpin–Tsai's model [15] is as follows:

$$\frac{E_c}{E_m} = \frac{1 + \xi\eta V_f}{1 - \xi\eta V_f'}$$

$$\eta = \frac{\frac{E_f}{E_m} - 1}{\frac{E_f}{E_m} + \xi'}$$

where E_c, E_f and E_m are modulus of elasticity of the composite, fibers, and the matrix, respectively. V_f and V_m are the volume fraction of the reinforcements and the matrix, respectively. The shape factor of the fibers:

$$\xi = 2\frac{L}{D}$$

Halpin–Tsai model for the effects of nano reinforcements:

$$E_c = \left[\frac{3}{8}\frac{1 + \left(\frac{2L_g}{3T_g}\right)\eta_L V_G}{1 - \eta_L V_G} + \frac{5}{8}\frac{1 + 2\eta_T V_G}{1 - \eta_T V_G}\right] E_P$$

$$\eta_L = \left[\frac{\frac{E_G}{E_P} - 1}{\frac{E_G}{E_P} + \frac{2L_G}{3T_G}}\right]$$

$$\eta_L = \left[\frac{\frac{E_G}{E_P} - 1}{\frac{E_G}{E_P} + 2}\right]$$

E_c indicates the elasticity modulus of the composites with randomly oriented glass fibers and E_G and E_P are the elasticity moduli of glass fibers and the matrix. V_G, T_g, and L_g refer the volume fraction, thickness, and length, respectively. Experimental results and the homogenization model were compared on elasticity modulus of composites by the different ratio of reinforcements. As viscoelastic materials, the mechanical response of the composites are highly dependent on strain rate. To examine the time dependent behavior of the rubber composites, the effects of glass fibers and rubber on time dependent behavior were studied by means of nanoindentation measurements. Oliver-Pharr method was used to determine elasticity modulus and hardness of the composites for finite element analysis of nanoindentation of rubber-based composites. The microstructure of the rubber-based composite material was examined by several representative volume elements (RVEs) by applying periodic boundary conditions. The physical properties of the material were related to the ratio of side length of the RVE to the radius of a particle. RVE models with different L/R values were studied to verify the stability of the model. The equivalent elastic modulus values of the composite materials were calculated.

13.4 Conclusion

Recycled rubber based composites reinforced with glass fibers were designed; mechanical behavior, fracture characteristics, toughening mechanisms, and damage analyses of the composites were conducted. After investigating the fundamental mechanical characteristics, experimentally obtained moduli were compared with a homogenization material model. A continuum-based material model was performed for the macroscopic behavior of the composite materials and the results were numerically reproduced from mechanical tests. The model was implemented for FEA Software ABAQUS/Standard as a user subroutine UMAT for implicit nonlinear finite element calculations. Then, microstructure of the composite material was modeled and the behavior of several representative volume elements (RVEs) were simulated. The numerical study was carried out to observe the evolution of the strain energy release rate along the crack front and the experimental results were compared with finite element simulations. The microstructure of the rubber-based composite material was modeled and simulation of the behavior of several representative volume elements (RVEs) was carried out and the effect of different ratios of energy absorbing glass fibers was obtained.

References

1. Hung, P.Y., Lau, K.T., Cheng, L.K., Leng, J., Hui, D.: Impact response of hybrid carbon/glass fiber reinforced polymer composites designed for engineering applications. Compos. Part B Eng. **133**, 86–90 (2018)
2. Shokrieh, M.M., Rafiee, R.: Prediction of Young's modulus of graphene sheets and carbon nanotubes using nanoscale continuum mechanics approach. Mater Des. **31**(2), 790–795 (2010)
3. Spanos, K.N., Georgantzinos, S.K., Anifantis, N.K.: Investigation of stress transfer in carbon nanotube-reinforced composites using a multiscale finite element approach. Compos. Part B Eng. **63**, 85–93 (2014)
4. Viet, N.V., Wang, Q., Kuo, W.S.: A studying on load transfer in carbon nanotube/epoxy composites under tension. J. Model. Mech. Mater. **1** (1) (2017)
5. Shiuh-Chuan, H., Shou-Jan, L.: Analytical model for predicting the interfacial stresses of carbon nanotubes-reinforced nanocomposites. Eng. Comput. **31**, 353–364 (2014)
6. Armbrister, C.E., Okoli, O.I., Shanbhag, S.: Micromechanics predictions for two-phased nanocomposites and three-phased multiscale composites: a review. J. Reinf. Plast. Compos. **34**, 605–623 (2015)
7. Takayanagi, M., Uemura, S., Minami, S.: Application of equivalent model method to dynamic rheo-optical properties of crystalline polymer. J. Polym. Sci. Part C: Polym. Symp. **5**, 113–122 (1964)
8. Zeng, Q.H., Yu, A.B., Lu, G.Q.: Multiscale modeling and simulation of polymer nanocomposites. Prog. Polym. Sci. **33**, 191–269 (2008)
9. Peng, R.D., Zhou, H.W., Wang, H.W., Mishnaevsky Jr., L.: Modeling of nano-reinforced polymer composites: microstructure effect on Young's modulus. Comput. Mater. Sci. **60**, 19–31 (2012)
10. Wang, H.W., Zhou, H.W., Peng, R.D., Mishnaevsky Jr., L.: Nanoreinforced polymer composites: 3D FEM modeling with effective interface concept. Compos. Sci. Technol. **71**, 980–988 (2011)
11. Li, Y., Waas, A.M., Arruda, E.M.: A closed-form, hierarchical, multi-interphase model for composites—derivation, verification and application to nanocomposites. J. Mech. Phys. Solids. **59**, 43–63 (2011)
12. Mortazavi, B., Bardon, J., Ahzi, S.: Interphase effect on the elastic and thermal conductivity response of polymer nanocomposite materials: 3D finite element study. Comput. Mater. Sci. **69**, 100–106 (2013)
13. Sun, C.T., Vaidya, R.S.: Prediction of composite properties from a representative volume element. Compos. Sci. Technol. **56**, 171–179 (1996)
14. Nemat-Nasser, S., Hori, M.: Micromechanics: Overall Properties of Heterogeneous Materials. North-Holland (1999)
15. Halpin, J.C., Kardos, J.L.: The Halpin-Tsai equations: a review. Polym. Eng. Sci. **16**(5) (1976)

Chapter 14
Piezoelectric Actuators as Control Surfaces for Morphing Vehicle

M. M. Mennu, B. Tran, and P. G. Ifju

Abstract Conventional design of micro-aerial vehicles (MAVs) uses fixed airframe design optimized for the entire flight path. This compromise leads to sub-optimal flight characteristics during certain flight regimes. Birds' wings show great versatility during various stages of flight using feathers and wrist joints. A new design is proposed using piezoelectric patches known as macro-fiber composite (MFC) embedded directly on the surface of the wing and tail to serve as control actuators. In addition, sweeping mechanism was developed to mimic the folding action of birds for a stable dive maneuver. The use of MFCs and sweeping mechanism for controlling MAVs presents a unique challenge for optimizing the effectiveness of these actuators for all flight maneuvers. Numerical models were developed using structural and aerodynamic tools to optimize the location of the MFCs for maximum deflection and overall aerodynamic performance. Digital image correlation (DIC) was used to validate the full field deformation of the control surfaces under simulated aerodynamic loading.

Keywords Morphing · Piezoelectric · Macro-fiber composites · Digital image correlation · Finite element analysis

14.1 Introduction

Aviation industry throughout its development has reached many milestones through biological inspiration. The invention of flaps, slats, ailerons, etc. were all mechanical adoptions of nature for human flight. In the past several decades, multiple efforts have been made to replicate birds' flight in unmanned micro-aerial vehicle (MAV) [1]. These vehicles have the same low Reynolds number as their bird counterparts. Birds can adapt their wings and tails through changing the wing area, camber, and wing tip deflections based on the environment and the flight maneuvers. Thus, the adoption of such morphing behavior can be advantageous for MAVs to increase adaptability based on flight objectives. Current fixed wing designs of MAVs are optimized for the entire flight path which leads to a compromise at specific flight regimes. Conventional designs use widely available servos with hinge mechanisms for the control surfaces of such vehicles. A typical sortie mission of MAVs involves an initial take-off usually with a hand launch. Then, the vehicle ascends to a specific altitude at a certain rate. Once the vehicle reaches the altitude for flight, it then goes to the initial waypoint to start the loiter pattern. In loiter phase, the vehicle will be completing mission objectives such as reconnaissance by following a raster pattern. After completion, the vehicle then avoids unfriendly environments or being an easy target in the sky by rapidly descending. The descent is followed by a maneuver to the landing site where it can be easily recovered. Each individual flight regime provides unique challenges for optimizing the aerodynamic performance of the vehicle. The best example of optimized flight can be seen in birds with their capacity to morph by sweeping their wings as well as controlling their feathers. Several groups including Ohanian [2], Bilgen [3], LaCroix [4], etc. have developed MAVs with the capacity to morph their wings using piezoelectric actuators known as macro-fiber composites (MFCs), developed in NASA [5], directly embedded onto the surface of the wings. However, the full potential of MFCs have not been realized as the primary actuators for all control surfaces of MAVs. In this research, the use of MFCs as control surfaces for the tail of a newly design MAV is discussed.

M. M. Mennu (✉) · B. Tran · P. G. Ifju
Department of Mechanical and Aerospace Engineering, University of Florida, Gainesville, FL, USA
e-mail: mmennu@ufl.edu; tranb@ufl.edu; ifju@ufl.edu

V. Chalivendra et al. (eds.), *Mechanics of Composite, Hybrid and Multifunctional Materials, Fracture, Fatigue, Failure and Damage Evolution, Volume 3*, Conference Proceedings of the Society for Experimental Mechanics Series,
https://doi.org/10.1007/978-3-030-86741-6_14

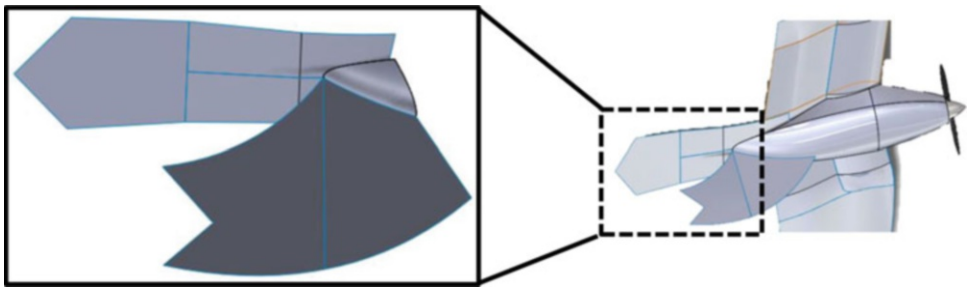

Fig. 14.1 Initial design of tail section of the micro-aerial vehicle with enlarged view

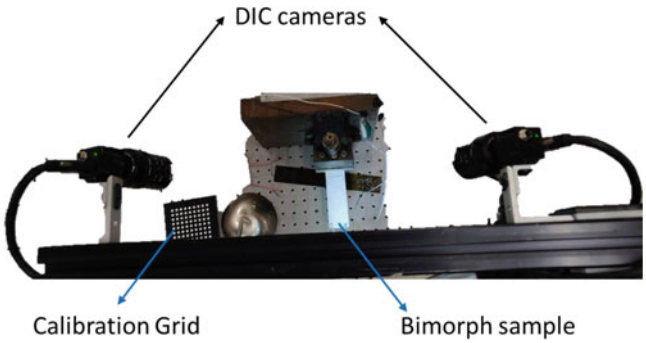

Fig. 14.2 Top-down view of experimental setup for measuring out of plane deflection of bimorph samples

14.2 Background

There are two main control surfaces that are included in the tail section of this MAV. These are the elevator and the rudder. The elevator is used for pitch control of the vehicle and the rudder is used for maintaining directional stability of the aircraft. There are several ways of designing this control surfaces either as separate sections or can be combined to form V-shape or X-shaped tails. These designs need to be compared both qualitatively and quantitatively to determine which configuration will allow the effective integration of MFC as control actuators as well as resemble a bird while in flight. Figure 14.1 shows the tail section of the MAV in design.

The tail section as observed uses two flat surfaces that can potentially incorporate MFCs for actuation. Therefore, it was appropriate to characterize these control surfaces using cantilever beam setup of thin carbon fiber reinforced plastic (CFRP) with MFCs attached to it. In order to have equal magnitude of deflection in either side, a bimorph configuration is necessary. Bimorph configuration consists of two MFCs attached on each side of the CFRP plate for actuation. Once a bimorph sample was fabricated, it was prepared for full field deformation measurement using DIC. The first step includes speckling the sample using an even coat of white paint followed by a random pattern of black dots using black spray paint. After the sample is prepared, DIC cameras are placed right above the cantilever setup to measure out of plane displacements. The cameras are placed equidistance and angled towards the sample to get the maximum out of plane resolution. The calibration grid is used to record the location and orientation of the cameras in relation to one another necessary for analysis in the DIC software. VIC-3D software, commercially available through Correlated Solutions [6], is used for processing all captured images and recording displacement data. The top-down view of the experimental setup is presented in Fig. 14.2.

14.3 Analysis

The initial design of this MAV included two sections for the elevator and rudder as seen in Fig. 14.1. FEA models for each section were developed to study the implementation of MFCs on this control surfaces and their effectiveness similar to previous work on the inboard wing [7]. The main challenge is understanding the behavior of MFC actuators when experiencing aerodynamic loads. For these simulations, the aerodynamic loads were modeled by introducing a distributed load into the FEA model. The various sections of the elevator had different layup configurations. The root and base sections of

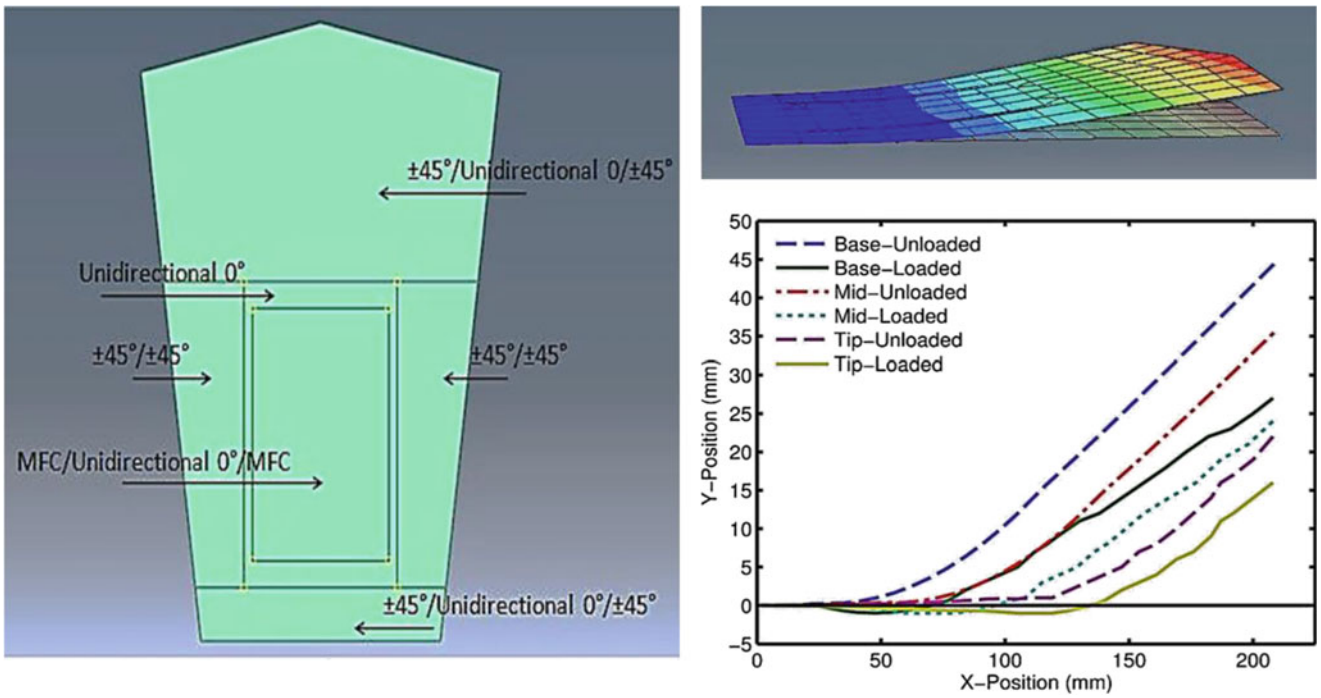

Fig. 14.3 Initial design study of elevator section with MFC actuators

the elevator were layered with quasi-isotropic layup of the composite to ensure maximum stiffness. Unidirectional carbon fiber was used as a substrate for the middle section of the elevator where the MFCs were placed. This substrate was chosen because it yields the maximum deflection compared to other layups of composite. The section surrounding this MFC region was layered with $\pm 45^{\circ}$ layers to ensure maximum compliance when the MFCs are being actuated. There were three locations of the MFC that were explored. MFC was placed closest to the root of the elevator, in the middle as well as closest to the tip of the elevator. These locations were modeled with a distributed load as well as without one. The results can be seen in Fig. 14.3.

A similar study was completed on the rudder section of the initial design configuration. The main difference for this section was the size of the MFC and the amount of load experienced by this section. The overall area of this rudder section is much smaller than the elevator section for better resolution on the directional control of the aircraft. Three different locations with the two loading conditions were studied. The results have been presented in Fig. 14.4. In both cases of the rudder and elevator, more deflection was observed when the MFC was placed closer to the base or the root of these control surfaces. The stiffness of the quasi-isotropic layup maintains the curvature from the end of the MFC region up to the tip. The simulated cases with aerodynamic loading showed a reduction of deflection compared to the unloaded cases. This reduction in deflection however does not reduce the effectiveness of these actuators because the onset of the aerodynamic loading is from the gained speed of the vehicle. Further analysis can be done by using fluid-structural interaction models to optimize this design. In addition, the use of two independent control surfaces each with bimorph configuration can be economically expensive. Other tail configurations that can potentially reduce the number of actuators and increase efficiency can also be explored with similar methods.

14.4 Conclusion

The design of a new MAV incorporating MFCs as actuators requires investigation on how to effectively implement them. To this extent, the tail configuration of the designed MAV with a rudder and elevator section has been studied. DIC was used as a full field measurement technique to acquire the material properties and deflection behavior of MFCs using a cantilever setup. Multiple locations of the MFCs on the control surfaces were investigated with simulated aerodynamic loading. Significant deflection can be observed with a bimorph setup but operating these many MFCs just for the tail can be costly.

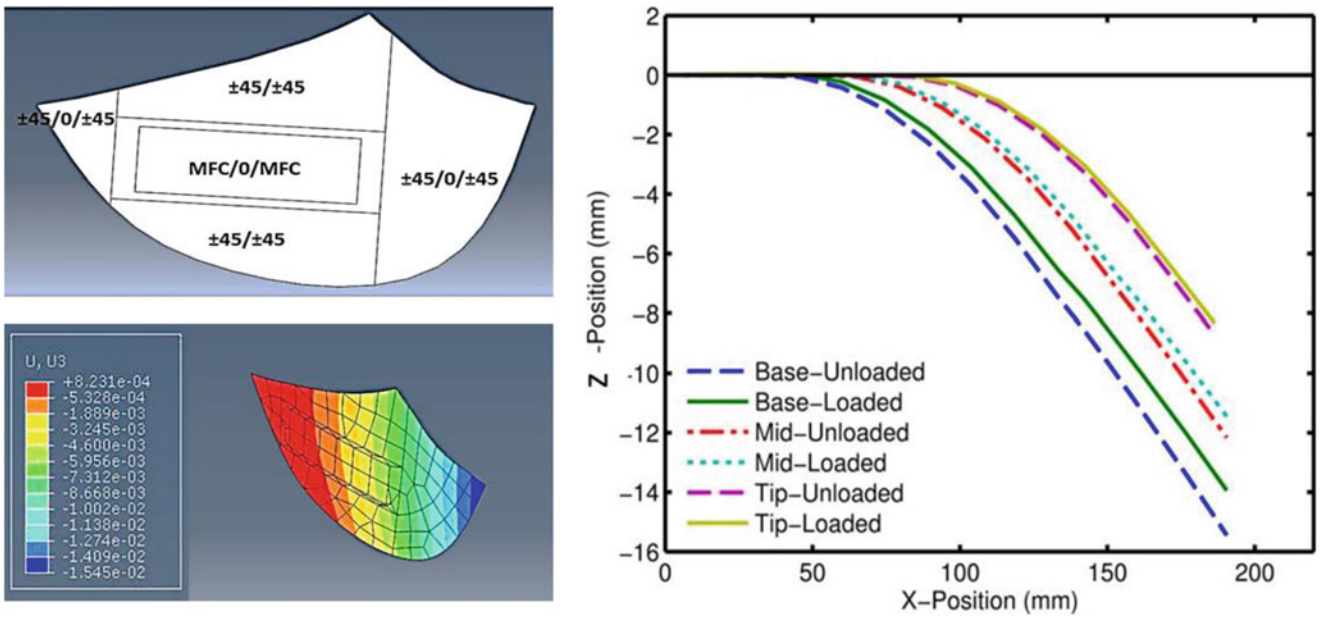

Fig. 14.4 Initial design study of rudder section with MFC actuators

Acknowledgements The authors would like to thank the STTR program under the Air Force Office of Scientific Research for the funding.

References

1. Barbarino, S., Bilgen, O., Ajaj, R.M., Friswell, M.I., Inman, D.J.: A review of morphing aircraft. J. Intell. Mater. Syst. Struct. **22**(9), 823–877 (2011)
2. Ohanian, O., et al.: Piezoelectric morphing versus servo-actuated MAV control surfaces. In: 53rd AIAA/ASME/ASCE/AHS/ASC Structures, Structural Dynamics and Materials Conference
20th AIAA/ASME/AHS Adaptive Structures Conference
14th AIAA (2012)
3. Bilgen, O., Kochersberger, K., Diggs, E.C., Kurdila, A.J., Inman, D.J.: Morphing wing micro-air-vehicles via macro-fiber-composite actuators. In: Collection of Technical Papers—AIAA/ASME/ASCE/AHS/ASC Structures, Structural Dynamics and Materials Conference, vol. 1, pp. 1005–1020 (2007)
4. Lacroix, B.W., Ifju, P.G.: Aeroelastic model for macrofiber composite actuators on micro air vehicles. J. Aircr. **54**(1), 199–208 (2017)
5. J. W. High and W. K. Wilkie, "Method of Fabricating NASA-Standard Macro-Fiber Composite Piezoelectric Actuators," 2003.
6. Correlated Solutions – VIC-3D.: [Online]. https://www.correlatedsolutions.com/vic-3d/. Accessed 10 Feb 2021
7. Mennu, M.M., Tran, B., Ifju, P.G., Santamaria, E.: Full-field deformation measurement of morphing wings. In: Conference Proceedings of the Society for Experimental Mechanics Series, pp. 101–104 (2020)

Chapter 15
Alternative Concretes: Study of Concrete Performance with Addition of Copper Tailings Reinforced and Steel Fiber

Vinicius L. Pereira, Isaías S. Almeida, Sabino A. Neto, Emin Bayraktar, and Lygia P. Ferreira

Abstract The growing demand for mineral leads to a significant increase in the number of tailings produced, which exceed the number of ores with economic value obtained. The process to obtain one ton of copper ore generates 90% of the total amount of waste, making urgent the measures to reuse it is tailings. Concrete with steel fiber has been applied in civil construction to improve the mechanical characteristics of the concrete; the steel fiber increases impact resistance, fatigue resistance, cracking control, and concrete post-cracking behavior. Considering that, this work aims to present a new alternative for the reuse of copper ore tailings in the construction industry, through the production of concrete reinforced with steel fibers. The feasibility of using the tailings was investigated by three mixture: a reference mixture (RR) and a mixture with 20% of tailings plus 2% of steel fiber (R1). Both mixtures, the water-cement ratio was 0.5, and plasticizer additive of water reduction was 2%. From the results obtained, it was possible to observe that both R1 presented satisfactory results regarding the mechanical evaluations performed, when compared with RR. Thus, it is possible to say that, considering this aspect, the manufacture of concrete with partial replacement of sand by copper tailings with the addition of steel fiber is feasible.

Keywords Concrete · Steel fiber · Copper tailings · Sustainability · Sossego mine

15.1 Introduction

The growing demand for mineral leads to a significant increase in the amount of waste produced, which exceeds the number of ores of economic value produced. The processing of one ton of copper ore generates 90% of waste from the total amount [1].

The copper ore tailings have a granulometry like that of natural sand, where 95.79% of the tailings exhibit granulometry of sandy strip, with 4.51% silty material. In addition, the minerals found in the mineralogical composition of the tailings also resemble sand, such as quartz and magnetite, in addition to presenting more resistant minerals such as clinochlorine, actinolite, and albite [2].

The addition of steel fibers to the concrete matrix helps to reduce the brittleness, especially of high-strength concretes, thereby reducing the appearance of micro cracks and macro cracks. However, steel fibers act as crack fasteners and not as crack inhibitors. The response of concrete with the addition of steel fiber in relation to the tensile and compressive strength is similar, as it mainly increases the toughness and ductility after peak. The increase in the steel fiber content in the concrete guarantees an increase in the deformation capacity, consequently there is a greater load-absorbing capacity of the concrete in axial compression. Additionally, the distribution of fibers in the concrete matrix is carried out at random since this material does not have a continuous body like other commercial fibers. However, an important factor to be considered in the efficiency of fibers in concrete is their orientation in the concrete matrix [3].

Steel fiber concrete has been applied in civil construction with the aim of improving the mechanical characteristics of concrete used for complex structural purposes. Steel fiber causes increased impact resistance, fatigue resistance, crack control, and post-cracking behavior of concrete [4].

V. L. Pereira (✉) · I. S. Almeida · S. A. Neto · L. P. Ferreira
Department of Construction Materials, University of South and Southeast Pará, Marabá, PA, Brazil
e-mail: vinicius.vlp@unifesspa.edu.br; isaias.almeida@unifesspa.edu.br; sabino.neto@unifesspa.edu.br; lpolicarpio@unifesspa.edu.br

E. Bayraktar
Department of Tribology and Materials, Supmeca-Paris, Saint-Ouen, France
e-mail: emin.bayraktar@supmeca.fr

V. Chalivendra et al. (eds.), *Mechanics of Composite, Hybrid and Multifunctional Materials, Fracture, Fatigue, Failure and Damage Evolution, Volume 3*, Conference Proceedings of the Society for Experimental Mechanics Series,
https://doi.org/10.1007/978-3-030-86741-6_15

Thus, the objective of this work is to present a new alternative for the reuse of copper ore tailings in the construction industry, through the production of concrete reinforced with steel fibers. The partial replacement of sand by copper ore tailing also seeks to reduce the mass exploitation of natural river sand, commonly used as fine aggregate in the production of concrete. Thus, consequently, it is desired to reduce the disposal of this waste in retention dams, collaborating with the reduction of impacts generated on the environment.

15.2 Background

The materials used in the experimental program were: CP V ARI cement, whose chemical, physical, and mechanical characteristics are in accordance with NBR 16697 [5]; crushed rock; natural sand; high-performance water-reducing plasticizer additive; steel fiber; and copper ore tailings, the latter from the Sossego mine located in the mineral province of Carajás. The materials were analyzed and characterized to obtain a better quality in the production of concrete reinforced with steel fiber and addition of copper tailings.

The steel fiber used was manufactured by the company MM Fibras para Concreto® and the technical data are available directly on the manufacturer's website. The fiber used is classified for concrete reinforcement purposes, reaching 800 MPa of mechanical strength per wire, with the corrugated steel wire model. In addition, ASTM A 820 was used for its manufacture. The fibers have the following dimensions: length of 40 mm, width of 2 mm, thickness of 0.7 mm considering 0.25 mm of variation, height of 2 mm and format 40.

To reinforced concrete was produced with steel fiber and addition of copper ore tailings; two different mixtures were prepared: a reference mixture (RR) and a mixture with 20% of tailings plus 2% of steel fiber (R1). All with a water-cement ratio of 0.5 and plasticizer additive to reduce water by 2%.

The discrimination of sample according to the levels of addition of steel fiber and copper tailings is shown in Table 15.1, and then, Table 15.2 shows the proportions in volume of the traces used.

The production of the specimens followed the specifications from NBR 5738 [6], respecting the molding and curing procedures, using a 120 L concrete mixer. After the preparation of the concrete, the mixtures were compacted manually in molds of cylindrical specimens with 10 cm in diameter and 20 cm in length, the molds were previously prepared with release agent. Compaction was carried out with a density rod according to the specified dimensions. After, they were cured initially for 24 h in the air, and then immersed in water saturated with lime; the samples were tested after the age of 28 days. The samples were tested for resistance to uniaxial compression after 28 days of curing.

15.3 Analysis

To determine the compression resistance, specimens with different percentages of steel fiber addition were followed the specifications from NBR 5739 [7], which determines the conditions for carrying out tests on cylindrical specimens. To carry out the test, the specimens were centered strictly in relation to the loading axis, and a constant loading was applied. In total, 3 specimens of each line were tested.

Table 15.1 Discrimination of the samples according to the content of substitution and addition of fiber

Sample	Copper tailings (%)	Steel fiber (%)	Number of specimens
RR	0	0	9
R1	20	2	9

Table 15.2 Proportion by volume of traces with water-cement ratio 0.50

Trace	RR	R1
Cement	1.00	1.00
Water	0.50	0.50
Coarse aggregate	2.25	2.25
Fine aggregate	1.35	1.05
Copper tailings	0	0.30
Steel fiber (%)	0	2

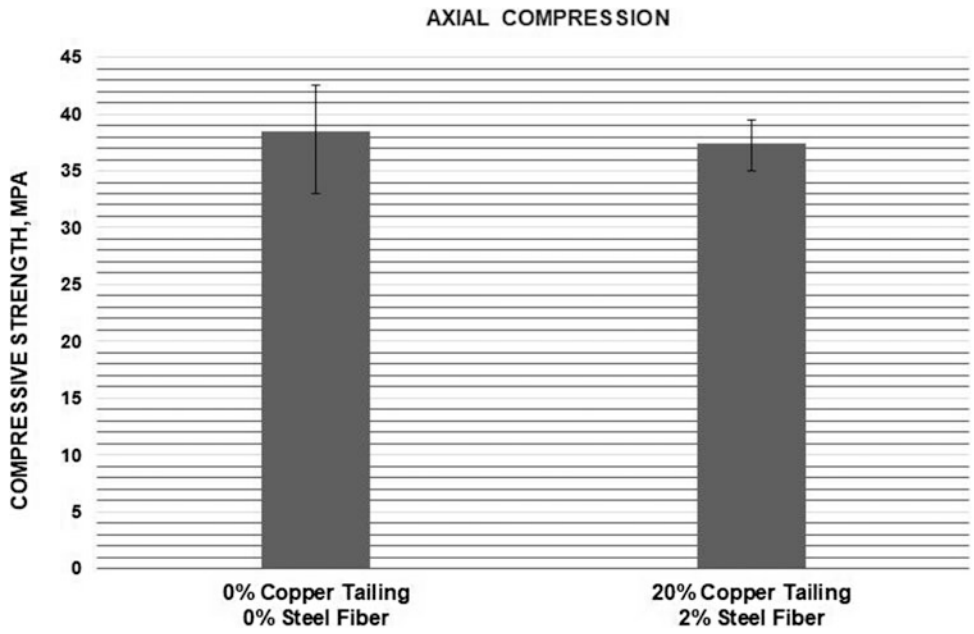

Fig. 15.1 Results of compression tests at age of 28 days

The results of resistance to uniaxial compression obtained in the mechanical tests showed a small difference in the average between RR and R1, where it was possible to observe only 2.73% difference. The strength of concrete with copper tailing reinforced with steel fiber (R1) showed satisfactory results about the mechanical evaluation performed, as shown in Fig. 15.1.

15.4 Conclusion

This work aimed to study a new alternative for the reuse of copper ore tailings in the civil construction industry, through the production of concrete reinforced with steel fibers.

The results obtained showed that the concrete with 20% replacement of sand by copper ore tailing and the addition of 2% of steel fiber (R1) presented satisfactory results on the mechanical evaluations. Thus, it is possible to say that, considering this aspect, there may be technical feasibility for the manufacture of concrete with partial replacement of sand by copper tailings with the addition of steel fiber.

Acknowledgements Unifesspa and Pibic for the financial support.

References

1. Soares, L.: Barragens de Rejeitos. Tratamento de Minérios. **5**, 831–896 (2010)
2. Pereira, V.L.: Avaliação das Propriedades Físicas e Mecânicas de Argamassas com Adição de Rejeito de Minério de Cobre da Província Mineral de Carajás. A aplicação do Conhecimento Científico na Engenharia Civil. **4**, 388–416 (2020)
3. Usman, M., et al.: Axial compressive behavior of confined steel fiber reinforced high strength concrete. Construct. Build. Mater. **230**, 2–10 (2019)
4. Rauecker, J.C.N., et al.: Uma abordagem experimental e numérica para determinação de curvas de compressão para concreto simples e reforçados com fibras de aço. Matéria. **24** (2019)
5. Associação Brasileira de Normas Técnicas: ABNT NBR 16697: cimento portland: requisitos. ABNT, Rio de Janeiro (2018)
6. Associação Brasileira de Normas Técnicas: ABNT NBR 5738: concreto: procedimento para moldagem e cura de corpos de prova. ABNT, Rio de Janeiro (2016)
7. Associação Brasileira de Normas Técnicas: ABNT NBR 5739: concreto: ensaio de compressão de corpos-de-prova cilíndricos. ABNT, Rio de Janeiro (2018)

Chapter 16
Cyclical Instrumented Indentation Testing for Fatigue Characterization of Metals

Luis S. Santos and Hugh A. Bruck

Abstract Fatigue testing methods for metals have traditionally used static test methods that have been modified for cyclic loading. One technique that has not been extensively applied to characterizing fatigue behavior of metals is indentation testing. New manufacturing processes for metals, such as selective laser sintering, are introducing new challenges in characterizing properties where the nature of the process can lead to greater spatial variability, making a technique for characterizing the localized variation in fatigue properties critical. Recently, we explored the use of cyclic instrumented indentation testing for locally characterizing the fatigue behavior of metals. The results indicate that cyclic instrumented indentation testing can be used to obtain fatigue behavior locally in metals, and potentially other materials, such as composites.

Keywords Instrumented indentation · Fatigue · S-N curve · Continuous stiffness measurement

16.1 Introduction

Traditional fatigue tests have been the main approach to obtain fatigue data for materials. As described in the ASTM standards [1–3], the specimens required for such tests are typically large and generate the aggregated fatigue properties of the entire specimen. Currently, with the proliferation of additive manufacturing (AM) and the development of advanced composite materials, designers are able to tailor microstructural features that can have a significant impact on the global fatigue behavior of the material. If a traditional test is used on these materials, then the influence of the microstructure cannot be isolated. Therefore, there is a need to investigate more localized testing approaches.

One promising approach is indentation testing. The load-unload technique by Oliver and Pharr [4], also known as the Oliver–Pharr method, has been the backbone to quantify the elastic modulus by indentation and has been successfully used to compute the hardness and elastic modulus of multiple materials like shape memory alloys [5], particle reinforced composites [6], human glioma cell line [7], polymers [8], bones [9], and more. The Oliver–Pharr method computes the elastic modulus from the contact stiffness at the beginning of the unloading procedure and is inherently limited to one measurement per indentation. The continuous stiffness measurement (CSM) technique offers an alternative by imposing a small oscillating signal on top of the original indentation signal to build a dynamic model [10]. The response of the dynamic model is then processed to determine the contact stiffness not only during the unloading procedure but during the entire indentation process. The contact stiffness is then used similarly to the Oliver–Pharr method to obtain the elastic modulus of the tested material, although CSM has also been applied to get creep measurements [11] and stress-strain curves [12]. CSM was used by Li and Bhushan [13] along with nanoindentation to study fatigue but limited their scope to the calculation of the contact stiffness only. Also, Xu et al. [14] used fatigue indentation to understand the depth propagation behavior suggesting that the indentation depth propagation has some similarities with fatigue depth propagation. Other researchers have used repeated indentation cycles to study the crack formation or propagation in brittle materials [15–18] and aluminum foam [19].

In this paper, we investigate the use of cyclical instrumented indentation testing to characterize the localized fatigue behavior of metals. An approach was developed to obtain the material stiffness behavior as a function of fatigue cycles, which opens the door to generating an S-N curve with a single test.

L. S. Santos · H. A. Bruck (✉)
Department of Mechanical Engineering, University of Maryland, College Park, MD, USA
e-mail: lss@umd.edu; bruck@eng.umd.edu; bruck@umd.edu

V. Chalivendra et al. (eds.), *Mechanics of Composite, Hybrid and Multifunctional Materials, Fracture, Fatigue, Failure and Damage Evolution, Volume 3*, Conference Proceedings of the Society for Experimental Mechanics Series,
https://doi.org/10.1007/978-3-030-86741-6_16

16.2 Materials and Setup

Control specimens for characterization were created by cutting a 4340 rod into 1″ lengths and then polishing the top surface. For cyclic instrumented indentation testing, a sphero-conical diamond indenter was attached it to a Bose ElectroForce 3330 to apply a load varying from 98 N to a maximum force. Tests were conducted at three different maximum forces (589 N, 735 N, and 883 N) and four frequencies (2 Hz, 4 Hz, 5 Hz, and 6 Hz).

16.3 Cyclical Instrumented Indentation Testing Using Continuous Stiffness Measurements (CSM)

Continuous Stiffness Measurements (CSM) is a technique used to measure the stiffness of a material by applying a small harmonic force to the traditional force profile required to produce an indentation [20]. The technique models the instruments and material as a single dynamic model where both the cyclic force, $F(t)$, and displacement, $z(t)$, are assumed to follow a harmonic trend and a dephased angle is expected between both variables, as shown in Fig. 16.1. Traditional CSM assumes that both the force and displacement amplitudes are constant and account for relative force and displacement. We have tried to address these issues and have included any pre-existing force, F_m, and pre-existing displacement, z_m. In addition, we assume that the force, displacement, and contact stiffness could change over time. Our updated model to described the behavior of the force and displacement are:

$$F(t) = F_m + F_0 e^{i\omega t}$$
$$z(t) = z_m + z_0 e^{i(\omega t - \varnothing)}$$

CSM has been useful to compute the contact stiffness during an indentation but it has some drawbacks.
With the same dynamic model as in Fig. 16.1, the governing equation is:

$$-m\omega^2 + D\omega i + K\left[\frac{z_m}{z_0 e^{i(\omega t-\phi)}} + 1\right] = \frac{F_m}{z_0 e^{i(\omega t-\phi)}} + \frac{F_0}{z_0} e^{i\phi}$$

Equating the real parts, we can relate the stiffness K with the displacement z and force F during each cycle. Since we are more interested in the result at the maximum force, then the equation reduces to:

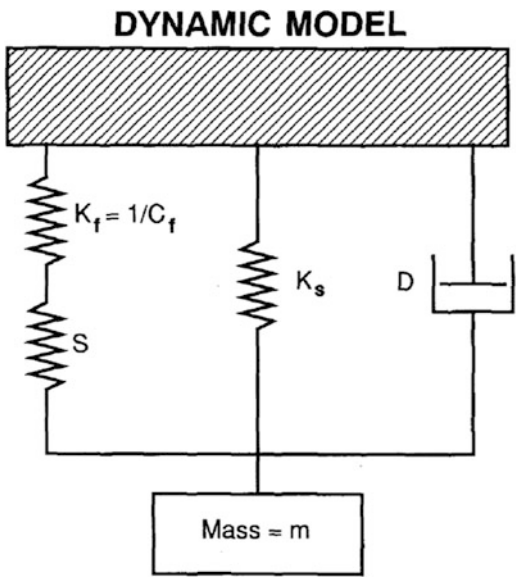

Fig. 16.1 Dynamic model used for CSM. The model includes an aggregated frame stiffness K_f, spring stiffness K_s, contact stiffness S, mass m, and damping constant D [4]

$$K\left[\frac{z_m}{z_0}\cos\phi + 1\right] - m\omega^2 = (F_m + F_0)\frac{\cos\phi}{z_0}$$

We noted that the traditional CSM equation is just a special case of our generalized model, when z_m and F_m are both zero. The above equation provides a way to compute the stiffness K to later compute the contact stiffness S, which are related as:

$$K = \left[\frac{1}{K_\mathrm{f}} + \frac{1}{S}\right]^{-1} + K_\mathrm{s}.$$

During a force-controlled fatigue indentation test, we know the force and frequency. Also, the displacement is collected as the system response. However, we still have to determine the frame stiffness K_f and spring stiffness K_s. So we use the generalized equation to calculate K and m. Then, we use the above equation to compute the stiffnesses K_f and K_s.

In order to calculate both machine stiffnesses, we ran several tests from 1 to 10 Hz every 1 Hz for 100 cycles with 4340 and wrought aluminum. We computed the contact stiffness S and fitted a curve to all the data points to obtain the machine parameters.

$$\begin{aligned} m &= 37.97\,\mathrm{kg} \\ K_\mathrm{f} &= 11,963,938\,\frac{\mathrm{N}}{\mathrm{m}} \\ K_\mathrm{s} &= -7,033,185\,\mathrm{N/m} \end{aligned}$$

16.4 Elastic Modulus

The unloading slope, S, for every cycle is as shown in Fig. 16.2. The unloading slope is graphically defined as the tangent of the force-displacement curve at the beginning of the unloading procedure.

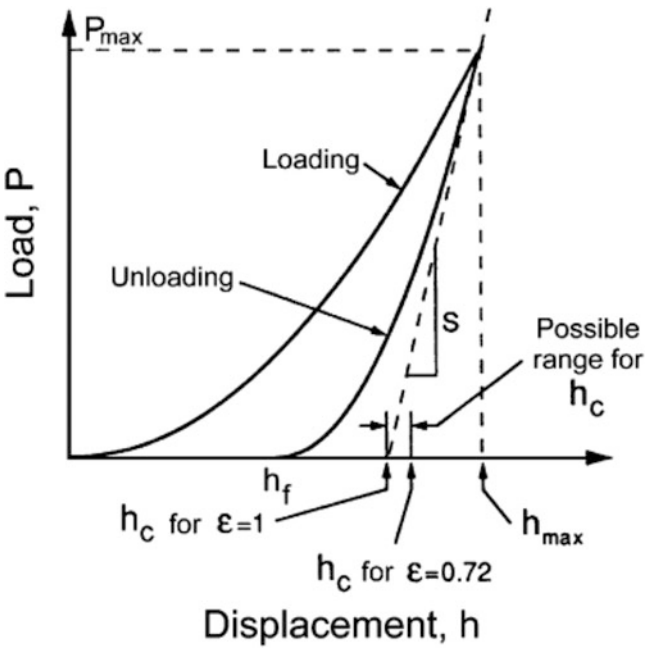

Fig. 16.2 Force-displacement curve for one cycle. S, the unloading slope, is graphically defined as the tangent of the curve at the major load [11]

The unloading slope is then used to calculate the contact or reduced stiffness, E_r, as follows:

$$S = 2\sqrt{\frac{A}{\pi}}E_r$$

where A is the projected area of the indentation that is a function of the indenter geometry and contact penetration depth, h_c. For a Berkovich indenter.

The contact penetration depth, h_c, is corrected to account for deformation on the material surface during indentation as:

$$h_c = h_{max} - \varepsilon\frac{F_{max}}{S}$$

where ε is a constant that depends on the indenter geometry. For a Berkovich indenter, ε would be 0.75.

We can then relate the reduced stiffness to the material stiffness as follows:

$$E_r = \frac{1-\nu_{mat}^2}{E_{mat}} + \frac{1-\nu_{ind}^2}{E_{ind}}$$

where the subscripts "mat" and "ind" refer to the material and indenter properties, respectively.

16.5 Results and Discussion

Indentation fatigue tests were conducted on 4340 specimens before and after heat treatment. Tests were conducted for 35,000 cycles at 2 Hz from 98 to 883 N, at 4 Hz from 98 to 735 N, and at 5 Hz or 6 Hz from 98 to 589 N, respectively. The elastic modulus results are presented in Fig. 16.3. All elastic modulus curves have a similar degradation trend. However, their absolute values vary due to the initial conditions associated with imperfections at the specimen surface. Therefore, results were normalized by the initial value, and are shown in Fig. 16.4. These results reasonably capture the degradation behavior of an S-N curve indicating that the technique can be potentially viable for reconstructing S-N curves.

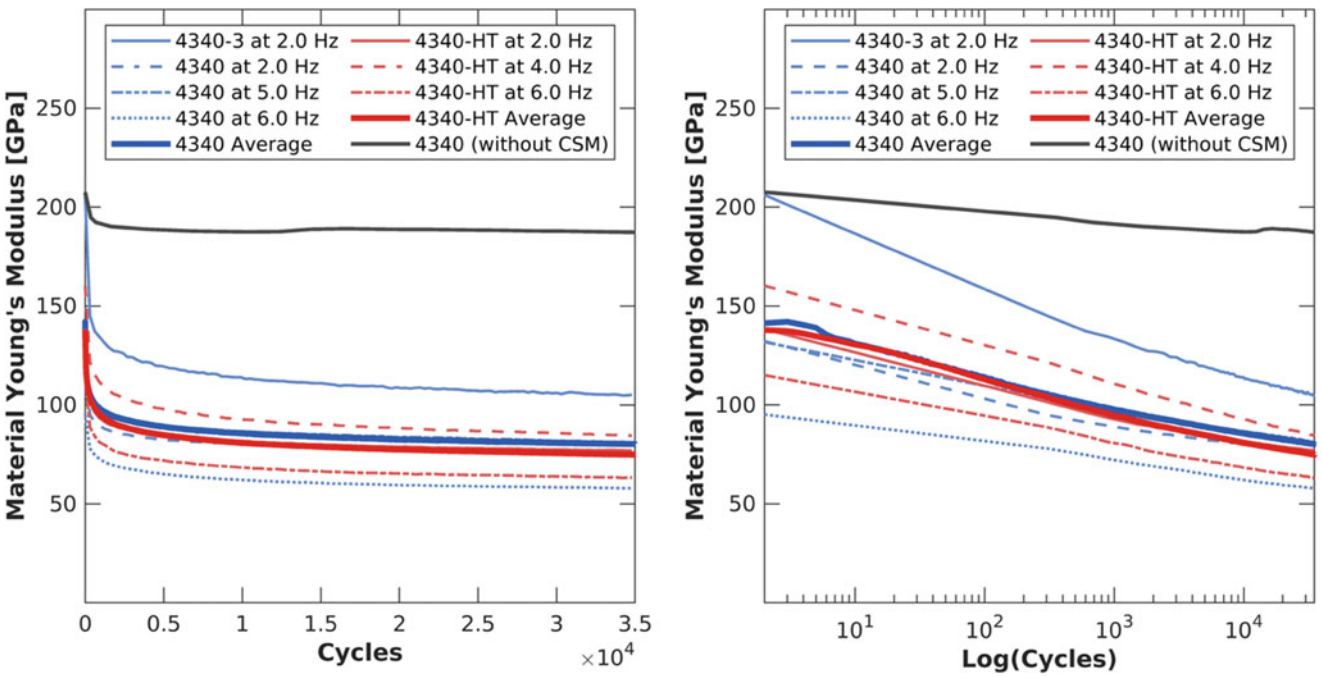

Fig. 16.3 Material elastic modulus obtained for 4340. Left: Linear cycles scale. Right: Log cycle scales

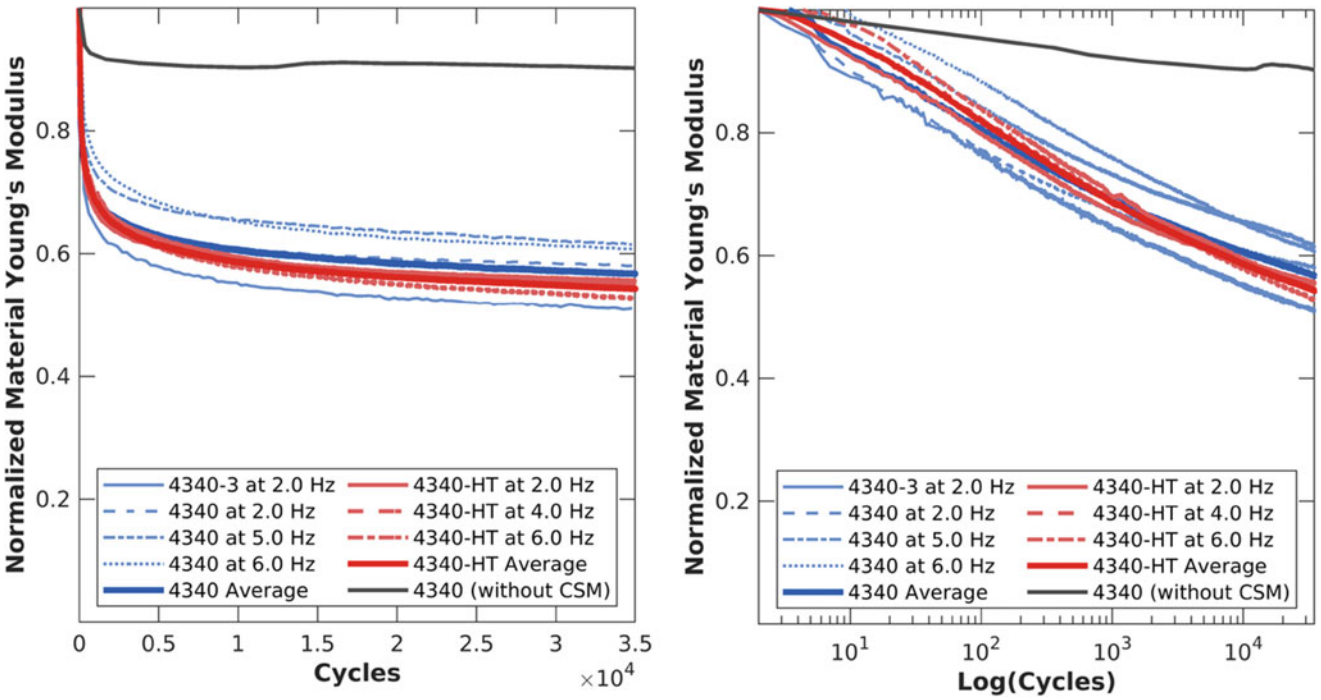

Fig. 16.4 Normalized material elastic modulus obtained for 4340. Left: Linear cycles scale. Right: Log cycle scale

16.6 Conclusions

In this study we proposed a generalized CSM equation that we used to model the dynamic behavior of fatigue indentation. The technique requires first calibrating the machine against known materials and correcting the penetration depth by using existing S-N data. It was observed that the technique is sensitive to small imperfections, like scratched on the polished surface of the specimens, which required normalizing the measurements by the initial measurement. Nevertheless, the approach is a promising start into producing localized fatigue properties for material with different geometric features and opens the door to generating a S-N curve from a single experimental test. This has important implications for being able to determine localized fatigue behavior that can impact the development of AM metals, as well as other materials, such as composites.

Acknowledgments This work was sponsored by Naval Air Warfare Center Aircraft Division, Pax River, MD under award number N004211910001. The opinions expressed in this paper do not necessarily represent those of the sponsor.

References

1. ASTM.: Standard test method for strain-controlled fatigue testing. ASTM Standard E606 (2012)
2. Dreyfuss, R.: Standard practice for conducting force controlled constant amplitude axial fatigue tests of metallic materials. In: Annual Book of ASTM, pp. 515–519. American Society for Testing and Materials (2003)
3. ASTM E73910.: Standard practice for statistical analysis of linear or linearized stress-life (SN) and strain-life (ε-N) fatigue data (2015)
4. Oliver, W.C., Pharr, G.M.: An improved technique for determining hardness and elastic modulus using load and displacement sensing indentation experiments. J. Mater. Res. **7**(6), 1564–1583 (1992)
5. Cole, D.P., Bruck, H.A., Roytburd, A.L.: Nanoindentation studies of graded shape memory alloy thin films processed using diffusion modification. J. Appl. Phys. **103**(6), 064315 (2008)
6. Yan, W., Pun, C.L., Simon, G.P.: Conditions of applying Oliver–Pharr method to the nanoindentation of particles in composites. Composit. Sci. Technol. **72**(10), 1147–1152 (2012)
7. Kontomaris, S.V., Stylianou, A., Nikita, K.S., Malamou, A., Stylianopoulos, T.: A simplified approach for the determination of fitting constants in Oliver–Pharr method regarding biological samples. Phys. Biol. **16**(5), 056003 (2019)

8. Tranchida, D., Piccarolo, S., Loos, J., Alexeev, A.: Accurately evaluating Young's modulus of polymers through nanoindentations: a phenomenological correction factor to the Oliver and Pharr procedure. Appl. Phys. Lett. **89**(17), 171905 (2006)
9. Zysset, P.K., Guo, X.E., Hoffler, C.E., Moore, K.E., Goldstein, S.A.: Elastic modulus and hardness of cortical and trabecular bone lamellae measured by nanoindentation in the human femur. J. Biomech. **32**(10), 1005–1012 (1999)
10. Li, X., Bhushan, B.: A review of nanoindentation continuous stiffness measurement technique and its applications. Mater. Charact. **48**(1), 11–36 (2002)
11. Li, X., Bhushan, B.: Continuous stiffness measurement and creep behavior of composite magnetic tapes. Thin Solid Films. **377**, 401–406 (2000)
12. Vachhani, S.J., Doherty, R.D., Kalidindi, S.R.: Effect of the continuous stiffness measurement on the mechanical properties extracted using spherical nanoindentation. Acta Mater. **61**(10), 3744–3751 (2013)
13. Li, X., Bhushan, B.: Nanofatigue studies of ultrathin hard carbon overcoats used in magnetic storage devices. J. Appl. Phys. **91**(10), 8334–8336 (2002)
14. Xu, B.X., Yue, Z.F., Wang, J.: Indentation fatigue behaviour of polycrystalline copper. Mech. Mater. **39**(12), 1066–1080 (2007)
15. Hoshide, T., Ohara, T., Yamada, T.: Fatigue crack growth from indentation flaw in ceramics. Int. J. Fract. **37**(1), 47–59 (1988)
16. Reece, M., Guiu, F.: Repeated indentation method for studying cyclic fatigue in ceramics. J. Am. Ceram. Soc. **73**(4), 1004–1013 (1990)
17. Lawn, B.R., Marshall, D.B., Anstis, G.R., Dabbs, T.P.: Fatigue analysis of brittle materials using indentation flaws. J. Mater. Sci. **16**(10), 2846–2854 (1981)
18. Cook, R.R., Lawn, B.R., Anstis, G.R.: Fatigue analysis of brittle materials using indentation flaws. J. Mater. Sci. **17**(4), 1108–1116 (1982)
19. Schmahl, M., Märten, A., Charité, P.Z., Fleck, C.: Nanofatigue behaviour of single struts of cast A356.0 foam: cyclic deformation, nanoindent characteristics and sub-surface microstructure. Mater. Design. **2020**, 109016 (2020)
20. Hay, J., Agee, P., Herbert, E.: Continuous stiffness measurement during instrumented indentation testing. Exp. Tech. **34**(3), 86–94 (2010)

Chapter 17
Toughening Mechanism of Recycled Rubber Based Composites Reinforced with Glass Fibers + Alumina Fibers for Military Applications

G. K-Çakır, Ö. Aslan, and E. Bayraktar

Abstract Military grade composites are used in many different applications for their low weight to protect the equipment from harm or destruction. In this research, low-cost devulcanized recycled rubber based composites were designed with short glass fibers + glass bubbles reinforcements. After determination (in wt% percentages) of the reinforcements with matrix, a special process was applied to complete successfully the manufacturing of these composites (silanization of the recycled rubber and devulcanization before blending it with epoxy resin and reinforcement). All of the details of these processes were given in former papers (Irez et al., Materials 12:2729, 2019; Irez et al., Polymers 12:448, 2020; Irez et al., Mechanics of composite and multi-functional materials, Springer, pp 59–70, 2017; Irez and Bayraktar, Mechanics of composite and multi-functional materials, Springer, pp 73–80, 2019). After that, the relevant toughening mechanisms for the most suitable reinforcements were analyzed in detail for front and rear parts in the military applications (such as military vehicles, boats, etc.). For this purpose, certain mechanical and physical properties (ISO 13586: 2000), (K_{IC}—Fracture toughness stress intensity factor and G_{Ic}—Critical energy release rate in mode I) have been determined by fracture toughness tests (static 3P bending test with single edge notch specimens). Microstructural and fracture surfaces analyses have been carried out by means of scanning electron microscopy (SEM).

Keywords Recycled composites · Fine glass-alumina fibers · Devulcanized rubber · Static 3P bending · SEM, fracture surface · Damage analyses

17.1 Introduction

Recycling of materials currently attracts considerable worldwide attention because of environmental and economic issues. Among the recyclable materials, recycled rubber is a widely used material in many industries and development of low-cost and lightweight materials to be used in the manufacture constitutes an important task. Moreover, recycled rubber containing composites can be suitable for applications where high toughness and high resistance to impact are desirable. In the literature, there are several studies on design and manufacturing of recycled rubber composites. Irez, Zambelis, and Bayraktar [1] studied the fracture behavior and damage analyses of recycled ethylene propylene diene monomer rubber modified epoxy based composites reinforced with alumina fiber. They have conducted three-point bending tests to investigate fundamental mechanical characteristics. Mechanical test results showed that the reinforcements improved the fracture toughness of these composites. Another study on recycled rubber based composites was performed by Irez, Bayraktar, and Miskioglu [2], and four different compositions were developed and characterized for their potential usage as structural materials. The matrix was

G. K-Çakır
Department of Mechanical Engineering, Atilim University, Ankara, Turkey

School of Mechanical and Manufacturing Engineering, Isae-Supmeca-Paris, Saint-Ouen, France
e-mail: gamze.cakir@atilim.edu.tr

Ö. Aslan
Department of Mechanical Engineering, Atilim University, Ankara, Turkey
e-mail: ozgur.aslan@atilim.edu.tr

E. Bayraktar (✉)
School of Mechanical and Manufacturing Engineering, Isae-Supmeca-Paris, Saint-Ouen, France
e-mail: emin.bayraktar@isae-supmeca.fr

V. Chalivendra et al. (eds.), *Mechanics of Composite, Hybrid and Multifunctional Materials, Fracture, Fatigue, Failure and Damage Evolution, Volume 3*, Conference Proceedings of the Society for Experimental Mechanics Series,
https://doi.org/10.1007/978-3-030-86741-6_17

prepared by treatment of epoxy with 10% recycled rubber. They stated that all of the experiments, scanning electron microscopy, nanoindentation, static (3PB), test results expose a combined effect of toughening mechanisms of high strength and ductile, lightweight and low-cost composites based on the rubber modified epoxy composites reinforced with nano magnetic iron oxide and auxiliary fine nickel and nano aluminum powders. These authors also studied fracture toughness analysis of epoxy-recycled rubber-based composite reinforced with graphene nanoplatelets for structural applications in automotive and aeronautics [3–10]. After manufacturing the composites, their bending strength and fracture characteristics were investigated by three-point bending (3PB) tests. Halpin–Tsai homogenization adapted to composites containing GnPs was used to estimate the moduli of the composites, and satisfactory agreement with the 3PB test results was observed. In addition, 3PB tests were simulated by finite element method incorporating the Halpin–Tsai homogenization, and the resulting stress–strain curves were compared with the experimental results. Mechanical test results showed that the reinforcement with GnPs generally increased the modulus of elasticity and the fracture toughness. They observed that these composites have the potential to be used to manufacture various components in the automotive and aeronautic industries as well as smart building materials in civil engineering applications.

The majority of the studies on recycled rubber composites show that recycled rubber reinforced with nano scale particles lead to develop physical and mechanical properties of the structures and also provide low-cost and lightweight composites for several application areas. In this work, various reinforcements including glass bubble microspheres, Al_2O_3 fiber, nano graphene platelets (GnPs), and nano silica have been used to provide multifunctionality to the composites. After the general characterizations of the composites, certain additional tests were carried out to identify toughening mechanisms by using Scanning Electron Microscopy, (SEM) on the fracture surfaces.

17.2 Experimental Conditions

Low-cost devulcanized recycled rubber based composites were reinforced with short glass fibers + glass bubbles reinforcements. After determination (in wt% percentages) of the reinforcements with matrix, a special process was applied to complete successfully the manufacturing of these composites (silanization of the recycled rubber and devulcanization before blending it with epoxy resin and reinforcement). All of the details of these processes were given in former papers [1–3, 7]. Chemical treated followed devulcanized recycled rubber were mixed with epoxy resin for obtaining a strong chemical bonding diffusion reinforced with different reinforcement (Table 17.1).

After blending of this mixture, they were milled during 4 h by adding "Zn-Stearate" as lubricant for homogenous distribution. For manufacturing of the composites, hot compaction was carried out at 230 °C during 20 min under the pressure of 6 tons after that the specimens produced with a diameter of 50 mm. Final rectangular shape specimens were cut for 3-point bending tests (ASTM STP 856) called Single Edge Notch Bending (SENB) test specimens (Fig. 17.1) to calculate fracture toughness and fracture energy values of these composites.

3P bending tests (SENB) were carried out with a constant speed of 1 mm/min. Fracture surface analyses were carried out by using Scanning Electron Microscope (SEM) on the damaged specimens. Microstructural analyses have also been carried out on the polished surfaces of these specimens (Distribution of the particles by mapping and also chemical analyses by EDS (Electro Discharge Spectrum)). All of the microhardness measurement have been carried out by using of "SHORE-D TESTS" following the ASTM 2240 and the results were presented in Table 17.2.

Table 17.1 Chemical compositions of the composites studied in this work (wt%)

Composites name	Matrix (rubber/epoxy)	TiB_2	(γ-Al_2O_3) fiber	Glass bubble	Al-chips	BN	Nano SiO2
A	80/20	5	5	5			
B	80/20	5	5		10		
C	80/20		10	10			5
D	80/20					5	10
E	80/20				10		
F	80/20	5					
G	80/20		10	5			

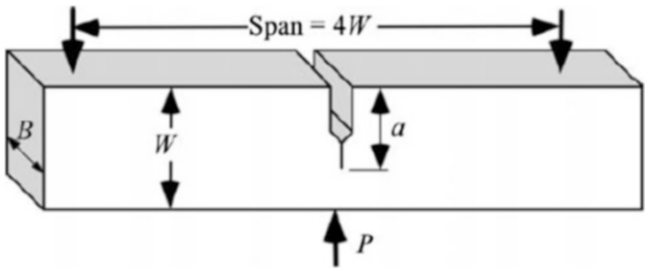

Fig. 17.1 3-Point single edge notch bending (SENB) test for fracture toughness, K_{Ic} and fracture energy, G_{Ic} characterization

Table 17.2 Shore-D hardness measurements of the composites

Composites name	Shore-D test ASTM 2240
A	80.5 ± 2.25
B	79.75 ± 3
C	80 ± 2
D	78.75 ± 1.5
E	71.5 ± 2
F	67.5 ± 2
G	80.25 ± 3

17.2.1 Materials Processing and Fracture Surface Analyses

The combination of epoxy and rubbers are reinforced with glass bubbles, alumina fibers, graphene nano platelets or nano silica. The toughness improvement in hybrid rubber based composites can increase the plastic zone in the structure and this leads the devulcanized rubber based composites to dissipate additional fracture energy. For this reason, the mixture of composite material is chosen as 80 wt % for devulcanized rubber and 20 wt % for epoxy. Moreover, glass bubble has a high strength to density ratio for use in demanding polymer processing operations for various plastic and rubber parts and applications. A perfectly spherical shape with an aspect ratio of one makes glass bubbles efficient volume fillers because they can be incorporated at very high volume loadings without increasing the viscosity to unacceptable levels for further polymer processing and shaping operations. Glass bubbles can provide excellent weight reduction, performance, processing, and dimensional stability characteristics when used with other reinforcing fillers [4–11].

The most common flexural test for composite materials is the three-point bending test. Flexural strength, elasticity modulus in bending (flexural modulus), and strain are obtained from the test results. Three-point bending tests are carried out according to the ASTM D790 standards. The test specimen is placed to the universal testing machine and force is applied until its failure. In addition, fracture toughness indicators such as critical stress intensity factor and critical strain energy release rate are investigated with notched specimens. During the tests, crosshead speed is selected between 1 and 2 mm/min and flexural strength and strain are obtained from the test results [8–10, 12–15].

Microstructure and surface damage evaluations are made by means of scanning electron microscopy (SEM). After the realization of bending tests, fracture surfaces are observed by means of scanning electron microscopy (SEM). Creating ideal interface for each composition provides good adhesion of the reinforcements in the rubber-based matrix.

17.3 Results and Discussion

17.3.1 Microstructure and Fracture Surface Observations

For this reason, the fracture surface analyses of the composites have been carried out by using Scanning Electron Microscope (SEM) to justify this idea. At the same time, detailed mapping analyses have also been done on the microstructures of the polished specimens for each composite for observing the distribution of the reinforcement in the matrix. Figures 17.2 and 17.3

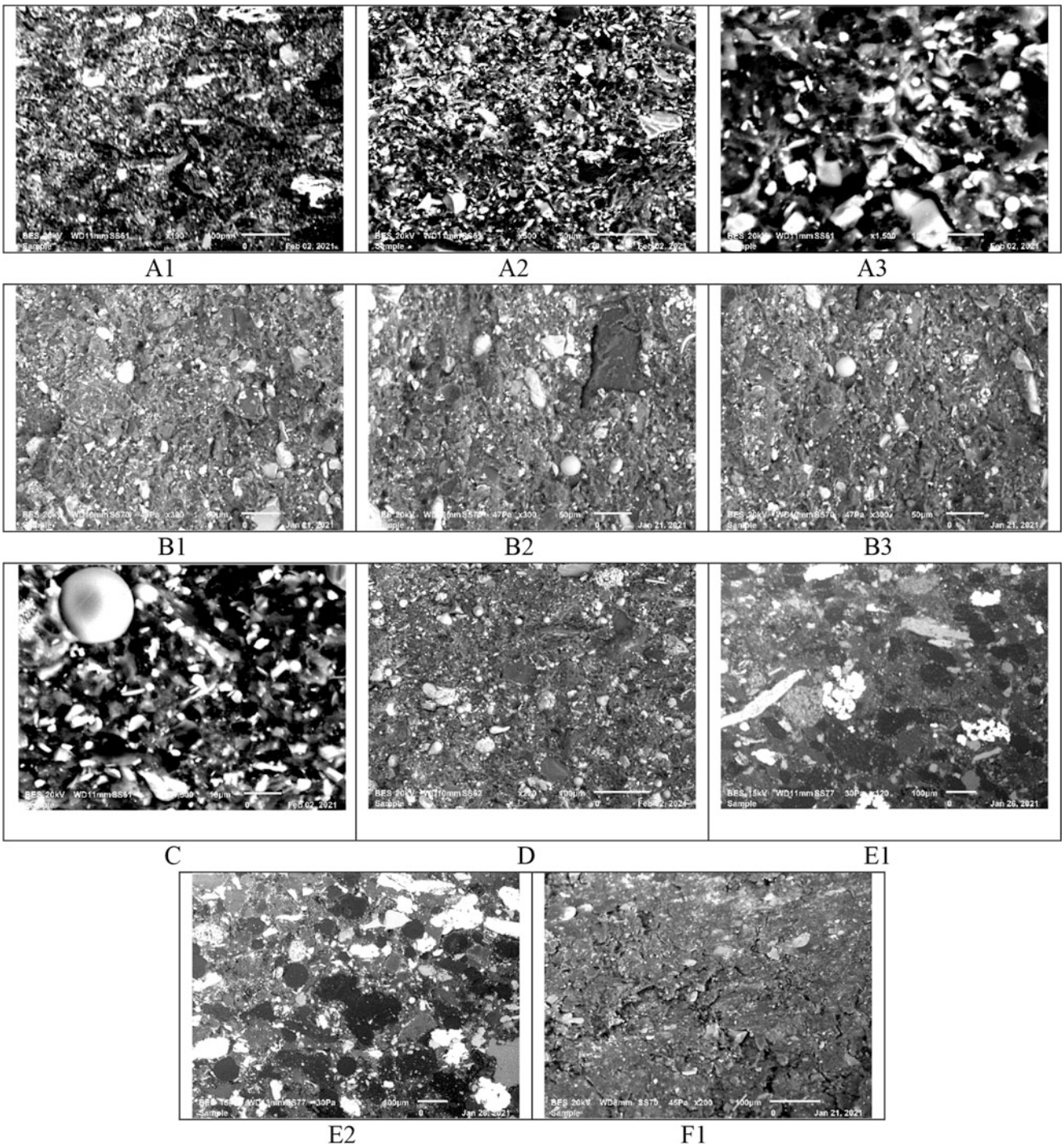

Fig. 17.2 Microstructure and fracture surface analyses for the different composites

give all of the details on the microstructure evolution with different reinforcements. On may observe a homogenous distribution of the reinforcement in the matrix with some agglomeration of the fine powders used as reinforcements in the matrix such as glass bubbles, GB, SiO_2, etc. Energy Dispersive Spectroscopy (EDS) is used to analyze the chemical composition of rubber-based composites and shown for some of the specimens in Fig. 17.4. Fracture surfaces of all of the compositions have shown that there is a strong cohesion between the reinforcements and matrix. The ceramic fibers and glass bubbles seems retain the cohesion during the fracture and they should play a bridge between two parts of the microstructure. Furthermore, some of the fracture surfaces present a hiding place structure due to the tough cohesion in the microstructure

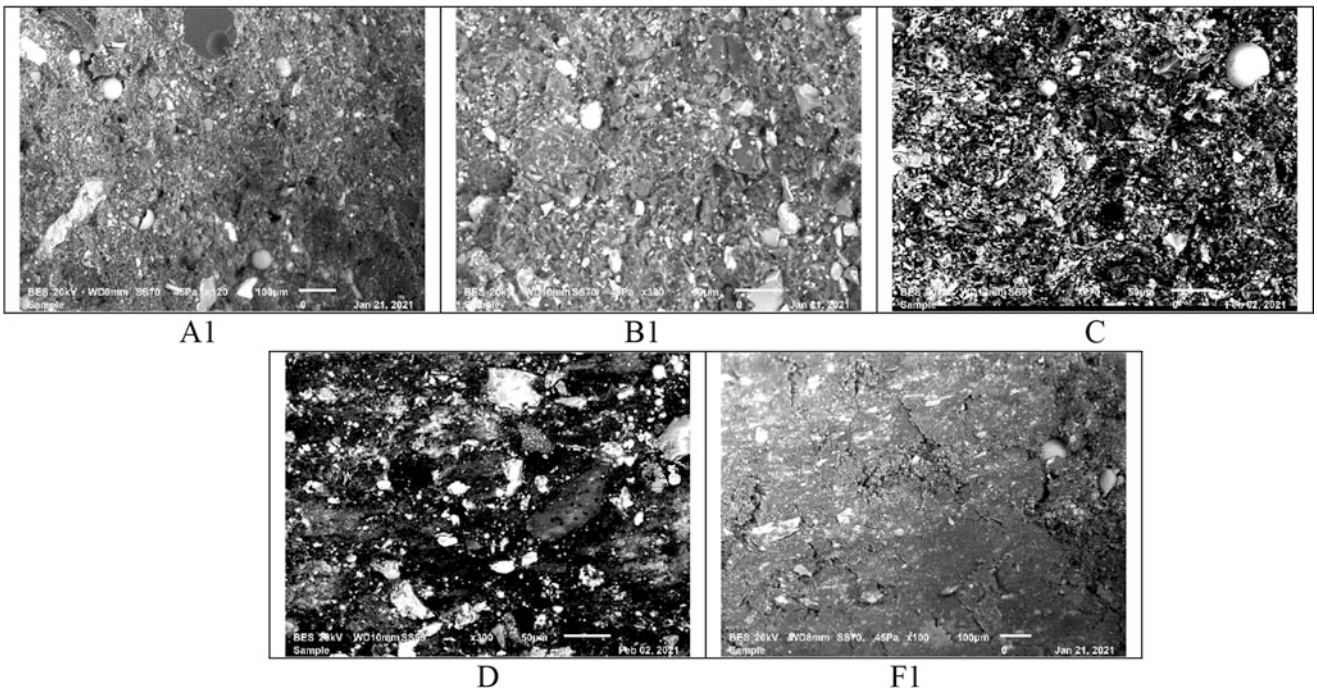

Fig. 17.3 Microstructure and fracture surface analyses for the different composites

related to the mutual chemical diffusion bonding. This property should be improved with the homogenous ball milling of the mixture to eliminate agglomeration of the fine reinforcements.

17.3.2 Mechanical and Physical Properties: Three-Point Bending Tests (SENB)-ASTM D 790

3P bending tests have been carried out with a constant speed of 1 mm/min for the specimens produced from each different type of composites called single edge notch bending (SENB). Three to four specimens have been tested for each composition and evolution of stress levels depending on the deformation for each composition were presented in Fig. 17.5. By using these graphs, fracture toughness and fracture energy values have been calculated.

Mechanical and physical properties are obtained by conducting the 3P bending test with single edge notch specimens suggested by ASTM D790 [5]. Flexural stress is calculated during three-point bending as

$$\sigma_{\mathrm{f}} = \frac{3FL}{2bh^2}$$

where L is the span length, P is the maximum bending load, b and h are the sample width and thickness, respectively. Flexural strain is

$$\varepsilon_{\mathrm{f}} = \frac{6Dh}{L^2}$$

in which D is the maximum deflection at the center of the specimen. The modulus of elasticity in bending is calculated from

$$E_{\mathrm{f}} = \frac{L^3 m}{4bh^3}$$

m is the tangent of the initial straight portion of the stress–strain curve.

The critical stress intensity factor in mode I loading is determined by testing of the SENB specimens under plane strain conditions as

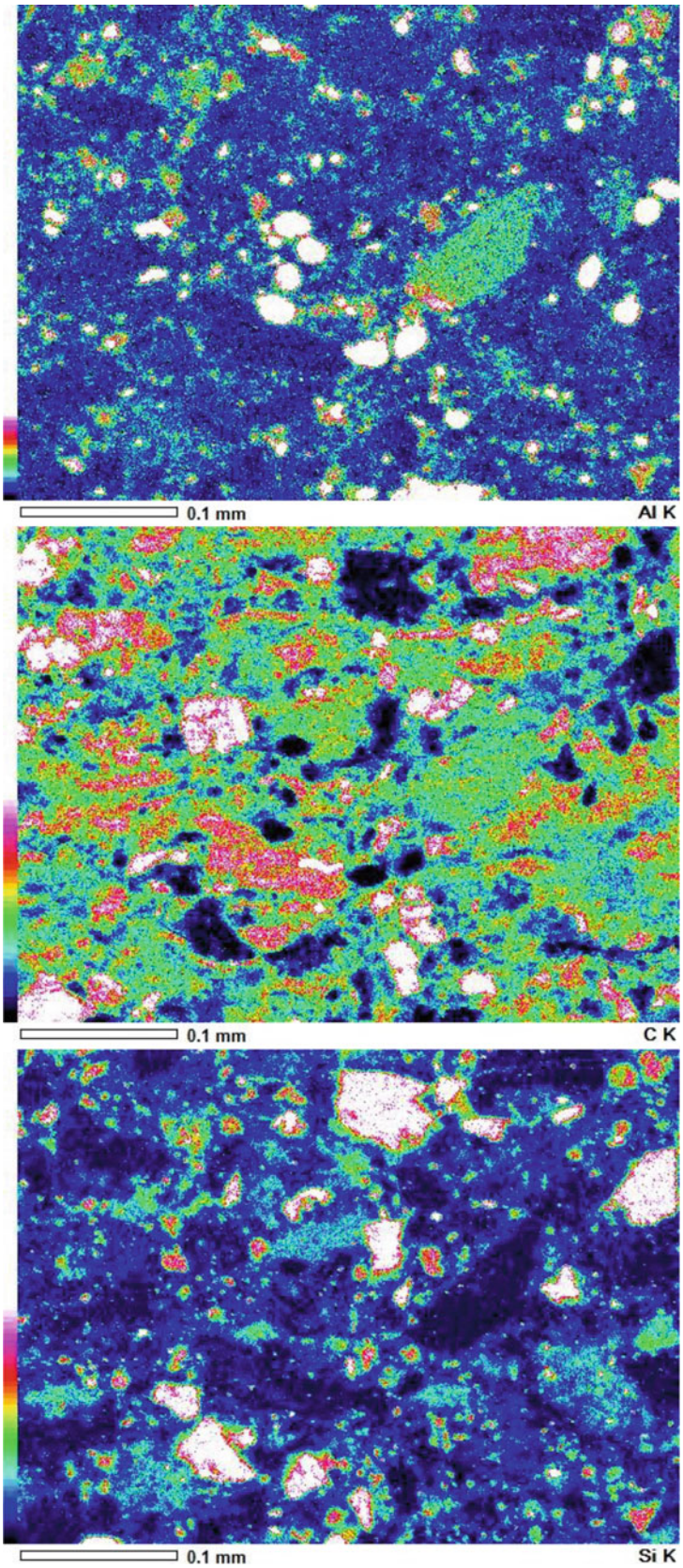

Fig. 17.4 Energy Dispersive Spectroscopy (EDS) chemical mapping for the specimen D

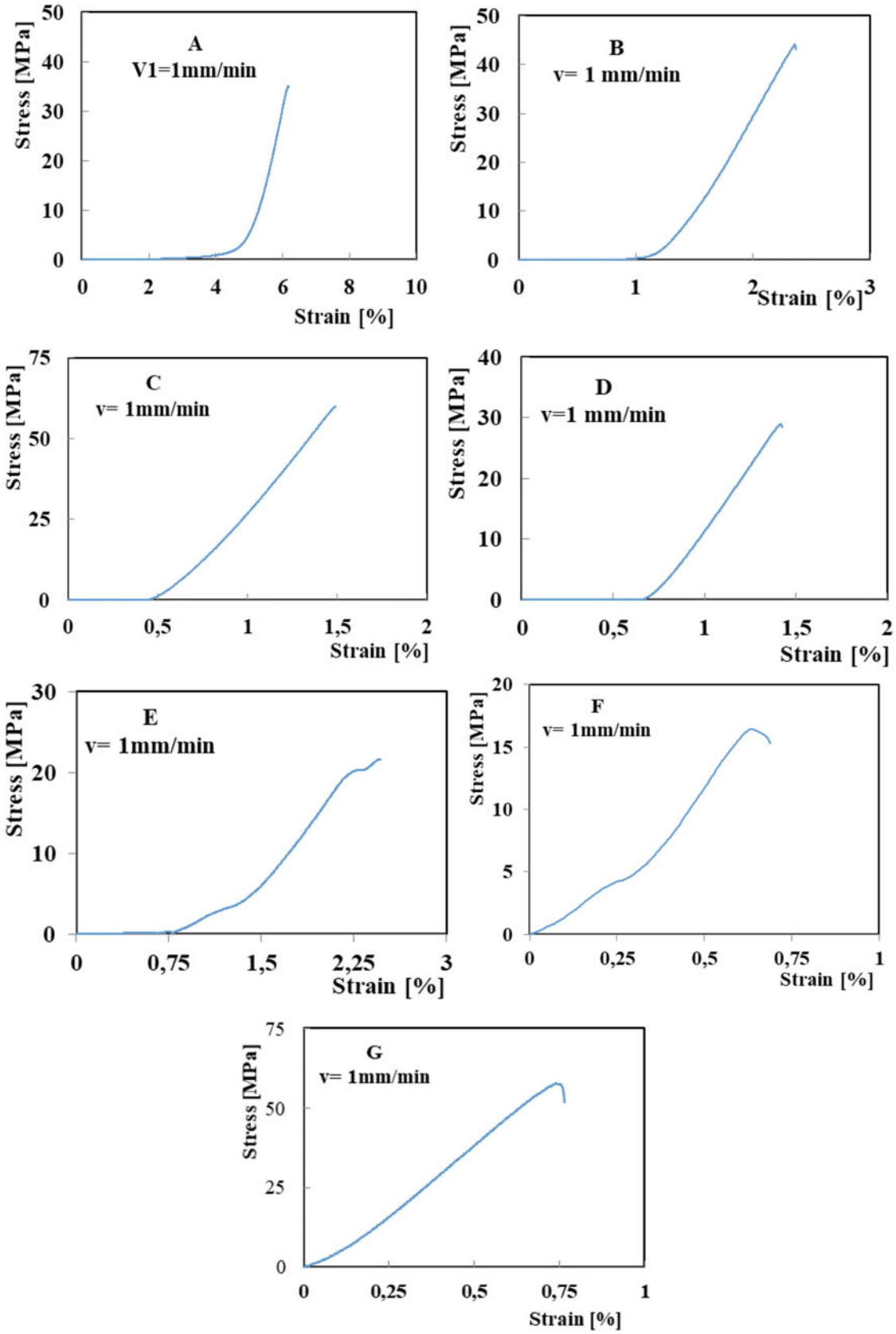

Fig. 17.5 Three-point single edge notch bending test results (3PB-SENB) for the different compositions

$$K_{\mathrm{Ic}} = \frac{F}{BW^{\frac{1}{2}}} f(x), \quad x = a/W$$

This equation is valid for $0 < x < 1$ where F is the maximum force, B is the thickness of the specimen, W is the width, and "a" is the total notch length. $f(x)$ is the geometry correction factor which is obtained by

$$f(x) = 6x^{1/2}\left[1.99 - x(1-x)\left(\frac{2.15 - 3.93x + 2.7x^2}{(1+2x)(1-x)^{3/2}}\right]\right.$$

Critical strain energy release rate (fracture energy) is calculated as

$$G_{\mathrm{Ic}} = \frac{K_{\mathrm{Ic}}^2}{E}$$

where E is the modulus of elasticity.

The dimensions of the test specimens are shown in Table 17.3. Fracture toughness stress intensity factor and critical energy release rate in mode I are calculated and presented in Table 17.4. It is observed that the rubber-based composites reinforced with glass bubbles, alumina and graphene nano plates and carbon nano tubes with a certain ratio have shown improvements in the mechanical properties, flexural stress and fracture toughness.

Table 17.3 Dimensions of the specimens

Specimen	L (mm)	W (mm)	B (mm)	a (mm)
A1	32	7	19	1.25
A2	32	7	19	1.25
A3	32	7.05	15.37	1.25
B1	32	7.18	20.8	1.25
B2	32	7.15	20.6	1.25
B3	32	7	20.88	1.25
C	32	6.45	18	1.25
D	32	7.66	17.33	1.25
E1	32	7.44	21	1.25
E2	32	7.87	9.12	1.25
E3	32	7.9	18.7	1.25
F1	32	8	15	1.25
F2	32	6	15	1.25
F3	32	5	14	1.25
G	32	5	18	11.25

Table 17.4 Comparison of mechanical properties of the specimens

Specimen	σ_{fB}	ε_{f}	E_{f} (MPa)	K_{Ic} (Mpa $\mathrm{m}^{1/2}$)	G_{Ic} (kJ/ m^2)
A1	34.97	6.18	388.88	1.89	9.19
A2	37.45	6.71	432.51	2.02	9.47
A3	33.49	3.20	1239.48	1.82	2.68
B1	44.27	2.37	1829.47	2.45	3.29
B2	51.65	2.18	2635.60	2.85	3.08
B3	45.02	1.09	4758.34	2.43	1.24
C	59.93	1.49	7010.73	2.99	1.27
D	28.99	1.42	2024.69	1.71	1.45
E1	26.54	5.21	192.26	1.52	12.09
E2	29.19	2.26	1675.87	1.77	1.88
E3	21.64	2.47	831.50	1.32	2.10
F1	12.55	3.57	336.06	0.78	1.79
F2	8.39	2.00	391.12	0.39	0.39
F3	16.46	0.91	5527.83	0.65	0.08
G	57.68	0.76	29759.11	2.28	0.17

Table 17.5 The effect of speed on K_{Ic} and G_{Ic} (kJ/m^2) values

Specimen	v (mm/min)	σ_{fB}	ε_f	W (mm)	B (mm)	K_{Ic} (Mpa m$^{1/2}$)	G_{Ic} (kJ/m^2)
A1	1	34.97	6.18	7	19	1.89	9.19
A2	1	37.45	6.71	7	19	2.02	9.47
A3	1	33.49	3.20	7.05	15.37	1.82	2.68
B1	1.5	44.27	2.37	7.18	20.8	2.45	3.29
B2	2	51.65	2.18	7.15	20.6	2.85	3.08
B3	1.5	45.02	1.09	7	20.88	2.43	1.24
C	1.1	59.93	1.49	6.45	18	2.99	1.27
D	1	28.99	1.42	7.66	17.33	1.71	1.45
E1	1	26.54	5.21	7.44	21	1.52	12.09
E2	1	29.19	2.26	7.87	9.12	1.77	1.88
E3	1	21.64	2.47	7.9	18.7	1.32	2.10
F1	1	12.55	3.57	8	15	0.78	1.79
F2	1	8.39	2.00	6	15	0.39	0.39
F3	1	16.46	0.91	5	14	0.65	0.08
G	1	57.68	0.76	5	18	2.28	0.17

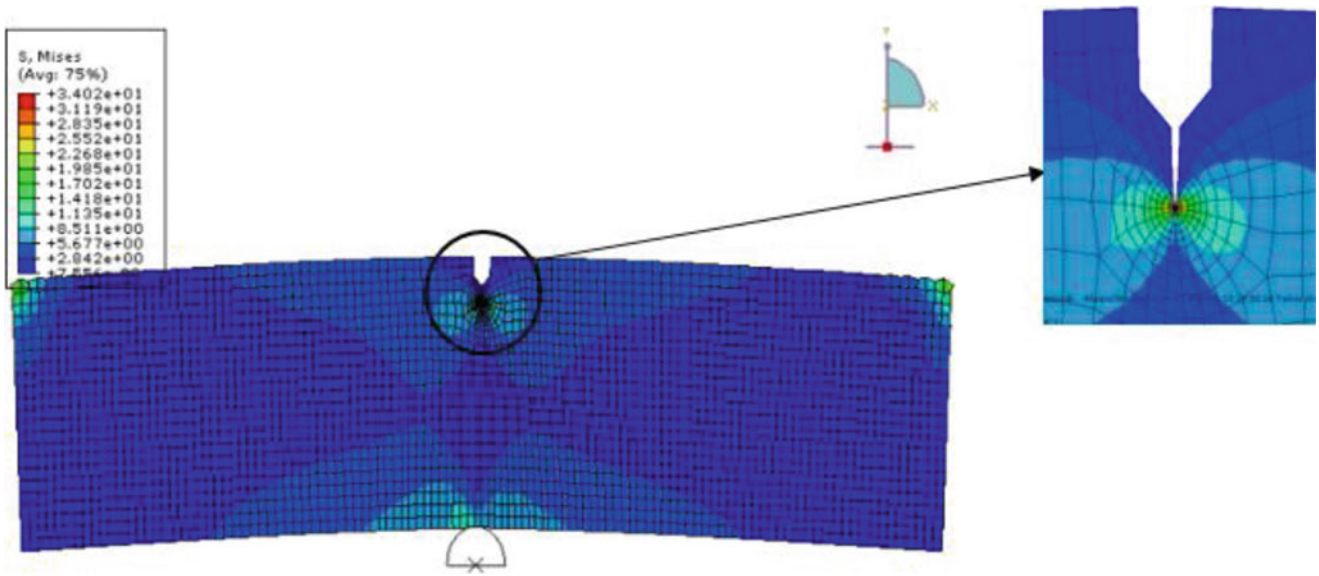

Fig. 17.6 Numerical model for 3P single edge notch bending (SENB) test for A1

During the tests, crosshead speed is selected between 1 and 2 mm/min and the change of the properties according to the speed is shown in Table 17.5. It can be said that the critical stress intensity factor increases with increasing crosshead speed.

Fracture surfaces obtained from 3 PB tests are analyzed by means of SEM. A good adhesion of the reinforcements in the composite is observed by creating ideal interface for each composition. The elastic stress analysis is performed using ABAQUS/Implicit. Symmetric boundary conditions are applied along the corresponding edges of symmetry. To implement the test result, the displacements were given at the center of the specimen. Figure 17.6 shows the typical configuration and mesh of one of the models for plane strain condition. In order to obtain high stress field around the crack, relatively fine mesh sizes are adopted in this region as seen in Fig. 17.7. Material properties obtained from the test result are used in the calculations. In linear elastic fracture mechanics, the stress intensity factor is used to characterize the fracture toughness of a brittle material. The fracture toughness is assumed as constant for a given specimen thickness. To check the validity of this assumption regarding the specimen configuration, the stress intensity factors are calculated for the maximum deflections observed from bending tests. Mechanical properties are implemented for finite element analysis for specimens A1, A2, A3, and B3 and the critical stress intensity factors are calculated very close to the values obtained by experimental values and shown in Table 17.6.

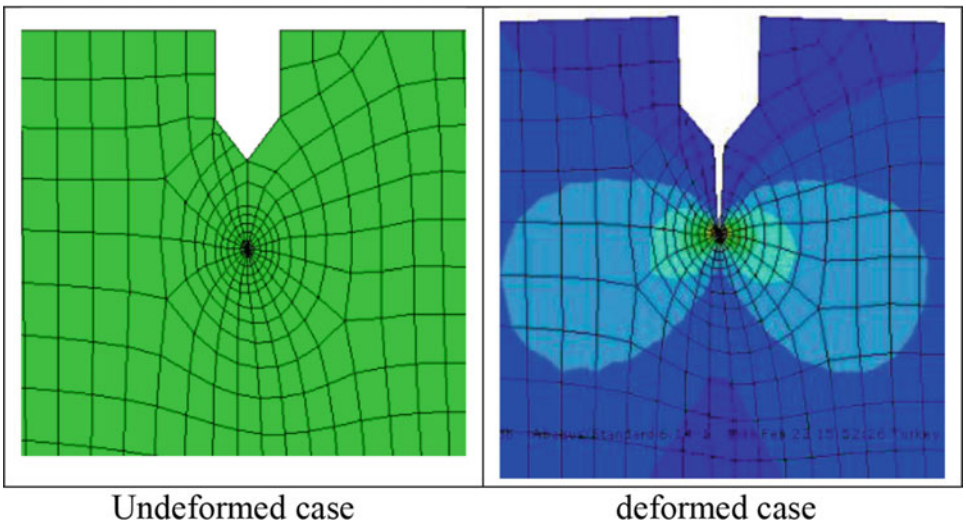

Fig. 17.7 Finite element mesh for the specimen according to the geometry given in Fig. 17.5

Table 17.6 Critical stress intensity factors obtained by numerical analysis

Specimen	E_b (MPa)	a/W	K_{ic} (MPa*m^(1/2))
A1	389	0.179	1.9
A2	433	0.179	2
A3	1240	0.177	1.8
B3	4758	0.179	2.3

17.4 Conclusion

Recycled rubber based composites reinforced with alumina fiber and glass bubble have been designed and manufactured in different wt% percentages. Toughening mechanisms have been analyzed and mechanical and physical properties (fracture toughness stress intensity factor and critical energy release rate) have been determined by fracture toughness tests. Microstructural and fracture surfaces analyses have been carried out by means of scanning electron microscopy. After fracture surfaces have been obtained from 3 PB tests and analyzed by means of SEM, a good adhesion of the reinforcements has been observed by creating ideal interface for each composition. It is observed that the rubber-based composites reinforced with glass bubbles, alumina, and graphene nano plates have shown improvements in the mechanical properties, flexural stress and fracture toughness. The improved toughening mechanisms are due to the formation of the cavitation and void formation because of debonding of the fine reinforcement particles in the rubber matrix which leads to void growth with consequent locally matrix expansion. For this reason, the mixture of devulcanized rubber (85 wt %) with solid powder epoxy resin (15 wt %) is significant for manufacturing the effective composite material. It is also observed from numerical analysis that the stress intensity factor is influenced by the depth and crack length of the specimen.

References

1. Irez, A.B., Zambelis, G., Bayraktar, E.A.: New design of recycled ethylene propylene diene monomer rubber modified epoxy based composites reinforced with alumina fiber: fracture behavior and damage analyses. Materials. **12**, 2729 (2019). https://doi.org/10.3390/ma12172729
2. Irez, A.B., Bayraktar, E., Miskioglu, I.: Fracture toughness analysis of epoxy-recycled rubber-based composite reinforced with graphene nanoplatelets for structural applications in automotive and aeronautics. Polymers. **12**, 448 (2020). https://doi.org/10.3390/polym12020448
3. Irez, A.B., Bayraktar, E., Miskioglu, I.: Mechanical characterization of epoxy—scrap rubber based composites reinforced with alumina fibers. In: Mechanics of Composite and Multi-functional Materials, vol. 6, pp. 59–70. Springer (2017). ISBN 978-3-319-63408-1). https://doi.org/10.1007/978-3-319-63408-1
4. Yalcin, B., Amos, S.E., Williams, M.J., Gunes, I.S., Ista, T.K.: 3M™ glass bubbles iM16K for reinforced thermoplastics. www.3M.com/glassbubbles (2016)
5. Designation: D 790–03 Standard Test Methods for Flexural Properties of Unreinforced and Reinforced Plastics and Electrical Insulating Materials. ASTM International, West Conshohocken

6. Zaimova, D., Bayraktar, E., Miskioglu, I.: Design and manufacturing of new elastomeric composites: mechanical properties, chemical and 179 physical analysis. Int. J. Composit. B. **1**(1), 1–12 (2016) (online 2017)
7. Irez, A.B., Bayraktar, E.: Design of a low-cost aircraft structural material based on epoxy: recycled rubber composites modified with multifunctional nano. In: Mechanics of Composite and Multi-functional Materials, vol. 5, pp. 73–80. Springer (2019). https://doi.org/10.1007/978-3-030-30028-9_11
8. Ferreira, L.M.P., Miskioglu, I., Bayraktar, E., Katundi, D.: Mechanical and tribological properties of scrap rubber reinforced with Al_2O_3 fiber, aluminium and TiO_2. In: Mechanics of Composite and Multi-functional Materials, vol. 7, pp. 37–44. Springer. ISBN 978-3-192 319-41766-0 (2016). https://doi.org/10.1007/978-3-319-41766-0
9. Masoud, F., Sapuan, S.M., Ariffin, M.K.A.M., Nukman, Y., Bayraktar, E.: Cutting processes of natural fiber-reinforced polymer composites. Polymers. **12**, 1332 (2020). https://doi.org/10.3390/polym12061332
10. Burak Irez, A., Bayraktar, E., Miskioglu, I.: Flexural fatigue damage analyses of recycled rubber—modified epoxy-based composites reinforced with alumina fibres. FFEMS Fatigue Fract. Eng. Mater. Struct. (2019)
11. Wan, C., Chen, B.: Reinforcement and interphase of polymer/graphene oxide nano composites. J. Mater. Chem. **22**, 3637–3646 (2012)
12. Burak Irez, A., Hay, J., Miskioglu, I., Bayraktar, E.: Scrap-rubber based composites reinforced with boron and alumina. In: Mechanics of Composite and Multi-functional Materials, vol. 6, pp. 1–10. Springer (2018)
13. Zhang, G., et al.: Effect of functionalization of graphene nanoplatelets on the mechanical and thermal properties of silicone rubber composites. Materials. **9**(2), 92 (2016)
14. Fu, S.-Y., Mai, Y.-W., Lauke, B., Yue, C.-Y.: Synergistic effect on the fracture toughness of hybrid short glass fiber and short carbon fiber reinforced polypropylene composites. Mater. Sci. Eng. **A323**, 326–335 (2002)
15. Dong, C., Davies, I.J.: Optimal design for the flexural behaviour of glass and carbon fibre reinforced polymer hybrid composites. Mater. Des. **37**, 450–457 (2012)

Chapter 18
Sensitivity Analysis of a Concrete Structure Subjected to Cyclic Loading Using a Polynomial Chaos Expansion Method

Henriette Marlaine Imounga, Emilio Bastidas-Arteaga, Serge Ekomy Ango, and Rostand Moutou Pitti

Abstract Cyclic loading is one of the main causes of degradation of reinforced concrete structures. The behavior of a reinforced concrete structure in fatigue can be represented by mechanical models, based on different theories (damage, fracture, plasticity ...), whose development requires knowledge of the characteristic parameters of the material and uncertainties associated. In this paper, we propose a polynomial chaos expansion (PCE) methodology to propagate parameter uncertainties in a damage model. The PCE will also be used to perform a sensitivity analysis of the model. Sensitivity analysis allows quantifying the effects of input variables or their combinations on the output variables of a model. The methodology is illustrated with a reinforced concrete beam subjected to cyclic loading. The results indicate that the deterministic model and PCE are close to the experimental results. The sensitivity analysis was also useful to determine which are the most influencing parameters for a reliability analysis.

Keywords Reinforced concrete · Cyclic loading · Polynomial chaos expansion · Sensitivity analysis · Reliability

18.1 Introduction

During their lifetime, reinforced concrete structures are subjected to stresses of various kinds which lead to their early degradation. Many digital models have been developed in order to represent with the greatest precision the behavior of concrete under mechanical loading. In the case of cyclic loads, several models based on damage theory allow the effects of micro-cracking in concrete to be evaluated after each loading cycle (load/unload). Their use requires, among other things, knowledge of the intrinsic parameters of the material which could be determined from experimental tests. These can contain uncertainties related to the implementation of the tests and the calculation methods used. However, models take time and experimental data is scarce. The work we propose consists of a meta-modeling of the mechanical behavior of a reinforced concrete beam subjected to cyclic loading. The meta-model, based on the polynomial chaos expansion method, allows the uncertainties of the input parameters to be propagated in the mechanical model and is used to perform a sensitivity analysis of the inputs to the outputs.

H. M. Imounga
Université des Sciences et Technique de Masuku, EPM, Franceville, Gabon

UBL, Université de Nantes, GeM, Nantes, France
e-mail: henriette.imounga@etu.univ-nantes.fr

E. Bastidas-Arteaga
UBL, Université de Nantes, GeM, Nantes, France
e-mail: ebastida@univ-lr.fr

S. Ekomy Ango
IRT, CENAREST, Libreville, Gabon

R. Moutou Pitti (✉)
IRT, CENAREST, Libreville, Gabon

Université Clermont Auvergne, CNRS, Clermont Auvergne INP, Institut Pascal, Clermont-Ferrand, France
e-mail: rostand.moutou_pitti@uca.fr

V. Chalivendra et al. (eds.), *Mechanics of Composite, Hybrid and Multifunctional Materials, Fracture, Fatigue, Failure and Damage Evolution, Volume 3*, Conference Proceedings of the Society for Experimental Mechanics Series,
https://doi.org/10.1007/978-3-030-86741-6_18

The paper is structured as follows. The first part describes the damage model used with the constitutive equations (Sect. 18.2). The PCE method is presented in Sect. 18.3. The Sect. 18.4 presents the numerical implementation. Finally, the results are presented and discussed in Sect. 18.5.

18.2 Mechanical Model

To model the concrete, we used the isotropic damage model developed by [1], and implemented in the CAST3M code. In the latter, the damage variable is a scalar which varies between 0 for sound concrete and 1 for cracked concrete. The model takes into account the residual strains and makes it possible to represent the hysteretic behavior as well as the unilateral effects (opening - reclosing of the crack) of concrete.

The different state laws are expressed by the following differential equations:

$$\begin{cases} \sigma = E\left((1-D)\langle\varepsilon_x\rangle_+ + \langle\varepsilon_x\rangle_-\right) + 2(1-D)\mu\varepsilon + 2D\mu(\varepsilon - \varepsilon^\pi) \\ \sigma^\pi = 2D\mu(\varepsilon - \varepsilon^\pi) \\ Y = \dfrac{E}{2}\langle\varepsilon_x\rangle_+^2 + \mu\varepsilon\cdot\varepsilon - \mu(\varepsilon-\varepsilon^\pi)\cdot(\varepsilon-\varepsilon^\pi) \end{cases} \tag{18.1}$$

where μ is a shear coefficient, σ^π is the frictional tensor, ε^π is the sliding tensor, and Y is the damage energy released rate.

Equation (18.2) gives the expression of the scalar damage variable.

$$D = 1 - \frac{1}{1 + \left(A_{\text{Dir}} H\left(\langle\varepsilon_{ij}\rangle_+\langle\sigma_{ij}\rangle_+\right) + A_{\text{Ind}}\left(1 - H\left(\langle\varepsilon_{ij}\rangle_+\langle\sigma_{ij}\rangle_+\right)\right)\right)(Y - Y_0)} \tag{18.2}$$

where A_{Dir} represents the brittleness in tension, A_{Ind} the brittleness in compression, Y_0 the damage initial threshold and H is Heaviside.

18.3 Expansion of Polynomial Chaos

The PCE is a meta-modeling technique which aims to approximate a computational model in the form of polynomial functions. The general decomposition of a PCE is written as follows:

$$\widehat{Y} = M^{PCE}(X) = \sum_{\alpha=0}^{P} y_\alpha \psi_\alpha(X) \tag{18.3}$$

where y_α is the coefficient of the PCE and $\psi_\alpha(X)$ a multivariate polynomial of degree α.

The post-processing of a PCE for the sensitivity analysis proposed by [2] facilitates the evaluation of expensive models in computation. The sensitivity analysis quantifies the influence of the variability of the input parameters (individually or combined) of a model on the output variables using the sensitivity indices [3, 4]. To quantify the impact of the selected input variables on the model, we calculate the Sobol's sensitivity indices directly deducted from the PCE coefficients, with the assumption that there is no correlation between the different variables.

18.4 Numerical Implementation

To perform the various analyses, we model a reinforced concrete beam subjected to a cyclic loading (10,000 cycles) of three-point bending with an alternating point load varying between 5.4 and 18 kN (Fig. 18.1).

The studies were carried out for a C40 concrete with 90 kg m^{-3} of admixture and a *w/c* ratio of 0.44 [5]. The following table presents the variability retained for the generation of the random variables (Table 18.1).

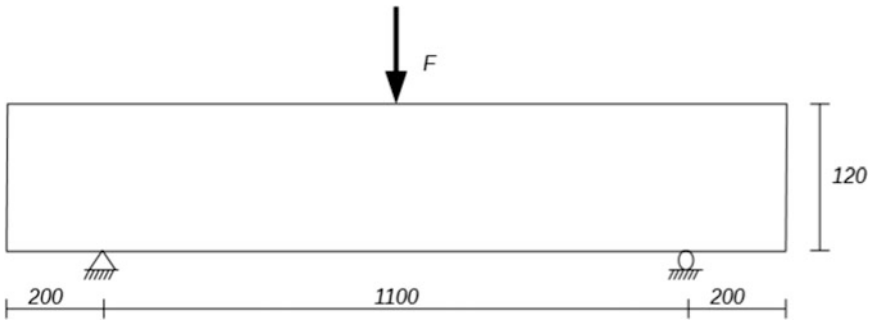

Fig. 18.1 Beam geometry configuration

Table 18.1 Variability of input parameters

Parameters	Notation	Value
Elasticity modulus (MPa)	E	Lognormal ($\mu = 35{,}000$; COV $= 0.12$)
Tensile strength (MPa)	f_t	Lognormal ($\mu = 3.5$; COV $= 0.13$)
Concentrate load (N)	F	Uniform on the interval [5.4; 18] $\times$ 103

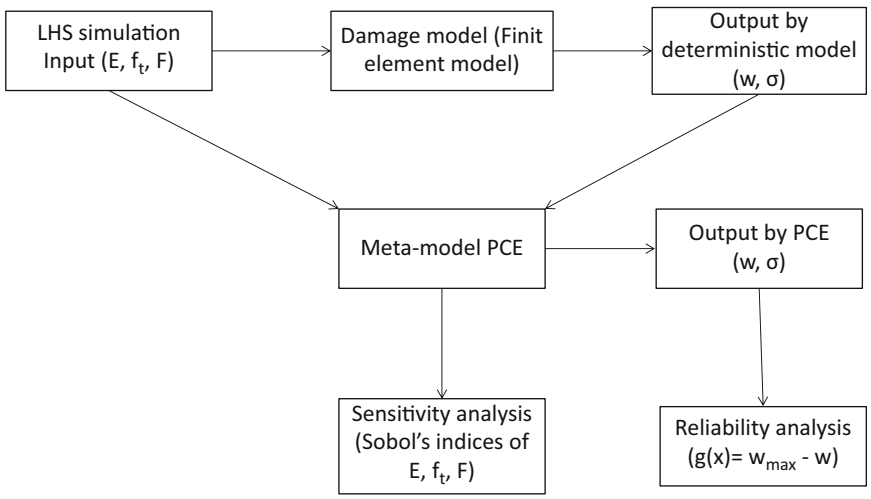

Fig. 18.2 Flowchart of the methodology

Figure 18.2 describes the methodology used to perform the sensitivity and reliability analyses. 200 LHS simulations of the three input variables are performed and fed into the finite element code to calculate deflection and tensile stress in concrete. The input and output values are then injected into the PCE; the PCE coefficients which make it possible to deduce the Sobol's indices are determined. At the exit of the meta-model we also obtain the values of the deflection and the stress, of which those of the deflection are used to calculate the reliability of the structure.

18.5 Results and Discussions

Table 18.2 presents the Sobol sensitivity indices of the input random variables on the damage model. One can thus establish an order of influence of the various input parameters on the deflection and the tensile stress in the concrete. The ultimate tensile stress (f_t) has negligible influence on the two outputs; the loading has a stronger influence on the stress which is logical. The sensitivity indices on the deflection of the Young's modulus and the charge intensity are very close (see Fig. 18.3). This analysis makes it possible to know the most influential parameters to prioritize in order to estimate the lifespan of a structure.

Table 18.2 Sensitivities of the input parameters

Parameters	Deflection	Stress
E	0.594	3.071×10^{-4}
f_t	1.793 × 10–6	3.724×10^{-6}
F	0.412	0.9997

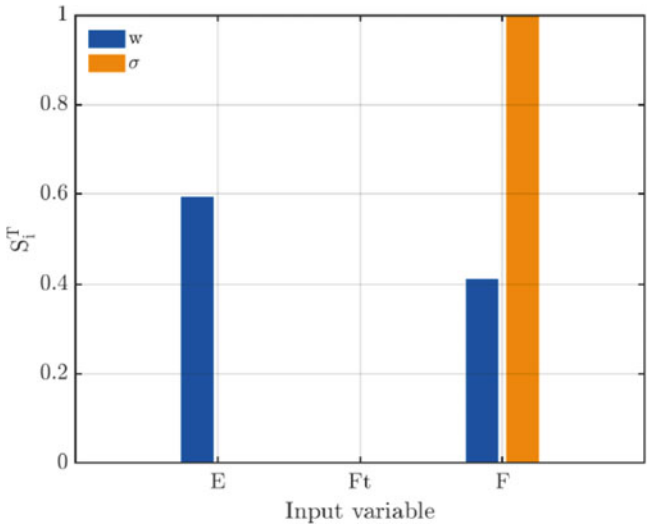

Fig. 18.3 Sobol's total indices

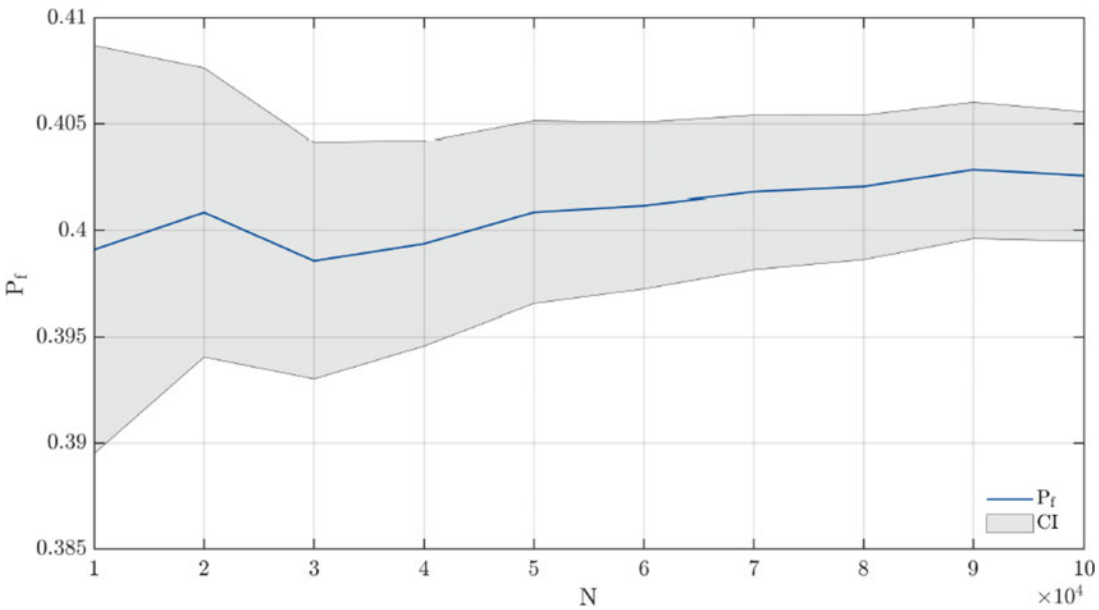

Fig. 18.4 Convergence of failure probability P_f

The probability of failure of the beam was calculated from the Monte Carlo simulation method. This method aims to estimate the probability of failure by probability sampling of the inputs of a model. For our example, the failure criterion is the maximum deflection taken equal to 0.8 mm and we obtain a failure probability of 0.402 with a reliability index of Beta = 0.2468 (Fig. 18.4).

18.6 Conclusion

The methodology used made it possible to highlight the influence of certain input variables on the damage model. It provides information on the variables whose variability will have the most impact on determining the lifespan of a structure. The use of the polynomial chaos expansion is quite interesting in terms of computation time which is relatively short for the number of cycles which is quite high. For a more complete study, the parameters of the damage model considered as deterministic in this study and whose values are extracted from the literature, will be modeled as random variables in order to evaluate the effects of their uncertainties on the output parameters of the model.

Acknowledgments The financial support of the Regional Council of "Pays de la Loire" within the framework of the BUENO 2018–2021 research program (Durable Concrete for Offshore Wind Turbines) is gratefully acknowledged.

References

1. Richard, B., Ragueneau, F., Cremona, C., Adelaide, L.: Isotropic continuum damage mechanics for concrete under cyclic loading: stiffness recovery, inelastic strains and frictional sliding. Eng. Fract. Mech. **77**(8), 1203–1223 (2010)
2. Sudret, B.: Global sensitivity analysis using polynomial chaos expansions. Reliab. Eng. Syst. Saf. **93**(7), 964–979 (2008). https://doi.org/10.1016/j.ress.2007.04.002
3. Crestaux, T., Le Maitre, O., Martinez, J.-M.: Polynomial chaos expansion for sensitivity analysis. Reliab. Eng. Syst. Saf. **94**(7), 1161–1172 (2009). https://doi.org/10.1016/j.ress.2008.10.008
4. Sobol, I.M.: Global sensitivity indices for nonlinear mathematical models and their Monte Carlo estimates. Math. Comput. Simul. **55**(1–3), 271–280 (2001). https://doi.org/10.1016/S0378-4754(00)00270-6
5. Wang, X.-H., Bastidas-Arteaga, E., Gao, Y.: Probabilistic analysis of chloride penetration in reinforced concrete subjected to pre-exposure static and fatigue loading and wetting-drying cycles. Eng. Fail. Anal. **84**, 205–219 (2018). https://doi.org/10.1016/j.engfailanal.2017.11.008